Secular cooling of the solid Earth, emergence of the continents, and evolution of Earth's external envelopes

Nicolas Flament

N° d'ordre : 550
N° attribué par la bibliothèque : __ENSL550

THÈSE

Refroidissement séculaire de la Terre solide, émergence des continents, et évolution des enveloppes externes de la Terre

présentée et soutenue publiquement le 9 Décembre 2009

par Nicolas Flament

en vue d'obtenir le grade de

Docteur de l'Université de Lyon - École Normale Supérieure de Lyon

Spécialité : Sciences de la Terre

Laboratoire de Sciences de la Terre

École Doctorale Matériaux de Lyon

et de

Docteur de l'Université de Sydney

School of Geosciences

devant la commission d'examen formée de

Rapporteur	Stephen Galer	Institut Max Planck (Mainz - Allemagne)
Rapporteur	Claude Jaupart	Institut de Physique du Globe (Paris)
Examinateur	Francis Albarède	École Normale Supérieure (Lyon)
Examinateur	Pascal Philippot	Institut de Physique du Globe (Paris)
Directeur	Nicolas Coltice	Université Lyon 1 (Lyon)
Directeur	Patrice Rey	Université de Sydney (Sydney - Australie)

À mes parents,
pour m'avoir transmis leur passion pour la géologie,
et pour leur soutien inconditionnel

Contents

Remerciements

Un grand merci à mes tuteurs, Nicolas Coltice et Patrice Rey. Cette thèse a très largement bénéficié de la complémentarité et de la diversité de leurs domaines d'expertise. Leur soutient a été primordial à l'aboutissement de ce projet, et j'ai particulièrement apprécié leur disponibilité pendant la rédaction de cette thèse. Merci aussi de m'avoir permis d'associer épanouissements personnel et professionnel en me proposant une thèse en cotutelle. Je ne peux qu'espérer que ce projet constitue le début d'une longue collaboration. Ce manuscrit a également bénéficié de discussions avec Laurent Husson, Anthony Dosseto, Nicolas Olivier et Gilles Dromart. Un grand merci aux deux rapporteurs de cette thèse, Steve Galer et Claude Jaupart. Leurs remarques et commentaires constituent un guide pour le futur. Je les remercie également, ainsi que Francis Albarède et Pascal Philippot, pour la discussion scientifique qui a suivi ma soutenance. Je remercie Isabelle Daniel et Nicolas Coltice pour avoir rendu mon agenda d'enseignement flexible, essentiellement par le recours à des projets TICE. Dans le cadre de cette cotutelle, j'ai bénéficié d'une bourse Lavoisier du Ministère des Affaires Etrangères et Européennes qui a permis le financement de voyages répétés.

À Lyon, je remercie tout le monde au R6. Le R6, c'est un peu comme le Nord, il vous rend triste deux fois, à l'arrivée, et au départ. J'epère que le cahier de citations continue de se remplir pour les visites à venir. Un grand merci, et une pensée particulière, à Dominique Barbe pour l'impression de multiple documents d'enseignement et de recherche. J'espère que ses soucis de santé ne seront bientôt plus qu'un mauvais souvenir. En Australie, je garde un excellent souvenir des camps de terrain, notamment dans les Pilbaras, où je compte bien retourner un jour. L'accueil australien a été très chaleureux, ce qui n'est pas étranger au fait que Sydney constitue la prochaine étape de mon parcours.

Merci à ma famille, qui a su s'adapter aux visites sporadiques et aux appels à des heures décalées. Embrasser deux cultures est un cadeau merveilleux, mais qui s'avère parfois difficile. Les mots me manquent pour remercier ma moitié, Kylie, qui m'a suivi à l'autre bout du monde, et qui m'a soutenu (plus encore que d'habitude) pendant la rédaction de mon manuscrit. Non seulement m'aide-t-elle à définir le cap, mais elle rend aussi le voyage facile et très agréable.

Avant-propos

L'évolution à long terme du niveau marin reste mal comprise, bien que les théories de l'expansion des fonds océaniques et de la tectonique des plaques aient été établies il y a plus de cinquante ans. La principale difficulté du problème de l'évolution séculaire du niveau marin réside dans la quasi-impossibilité d'appliquer les méthodes de la stratigraphie séquentielle aux formations précambriennes, du fait de de la qualité décroissante de l'enregistrement géologique pour les ères les plus anciennes. Il est donc nécessaire de développer des théories et des modèles, et de les confronter aux données géologiques et géochimiques disponibles. Une autre difficulté vient de l'approche uniformitariste de la plupart des études publiées sur le sujet à ce jour, dans lesquelles le niveau marin est supposé constant depuis le début de la tectonique des plaques sur Terre, possiblement vers la fin de l'Archéen.

À l'échelle de l'histoire de la Terre, le niveau marin est principalement contrôlé par l'évolution thermique du manteau et par la croissance des continents. Pour que le niveau marin reste constant, il faut qu'il y ait un équilibre entre refroidissement du manteau et croissance continentale. Dans cette thèse, nous explorons les conséquences d'un manteau plus chaud et d'un moindre volume de croûte continentale pour le niveau marin archéen. Dans la première partie, nous proposons un modèle physique pour estimer le niveau marin et la quantité de terres émergées pour des conditions archéennes plausibles. Dans la deuxième partie, nous nous concentrons sur l'éruption sous-marine de provinces magmatiques effusives mises en place sur de la croûte continentale, phénomène fréquent à l'Archéen mais rare par la suite. Nous abordons ce problème en combinant modèles numériques et données géologiques de terrain à l'échelle régionale. Dans la troisième partie, nous présentons un modèle intégré, qui permet d'explorer les effets de scenarii de croissance continentale contrastés sur l'évolution du niveau marin et de la quantité de terres émergées. La dernière partie aborde les conséquences de changements du niveau marin et de la surface de terres émergées pour l'évolution de l'atmosphère et de la vie primitive.

L'un des objectifs de cette étude est d'établir les liens entre l'évolution de la Terre solide et de ses enveloppes externes. La principale difficulté est l'évaluation des hypothèses, notamment en ce qui concerne l'évolution du volume des océans et des continents, qui sont restent largement inconnues et débattues. Des observations géologiques et géochimiques de premier ordre permettent toutefois de valider les résultats de nos modèles.

Résumé en français

Les océans s'approfondissent au cours des temps géologiques du fait du refroidissement à long terme du manteau terrestre. En parallèle, le refroidissement de la lithosphère continentale se traduit par une augmentation des altitudes qu'elle peut supporter. La combinaison de ces deux effets implique une augmentation de la surface de terres emergées au cours du temps. Cette émergence progressive des continents modifie l'importance des processus d'altération et d'érosion des silicates et influe donc sur la composition de l'atmosphère et des océans, avec des conséquences importantes pour le climat et pour la vie.

Parmi les objectifs de ce travail figurent l'estimation du niveau marin et de la surface de terres émergées à l'Archéen, ainsi que leur évolution respective. Ceci permet de faire le lien entre l'évolution des enveloppes internes et externes de la Terre du fait de changement dans l'efficacité des processus d'érosion des silicates.

Le **chapitre 1** a pour but de poser le problème, en proposant un tour d'horizon des connaissances, mais aussi des incertitudes, relatives à l'enregistrement géologique archéen : ses caractéristiques, sa représentativité, ainsi que les messages de la pétrologie et de la géochimie quant à l'évolution de la température du manteau et du volume total de croûte continentale. Les changements géologiques de premier ordre observés vers la transition Archéen/Protérozoïque sont également présentés.

Dans le **chapitre 2**, nous proposons un modèle physique qui permet d'évaluer la surface de terres émergées en fonction de la température du manteau, de la fraction de croûte continentale existante et de la distribution de l'altitude des continents (hypsométrie). A l'Archéen, le manteau terrestre était probablement environ 200°C plus chaud qu'aujourd'hui, et la surface totale de continents était de 20% à 80% de la surface continentale actuelle. Des températures mantelliques élevées engendrent des changements bathymétriques et isostatiques qui imposent une hausse du niveau marin, en partie compensée par la moindre surface de continents. Des modèles numériques suggèrent que la surface de terres émergées était au maximum de 15% de la surface terrestre à la fin de l'Archéen, résultat cohérent avec de nombreuses observations géologiques et géochimiques. Ces résultats ont été publiés dans la revue *Earth and Planteray Science Letters*. S'ensuit une réflexion complémentaire, postérieure à la publication de ces travaux, qui explore plus avant les effets sur le niveau marin et la surface de terres émergées a) de changements de densité et d'épaisseur de la croûte océanique ; b) de changements d'épaisseur de la croûte continentale; c) de changement de la profondeur des rides, en lien avec l'évolution du volume des océans; et d) de le la formation d'un supercontinent.

Dans le **chapitre 3**, afin d'estimer le refroidissement à long terme de la croûte continentale, nous présentons une étude des séries volcano-sédimentaires de la province magmatique du Fortescue (2775-2630 Ma) dans le craton des Pilbaras, en Australie Occidentale. Des observations structurales et sédimentologiques indiquent un dépôt de type flexural de ces séries et permettent d'évaluer le temps nécessaire à la relaxation de l'anomalie topographique qu'elles constituent. Des modèles numériques du comportement thermo-mécanique d'une lithosphère continentale indiquent que pour rendre compte des données géologiques, la température au

Moho devait être supérieure à 580°C lors de la mise en place du Groupe Fortescue. Des données de flux de chaleur disponibles pour les Pilbaras permettent d'estimer que la croûte continentale y a refroidi d'environ 200°C depuis 2,7 Ga. Une partie de ces travaux à été soumise à la revue *Geology*. S'ensuit une réflexion complémentaire sur l'environnement de dépôt des carbonates affleurant dans le Groupe Fortescue. Le caractère lacustre ou marin de la Formation Tumbiana est particulièrement sujet à débat. Nos données géochimiques et observations sédimentologiques pour cette formation sont favorables à un environnement de dépôt marin.

Dans le **chapitre 4**, chapitre de synthèse, nous proposons d'évaluer les effets de la croissance continentale sur l'évolution de la température du manteau, du niveau marin, de la surface de terres émergées et de la composition isotopique en strontium des océans. Pour se faire, nous avons développé un modèle fondé sur un modèle d'évolution thermique publié qui dépend de la croissance continentale. Un modèle géochimique, couplé au modèle thermique, permet d'évaluer l'évolution du $^{87}Sr/^{86}Sr$ dans les océans en fonction de la croissance continentale et de la surface émergée. La comparaison de scenarii de croissance continentale contrastés montre que la surface calculée de terres émergées, de moins de 5% de la surface de la Terre à l'Archéen, dépend peu de la croissance continentale. Cette estimation est moindre que précédemment car la croissance continentale impose des températures du manteau élevées. Ces modèles permettent également de réconcilier les données sur l'évolution du $^{87}Sr/^{86}Sr$ des carbonates marins avec une croissance continentale précoce en tenant compte de la surface réduite de terres emergées et de l'altitude moins élevée des continents à l'Archéen. Ce chapitre servira de base à l'élaboration d'un manuscrit.

Enfin, dans le **chapitre 5**, nous discutons qualitativement les effets de l'approfondissement séculaire des rides océaniques et de l'augmentation séculaire de la surface de terres émergées prédits par nos modèles sur la composition des océans et de l'atmosphère, ainsi que sur l'évolution de la vie primitive. L'approfondissement des rides océaniques pourrait expliquer l'évolution observée du $\delta^{18}O$ des carbonates marins. Des rides moins profondes à l'Archéen auraient aussi diminué la quantité de dioxyde de carbone piégé dans la crôute océanique, augmentant ainsi la concentration en carbone dans l'océan et dans l'atmosphére. Ceci aurait pu contribuer à un climat chaud à l'Archéen. Quant à l'émergence des continents, elle aurait engendré une augmentation de l'apport de phosphate, concentré dans les continents, à l'océan. Or le phosphate est un nutriment essentiel à la biosphère. L'émergence des continents aurait donc permis une augmentation de la biomasse, et de l'activité de cyanobactéries photosynthétiques. L'augmentation de l'activité de ces micro-organismes aurait pu contribuer à l'oxydation de l'atmosphère survenue il y a environ 2,4 Ga.

Les résultats de nos modèles sur l'évolution du $^{87}Sr/^{86}Sr$ des carbonates marins, ainsi que les discussions qualitatives du **chapitre 5**, montrent que les effets d'une surface réduite de terres émergées, d'altitudes continentales moins élevées et de rides océaniques moins profondes doivent être pris en compte dans les futures modélisations du climat et de la composition des océans et de l'atmosphère archéens.

1

From the Archaean to the Phanerozoic

Contents

1.1 Our Archaean heritage

1.1.1 The Archaean eon

The Archaean spans one and a half billion years of the Earth's history from 4.0 Ga to 2.5 Ga, which makes it the second longest eon. Together with the Hadaean (4.57 Ga to 4.0 Ga), it represents nearly half of Earth's history (Fig. 1.1). The unique characteristics of modern Earth (the presence of water in its three phases - liquid, solid and gas - and the operation of plate tectonics that shape the surface of the Earth and recycle continental crust into the mantle) have their roots in these eons. Studies of the Hadaean and Archaean Earth aim to understand the evolution of our planet, but also try to define criteria in the quest to identify Earth-like exoplanets in the early stages of their evolution. Archaean terranes are also studied for economical purposes, since many are diamondiferous and/or rich in mineral resources.

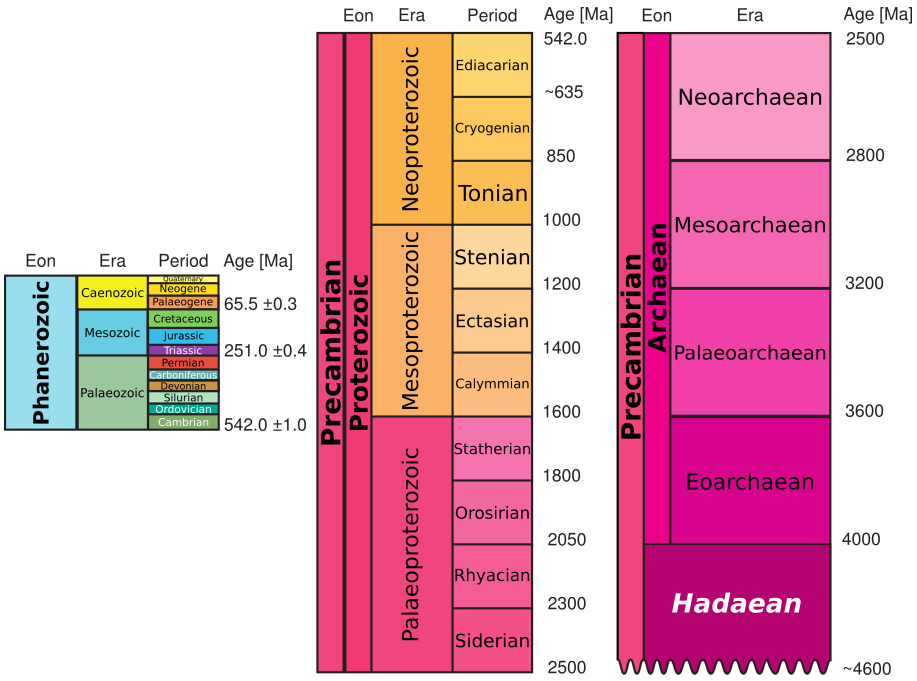

Figure 1.1: International stratigraphic chart plotted to scale to show the relative time span of the different eras. Modified from the chart of the International Commission on Stratigraphy available at http://www.stratigraphy.org/upload/ISChart2009.pdf.

Throughout over half a century of research, high quality geological, geochemical and geochronological data have accumulated on Precambrian ($\geq$ 542 Ma) terranes. Despite these data, global geochronology remains poorly defined in the Precambrian compared to the Phanerozoic ($\leq$ 542 Ma) stratigraphy that is established with a resolution of the order of five million years. The Phanerozoic stratigraphy is notably defined by the presence or absence of hard-shelled fossils. Such fossils are absent from the Precambrian record. Indeed, the end of the Precambrian is marked by the appearance of such fossils in the geological record. Moreover, older terranes

generally represent a smaller area of the surface of the Earth, and have longer been exposed to subsequent geological processes. This often results in complex structures and poor stratal preservation of sediments and is reflected by the time resolution of the global Precambrian geological record.

Because of these difficulties inherent to the Archaean geological record, many important questions are still shrouded in mystery regarding the Archaean Earth: How much hotter was the Archaean mantle? When did plate tectonics begin on Earth? When was the bulk of the continental crust formed? What was the volume of the Archaean oceans? What was the composition of the Archaean atmosphere? Was it oxidant or reducing? When did life appear? These questions can be summed up as follows: when, how, and why did Earth acquire its present unique characteristics that are liquid water, an oxygen-rich atmosphere, plate tectonics and life?

1.1.2 A quick overview of the Archaean rock record

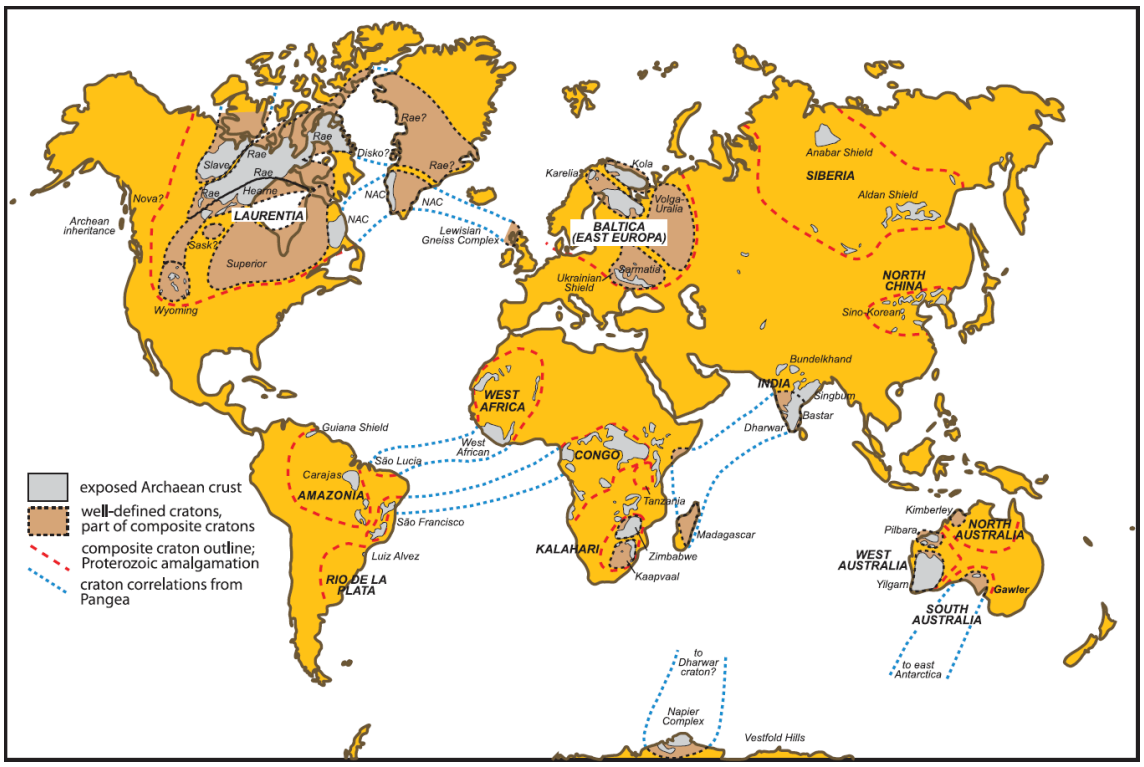

Figure 1.2: Global distribution of Archaean cratons. In grey: exposed Archaean crust; in brown: definable fragments of composite cratons (Bleeker, 2003); black dotted lined: approximate outline of composite cratons; red dashed lines: estimated extent of Archaean segments amalgamated during the Proterozoic; blue dotted lines: correlations between Archaean cratons inferred from the break-up of Pangea (Bleeker, 2003). This figure is from Pearson and Wittig (2008).

Archaean rocks are preserved in approximately 35 fragments of continental lithosphere called cratons (Fig. 1.2; Bleeker, 2003). A useful estimate by Artemieva (2006), based on the thermal age of the lithosphere, suggests that cratons of age between 3.6 and 2.95 Ga account for 11.2%

of the total area of emerged continental lithosphere and cratons of age between 2.95 and 2.5 Ga account for 5.9% of this area. These areas add up to 17.1% of emerged land or 4.7% of the Earth's surface, compared to around 18% of the Earth's surface covered by emerged Phanerozoic continental lithosphere (Artemieva, 2006).

Archaean cratons and Phanerozoic continental lithosphere differ by their density, their thickness, their surface heat flow and the thickness of their continental crust. The continental root of Archaean cratons, given here as the thickness of the thermal boundary layer that roughly corresponds to the 1300°C isotherm, ranges between 170 and 350 km compared to 60-140 km for the thickness of Phanerozoic continental lithosphere (Artemieva, 2009). The average density of Archaean cratons (3310 ± 16 kg m^{-3}) is significantly lower than that of Phanerozoic continental lithosphere (3365 ± 20 kg m^{-3} Artemieva, 2009). The surface heat flow of Archaean terranes (20-50 mW m^{-2}) is lower than that of Phanerozoic terranes (50-120 mW m^{-2}). Finally, Archaean continental crust is slightly thinner than average (Durrheim and Mooney, 1994). The present-day thickness of Archaean continental crust ranges between 32 and 50 km, compared to a range of 25 to 70 km for Phanerozoic continental crust, depending on the tectonic context (Artemieva, 2009).

Artemieva (2009) further separated Archaean continental lithosphere into two groups: one group composed of the Western Australian, Indian, South African and South American cratons with lithospheric roots 170-250 km thick and continental crust 32-40 km thick, and relatively high surface heat flow (40-50 mW m^{-2}); and the other group including the Siberian, Baltic, Canadian and West African cratons that display thicker lithospheric roots (250-350 km) and continental crust (40-50 km), and relatively low surface heat flow (20-45 mW m^{-2}). The necessity to separate Archaean cratons into at least two groups based on their lithospheric characteristics suggests that all cratons might not have been formed by one single universal process.

The typical Archaean lithological association consists of the so-called "granite-greenstone". Archaean granitoids are calcium-rich and sodium-rich and belong to the tonalite-trondhjemite-granodiorite (TTG) series that are the result of partial melting of eclogite facies basaltic crust (Barker and Arth, 1976). As for greenstone belts, these consist of an association of preponderant mafic to ultramafic volcanic rocks with felsic volcanic rocks and sedimentary rocks. Because of their mafic composition, greenstone belts have been proposed to be remnants of Archaean oceanic crust (*e.g.* Kusky and Kidd, 1992). However, a review by Bickle et al. (1994) of greenstone belts previously identified as ophiolites concluded that Archaean greenstone belts are not oceanic crust. Of importance to the conclusion of Bickle et al. (1994) are the contamination of mafic rocks by continental crust and the intrusive relationship of greenstone belts with older basement. This makes greenstone belts autochtonous terranes, and not allochtonous terranes as proposed, for example, by Kusky and Kidd (1992) for the Belingwe greenstone belt. Since then, no ophiolites older than ∼ 1 Ga have been identified in the geological record (Condie and Kröner, 2008). Claims for the oldest (3.8 Ga) ophiolite in the Isua greenstone belt, Greenland (Furnes et al., 2007) have been rejected since zircon geochronology shows that the units of this putative

ophiolite (gabbro, sheeted dike complex and pillow lavas) are not coeval but could differ in age by up to 100 Myr, and because the polarity of pillow basalts is reversed to that expected for an ophiolite (Nutman and Clark, 2007). Until an ophiolite is clearly identified in the Archaean record, greenstone belts cannot be considered as remnants of oceanic crust.

1.2 Secular cooling of the solid Earth

1.2.1 Petrological evidence for a hotter Archaean mantle

Mafic volcanics contained in greenstone belts are nevertheless central to the study of Archaean geology. Evidence for a hotter mantle in the Archaean comes from the occurrence of ultramafic volcanic rocks (wt.% MgO $>$ 18) that were first identified in the Komati Formation in the Barberton greenstone belt, South Africa and were thus named komatiites (Viljoen and Viljoen, 1969). Based on a compilation of geological maps and stratigraphic sections, Condie (1993) estimated that komatiites represent $\sim$ 15 % of rocks in terranes older than 3.5 Ga, $\sim$ 6 % in terranes between 3.5 Ga and 2.5 Ga, and less than 1% in post-Archaean terranes (including the well-studied example of Cretaceous komatiite lava flows from the Gorgona Island, *e.g.* Nisbet et al., 1993). The relatively low abundance of komatiites suggests that they could have erupted in restricted environments such as mantle plumes or subduction zones.

Experimental investigation under high pressure and high temperature of komatiites from the Komati Formation revealed that the water content of these rocks was very low ($<$ 0.2 wt.% H_2O), which in turn implied that their eruption temperature was of 1650 $\pm$ 20°C at atmospheric pressure (Green et al., 1975). This eruption temperature translates into an extraction temperature of the magma up to $\sim$ 1900°C for a depth of $\sim$ 200 km (pressure of 6 GPa; Nisbet et al., 1993). Because such temperatures probably reflect a maximum temperature in mantle plume settings and because mantle plumes are $\sim$ 300°C hotter than the surrounding mantle, this implies that the potential temperature of the upper Archaean mantle was of up to $\sim$ 1600°C (Nisbet et al., 1993). This temperature estimate is significantly higher than the present-day temperature of the upper mantle of about 1300°C. However, some authors have suggested that komatiites are not as dry as initially proposed (Parman et al., 1997), but contain up to 3 wt.% H_2O. This has led to a second model, in which komatiites are formed in subduction environments. In this model, the Archaean mantle would only be $\sim$ 100°C hotter than present (Grove and Parman, 2004). The latest argument regarding the water content of komatiites is based on the determination of the oxidation state of iron in Barberton komatiites (Berry et al., 2008), and pleads in favour of anhydrous melting. Regardless of the water content of komatiites, the decline in their relative abundance in the rock record through geological time reflects the secular cooling of the mantle.

Another line of evidence used to constrain the temperature of the mantle through time is the study of the petrology and geochemistry of mid-oceanic ridge basalts (MORBs) and hotspot-type MORBs through time. Abbott et al. (1994) identified MORB-like rocks from their rare earth element (REE) pattern. They then calculated the eruption temperature of these suites

from their chemical composition and converted the results to potential mantle temperature. The range of mantle temperatures described by MORBs at any given time is $\sim 200°C$, reflecting the compositional range of the suites. The results of Abbott et al. (1994) suggest that the mantle was 137-187°C hotter than present 2.8 Ga ago (see Fig. 1.4). The limiting factors of this result are that Archaean greenstone belts represent hotspot-type MORBs rather than normal MORBs, and that Archaean ultramafic rocks (komatiites and komatiitic basalts) have been studied more than normal Archaean basalts because they fascinate petrologists and are at the centre of a scientific debate. Both of these sampling biases tend to shift the Archaean temperature estimates of Abbott et al. (1994) toward higher values.

Finally, Coltice et al. (2009b) used available xenon isotope data to constrain the thermal history. There are three main xenon isotopic systems for which the parent nuclide present very different time lives of 15.7 Ma, 82 Ma and 4.45 Ga. The measurement of xenon anomalies thus allow for the investigation of magma differentiation and degassing at very different time scales. Coltice et al. (2009b) concluded that to be consistent with the xenon isotope data, the upper mantle must have cooled by $\sim 200°C$ during the Hadaean and by 100 to 250°C since 4 Ga. Overall, petrological and geochemical data constrain the range of temperature for the Archaean mantle to between 100 and 300°C hotter than present.

1.2.2 Thermal evolution models

Higher temperatures in the Archaean mantle are also expected from a theoretical point of view since the radiogenic heat production of uranium, thorium and potassium decay with time and must have been higher in the past (Wasserburg et al, 1964; Bickle, 1978). Fig. 1.3 shows the variation of radiogenic heat production through time. Heat production was double at 2.7 Ga and triple at 3.7 Ga. The evolution of the temperature of the mantle depends on the balance between heat production and heat loss for the Earth. At present, the total heat loss of the Earth to space of about 44 TW (Pollack et al, 1993) is greater than the radiogenic heat production of the bulk silicate Earth (mantle and continental crust) of about 30 TW (see Tab. 1.1). While in details other heat sources have to be considered to explain the secular cooling of the Earth (see Jaupart et al., 2007, for a recent review), it is mainly controlled by this imbalance between heat loss and heat production.

Because the process governing heat transport in the Earth is solid-state mantle convection that ultimately drives seafloor spreading and plate tectonics, thermal evolution models are based on parametrised convection models using the scaling law

$$Nu \propto Ra^{\beta},$$

where Nu is the Nusselt number, which is the ratio of convective to conductive heat flow, and Ra is the Rayleigh number, which is a measure of the convective potential on a fluid system. The exponent β determines the sensitivity of surface heat flux with respect to the vigour of convection.

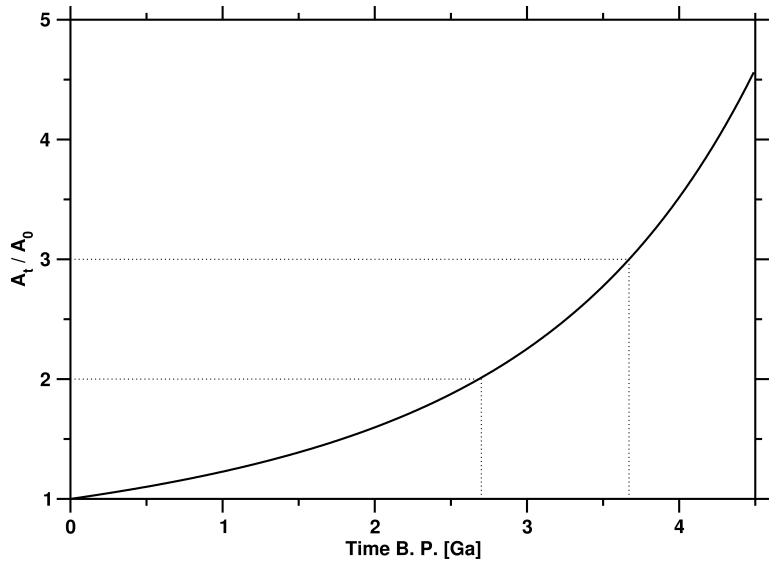

Figure 1.3: Variation in crustal heat production through time using the rates of heat release of heat producing elements given in Turcotte and Schubert (2002). See also Mareschal and Jaupart (2006).

Experimental and numerical studies show that the value of β is between 1/4 and 1/3 for thermal convection (see Christensen, 1985, for a review). Davies (1980) and Christensen (1985) pointed out that parametrised convection models using classical parameters predict a runaway increase of mantle temperatures going back in time (also referred to as "thermal catastrophe"). Because this is not consistent with the petrological constraints presented in the previous section, Christensen (1985) concluded that the coupling between heat loss by convection and mantle temperature must be weak and that β must be lower than 0.05 for the Earth. However, the models of Christensen (1985) are valid for a stagnant-lid Earth. A corollary conclusion of his results is therefore that the Earth cannot be approximated by a stagnant-lid thermal convecting system, as indicated by the operation of plate tectonics.

Table 1.1: Concentration of heat producing elements in the bulk silicate Earth, and in the average present-day and Archaean continental crust. Heat productions are calculated using rates of heat release for each element from Turcotte and Schubert (2002). The mass of the continental crust is taken as 2.6×10^{22} kg.

	K_2O (wt.%)	Th (ppm)	U (ppm)	A (pW kg^{-1})	H (TW)
Bulk Silicate Earth [a]	0.024	0.079	0.020	4.7	28.3
Average continental crust [b]	1.88	5.6	1.42	341	8.9
Archaean continental crust [b]	1.2	3	0.7	189	-

[a] From McDonough and Sun (1995)
[b] From Rudnick and Fountain (1995)

Two thermal evolution models that predict a weak coupling between heat loss by convection and mantle temperature, and that are consistent with petrological constraints were recently published (Fig. 1.4; Korenaga, 2006; Labrosse and Jaupart, 2007). The model of Korenaga (2006)

is built on a classical parametrised model but takes small-scale convection and the delayed subduction of a thick, buoyant oceanic lithosphere predicted for a hotter mantle (see section 1.3.1) into account. Both of these effects decrease the sensitivity of mantle temperature with respect to convective heat loss. As for the model of Labrosse and Jaupart (2007), it is empirical, based on the present-day age distribution of the oceanic floor. These models will be further discussed and their results will be used in section 2.2.

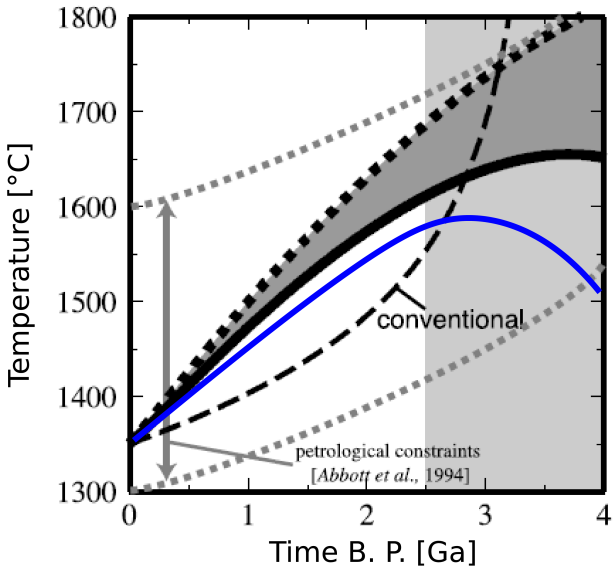

Figure 1.4: Proposed thermal evolution models that are consistent with petrological constraints from (Abbott et al., 1994). The conventional parametrised model results in a runaway increase of temperature going back in time. Thick black and thick black dotted curves are from Korenaga (2006) for different radiogenic heat productions of the silicate Earth. The blue curve is from Labrosse and Jaupart (2007) for a pulse in crustal growth at 2.7 Ga. Figure modified from Korenaga (2006).

Thermal evolution models are valid for solid state convection and cannot be used to predict mantle temperatures for which the mantle would melt, resulting in the formation of a magma ocean (Labrosse and Jaupart, 2007). Because of a lower viscosity, the convection of a magma ocean would be more vigorous and heat loss would occur on a shorter time scale (Solomatov, 2000). Based on a review of phase diagrams of mantle minerals determined experimentally, Jaupart et al. (2007) concluded that the upper mantle temperature threshold for the establishment of solid-state convection is 200 ± 100 K hotter than present. Taking the uppermost limit, the temperature of the upper Archaean mantle must have been at most 300 K hotter than present for solid-state convection to occur.

1.2.3 Geological evidence for a hot Archaean continental crust

The heat-producing elements uranium, thorium and potassium are incompatible (they concentrate in the melt phase during partial melting of the mantle) and are thus concentrated in the continental crust (Tab. 1.1). In Phanerozoic continental crust, a characteristic superficial layer

($\sim$ 5 km) enriched in heat-producing elements compared to the bulk of the continental crust is observed. However, this is not true of all Archaean continental crusts in which radiogenic elements are possibly distributed homogeneously, resulting in higher temperatures at the base of the crust (Mareschal and Jaupart, 2006). Finally, the crustal heat production of an average Archaean continental crust would have been of 380 pW kg^{-1} at 2.7 Ga, and of 570 pW kg^{-1} at 3.7 Ga (Tab. 1.1 and Fig. 1.3). Archaean continental crust thus is expected to have been hotter than present-day continental crust because of a higher radiogenic heat production and because of a more homogeneous distribution of heat producing elements.

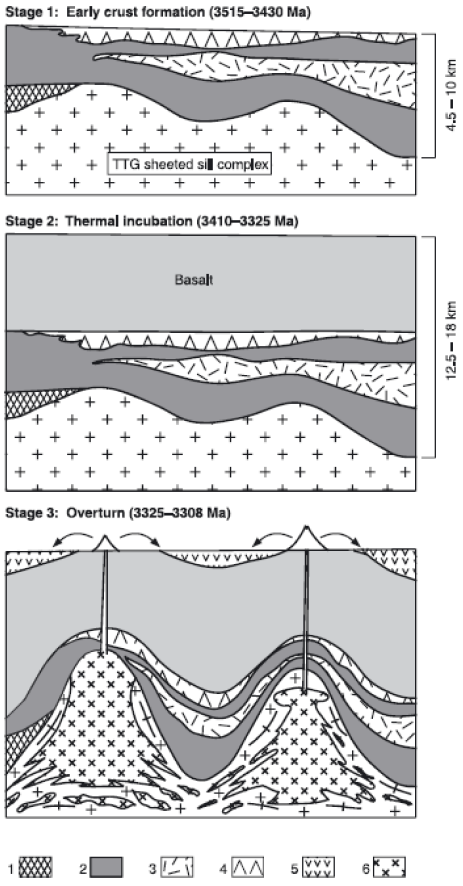

Figure 1.5: Schematic diagrams showing the three initial stages of crustal diapirism in the East Pilbara terrane. 1), 3), 4) and 5) felsic volcanics; 2) basalt; 6) granite melts from older TTG. Figure from Van Kranendonk et al. (2007).

Some Archaean crustal structures point to hot Archaean continental crust. One feature of Archaean continental crust that is not observed in the post-Archaean is crustal diapirism (Fig 1.5). Crustal diapirs are formed by a process that was called "sagduction" by Goodwin and Smith (1980). In this process, a thick pile of basalts, accumulated on top of continental crust (such as a continental flood basalt), acts as a thermal insulator so that the temperature rises in the continental crust (West and Mareschal, 1979; Rey et al., 2003). This results in the partial melting of the lower crust and in the rise of hot, light granitic material (TTGs, stage

3 of Fig. 1.5) and in the sinking of the denser basalts. The sagduction process can occur if the continental crust is ductile on geological time scale, which implies a relatively low viscosity (Mareschal and West, 1980). The viscosity of crustal rocks is temperature-dependent and is often defined using

$$\eta = \eta_0 \exp(Q/RT)\,, \tag{1.1}$$

where η_0 is a reference viscosity (at surface temperature), Q is the activation enthalpy, R is the gas constant and T is the temperature. If follows from Eq. 1.1 that the viscosity decreases exponentially with temperature. Crustal diapirs preserved at ∼3.3 Ga in the East Pilbara Terrane (Collins et al., 1998; Van Kranendonk et al., 2004a), at ∼2.7 Ga in the Slave province (Bleeker, 2002) and in the Yilgarn Craton (Campbell and Hill, 1988), and at ∼3 Ga in the Dharwar Craton (Bouhallier et al., 1995) are thus evidence for elevated crustal temperatures. Further evidence for hot Archaean crust comes from seismic profiles of the Canadian Shield and of the Kaapvaal Craton that show a flat Moho (Mareschal and Jaupart, 2006, and references therein). This suggests the flow of ductile, low viscosity, lower continental crust on geological time scales (Mareschal and Jaupart, 2006). Following the same reasoning as above, this is again evidence for a hot Archaean continental crust.

There are two solutions to explain the observation of ductile continental crust in the Archaean. The first solution consists is that crustal temperatures were overall elevated because of a higher radiogenic heat production (*e.g.* Mareschal and Jaupart, 2006). Alternatively, hot, ductile continental crust could occur in places where the continental crust is particularly thick, as is the case of present-day Tibet. England and Bickle (1984) proposed that the observation of high-grade metamorphic terrane reflected erosion following crustal thickening. On this basis, they suggested that the Archaean continental geotherms were similar to present-day ones and that elevated mountain belts existed in the Archaean. However, as we shall discuss in later chapters, erosion following crustal thickening is not the only way to exhume high-grade metamorphic terrane. For instance, the process of sagduction results in the exhumation of high-grade metamorphic terranes in the absence of significant crustal thickening (*e.g.* McGregor, 1951).

1.3 A biased rock record?

1.3.1 When did plate tectonics begin on Earth?

The theory of plate tectonics is based on the movement of rigid plates at the surface of the Earth, as proposed by Wilson (1965). The drifting continents collide, aggregate in supercontinents and break-up. This triggers complex deformation over long distances such as the ∼ 2500 km-long Himalayan mountain belt. In contrast, oceanic processes are geometrically simpler, and essentially occur at mid-oceanic ridges and subduction zones. As a result, the theory of plate tectonics is particularly successful in explaining oceanic tectonics. The final piece of evidence

that validated the theory of plate tectonics, the identification of magnetic anomalies in the ocean floor, was not discovered until the 1960's because it was not readily accessible (Vine, 1966). Because there is no Archaean oceanic rock record, Earth scientists studying the Archaean face the same problem as the pioneers of the theory of plate tectonics: they only have access to the piece of the puzzle (the continents) that is harder to decipher. Identifying Archaean continental tectonic processes is also difficult because the record of original events is often modified by subsequent events. Nevertheless, it is worth noting that the absence of oceanic crust from the Archaean rock record suggests that an active process existed that recycled oceanic crust. However, this process does not necessarily have to be similar to present-day seafloor spreading.

With petrological evidence for a hotter mantle, and thermal evolution models suggesting a hotter mantle back in geological time, Archaean plate tectonics models flourished in the late 1970's and early 1980's. Bickle (1978) suggested that a greater heat loss in the Archaean would likely be accommodated by faster generation and recycling of oceanic crust. Sleep and Windley (1982) pointed out that a hotter mantle would result in a greater degree of partial melting beneath mid-oceanic ridges and thus in the formation of thicker oceanic crust. Hoffman and Ranalli (1988) suggested that the lower part of such a thick oceanic lithosphere would be ductile and thus prone to delamination. Arndt (1983), on the contrary, suggested that the oceanic crust would mostly differ with present-day oceanic crust by its komatiitic composition rather than by its thickness. His model was, however, based on the strong assumption that modern-like plate tectonics were operating in the Archaean. Abbott and Hoffman (1984) pointed out that hotter, younger oceanic lithosphere would be more buoyant and likely recycled in flat subduction settings. In this respect, it is worth noting that young lithosphere subducts on modern Earth, and that the flat subduction zones observed at present do not primarily correlate with the age of the subducting lithosphere but with the subduction of oceanic plateaus (Gutscher et al., 2000). It thus seems that the thickness and the buoyancy of subducting lithosphere prevails over its age in determining the geometry of the subduction zone. It is important to note that all of the models mentioned above are oceanic tectonic models that are theoretical and difficult to test.

When interpreted as representative of Archaean deformation processes, the preservation of crustal diapiric structures (Fig 1.5) has led to the conclusion that heat loss by the Archaean Earth was due to voluminous magmatism and that plate tectonics were not operating in the Archaean (*e.g.* Hamilton, 1998). In sharp contrast, some authors rejected the "vertical tectonic" model for the formation of crustal diapirs and proposed to accommodate it in the framework of modern plate tectonics (*e.g.* De Wit, 1998). While crustal diapirism does not preclude the operation of plate tectonics, it implies that two contrasting styles of crustal deformation (horizontal and vertical) existed during the Archaean (Condie and Benn, 2006). This can be seen as a warning that uncritical uniformitarianism should be avoided when addressing the problem of Archaean plate tectonics. While it is important to look for similarities between Archaean processes and Phanerozoic processes drawn by plate tectonics (*e.g.* Condie and Kröner, 2008), it is equally important to assess the differences between Archaean and Phanerozoic processes (Bleeker, 2002).

Differences are to be expected because in the Archaean, the mantle and continental crust were hotter than in the Phanerozoic.

In their literature review on the age of first appearance and widespread distribution of petrotectonic assemblages such as ophiolites, forearc basins, passive margins and continental rifts, and on other indicators such as geochemical data and paleomagnetism, Condie and Kröner (2008) concluded that modern-*like* plate tectonics started at around 3 Ga and were widespread by 2.7 Ga. These estimates are likely to change as the amount of high precision data available on Archaean terranes data grows. It is also important to remember that much of the data used in this review was obtained with the aim of identifying processes that *resemble* plate tectonics, which is probably the main bias in answering the question.

1.3.2 Are cratons representative of the Archaean?

We have seen in previous sections that with no oceanic crust preserved, the Archaean rock record *is* biased. The thick and depleted lithospheric roots of all of the preserved Archaean cratons suggest another possible bias: it is possible that the cratons that developed a root and where thus stabilised (a process sometimes referred to as *cratonisation*) were the exception rather than the rule in the Archaean. Evidence for the roots of Archaean cratons comes from the occurrence of diamonds brought to the surface from underneath all cratons (Fig. 1.6). However, this does not constrain the age of cratonic roots. The oldest dated diamonds are $>$ 4.2 Ga microdiamond inclusions from the Jack Hills zircons (Menneken et al., 2007), but further support is needed to conclude that these diamonds were formed in thick continental roots. Placer diamonds (that occur in sedimentary deposits) from the $\sim$ 2.75 Hardey Formation of the Fortescue Group, Pilbara Craton, Australia and from the $\sim$ 2.7 Ga Witwatersrand basin, Kaapvaal Craton (Konstantinovskii, 2003) are necessarily of Archaean age. There is also good evidence from Re-Os isotopic dating that the age of the cratonic roots is Archaean and that some cratonic roots have been preserved for around 3 Gyr (Carlson et al., 2005). Finally, the recent identification of negative ^{142}Nd anomalies (formed within 400 Myr of the formation of the Earth) in $\sim$ 1.48 Ga-old mantle-derived rocks from the Bastar Craton, India (Upadhyay et al, 2009) suggests that these rocks were preserved in the lithospheric mantle from $\sim$ 4.2 Ga until $\sim$ 1.5 Ga. It thus seems that Archaean continental crust and underlying cratonic roots are of Archaean age.

The question of whether Archaean cratons are representative of the Archaean thus depends on the universality of the process resulting in the formation of continental roots. Three models have been proposed to explain the formation of the thick, cold cratonic keels composed of melt-depleted peridotitic mantle (Fig. 1.7): a) a single plume model (Boyd, 1989); b) stacking and accretion of oceanic lithosphere (Helmstaedt and Schulze, 1989); c) accretion and thickening of sub-arc lithospheric mantle (Jordan, 1988). Lee (2006) argued that the plume model was unlikely because the pressures at which cratonic peridotites melted ($\lesssim$ 4 GPa) are lower than expected in a plume setting ($\geq$ 7 GPa). Unfortunately, the geochemical distinction between the two remaining subduction-related processes is not obvious (Lee, 2006). Arndt et al. (2009)

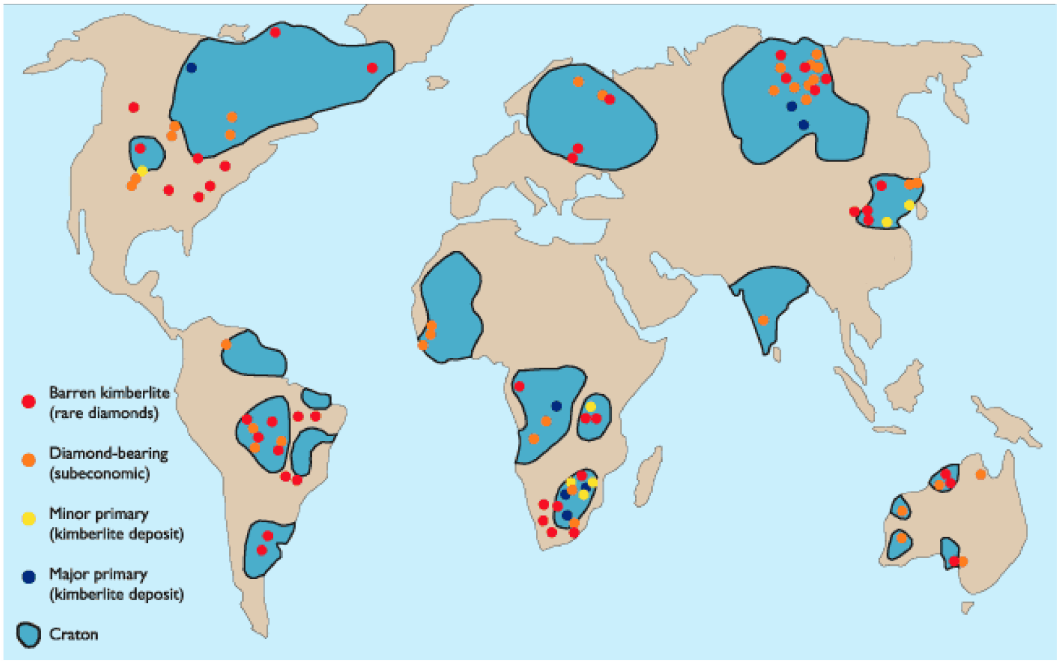

Figure 1.6: Distribution of kimberlites worldwide. Modified from http://www.geus.dk/minex/minex-22-dk.htm.

pointed out that the melting process would most likely be polybaric and fractional in the plume model. They suggested that the pressure deduced by Lee (2006) from isobaric partial melting calculations represents the last stage of this polybaric fractional melting process and is thus not a valid argument against the plume model. On the basis of petrological modelling, Arndt et al. (2009) favoured the plume model. The model of stacking and accretion of oceanic lithosphere is seducing in that it explains the formation of diamonds: subducting oceanic lithosphere would provide the necessary carbonate-rich fluids (Pearson and Wittig, 2008; Stachel and Harris, 2008; Wyman et al., 2008). It is worth noting that the sub-arc lithospheric mantle of scenario c) would have been metasomatised and would likely contain the carbon and oxygen necessary for the formation of diamonds. One problem with scenario b) is that the dense eclogitic material material has to be lost to the mantle to allow the continental root to become neutrally buoyant (Pearson and Wittig, 2008). Gravity-driven processes could explain the recycling of eclogitic material into the asthenospheric mantle (Vlaar et al., 1994). However, numerical modelling by Arndt et al. (2009) showed that the eclogitic material would likely drag down the overlying layer of depleted harzburgite into the mantle and the root would thus fail to form. In scenarii a) and b), the cratonic root could be neutrally buoyant from the onset (Lee, 2006; Arndt et al., 2009).

If the plume model is correct (proto-) continental material that happened to be located above a plume was preferentially preserved. Alternatively, assuming that a form of plate tectonics was operating in the Archaean, and that subduction processes always resulted in stacking and accretion of oceanic crust or in thickening of sub-arc lithospheric mantle, the most likely scenarii of cratonic root formation imply that (proto-) continents presenting at least one convergent

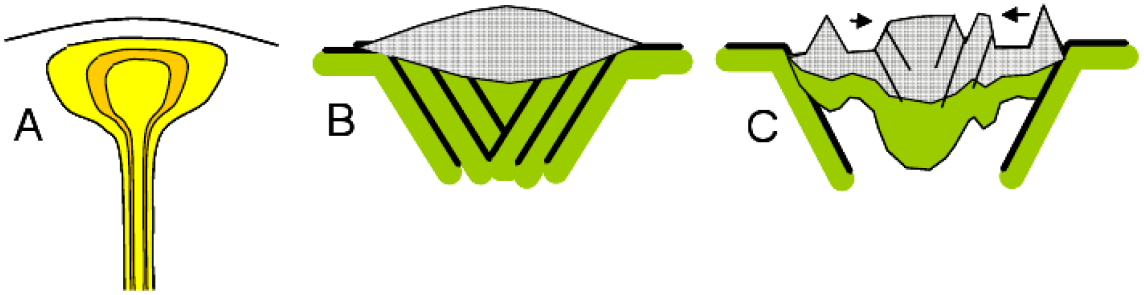

Figure 1.7: Three proposed scenarii to explain the formation of cratonic roots (vertical scale exaggerated). See text for details. From Lee (2006).

margin would have been preserved preferentially over (proto-) continents surrounded by passive margins which would not have developed a thick cratonic root and would have been recycled in the mantle. This is consistent with the absence of passive margins in the Archaean record until $\sim$ 2.7 Ga (Condie and Kröner, 2008). The absence of passive margins in the Archaean geological record is also predicted by numerical modelling. Hynes (2008) proposed that for a hotter mantle, the production of a large volume of melt would offset the thermal subsidence of a stretched continental margin and would thus limit the accommodation space for sediments.

The Archaean rock record is thus biased since it did not preserve oceanic material, and presumably did not preserve all continental material. Alternative models to plate tectonics that would result in crustal recycling include unstable stagnant lid similar to present-day Venus (Solomatov and Moresi, 1996) and "drip tectonics" in which the buoyant oceanic crust is decoupled from the underlying lithospheric mantle (Davies, 1993). In both of these models, dense eclogitised continental crust can sink back into the mantle. A limit to the unstable stagnant lid model based on a comparison between Venus and the Earth is that Venus is dry whereas the Earth is not. It is worth noting that some variety was preserved in the Archaean record, as indicated by differences in crustal and lithospheric thickness (Artemieva, 2009) and styles of continental tectonics (Condie and Benn, 2006).

1.3.3 An Archaean paradox: how to make hot continental crust on top of a cold cratonic root?

We have seen in the previous sections that there is evidence for both hot, flowing lower and middle continental crust and cool, strong continental lithosphere in the Archaean. This is a paradox that needs to be addressed when studying Archaean lithospheric deformation. One explanation is that the lithospheric geotherm (evolution of the temperature with depth) of cratons is not in steady-state but transient (Mareschal and Jaupart, 2006). In the process of lithospheric formation, the root is depleted in radiogenic elements compared to the overlying continental crust. Thus, the continental crust is hot because of a high heat production, and loses heat to the continental root. From their calculations of transient effects on lithospheric geotherms, Mareschal and Jaupart (2006) concluded that the time needed for crustal radiogenic

heat production to heat the cratonic root is 1 to 2 Ga depending on lithospheric thickness. Because radioactive decay is relevant on such time scales, the maximum temperature at the base of the lithosphere is 30% lower than when assuming a steady-state geotherm Mareschal and Jaupart (2006). This partly explains the thermal decoupling between the crust and the lithospheric mantle.

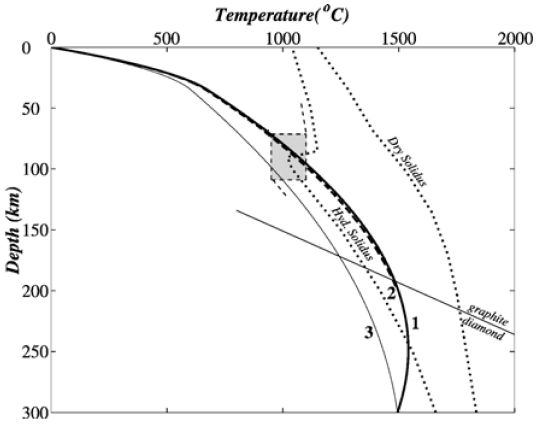

Figure 1.8: Example of turning lithospheric geotherm (curve labelled 1). This geotherm is obtained for a lithosphere 300 km thick, a rate of heat production in the lithospheric mantle of 0.04 μW m^{-3} and an age of 3 Ga. The transition curve from graphite to diamond (solid line), hydrous (0.2 wt.% water) and dry solidus for peridotite (dotted lines), and carbonatite melt field (shaded area) bounded by the carbonate solidus at low temperatures and amphibole breakdown at high temperature are also shown. This figure is from Michaut and Jaupart (2007).

Michaut and Jaupart (2007) showed from transient thermal modelling (over multi Ga timescale) that above a critical value of radiogenic heat production in the continental lithosphere, cratonic roots cool more rapidly than the surrounding mantle. This threshold value decreases with increasing lithospheric thickness. Above the threshold value, the loss of heat from the lithospheric root to the mantle results in "turning geotherms" with a negative temperature gradient at the base of the lithosphere (see Fig 1.8). This allows for hot continental crust ($T_{Moho} > 600$°C) and for the formation of diamonds at depth $\geq$ 200 km (Fig 1.8; Michaut and Jaupart, 2007). However, as they point out, a severe limitation of turning geotherms is that the middle part of the lithosphere would be characterised by high temperature and low viscosity (Eq. 1.1). The base of the lithosphere would thus tend to be delaminated and recycled into the mantle and the diamond-bearing part of the lithosphere would likely be lost in this process.

The thermal decoupling between Archaean continental crust and cratonic roots could thus be due to the repartition of radiogenic elements within the continental lithosphere and to the long time needed for the lithosphere to reach a thermal steady state.

1.4 Volume of continental crust and of oceans through time

The Archaean Earth might have differed from modern Earth by the amount of continental crust and of liquid water that were present at its surface.

1.4.1 When was the bulk of the continental crust formed?

Crustal growth is the difference between the production of new continental crust and the recycling of crustal material into the mantle. This problem of crustal growth has fascinated geologists over the years, and many crustal growth models have been proposed. The recent reviews of Rino et al. (2004) and of Harrison (2009) list 12 and 13 crustal growth models, respectively. These curves strongly differ from one another, and the estimate of crustal fraction at 3.8 Ga ranges from 0 to 1. The debate over the concept of crustal growth itself has sometimes been vigorous (Armstrong, 1991). In this section, several end-member crustal growth models are presented (Fig. 1.9) and the way they are estimated is discussed.

Delayed, slow growth models (Hurley and Rand, 1969; Taylor and McLennan, 1985, in Fig. 1.9) start after 4 Ga, which reflects the absence of a Hadaean rock record. Indeed, the Hadaean is defined as the period before the oldest known rock. At present, this limit is set by the 4.03 Ga orthogneisses from Acasta in the Slave Craton, Canada (Bowring and Williams, 1999).

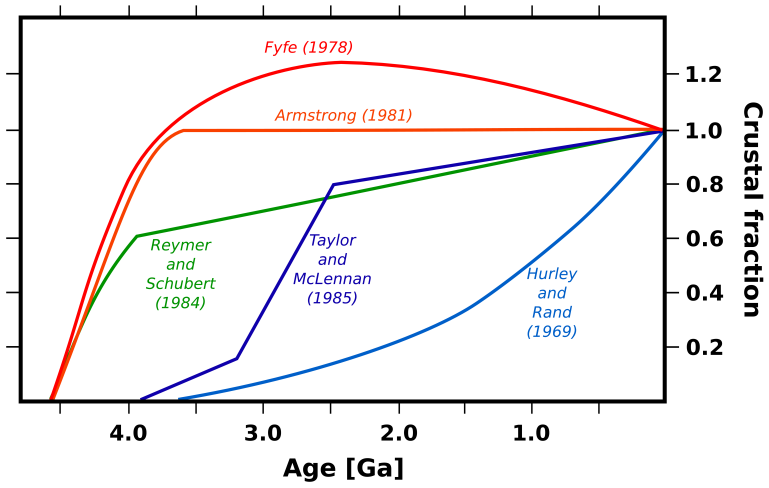

Figure 1.9: Five of the many crustal growth models proposed over the last forty years. Modified from Campbell (2003).

Models based on the age distribution of mineral and continents

Gastil (1960) pointed out that the age distribution of preserved mineral described peaks. Hurley and Rand (1969) extended this observation to the age and space distribution of continental crust and used their results to propose the first published crustal growth curve. In this approach,

only the preserved material is taken into account and there is no recycling into the mantle. For this reason, this "crustal growth curve" should rather be called a "crustal preservation curve". This curve provides a lower bound for crustal growth models, and subsequent curves produced using the same method resulted in a shift of the curve upward because of a larger dataset (Armstrong, 1991, and references therein). Many ages are have been determined using the U-Pb composition of zircons. On problem with these ages is that subsequent thermal events would favour chemical diffusion and could thus alter the U-Pb signal. Indeed, Kemp et al. (2006) showed in an integrated study of the U-Pb, oxygen and Lu-Hf isotope compositions of detrital zircons that there can be a significant discrepancy (of the order of a billion years) between the U-Pb crystallisation age an Hf model age of minerals. The oxygen isotope composition is characterised to ensure that the source of the detrital zircons did not contain any sedimentary component that would alter the Hf model age. Thus, crustal growth models based on the age distribution of minerals should be considered with caution. Furthermore, Gurnis and Davies (1986) showed that the age distribution of continents is an artifact due to preferential recycling of younger terranes.

Models based on the sedimentary record

The most consensual crustal growth model is probably that proposed by Taylor and McLennan (1985). This model is essentially based on changes in the geochemical composition of rare earth element pattern of fine-grained sedimentary rocks used as a proxy for the composition of the upper continental crust. Taylor and McLennan (1985) noticed that Archaean fine-grained sediments have a mafic composition whereas post-Archaean sediments are more differentiated. This led them to propose a crustal growth model that predicts a pulse in crustal growth at $\sim$ 2.7 Ga. However, the data on Archaean sediments used by Taylor and McLennan (1985) are biased toward greenstone-type environments, which partly explains their results (*e.g.* Condie, 1993). Regardless of this possible sampling bias, the link between the composition of fined-grained sediments and crustal growth, if any, is tame. Hawkesworth and Kemp (2006) recently proposed from the Hf model age of sedimentary and igneous zircons that it may take up to one billion year for newly produced continental crust to dominate the sedimentary record. Moreover, from the point of view of the secular evolution of sea level, it is also worth noting that only the emerged fraction of the continental crust is taken into account in this model. However, there is no reason why newly produced continental crust should emerge and be eroded instantaneously.

Models based on the freeboard argument

Reymer and Schubert (1984) estimated Phanerozoic crustal addition rates as the difference between addition by arc magmatism and subducting sediments at subduction zones. These estimates are based on the interpretation of seismic profiles and present large uncertainties. Reymer and Schubert (1984) concluded that the Phanerozoic crustal growth rate is about 1 km^3 a^{-1}.

However, their estimate of total substraction rate of about 1 km^3 a^{-1} is much lower than that of 1-3 km^3 a^{-1} proposed by Armstrong (1981). Because of the uncertainty in estimating addition and substraction rates, Reymer and Schubert (1984) give a second estimate of about 0.9 km^3 a^{-1} based on the argument of constant continental elevation of continents since the end of the Archaean (the "freeboard" argument of Wise, 1974). However, as we will discuss at length in later sections, numerical modelling and geological evidence do not support the constant freeboard hypothesis.

Steady-state model

Armstrong (1981) made the case for important sediment recycling at subduction zones and for a constant volume of continental crust through time. He stressed the uncertainty in estimating the rate of crustal production and recycling, and carried out geochemical calculations to show that the observed isotopic composition of Pb, Sr and Nd in the crust, mantle, sediments and sea water are compatible with a constant volume of continental crust through time. Based on low estimates of crustal addition rates and relatively elevated rates of subducting sediments, Fyfe (1978) concluded that the amount of continental crust is currently decreasing. His estimate constitutes the upper end-member of proposed crustal growth curves.

The accumulation of high precision isotopic evidence for an early silicate differentiation of the Earth over the last decade has renewed the interest in steady-state models (see Harrison, 2009, for a recent review). Positive ^{142}Nd anomalies in rocks from the 3.8 Ga Isua greenstone belt in West Greenland (Boyet et al., 2003; Caro et al., 2003) and the hafnium isotopic composition of zircons older than 4 Ga from Jack Hills, Yilgarn Craton, Western Australia (Blichert-Toft and Albarède, 2008) both point to an early extraction of continental material. They imply that continental growth had started by $\sim$ 4.3 Ga. It should be noted that Nd and Hf isotopic anomalies in Archaean rocks have been reported since the 1980's (*e.g.* Patchett et al., 1981) but have been traditionally accommodated in the preferred delayed continental growth model as deplored by Armstrong (1991).

Armstrong (1991) stressed that there is no need for continental growth on a plate tectonics Earth. As we saw in section 1.3.1, it is not clear whether plate tectonics were widespread before 2.7 Ga. Moreover, Rudnick (1995) pointed out that the bulk andesitic composition of the continental crust is not compatible with the current main process of crustal addition in which the protolith of the continental crust is basaltic. Possible mechanisms to make andesitic continental crust in the Archaean include hot subduction, accretion of oceanic plateaus and intraplate crustal growth by reworking of proto-continental crust as shown by Fig 1.5 (Rudnick, 1995; Albarède, 1998b). Crustal addition and recycling processes were therefore probably different in the Archaean compared to the present, which makes quantitative estimates of past crustal volumes difficult.

1.4.2 What was the volume of the Archaean oceans?

Despite being called the blue planet, the Earth is not a water-rich body: the mass of the oceans ($\sim 1.5 \times 10^{24}$ g) translates into only 0.025 wt.% H_2O over the whole Earth (5.97×10^{27} g). The amount of water stored in the mantle is largely undetermined but probably adds up to a few oceans worth, which means that the bulk water content of the Earth is $< 0.2\%$ (Marty and Yokochi, 2006). This water-content is low compared to that of carbonaceous chondrites (10 wt.% H_2O) and of comets (50 wt.% H_2O) (Marty and Yokochi, 2006, and references therein). This is readily explained by the fact that the Earth was formed in a volatile-poor part of the solar nebula. It is estimated that around 90% of its water is probably of extraterrestrial origin (Marty and Yokochi, 2006) and was acquired during an event that is called the "late veneer". Marty and Yokochi (2006) concluded from their review of isotopic constraints for the provenance of Earth's water that asteroids were the primary contributors to this late veneer, with comets and interplanetary dust playing a minor role.

Even though early Earth possibly contained as little as 10% of its total present-day water, the oceans possibly accumulated quickly at the surface of the Earth. The $\delta^{18}O$ signature of Hadaean zircons from Jack Hills, Yilgarn Craton, Western Australia was interpreted by Mojzsis et al. (2001) and by Wilde et al. (2001) as indicating the presence of clay minerals in their source. Because the only known processes to form clay minerals involve liquid water, this piece of evidence has been interpreted as reflecting the presence of liquid water at or near the Earth's surface by ~ 4.3 Ga. There is also evidence for deep-water environments in Archaean greenstone belts: sedimentary structures of the ~ 3.46 Ga Marble bar chert and Chinaman Pool chert in the Pilbara Craton point to a deep-water environment (Dromart et al., 2008). A water depth greater than 1000 m is also inferred from volcanic textures and sedimentary facies for the depositional setting of the 3.235 Ga Sulphur Springs volcanogenic massive sulphide (Vearncombe et al., 1995). More direct evidence for early oceans comes from the occurrence of pillow basalts in the 3.8 Ga Isua greenstone belt, Southwest Greenland (Fig.1.10). In this last case, it is difficult to estimate the deposition depth.

In the lack of strong constraints regarding the total amount of water stored in the mantle, it is difficult to estimate past oceanic volume. The volume of Archaean oceans could have been smaller than present, which implies that water would have accumulated at the Earth's surface from the degassing mantle and from extraterrestrial sources. Alternatively, the volume of Archaean oceans could have been greater than present, which implies that water would have been recycled into the mantle at subduction zone over Earth's history. The hypothesis of a constant volume of ocean since ~ 3.8 Ga is often made, based on the evidence listed above.

1.5 Late-Archaean changes at the Earth's surface

Cooling of the solid Earth, probable changes in the volume of continental crust, and possible changes in the volume of ocean would have had important consequences on the Earth's external

Figure 1.10: Metric scale pillow lavas in the 3.8 Ga Isua greenstone belt, Southwest Greenland. Pillow lavas indicate the eruption and fast cooling of mafic lavas in a subaqueous setting. (Photo: M. Boyet)

envelopes. The first likely consequence is a change in sea level. Several first order geological observations indicate differences in sea level and in environment between the Archaean and the Phanerozoic. Subaqueous flood volcanism on top of continental crust is widespread in the Precambrian but rare to absent in the Phanerozoic (Arndt, 1999). A recent compilation by Kump and Barley (2007) shows that only $\sim$ 20% of Archaean large igneous provinces (LIPs) and continental flood basalts (CFBs) are subaerial, compared to $\sim$ 80% in the post-Archaean. All post-Archaean CFBs are subaerial. This suggests higher sea levels in the Archaean. On the other hand, there is evidence for emerged continents in the Archaean. The oldest unconformity was reported in the Pilbara Craton, where subaqueous 3.46 Ga basalts were deposited at an angle on an erosional surface in felsic volcanics (Buick et al., 1995). Clastic sediments are also observed in Archaean cratons (Nisbet, 1987), but grain-size statistics on detrital zircons in quartzite samples from the Slave Province suggests that Archaean clastic sediments are of more localised provenance than Phanerozoic clastic sediments (Sircombe et al., 2001). Lowe (1994) also noted that limited sediments were supplied to continental margins in the early Archaean. This suggests that the area of emerged land was reduced in the Archaean compared to the Phanerozoic. Continental margins would also have differed. Eriksson and Fedo (1994) reported an increase in the amount of stable-shelf sediments throughout the Archaean. The first giant carbonate platform occurs in the 2.9 Ga Steep Rock Group, Superior Province (Wilks and Nisbet, 1985) and Eriksson et al. (2005) noted an enlargement of epereic seas around the Archaean-Proterozoic boundary. This suggests a change in sea level linked to continental stabilisation throughout the Archaean.

Large, stable continental shelves and carbonate platforms are particularly important since they are associated with the occurrence of stromatolites formed by photosynthetical micro-

organisms (Buick, 1992; Lepot et al., 2008). The enlargement of stable shelves would have favoured the spreading of such photosynthetical micro-organism, and the burial of reduced carbon. Both of these processes could have contributed to the possible accumulation of oxygen in the atmosphere from around 2.3 Ga, an event referred to as the Great Oxidation Event (*e.g.* Holland, 1999). The increase in emerged land area suggested by more widespread subaerial flood volcanism in the post-Archaean would also have resulted in enhanced weathering and erosion processes. This would in turn have had an impact on the composition of the atmosphere regulated by weathering processes and on the composition of the oceans due to an increased input of continental material (Rey and Coltice, 2008).

Problematic and outline

Archaean cratons are a characterised by thick, depleted lithospheric roots and low surface heat flow. The Archaean rock record is probably biased, because the continental material under which such lithospheric roots were formed was preferentially preserved, and because no Archaean oceanic material has been preserved in ophiolites. Despite this sampling bias, it can be inferred from the petrological and geochemical data that the Archaean mantle was 200 ± 100°C than present. Because of a higher radiogenic heat production, the continental crust was also hotter in the Archaean, and gravity played a more important role in crustal dynamics than in the Phanerozoic. This is notably indicated by the preservation of crustal diapirs that are unique to the Archaean. Because of these higher temperatures, plate tectonics differed from present-day. It is not clear whether plate tectonics were operating at all before ∼ 3 Ga.

The volume of continental crust and of oceans are poorly constrained through time. In the Archaean, the volume of continental crust was possibly reduced compared to present, but estimates largely differ between crustal growth models. It is possible that the oceans accumulated relatively quickly (by ∼ 3.8 Ga) at the Earth's surface. Subaqueous flood volcanism was common in the Archaean whereas it is absent in the Phanerozoic. This suggests higher sea levels in the Archaean.

As the mantle and the continental crust cooled down, plate tectonics and crustal deformation became more similar to present-day ones. Features of modern-like plate tectonics are more widespread in the geological record from ∼ 2.7 Ga. Towards the Archaean/Proterozoic boundary, subaerial continental flood basalts and large epereic seas on stable continental shelves became more common, and the atmosphere became oxidant.

The present contribution focuses on the impact of the secular cooling of the solid Earth on the evolution of its exogenic envelopes. In a first chapter, we will consider the consequences of higher mantle temperatures and of a reduced continental area on sea level and on the area of emerged land. To this end, we developed numerical isostatic models. The results of this work suggest that the area of emerged land was less than 15% in the Archaean, compared to 27.5% today. In a second chapter, we will discuss the consequences of a hotter continental crust on sea level. Thermal-mechanical models suggest that lower crustal flow was an efficient process maintaining Archaean continental flood basalts below sea level. Confronted to our modelling results, field observations from the Fortescue Group in the Pilbara Craton suggest that the continental crust has cooled by approximately 200°C over the last 2.7 billion years. In a last chapter, we will couple thermal evolution models to crustal growth curves to investigate the impact of the timing of crustal growth on mantle temperature and on the area of emerged land. These models show that early crustal growth model do not account for geological observations that suggests some land was emerged in the Archaean. They also reconcile early crustal growth models with the evolution of the composition of the oceans in radiogenic strontium constrained by marine carbonates.

2

Consequences of the secular cooling of the Earth for the emergence of the continents

Contents

2.1 Sea level change and the area of emerged land

The area of emerged land depends on sea level and on the distribution of continental elevations as a function of continental area that is given by the continental hypsometric curve. Due to the occurrence of plate tectonics, the Earth displays a unique hypsometric curve that consists of a continental domain and an oceanic domain (Fig. 2.1). A change in the area of emerged land can thus be due to a change in sea level, to a change in the continental part of the hypsometric curve, or both.

Sea level change is an actual topic in a context of global warming (be it anthropogenic or not) and sea level rise. The predictions of the Intergovernmental Panel on Climate Change (IPCC) for the next century are of between 0.2 and 0.6 m (Intergovernmental Panel on Climate Change, 2007). This sea level rise is at the centre of the political and economical debate because it would imply the flooding of coastal areas on which many large cities are built. Fig. 2.1 shows that small changes in sea level trigger flooding of large areas because of the gentle slope described by the continents between 200 m and -200 m.

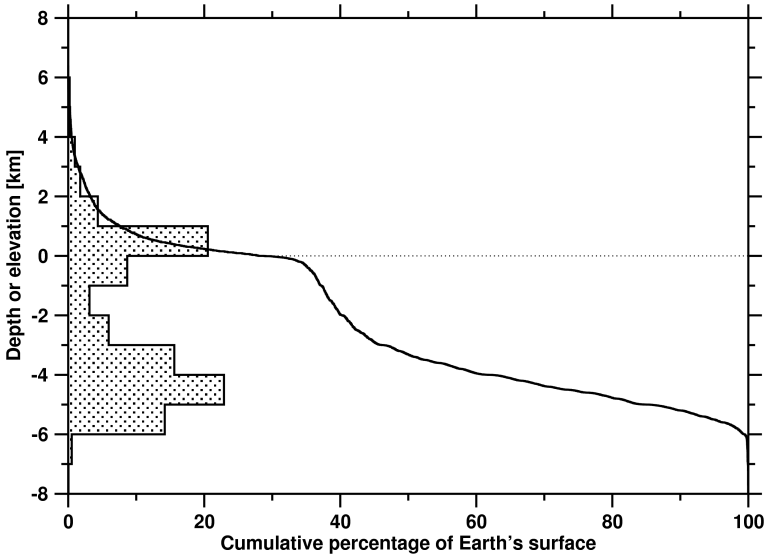

Figure 2.1: Hypsometry of the Earth compiled from eTOPO2 data (NOAA, 2006). The histogram illustrates the bimodal distribution of elevations on Earth with a peak at $\sim$ 500 m for the continents and a peak at $\sim$ -4500 m for the oceans.

Despite being a serious concern for humanity, the present sea level rise is small compared to sea level change on geological time scales. An estimation of Phanerozoic sea level change and flooded continental area are presented in Fig. 2.2. These curves show variations in sea level of $\sim$ 350 m and variations in the flooded area of continents of up to 40×10^6 km^2 (8% of the Earth's surface). The difference of more than two orders of magnitudes between sea level change at human scale and sea level change on a geological time scale is due to the fact that several mechanisms affect sea level at different amplitudes and over different time periods (Tab. 2.1, and Fig. 2.3). When studying sea level change, it is thus necessary to consider mechanisms of

relevant time scale and amplitude. For instance, if thermal expansion of seawater and melting continental ice sheets are relevant to global warming (Fig. 2.3), they describe high-order cycles that are not relevant to the study of secular[1] sea level change.

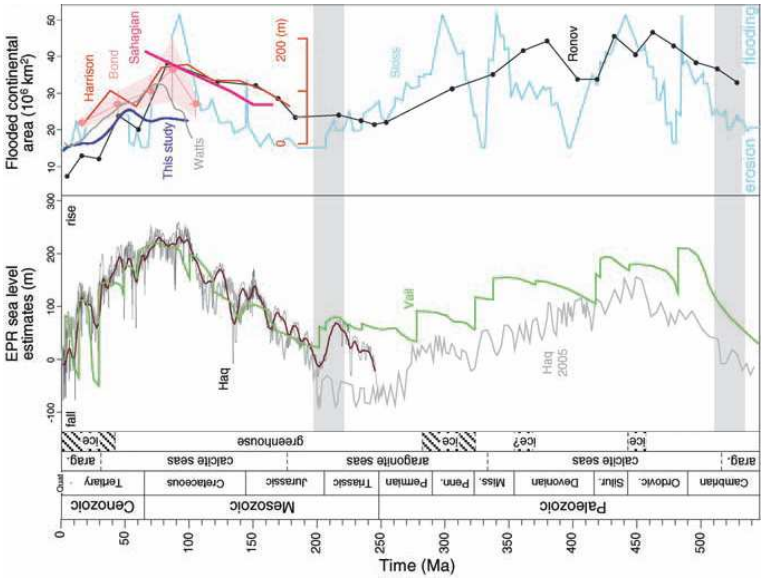

Figure 2.2: Estimates of Phanerozoic sea level change and flooded continental area. EPR stands for Exxon Production Research. From Miller et al. (2005) - see therein for references.

In sea level change studies, a distinction must also be made between absolute (*eustatic*) sea level change, with reference to a fixed datum such as the centre of the Earth, and *relative* sea level change, with reference to a moving point at the surface of the Earth (see Eriksson, 1999, for a recent review). The production of global eustatic curves such as shown in Fig. 2.2 is based on the interpolation of relative sea level change from different study areas using the methods of sequence stratigraphy (Vail et al., 1977). These methods consist in identifying unconformity bound sedimentary units at different scales (also called orders) and explain these units in terms of sea relative sea level change and sedimentary supply, as a function of geological time. Because of abundant sedimentological and geochronological data, and because of the interest of fossil fuel industries, Phanerozoic sea level changes of time scale as short as 0.1-0.5 Myr can be identified (Eriksson, 1999). Geochronology is facilitated by the occurrence of hard shelled fossils in the Phanerozoic. Fossils are used to define biostratigraphic stages that can be calibrated in time where absolute geochronological data are available. However, there are virtually no hard shelled fossils in the Precambrian, which results in a poorly defined stratigraphy. Stratal preservation is also often poorer in the Precambrian record. For these reasons, and because of more erratic tectonic controls on the formation of Precambrian basins, the principles of sequence stratigraphy cannot be applied directly to Precambrian terranes (Catuneanu et al., 2005). This in turn impedes global studies of Precambrian sea level change based on the sedimentary record. In a

[1] "*Secular*" is taken herein in the geological sense and refers to a long-term evolution over millions of years rather than centuries.

study of relative sea level change on several cratons, Eriksson et al. (2007) nevertheless identified the effect of a global glaciation event between 2.4 Ga and 2.2 Ga and of two superplume events at 2.7 Ga and 2.2 Ga on global sea level.

Table 2.1: Amplitude, rate and time period of mechanisms responsible for sea level change (modified after Eriksson, 1999).

Mechanism	Maximum size (m)	Average rate (mm ky^{-1})	Time period (Ma)
Oceanic crustal thickness	2800	0.5 [a]	1000
Crustal growth	2000	0.3-2.6 [b]	100-1000 [b]
Local tectonism	1000	10 000	<10
Mid-ocean ridges (secular) [c]	240-1000	0.06-0.4 [a] [c]	1000
Mid-ocean ridges (pulse)	350	7.5	70
Glacioisostacy	250	10 000	<0.1
Geoid relief	250	5000	<0.1
Hot-spot seafloor movements	100	Very slow	100
Intraplate stress	100	10-100	10
Orogeny	10-70	1.0	70
Sedimentation onto seafloor	60	1.1	70
Tsunamis and landslides	27	Instantaneous	Hours
Flooding/desiccation, small basin	15	Instantaneous	<0.013

[a] Assuming a secular cooling of the mantle of 50 K Ga^{-1}.
[b] The rate and time period of crustal growth depend on crustal growth models.
[c] The amplitude and rate of the effect of seafloor spreading depends on thermal evolution models.

Mechanisms such as glaciations and superplumes are however transient and thus not relevant to the study of the *secular* evolution of sea level. The only mechanisms relevant to the study of the secular evolution of eustatic sea level are global mechanisms of large amplitude ($>$ 50 m) occurring over time scales longer than 50 Myr. From Tab. 2.1, and Fig. 2.3, this leaves only six known mechanisms: changes in the thickness of the oceanic crust, in the area of continents (crustal growth), in the activity of mid-oceanic ridges (seafloor spreading), hot-spot seafloor movement, continental orogeny, and sedimentation onto the seafloor. Three of these six mechanisms (thickness of the oceanic crust, seafloor spreading, hot spots) are directly related to the temperature of the mantle. The secular evolution of sea level is thus closely related to the thermal evolution of the Earth.

Changes in the activity of mid-oceanic ridges have long been identified as a potential mechanism for sea level change: based on tectonic reconstructions of the volume of mid-oceanic ridges between 110 and 10 Ma, Hays and Pitman (1973) attributed Cretaceous high sea level to a pulse in the activity of mid-oceanic ridges. However, Cogné and Humler (2004) argued from the measurement of remaining oceanic surfaces and isochron maps that spreading rates at mid-oceanic ridges have been constant over the last 180 Ma. They suggest that a change in mantle temperature rather than a change in seafloor spreading rate could explained the observed Cretaceous sea level high. Assuming that the effect of mid-oceanic ridges controls the evolution of sea level, Turcotte and Burke (1978) used the observed Phanerozoic sea level change to estimate the evolution of the heat flux from the mantle. They suggested that high sea level reflect high

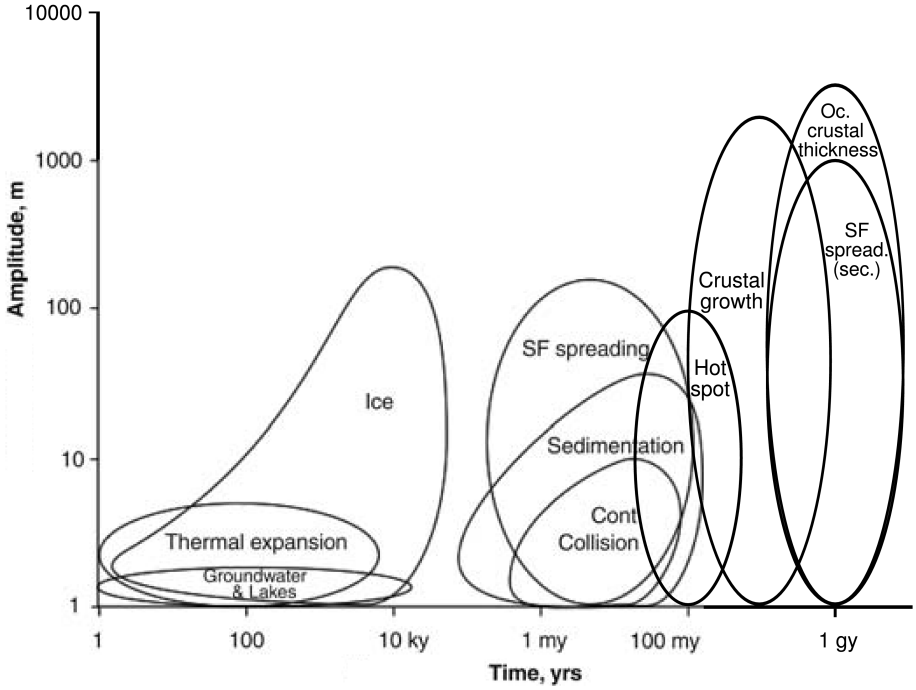

Figure 2.3: Amplitude of sea level change mechanisms as a function of time period (modified after Miller et al., 2005).

heat flow at mid-oceanic ridges and that in periods of high sea level, the ridge contribution to total surface heat flow can be of up to 50%. The way that changes in heat flux affect seafloor bathymetry can be explained as follows. New oceanic crust and lithosphere are produced at the mid-oceanic ridge, and the oceanic lithosphere gets cooler and thus denser as it spreads away from the ridge. In an isostatic model in which the mid-oceanic ridge is the reference, the seafloor gets deeper away from the ridge (Fig. 2.4). Faster seafloor spreading for a higher heat flux (or a hotter mantle) results in the subduction of younger oceanic lithosphere and thus in a less pronounced bathymetry (Fig. 2.4). Ultimately, this translates into higher sea levels for a hotter mantle. The effect on sea level of a pulse in mid-oceanic ridge activity, over a time scale of approximately 70 Myr, and of a secular change in seafloor bathymetry, over a time scale of approximately 1 Gyr, are separated in Tab. 2.1 and in Fig. 2.3. The secular change is of greater amplitude (1000 m compared to 350 m) because of greater changes in heat flux.

Fig. 2.4 also illustrates that the amplitude of the effect of seafloor spreading on sea level depends on the thermal model adopted: the change in bathymetry is four times more important for a conventional parametrised convection model compared to an empirical thermal evolution model assuming a triangular age distribution of ocean floor (Labrosse and Jaupart, 2007). Because the effect of seafloor spreading depends on the rate of seafloor spreading, it is also different in a model predicting sluggish plate tectonics for a hotter mantle (Korenaga, 2006) compared to conventional parametrised models (Fig. 2.5). In the model of Korenaga (2006), the oceanic bathymetry is more pronounced in the Archaean because of slower spreading rates, which results

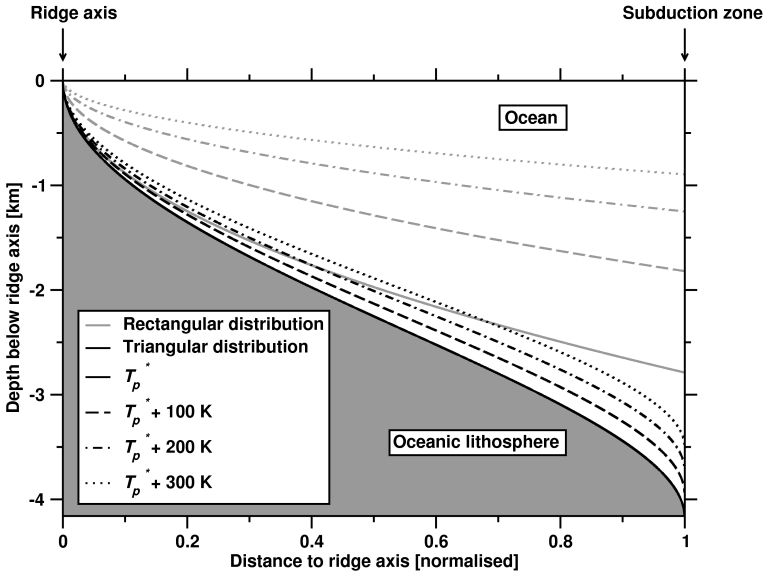

Figure 2.4: Effect of a change in mantle temperature on oceanic bathymetry calculated in a half-space cooling model. Results are shown for a triangular distribution of subduction age and for a rectangular distribution (see Labrosse and Jaupart, 2007, for details on the age distribution of seafloor).

in a lower sea level in the Archaean. Because of such differences, it is important to compare the secular evolution of sea level predicted by different thermal evolution models.

Galer (1991) pointed out that a thicker Archaean oceanic crust because of higher mantle temperature would trigger important changes in eustatic sea level. Indeed, this is potentially the largest effect to consider when studying secular sea level change (Tab. 2.1 and Fig. 2.3). As for sea level change related to crustal growth, its amplitude is similar regardless of the crustal growth model: redistributing the volume of oceans over the whole Earth would result in a change in sea level of up to 2000 m. However, there is no consensual crustal growth curve to date (see Fig. 1.9), and the rate of sea level change due to crustal growth depends on the adopted model (Tab. 2.1).

The presence of hot spots below the ocean floor results in an uplift of the ocean floor, and thus in a decrease of the volume of the oceanic reservoir. This translates into higher sea level. It is worth noting that hot spots can also occur below continents. In this case, they trigger an uplift of the continent and a high relative sea level, as in the case of present-day Africa. Sea level change associated to hot spot seafloor movement occurs on a timescale ten times shorter (100 Myr compared to 1 Gyr) and with an amplitude ten times smaller (100 m compared to between 1000 and 3000 m) than that of the mechanisms mentioned above. Hot spot seafloor movement is thus a second order mechanism when studying the secular evolution of sea level. If anything, a hotter Archaean mantle would have resulted in more frequent hot spots, possibly affecting larger areas. One notable example is that of the superplume event at 2.7 Ga that is recorded over all Archaean cratons. However, in the lack of Archaean oceanic crust, oceanic hot spots cannot readily be identified. One possibility is that oceanic hot spots would have resulted

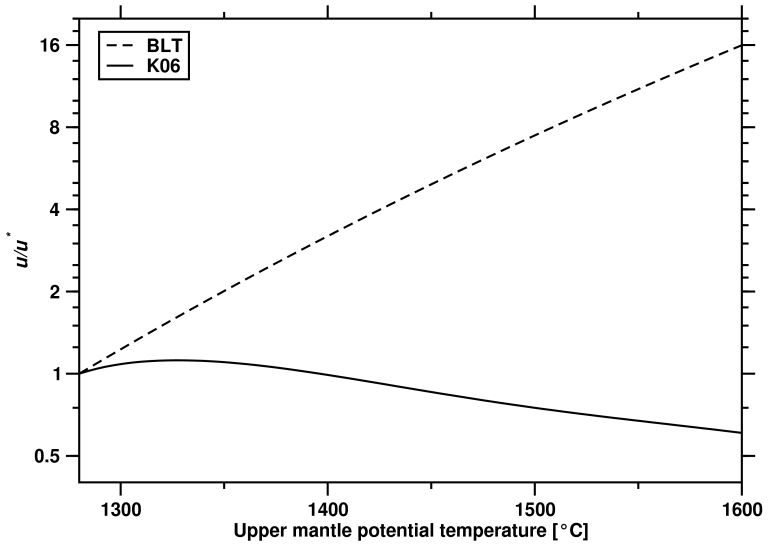

Figure 2.5: Oceanic spreading rate normalised to present day as a function of mantle temperature predicted by a conventional parametrised thermal evolution model (BLT) and by the model of Korenaga (2006) (K06).

in the formation of buoyant oceanic plateaus that were later reworked into continental crust by magmatic processes (Rudnick, 1995; Albarède, 1998b, see also section 1.4.1). Hot spot seafloor movement is not taken into account in the present study because this second-order effect is hard to reconstruct for distant geological time.

The next mechanism to consider is sedimentation onto the seafloor. The maximum amplitude of this mechanism ($\sim$ 60 m) is between 4 and 50 times lower, and its time scale between 10 and 1000 times shorter than that of crustal growth, secular seafloor spreading and oceanic crustal thickness. Moreover, a sedimentary load is compensated by subsidence in the long term, which further decreases the amplitude of sea level change it triggers. The possible increase of sedimentary input to the oceans with increasing crustal fraction could be of interest to the modellisation of the secular evolution of sea level. This would result in lower sea level back in geological time. However, Precambrian sedimentation rates are poorly constrained, and they depend on weathering and erosion rates with complex climatic feedback. The effect of sedimentation onto the seafloor is thus not taken into account in the present study. The opposing effect of hot spot seafloor movement that occurs on a longer timescale and a greater amplitude, and is also neglected here, could cancel out the effect of sedimentation onto the seafloor.

The amplitude of change in sea level due to continental orogeny is also relatively low (< 70 m), and orogenies occur over a timescale of the order of 70 Ma (Tab. 2.1). On a plate tectonics Earth, orogenies are not transient despite their short timescale. They are dynamically necessary in the theory of plate tectonics that are a continuous process. The effect of a secular change in mountain building due to the strengthening of the lithosphere as it cools down (Rey and Houseman, 2006) can readily be incorporated in the hypsometric curve. While a change in the hypsometric curve does not significantly affect sea level, its effect on the area of emerged land

is important (Fig. 2.1) and is thus relevant to the present study.

Most, if not all, studies of the secular evolution of sea level are based on the hypothesis of a constant freeboard through time since the end of the Archaean. This assumption is based on the observation that eustatic sea level has remained within $\sim$ 200 m of its present value throughout the Phanerozoic (Fig. 2.2) and that plate tectonics were operating by 2.5 Ga. For constant freeboard to be maintained over time, there must be a balance between crustal growth and secular cooling. This would be coincidental since two mechanisms of thermal origin, a thicker oceanic crust and a less pronounced oceanic bathymetry, can counter-balance crustal growth (Fig. 2.3). Furthermore, the observation of common submarine flood volcanism in the Precambrian as opposed to the Phanerozoic (Arndt, 1999) points to higher sea level in the Precambrian. This is not in agreement with the hypothesis of a constant freeboard through time. For this reason, we do not make the assumption of a constant freeboard in the modelling study presented in the next section. The main questions motivating this study are: Under which conditions can freeboard be constant? What was the area of emerged land in the Archaean? What is the effect of thermal evolution models on the predicted evolution of sea level? Did the geological record preserve any evidence of the secular evolution of sea level and of the area of emerged land?

2.2 A case for late-Archaean continental emergence

Foreword

We saw in the previous section that in the long-term, the evolution of sea level is mainly controlled by the temperature of the mantle and by the total area of continental crust. In the following article, we build an isostatic freeboard model (*e.g.* Galer, 1991) to investigate the effect of a hotter mantle and of a reduced continental area on sea level. We make the assumption of a constant oceanic volume and of a constant thickness of the continental crust, and we carry out a Monte Carlo analysis to assess the sensitivity of our models to these two parameters.

In order to evaluate the area of emerged land, we incorporate the continental hypsometric curve to the models, which is the main novel aspect of this study. Because of the shape of the continental hypsometric curve, taken from Harrison et al. (1981), solving for the emerged area of continents involves the evaluation of the Gauss hypergeometric function ${}_2F_1$. We evaluate this function numerically. We also investigate the effect of a lower maximum continental elevation as suggested by thin sheet modelling of hot continental lithospheres in convergent regime (Rey and Coltice, 2008).

Modelling results are presented for a range of mantle temperatures and crustal fraction since both probably varied during the Archaean. They suggest that in the Archaean, the area of emerged land was reduced by half compared to the present. This result is consistent with many first order geological and geochemical observations.

The following is an article entitled *A case for late-Archaean continental emergence from thermal evolution models and hypsometry* by Nicolas Flament, Nicolas Coltice and Patrice Rey (2008) published in *Earth and Planetary Science Letters* 275, p. 326-336.

Abstract

The secular cooling of the Earth's mantle and the growth of the continental crust together imply changes in the isostatic balance between continents and oceans, in the oceanic bathymetry and in the area of emerged continental crust. The evolution of these variables is of fundamental importance to the geochemical coupling of mantle, continental crust, atmosphere and ocean. To explore this further, we developed a model that evaluates the area of emerged continental crust as a function of mantle temperature, continental area and hypsometry.
In this paper, we investigate the continental freeboard predicted using different models for the cooling of the Earth. We show that constancy of the continental freeboard (± 200m) is possible throughout the history of the planet as long as the potential temperature of the upper mantle was never more than 110-210°C hotter than present. Such numbers imply either a very limited cooling of the planet or, most likely, a change in continental freeboard since the Archaean. During the Archaean, a greater radiogenic crustal heat production and a greater mantle heat flow would have reduced the strength of the continental lithosphere, thus limiting crustal thickening due to mountain building processes and the maximum elevation in the Earth's topography [Rey, P. F., Coltice, N., Neoarchean strengthening of the lithosphere and the coupling of the Earth's geochemical reservoirs, Geology 36, 635-638 (2008)]. Taking this into account, we show that the continents were mostly flooded until the end of the Archaean and that only 2-3% of the Earth's area consisted of emerged continental crust by around 2.5 Ga. These results are consistent with widespread Archaean submarine continental flood basalts, and with the appearance and strengthening of the geochemical fingerprint of felsic sources in the sedimentary record from $\sim$ 2.5 Ga. The progressive emergence of the continents as shown by our models from the late-Archaean onward had major implications for the Earth's environment, particularly by contributing to the rise of atmospheric oxygen and to the geochemical coupling between the Earth's deep and surface reservoirs.

Keywords: Archaean; continental emergence; continental freeboard; crustal growth; hypsometry; thermal evolution Cretaceous

2.2.1 Introduction

The analysis of eustatic sea level (e.g. Vail et al., 1977; Haq et al., 1987; Miller et al., 2005) has led to the conclusion that continental freeboard (the average elevation of emerged continental crust above sea level) has remained constant throughout the Phanerozoic. This hypothesis has been extended throughout the entire Proterozoic on the premise that tectonic processes have been the same since the end of the Archaean (2.5 Ga) (Wise, 1974). This constancy in continental freeboard has also been used to constrain the evolution of other interdependent parameters such as crustal growth rates (Reymer and Schubert, 1984; Schubert and Reymer, 1985), sedimentation rates (McLennan and Taylor, 1983), ocean volume (Kasting and Holm, 1992; Harrison, 1999),

crustal thickness (Hynes, 2001), depth of mid-oceanic ridges (Galer, 1991; Kasting and Holm, 1992) and mantle temperature (Galer, 1991; Galer and Mezger, 1998).

However, the widespread occurrence of continental flood basalts emplaced on top of immersed continents (Arndt, 1999; Kump and Barley, 2007) suggests higher sea levels in the Archaean. Furthermore, the geochemical fingerprints of felsic sources do not appear in the geological record before the end of the Archaean (Veizer and Compston, 1976; McLennan and Taylor, 1980; Taylor and McLennan, 1985; Shields and Veizer, 2002; Valley et al., 2005). These observations could indicate that the differentiated continental crust was mostly isolated throughout the Archaean (Rey and Coltice, 2008) because it was widely covered by mafic volcanism, and because the continents were largely immersed throughout the Archaean. The timing of continental emergence has long been questioned. Despite a lack of data and physical models, Hargraves (1976) proposed a late emergence during the Proterozoic, a hypothesis disputed by Windley (1977) and by Vlaar (2000) who both argued in favour of a continental emergence near the Archaean/Proterozoic boundary.

In this paper, we propose a model to quantify emerged crustal area as a function of mantle temperature, hypsometry (the global areal distribution of the Earth's surface elevations) and continental area. Because there is no consensual thermal evolution model for the Earth as yet, we present the continental freeboard and area of emerged continental crust as calculated using three different thermal evolution models: two models based on marginal stability analysis of the oceanic lithosphere (Korenaga, 2006) and one model based on the observation of the present-day distribution of seafloor ages (Labrosse and Jaupart, 2007). The choice of thermal evolution model is critical in the calculation of continental freeboard. For realistic thermal evolution models (Korenaga, 2006; Labrosse and Jaupart, 2007), constancy of continental freeboard ($\pm$ 200 m) can be achieved if the potential temperature of the mantle was never more than 110-210°C hotter than present. Previous results from continental freeboard models (Galer, 1991; Galer and Mezger, 1998) fall within this range.

For a late-Archaean balance of parameters (mantle potential temperature 150°C hotter than present and 80% of present continental area) and for constant hypsometry, we calculate that the area of emerged continental crust was less than 12% of the Earth's area. Physical models suggest that mountain building processes were less efficient during the Archaean, due to a reduced strength of the continental lithosphere (Rey and Houseman, 2006; Rey and Coltice, 2008). Including this effect in the evolution of the hypsometry has a major impact on the calculated emerged area of continental crust. For the late-Archaean, we calculate that the emerged area of land was only 2-3% of the Earth's area and therefore predict that the continents were largely flooded. These results are of fundamental importance to the understanding of the coupling of the Earth's geochemical reservoirs. We show that they are consistent with a large number of global geochemical trends in the late-Archaean record.

2.2.2 Model formulation

Isostasy

Because of isostatic equilibrium between continents and oceans, a change in sea level h_f with respect to present-day can be written as

$$\Delta h_f = \Delta d_r \left(1 - \frac{\rho_w}{\rho_m}\right) + \Delta d_{oc} \left(1 - \frac{\rho_{oc}}{\rho_m}\right) - \Delta d_{cc} \left(1 - \frac{\rho_{cc}}{\rho_m}\right) \ , \tag{2.1}$$

where Δd_r, Δd_{oc} and Δd_{cc} are changes in the depth of ridge crests (Reymer and Schubert, 1984), the thickness of the oceanic crust (Galer, 1991) and the thickness of the continental crust (Galer and Mezger, 1998) respectively (all parameters are listed in Tab. 2.2). The densities are ρ_m for the mantle, ρ_{oc} for the oceanic crust, and ρ_w for seawater.

Table 2.2: Variables used in the models. Asterisks indicate present values.

Symbol	Meaning	Value	Std deviation	Unit
α_R	coefficient of thermal expansion (rectangular system)	2.3×10^{-5}		K^{-1}
α_L	coefficient of thermal expansion (triangular system)	2×10^{-5}		K^{-1}
κ	thermal diffusivity	8×10^{-7}		$m^2\ s^{-1}$
ρ_{cc}	mean density of the continental crust	2800	$\pm$ 100 [a]	kg m^{-3}
ρ_{oc}	mean density of the oceanic crust	3000	$\pm$ 100 [a]	kg m^{-3}
ρ_m	mean density of the upper mantle	3300	$\pm$ 100 [a]	kg m^{-3}
ρ_w	mean density of sea water	1030	$\pm$ 10 [a]	kg m^{-3}
A^*_{cc}	total area of continents	2.17×10^{14} [b]		m^2
A_E	area of the Earth	5.1×10^{14}		m^2
A^*_f	area of emerged continents	1.4×10^{14}		m^2
A^*_{oc}	total area of oceans	2.93×10^{14} [b]		m^2
A^*_{sh}	area of the continents, shelf included	1.75×10^{14}		m^2
a	constant in the hypsometric function	0.0388		
b	constant in the hypsometric function	0.608		
d^*_b	average depth below ridges	1859		m
d^*_{cc}	continental crustal thickness	41.1 [c]	$\pm$ 6.2 [c]	km
d_{cc}	Archaean continental crustal thickness	41.1	$\pm$ 7 [d]	km
d_{max}	maximum depth of the continental slope	2446		m
d^*_{oc}	oceanic crustal thickness	7075	$\pm$ 700 [e]	m
d_{oc}	oceanic crustal thickness for $T^*_p = 1430°C$	20870	$\pm$ 2500 [d]	m
d^*_r	ridge depth	2446		m
E	activation energy in the viscosity law	300		kJ
f^*	continental freeboard	8850		m
h^*_f	sea level above the edge of the continental shelf	200		m
h^*_{max}	maximum elevation above continental shelf	9050		m
R	universal gas constant	8.314		J $mol^{-1}K^{-1}$
t^*_s	mean subduction age of the ocean floor	90		Ma
t^*_{max}	maximum age of the oceanic lithosphere	180		Ma
T^*_p	potential temperature of the upper mantle	1280		°C
u^*	oceanic half-spreading rate	2.59 [f]		cm a^{-1}
V_o	total volume of oceans	1.36×10^{18}	$\pm$ 2×10^{17} [g]	m^3
z	exponent in the hypsometric function	0.706		

[a] Galer (1991)
[b] Schubert and Reymer (1985)
[c] Christensen and Mooney (1995)
[d] Galer and Mezger (1998)
[e] White et al. (1992)
[f] Cogné and Humler (2004)
[g] Harrison (1999)

The thickness of continents may have changed over the Earth's history, although seismic studies (e.g. Christensen and Mooney, 1995) show that the present mean thickness of Precambrian shields and platforms (41.5 ± 5.8 km) is similar to the average thickness of the continental crust (41.1 ± 6.2 km). We therefore assume a constant thickness of the continental crust ($\Delta d_{cc} = 0$ in Eq. 2.1) in this study.

Change in Δd_{oc} is a function of the mantle temperature, and change in Δd_r depends upon both mantle temperature and ocean volumetric budget.

Thickness of the oceanic crust

Sleep and Windley (1982) suggested that a hotter mantle in the Archaean would imply a thicker oceanic crust. Models of isentropic decompression melting have been developed to predict the thickness of the oceanic crust as a function of mantle potential temperature T_p (McKenzie, 1984), eventually taking into account the limiting effect induced by the pressure of the crustal overburden (Vlaar and van den Berg, 1991). However, this effect is significant only when considering high mantle temperatures ($T_p > 1560$°C). When using isentropic decompression melting models, the thickness of the oceanic crust is generally assumed to be equal to the calculated thickness of melt, which completely ignores the role of dynamic extraction that could significantly affect the results (Sramek et al., 2007). Therefore, changes in oceanic crustal thickness should be assigned ± 2.5 km uncertainties for a given temperature (Galer and Mezger, 1998). We compared the oceanic crustal thickness calculated using the model of McKenzie (1984) and the parametrisation of the peridotite solidus and liquidus given by McKenzie and Bickle (1988) with that calculated using the model of Korenaga (2006). The difference between both parametrisations for a mantle potential temperature 200°C hotter than present is very close to the uncertainty range: the oceanic crustal thickness calculated by McKenzie and Bickle (1988) is only 2.7 km thicker than the one calculated by Korenaga (2006). The melt height produced for present-day upper mantle potential temperature ($T_p = 1280$°C) fits the observed 7 km-thick oceanic crust for both parametrisations. Due to the lack of a two-phase model taking dynamic extraction into account, the model of McKenzie (1984) is used in this study.

Ocean volumetric budget

As depicted in Fig. 2.6, the volume of the ocean V_o is divided into V_a the reservoir above the mid-oceanic ridge, V_b the reservoir below the mid-oceanic ridge, V_s the reservoir above the continental slope, and V_l the volume due to change in the hypsometric curve after water loading or unloading:

$$V_o = V_a + V_b + V_s + V_l \ . \tag{2.2}$$

The volume V_a depends on the total oceanic area A_{oc} and depth of the ridges d_r and is written

$$V_a = A_{oc}\, d_r \ . \tag{2.3}$$

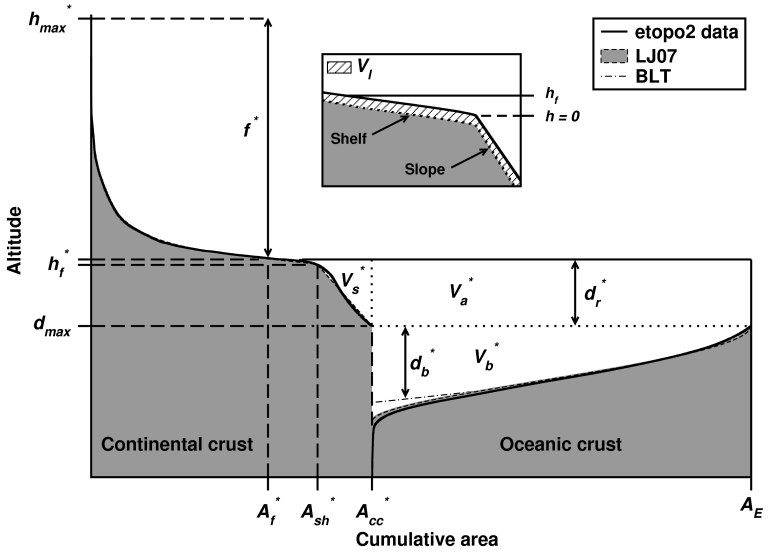

Figure 2.6: Schematic diagram illustrating the parameters relating to the area of emerged continents (see Tab. 2.2 for definitions). Changes in continental freeboard f are equal and opposite to changes in sea level h_f. The oceanic portion of the observed hypsometry is flipped horizontally to better illustrate tectonic processes. Both rectangular (BLT) and linear (LJ07) seafloor age distributions are shown. The inset diagram shows the relationships between reference level $h = 0$, sea level h_f, continental shelf and continental slope (not to scale). The volume caused by isostatic adjustment of the continent V_l is also illustrated in the inset diagram for a hypothetical raise in sea level. Note that V_l^* =0.

Bathymetry

The volume of the reservoir V_b depends on the seafloor bathymetry, caused by cooling of the ocean lithosphere, which is modelled here with the theory of semi-infinite half-space cooling combined with isostasy (e.g. Turcotte and Schubert, 1982):

$$d_b(t) = \frac{2\rho_m \alpha\, T_p}{\rho_m - \rho_w}\sqrt{\frac{\kappa\, t}{\pi}} \ ,$$

where d_b is the depth below ridge axis, α is the thermal expansivity, κ is the thermal diffusivity and t is the age of the oceanic floor. For a given distribution of area of the ocean floor with age dA/dt, the volume of the reservoir V_b can therefore be written as

$$V_b = \int_0^{t_{max}} d_b(t)\frac{dA}{dt}dt \ ,$$

where t_{max} is the maximum age of the ocean floor. Different age distribution models can be derived, depending on the mode of mantle cooling (Labrosse and Jaupart, 2007). In the following, we explore changes in bathymetry as a function of the potential temperature of the mantle T_p

and of the area of continental crust A_{cc} for different distribution models.

Two different approaches can be used to calculate the distribution of seafloor ages, but they are mutually exclusive. The first is based on boundary layer stability analysis, stating that subduction starts when a plate reaches a threshold age at which the thermal boundary layer becomes gravitationally unstable. As a consequence, such models imply a rectangular distribution of seafloor ages:

$$\frac{dA}{dt} = C_0 \quad \text{for} \quad t < t_s \ ,$$

where C_0 is the global rate of seafloor spreading and t_s is the age of subduction of the oceanic floor. For this distribution, the total area of the ocean floor is:

$$A_{oc} = C_0 t_s \ ,$$

and the present-day subduction age is $t_s^* = 90$ Ma. The boundary layer theory implies that the age of subduction depends on mantle convective vigour through convection velocity:

$$t_s = t_s^* u^* / u \ ,$$

where u is the half spreading rate at mid-oceanic ridges. For Rayleigh-Bénard convection, a given potential temperature T_p gives u as

$$u(T_p) = u^* \left(\frac{T_p}{T_p^*} \frac{\eta(T_p^*)}{\eta(T_p)} \right)^{2/3} \ , \tag{2.4}$$

where the viscosity itself depends on the potential temperature of the mantle T as (Davies, 1980)

$$\eta = \eta_0 \ \exp\left(\frac{E}{R\,T} \right) \ ,$$

where E is the activation energy. This model is referred to hereafter as the Boundary Layer Theory (BLT). It implies a strong feedback between T_p and heat flow, suggesting larger radiogenic heat production or core heat flow than what is usually proposed from cosmochemical arguments (see Jaupart et al., 2007, for a recent review).

For this reason it has been proposed (Arndt, 1983; Korenaga, 2006) that the positive buoyancy of the oceanic lithosphere could delay the onset of subduction if the oceanic crust is thick enough. The positive buoyancy of the oceanic lithosphere is due to the change of partitioning intrinsic density between the oceanic crust and the underlying depleted mantle with change in mantle temperature. Including this chemical effect and small scale convection in the classical boundary layer theory reduces the dependence of u on T_p. This model, hereafter referred to as K06, proposes a moderate thermal evolution of the mantle which is more consistent with petrological constraints on the mantle temperature in the Archaean (Abbott et al., 1994). The

advantage of the boundary layer approaches BLT and K06 is that the distribution of seafloor ages can readily be calculated for any given mantle temperature.

However, these models could be in contradiction with the observed present-day distribution of ages of the seafloor. Indeed, different oceanic lithospheres have different ages of subduction and the probability of subduction is approximately the same for any age (Sclater et al., 1981; Parsons, 1982; Rowley, 2002; Cogné and Humler, 2004; Labrosse and Jaupart, 2007). Hence the distribution is triangular:

$$\frac{dA}{dt}(x) = C_0 \left(1 - x\,\frac{t}{t_{max}}\right) \ ,$$

where t_{max} is the maximum age of the lithosphere and $x = A_{cc}/A^*_{cc}$ is the areal fraction of present continental crust. For this distribution, the area of oceans can be derived as

$$A_{oc} = \frac{(2-x)C_0\, t_{max}}{2} \ .$$

One problem of this approach is that there is no physical model as yet for a relationship between the maximum age of the lithosphere t_{max} and T_p. Labrosse and Jaupart (2007) inferred from their parametrisation of the thermal evolution of the Earth that t_{max} must be larger than 104 Ma at all ages. The authors also proposed that the deviation from the rectangular distribution of ages is caused by the presence of continents. Hence, as in their models, our model for the seafloor age distribution evolves from rectangular to triangular as a linear function of x (Labrosse and Jaupart, 2007). This model is referred to hereafter as LJ07.

For each model, the coefficient of thermal expansion α is adjusted so that the calculated ridge depth is equal to the present-day ridge depth (see Tab. 2.2). The area of continents at a depth greater than d_{max} is neglected in all models. The depth of mid-oceanic ridges is allowed to change through time (Eq.2.1). The plots of present-day bathymetry for both distribution systems are shown in Fig. 2.6. The triangular distribution gives a better fit to the data as expected since it is an empirical model.

Hypsometry

The volume V_s of the water reservoir over the continent is a function of the hypsometric curve $f(A)$:

$$V_s = (A_{cc} - A_f)(h_f + d_{max}) - \int_{A_f}^{A_{cc}} f(A)\ dA \ , \tag{2.5}$$

where A_f is the area of emerged continents. The hypsometric curve is described by a function modified from Strahler (1952) and Harrison et al. (1981) until the edge of the continental shelf, and the continental slope is taken as a linear function. This can be written as

$$f(A) = \begin{cases} b \cdot h_{max} \left(\frac{1-A/A_{sh}}{a+A/A_{sh}} \cdot a\right)^z & \text{if } A \le A_{sh} \\ \\ \frac{A-A_{sh}}{A_{cc}-A_{sh}} d_{max} & \text{if } A > A_{sh} \ , \end{cases} \tag{2.6}$$

where h_{max} is the maximum elevation of the continents, and a, b and z are constants determined to fit the eTOPO2 data (NOAA, 2006). Values are given in Tab. 2.2 for a correlation coefficient $R^2 = 0.999$. Sea level is always above the reference level ($h = 0$), defined at the edge of the continental shelf in $A = A_{sh}$.

The volume V_l, caused by isostatic adjustment after a sea level change over the continent (see Fig. 2.6), is given by

$$V_l = \begin{cases} \frac{\rho_w}{\rho_m} \left[\int_{A_f}^{\hat{A_f}} (h_f - h)\ dA + \int_{\hat{A_f}}^{A_{cc}} (h_f - \hat{h_f})\ dA \right] & \text{if } h_f > \hat{h_f} \\ \\ \frac{\rho_w}{\rho_m} \left[\int_{\hat{A_f}}^{A_f} (h - h_f)\ dA + \int_{A_f}^{A_{cc}} (h_f - \hat{h_f})\ dA \right] & \text{if } h_f < \hat{h_f}\ , \end{cases}$$

with $\hat{A_f}$ and $\hat{h_f}$ being respectively the area of emerged continents and sea level before water loading or unloading. h is defined using the hypsometric curve $f(A)$ (Eq. 2.6). For a transgression, $A_f < \hat{A_f} < A_{cc}$ and V_l is positive. As for a regression, $\hat{A_f} < A_f < A_{cc}$, and V_l is negative, therefore the continent is uplifted. V_l is zero today since the observed hypsometric curve is the reference.

Eustatic sea level is determined by iterative computing of V_o from Eq. 2.2 until constancy of ocean volume is reached. In this process, V_a is calculated from Eq. 2.3 with d_r computed from Eq. 2.1 and the integral of $f(A)$ in Eq. 2.5 is calculated numerically.

2.2.3 Influence of thermal evolution models on continental freeboard

In this section, we explore the dependencies of continental freeboard and area of emerged continents on mantle potential temperature and continental area, assuming constant hypsometry and ocean volume.

Continental freeboard

For a given continental area, sea level increases as temperature increases, due to the combination of two processes: thickening of the buoyant oceanic crust and flattening of the seafloor. The former process has an identical effect in the BLT, K06 and LJ07 models. However, models differ in the parametrisation of the flattening of the bathymetry. Indeed, in the BLT model, spreading rates are very sensitive to mantle temperature. Hence, for mantle temperatures more than 100°C hotter than present-day, the bathymetry is almost flat, the volume of the reservoir below ridges V_b is reduced and sea level is high. The K06 model, however, proposes a reduced sensitivity of spreading rate to temperature and the LJ07 model proposes a modest change in the maximum age of the ocean floor. Flattening of the bathymetry is thus buffered in these two models. As a consequence, K06 and LJ07 models have a lower sensitivity to T_p than the BLT model.

Continental freeboard is also sensitive to the fraction of the Earth's area covered by continental plates. As new continental crust is produced, the total area of the continents A_{cc} increases while the total area of the oceans decreases. Removing the continental crust entirely would result in a decrease in sea level of $\sim$ 1000 m. The dependency of continental freeboard on continental area is the same in the BLT and K06 models but is slightly different in the LJ07 model, in which the seafloor age distribution changes with continental area.

Fig. 2.7 shows the contours of constant continental freeboard as a function of continental area and mantle temperature for each model. The constant freeboard hypothesis allows for sea level variations of $\pm$ 200 m, which is the amplitude of Phanerozoic sea level change (Haq et al., 1987; Miller et al., 2005). The slope of the contours shows that continental freeboard calculated using the BLT model is more sensitive to mantle temperature than other thermal evolution models. Constant freeboard ($\pm$ 200 m) can be achieved if mantle temperature did not exceed its present-day value by more than 90°C (75-110°C) for the BLT model, 160°C (130-190°C) for the K06 model, 190°C (165-210°C) for the LJ07 model with t_{max} = 180 Ma, and 140°C (120-165°C) for the LJ07 model with t_{max} = 104 Ma. The temperature calculated by the K06 model is close to the temperature suggested by Galer (1991). Both the K06 and LJ07 models can accommodate a greater mantle temperature than the BLT model, keeping continental freeboard constant.

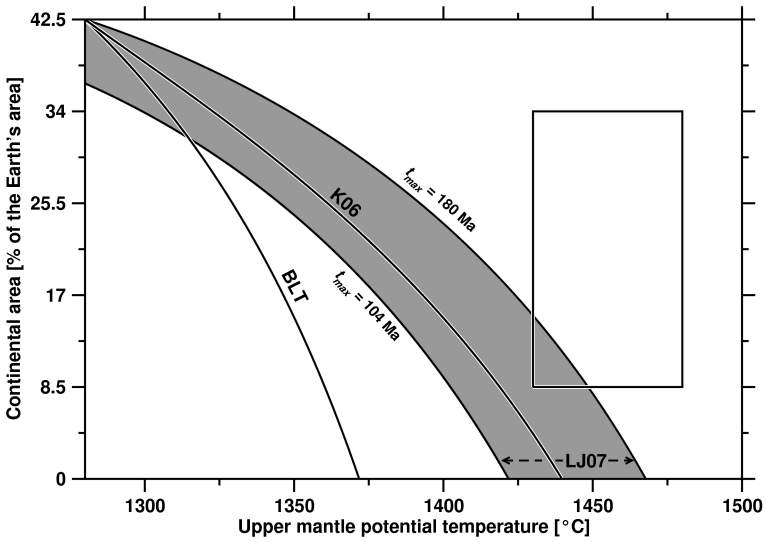

Figure 2.7: Contours of constant continental freeboard as a function of continental area and mantle temperature, for present hypsometry. Results are presented for each model. The shaded area shows the variability of the continental freeboard with t_{max} for the linear seafloor age distribution model (LJ07). The box shows the possible range of parameters in the Archaean: the mantle was probably 150-200°C hotter than present and the continental area increased from 20% to 80% of present.

To achieve constancy of the freeboard, a change in mantle temperature must be counterbalanced by a change in continental area (Schubert and Reymer, 1985). For the BLT model, a cooling of 30°C is necessary to balance 30% of crustal growth, while a cooling of $\sim$ 60°C is required for other models. If most of the continents were produced very early in the Earth's

history, the constancy of continental freeboard within the Archaean and Proterozoic could not be achieved because cooling is supposedly between 50 and 100°C Ga^{-1} (Jaupart et al., 2007). For all thermal evolution models, keeping continental freeboard constant throughout most of the Earth's history could be very difficult if the episodicity of crustal production (Rudnick, 1995; Condie, 2000) is not matched by an episodicity of mantle cooling.

Area of emerged continental crust

One novel aspect of our approach is the calculation of the area of emerged continental crust. Today, continents represent 42.5% of the Earth's area (Schubert and Reymer, 1985), and emerged crustal area represents only 27.5%. At constant freeboard, the change in the fraction of emerged crust is proportional to the change in continental area (see Fig. 2.8). However, as expected from the freeboard equations, the greater the mantle temperature, the higher the sea level and the smaller the emerged crustal area. For present-day continental area and hypsometry, an increase in mantle temperature of 100°C would reduce the area of emerged continental crust to $\sim$ 9-16% depending on the thermal evolution model.

All other parameters being constant, the area of emerged continental crust varies with the total area of continental crust. However, there is a trade-off between continental area and emerged area: a larger continental area generally leads to a greater emerged area, but it also triggers an increase in sea level. As expected, the BLT model presents the highest sensitivity to mantle temperature. For a hotter mantle, this model thus proposes an emerged continental area much lower than that proposed by the more conservative LJ07 and K06 models (Fig. 2.8).

For low temperature and large continental area, the area of emerged continental crust is not sensitive to continental growth. The emerged area can only increase with continental growth for a hot mantle, where continental freeboard is highly sensitive to mantle temperature. Hence, a pulse of crustal growth during the Archaean would have resulted in a net increase of emerged area. The area of emerged continental crust depends mainly upon mantle temperature whereas continental freeboard depends on the ratio of crustal growth to mantle cooling.

2.2.4 Area of emerged continental crust in the Archaean

Mantle temperature and continental area in the Archaean

It is generally agreed that the temperature of the mantle has decreased over time while the continental area has increased. The main argument for a hotter mantle in the Archaean is based on the petrography and geochemistry of komatiites (Green et al., 1975; Nisbet et al., 1993). Temperature estimates depend on the water content of komatiites. Arndt et al. (1998) argued that while some komatiites formed from hydrous melt, most were dry. Dry komatiites, erupted in a plume environment, would suggest a mantle temperature 200-300°C hotter at 3.5 Ga (Nisbet et al., 1993) compared to a 100-200°C hotter mantle for hydrated komatiites erupted in a subduction environment (Grove and Parman, 2004). Abbott et al. (1994) concluded from their

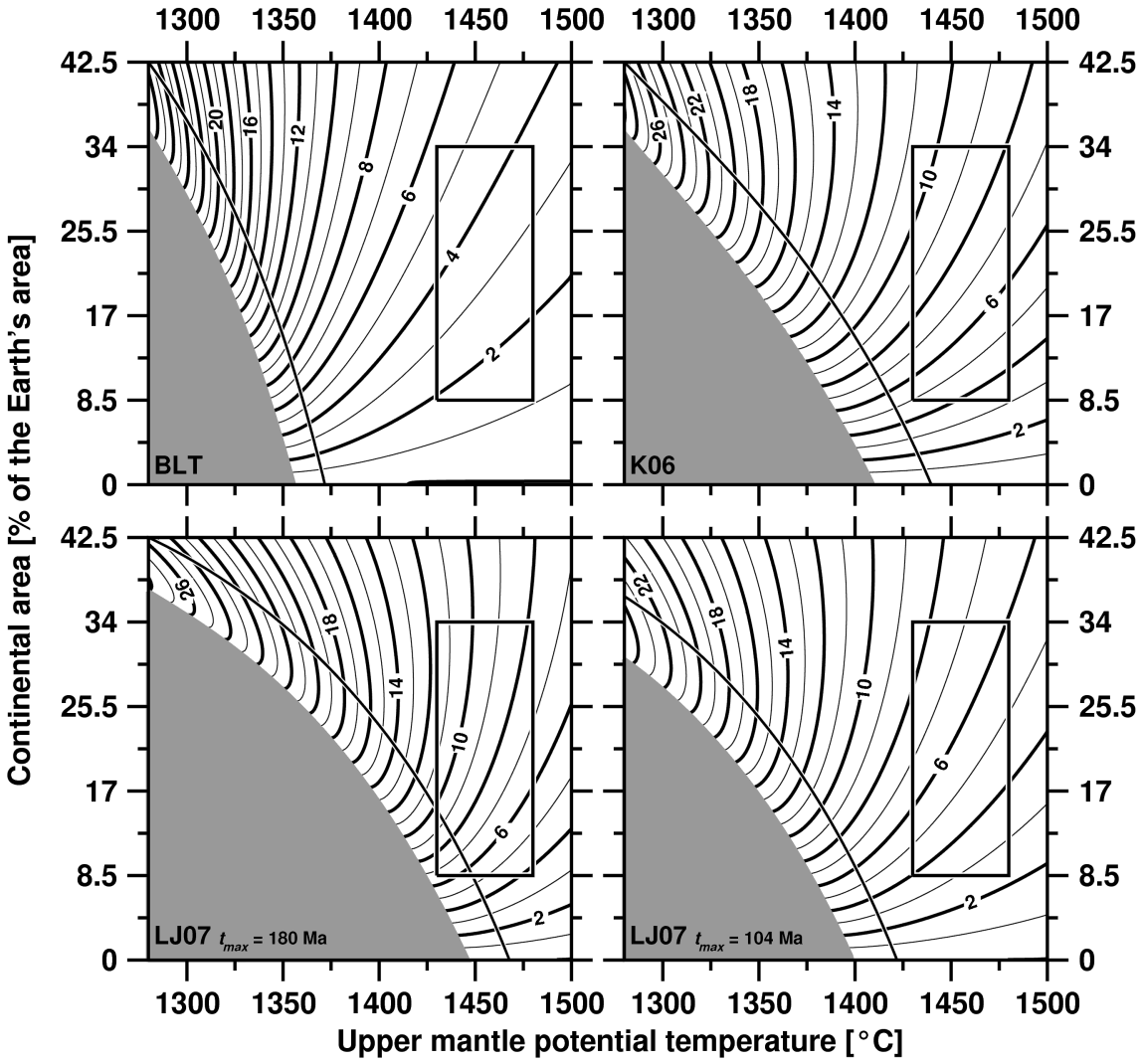

Figure 2.8: Contours of the area of emerged continental crust (in % of the Earth's area) as a function of continental area and mantle temperature for present hypsometry. Results are presented for each model. The shaded area in each diagram shows the conditions within which the continental slope would emerge. The thick black lines are the contours of constant continental freeboard. The boxes are as defined in Fig. 2.7.

petrological and geochemical study on mid-ocean ridge basalts that the potential temperature of the mantle at 2.8 Ga was 137-187°C greater than present. Using these constraints, we assume that the mantle was 150-200°C hotter during the Archaean.

Most models of continental growth show that the volume of continental crust has increased over time (e.g. Campbell (2003) and Rino et al. (2004) for recent reviews), with many pointing toward a major growth pulse during the Neoarchaean (2.9-2.5 Ga). Following the work of Campbell (2003) based on Nb/U ratios in Archaean basalt-komatiite suites, we assume that the continental crust grew from $\sim$ 20% of the present continental area at around 4 Ga to 80% by 2.5 Ga.

Putting these considerations of mantle temperature and crustal growth together, and assuming constant hypsometry, the calculated area of emerged continents in the Archaean is between 1 and 12% of the Earth's area (Fig. 2.8).

Hypsometry in the Archaean

The hypsometric curve is an expression of the balance between mountain building processes and erosion processes. Orogenies are expected to produce high plateaus and high peak elevations that erosion processes can flatten down in a few hundred million years (Harrison, 1994). Considering the present-day variation in hypsometry from one continent to another (e.g. Harrison et al., 1981) we propose that the global hypsometry could have fluctuated during the Phanerozoic between an orogenic end-member and an anorogenic end-member (see Fig. 2.9). The orogenic end-member for the Phanerozoic is illustrated by the present-day hypsometry of Asia, which supports the highest plateau and highest peak on Earth, built over the last 50 Ma. The Earth's present-day hypsometry is actually very close to this end-member. In contrast, the global hypsometry during the upper-Jurassic/lower-Cretaceous, a time of continental flooding, is likely to have been closer to that of the anorogenic end-member, present-day Australia.

Assuming that the overall shape of the end-member hypsometric curves (described by Eq. 2.6) has remained constant over time, the secular evolution of the global hypsometry depends only upon the maximum elevation. Harrison (1994) proposed that early in the Earth's history, a greater generation of radioactive heat would imply greater rates of mountain building and thus higher continental elevations. In contrast, Rey and Houseman (2006) argued that a greater production of radiogenic crustal heat and a greater mantle heat flow would reduce the strength of the continental lithosphere and thus its ability to sustain high mountain belts (Rey and Houseman, 2006). Assuming conservative present-day strain rates (10^{-15} to 10^{-14} s^{-1}), the maximum elevation of orogenic plateaus during the Neoarchaean would have been 1800-2200 m (Rey and Coltice, 2008), allowing for a dynamically supported maximum elevation up to $\sim$ 3600 m. Fig. 2.9 shows possible orogenic and anorogenic hypsometry end-members for the Neoarchaean. The proposed Neoarchaean orogenic end-member is very close to the present-day anorogenic end-member.

This reduced maximum elevation is at odds with some previous works, which have argued

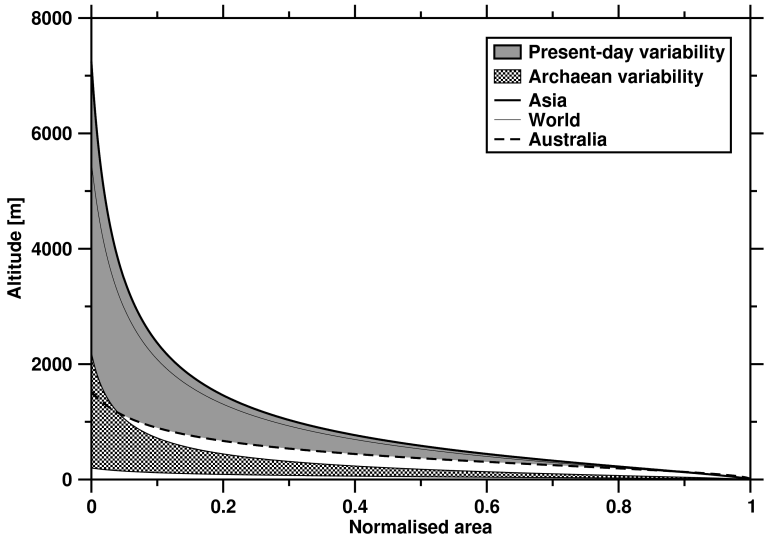

Figure 2.9: Variability of continental hypsometric curves for the present-day and for the Neoarchaean. The area is normalised. The datum of the ordinate axis is the altitude at the edge of the continental shelf (currently -200 m). The hypsometric curves for Asia and Australia are built using parameters from Harrison et al. (1981). The world hypsometric curve is that compiled from the eTOPO2 data.

that Archaean orogenic processes and mountain belts were similar to their modern counterparts. For instance, England and Bickle (1984) argued that orogenic crustal thicknesses could have been up to 70 km in the Archaean "by noting that pressures in high-grade gneiss belts of 8-10 kb imply overburdens of 28 to 35 km [...] with 35 km of crust preserved beneath the sampled locality". Their paper is one of the cornerstones of uniformitarianism as it concludes that Archaean geothermal gradients were similar to present-day ones. A quarter of a century of research has shown that erosion following instantaneous thickening is not the only process able to exhume high-grade metamorphic terranes. Firstly, it should be noted that exhumation of deep crustal levels may occur with little finite crustal thickening when erosion rates are similar to crustal thickening rates. Secondly, exhumation of deep crustal levels in metamorphic core complexes occurs in association with horizontal extension and thinning of the crust. Thirdly, the coeval sagduction of dense greenstone covers and exhumation of their felsic basement, a process described in many Archaean cratons (McGregor, 1951; Dixon and Summers, 1983; Bouhallier et al., 1995), is known to have exhumed kyanite bearing assemblages (Delor et al., 1991; Collins et al., 1998). Therefore, one cannot assume that 8-10 kb high-grade gneiss terranes are proof of a 70 km-thick orogenic crust in the Archaean, nor that Archaean continental geotherms were similar to modern ones.

Flooded continents in the late-Archaean

Assuming that the hypothesis of warmer and weaker continental lithospheres in the Archaean is valid, the effect of decreasing the maximum elevation in the present-day global hypsometric curve is a decrease in the area of emerged continental crust as shown in Fig. 2.10. Note that, however,

the relationship between maximum elevation and area of emerged continental crust can differ depending on mantle temperature. We represent a late-Archaean configuration in Fig. 2.11, based on the hypsometry of our proposed Neoarchaean orogenic end-member (see Fig. 2.9). We use the LJ07 model, allowing the maximum age of the ocean floor to vary between 104 and 180 Ma, since the results for the K06 model fall within these limits. For a maximum oceanic floor age t_{max} of 180 Ma, the calculated emerged crustal area is 3.1% of the Earth's area. For t_{max} =104 Ma, it is 1.8%. It is worth noting that a small increase in total continental area from 34% to 42.5% since the end of the Archaean has resulted in a large increase in emerged area, of approximately 25% of the Earth's area. Our models show that large submerged continental areas existed in the late-Archaean. For a maximum oceanic floor age of 180 Ma (104 Ma) we calculate that $\sim$ 24% ($\sim$ 25.5%) of the Earth's area is covered by water $\sim$ 800 m ($\sim$ 1100 m) deep. Note that these are maximum depths, as sedimentation processes are not taken into account here.

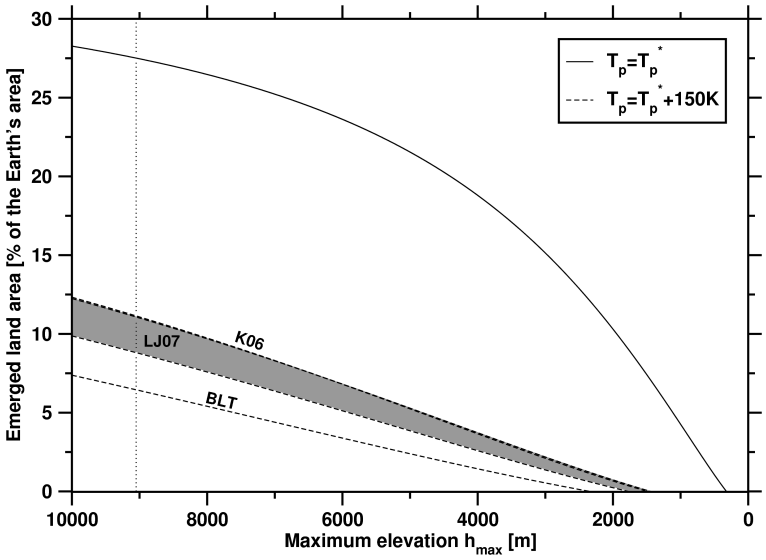

Figure 2.10: Changes in the area of emerged continental crust as a function of the elevation of the highest peak on Earth, for present-day continental area ($x = 1$) and hypsometry. The thick curve is calculated for present mantle temperature and is the same for all models. The thin curves are illustrated for each model and for a mantle temperature 150°C greater than today. The shaded area shows the variability of emerged area with t_{max} for the linear seafloor age distribution model (LJ07). In this calculation the results for the K06 model are very close to those for the LJ07 model with t_{max} = 180 Ma. The dotted line shows the present-day maximum elevation.

Uncertainty in the calculation of the area of emerged land

We have shown that the calculation of the area of emerged land depends upon the chosen thermal evolution model for the Earth. The results of the calculation are also affected by the natural variability associated with each of the parameters used for the computation, especially the thickness of the continental crust and the volume of the ocean. To illustrate the uncertainty in the calculation of the area of emerged land due to this natural variability, we performed a Monte Carlo analysis for the model presented in Fig. 2.11 assuming a maximum oceanic floor age

of 104 Ma. The input parameters are described by Gaussian distributions using the mean values and standard deviations listed in Tab. 2.2. From 10^5 realisations, we predict a distribution of the area of emerged land and of sea level.

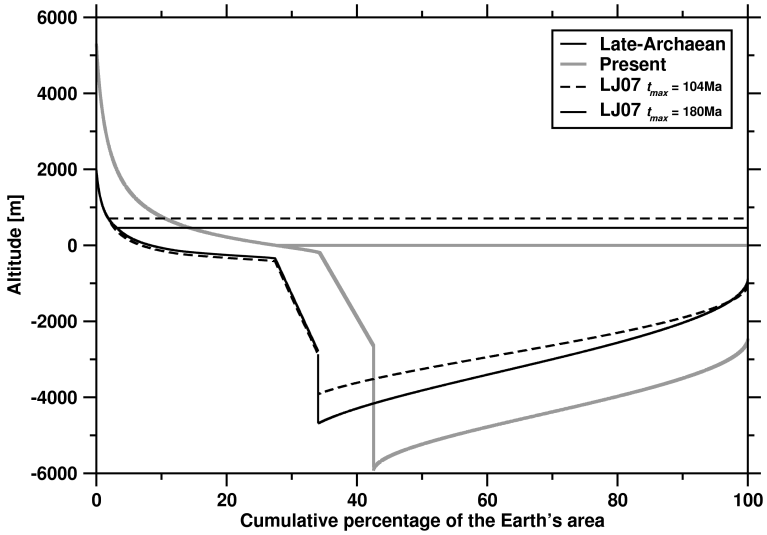

Figure 2.11: Calculated hypsometry, bathymetry and sea level for a late-Archaean configuration ($\sim$ 2.5 Ga, x =0.8, T_p = 1430°C, h_{max} = 3615 m) for the LJ07 model. The plain dark lines are for a maximum oceanic floor age of 180 Ma and the dashed lines for a maximum oceanic floor age of 104 Ma. The lighter lines represent present-day hypsometry, bathymetry and sea level for the LJ07 model.

We analyse both the predicted distributions for the effect of density, crustal thicknesses and ocean volume variabilities. Three types of configurations can be obtained in which continents are (a) entirely emerged, (b) partially flooded or (c) entirely flooded. The input and output of these analyses are summarised in Tab. 2.3. The predicted distributions have large standard deviations, up to 100% of the mean value for A_f and 50% for h_f. This is caused by the large variability we have considered for densities, thicknesses and ocean volume. The predicted distributions of the area of emerged land present a positive skew which explains the observed differences between mean and median. The medians for A_f range between 1.79 and 2.84% of the Earth's surface. Hence, the model presented before in Fig. 2.11 is one of the most probable.

Taking all variabilities into account, the input parameters of models predicting partial flooding (64% of all the realisations) are consistent with that obtained in the determinist approach for a change in the thickness of the continents of -2.1 $\pm$ 6.1 km. For complete flooding to be obtained (9% of the trials) the continental crust has to be about 10 km thinner than present. For a crust much thicker than present (10.2$\pm$ 6.1 km), and a reduced ocean volume (about 10% lower than present), continents can be entirely emerged. This situation is obtained for 27% of the trials. The calculated thickening of the crust necessary to entirely emerge the existing continents in the Archaean is twice that proposed by Galer and Mezger (1998) and abundant geological and geochemical evidence suggesting flooded continents in the Archaean (see next section) would advocate for Archaean continents slightly thinner or as thick as present-day ones.

Table 2.3: Effect of uncertainties on densities and natural variability in continental and oceanic crustal thicknesses and oceanic volume for the calculation of the area of emerged land for the example in Fig. 2.11 with $t_{max} = 104$ Ma. The information is given in the form mean(standard deviation) or mean/median(standard deviation) when three numbers are present.

			Input error and uncertainties						Monte Carlo output	
Variability incorporated	Result	N	ρ_{oc}/ρ_m	ρ_{cc}/ρ_m	ρ_w/ρ_m	Δd_{oc} [km]	Δd_{cc} [km]	V_o [$\times 10^{18}$m^3]	h_f [m]	A_f [$\%A_E$]
None	$1 < A_f < A_{sh}$	-	0.91(-)	0.85(-)	0.312(-)	13.8(-)	0.0(-)	1.36(-)	855.9(-)	2.04(-)
Densities	$0 < A_f < A_{sh}$	95900	0.91(3.7×10^{-2})	0.85(3.9×10^{-2})	0.312(9.5×10^{-3})	-	-	-	727.9/718.3(344.2)	4.28/2.75(4.39)
	Entirely emerged	4099	1.00(1.6×10^{-2})	0.89(3.9×10^{-2})	0.327(8.5×10^{-3})	-	-	-	-	-
	Entirely flooded	1	0.74 (-)	0.80(-)	0.266(-)	-	-	-	-	
Thicknesses	$0 < A_f < A_{sh}$	69560	-	-	-	13.9(2.6)	-2.5/-2.1(5.6)	-	965.2/919.2(571.6)	4.05/1.79(5.49)
	Entirely emerged	24015	-	-	-	13.2(2.6)	12.0/11.0(4.8)	-	-	-
	Entirely flooded	6425	-	-	-	14.7(2.6)	-18.1/-17.4(3.9)	-	-	-
Ocean volume	$0 < A_f < A_{sh}$	99284	-	-	-	-	-	1.36(0.20)	707.2/703.2(276.5)	3.84/2.84(3.32)
	Entirely emerged	716	-	-	-	-	-	0.8(0.06)	-	-
All	$0 < A_f < A_{sh}$	63995	0.91(3.8×10^{-2})	0.85(3.9×10^{-2})	0.312(9.7×10^{-3})	13.9(2.6)	-2.1/-1.9(6.3)	1.38(0.20)	942.8/883.6(577.6)	4.29/1.93(5.66)
	Entirely emerged	26683	0.93(4.2×10^{-2})	0.85(4.1×10^{-2})	0.314(1.0×10^{-2})	13.4(2.6)	10.1/9.8(6.1)	1.29(0.20)	-	-
	Entirely flooded	9322	0.88(3.5×10^{-2})	0.82(3.3×10^{-2})	0.307(8.6×10^{-3})	14.6(2.6)	-14.1/-13.8(5.7)	1.43(0.22)	-	-

Geological and geochemical footprints for a late-Archaean emergence of continents

Largely flooded continents at the end of the Archaean as shown by our models are consistent with the observation of widespread volcanism on submerged continental platforms (Arndt, 1999; Kump and Barley, 2007). The histogram in Fig. 2.12a shows that more than 80% of the Archaean Large Igneous Provinces (LIPs) were emplaced in subaqueous conditions, compared to less than 30% after 2.5 Ga (Kump and Barley, 2007). Assuming no sampling bias, this fraction of emerged LIPs is a direct measure of the fraction of emerged continents. Note that the proportion of emerged continental crust at 2.5 Ga calculated using our model (10%, Fig. 2.11) is consistent with the observation that $\sim$ 15% of the LIPs emplaced between 2.75 and 2.5 Ga are subaerial (Fig. 2.12a). Further research regarding the subaerial or submarine nature of LIPs of different ages would better constrain the fraction of emerged continental crust over time. Moreover, this increase in the amount of stable-shelf sediments throughout the Archaean (Eriksson and Fedo, 1994) leading up to the formation of giant carbonate platforms at 2.9 Ga (Wilks and Nisbet, 1985) and between 2.6-2.4 Ga (Eriksson et al., 2005) confirms that continental crust mainly evolved below sea level.

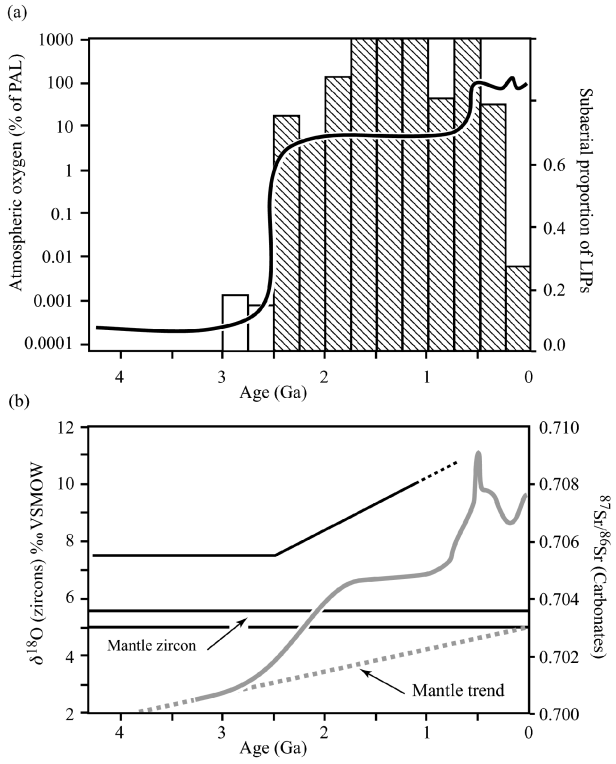

Figure 2.12: Geological and geochemical evidence for a possible late-Archaean emergence of the continents. a) Histogram: proportion of subaerial LIPs through time (from Kump and Barley, 2007); Curve: evolution of atmospheric oxygen in percentage of Present Atmospheric Level (from Kump, 2008). b) Black lines: evolution of the δ^{18}O of detrital and inherited zircons (from Valley et al., 2005). The mantle value is 5.3$\pm$ 0.3‰; Grey lines: evolution of the isotopic ratio ^{87}Sr/^{86}Sr of the mantle (dotted line) and of marine carbonates (plain line) (from Shields and Veizer, 2002). These signals all indicate a major change at the end of the Archaean (2.5 Ga).

The reduced area of emerged continents (up to 3% of the Earth's area, which is roughly the size of South America) and maximum elevations (approximately 3600 m) calculated using our models would still account for the common occurrence of clastic sediments and basins in the Archaean (Nisbet, 1987), including the oldest known unconformity dated at 3.46 Ga (Buick et al., 1995). Nevertheless, Archaean clastic sediments are known to be not as well mixed as present-day ones (Sircombe et al., 2001), and some authors have noted that limited sediments were supplied to continental margins in the early Archaean (Lowe, 1994). This is compatible with a reduced emerged continental area and smaller drainage basins (Bleeker, 2002).

A reduced area of emerged continental crust is also consistent with the lack of felsic fingerprints in the sedimentary record before $\sim$ 2.5 Ga, which was explored by: a) Taylor and McLennan (1985) who showed that the geochemical composition of black shales, a proxy for the composition of emerged continental crust, changed from mafic-dominated to felsic-dominated at $\sim$ 2.5 Ga; b) Veizer and Compston (1976) who showed that the isotopic ratio $^{87}Sr/^{86}Sr$ of marine carbonates separated from the calculated mantle evolution before $\sim$ 2.5 Ga towards more radiogenic values after $\sim$ 2.5 Ga (Fig. 2.12b). This shift in composition implies a change from a "mantle"-buffered to a "river"-buffered ocean because the felsic continental crust is a major reservoir for radiogenic strontium (Shields and Veizer, 2002); c) Valley et al. (2005) who showed that the $\delta^{18}O$ signature of igneous zircons changed from mildly-evolved magmatic values ($5 < \delta^{18}O < 7.5$ ‰) before 2.5 Ga to values increasingly greater than 7.5 ‰ after 2.5 Ga (Fig. 2.12b). They interpreted this change in $\delta^{18}O$ as an increase in the intra-crustal recycling of high $\delta^{18}O$ felsic sediments.

The appearance of the felsic signature in the sedimentary record is generally interpreted as a major pulse in crustal growth at $\sim$ 2.7 Ga (Taylor and McLennan, 1985; Shields and Veizer, 2002; Valley et al., 2005). However, the discrepancy between the U-Pb crystallisation age and the Hf model age of low $\delta^{18}O$ detrital and inherited zircons of the Gondwana supercontinent (Kemp et al., 2006) has lead to the conclusion that it could take up to one billion years for newly formed continental crust to dominate the sedimentary record (Hawkesworth and Kemp, 2006). Hawkesworth and Kemp (2006) attributed this time lag to the emplacement of new crust by under- or intra-plating within older crust, delaying its erosion and contribution to the sedimentary record. However, we attribute this delay to the fact that the felsic continental crust was both largely covered under LIPs and mostly flooded during the Archaean. Hence, the anomalies in the sedimentary record after 2.5 Ga do not necessarily represent a pulse in crustal growth at $\sim$ 2.7 Ga, but rather the emergence of the continents allowing for the erosion of the mafic cover and the exhumation of the felsic reservoir. Finally, this emergence of the continents would most likely contribute to the rise of the atmospheric oxygen at $\sim$ 2.5 Ga (see Kump, 2008, for a recent review; Fig. 2.12a) as it would result in the reduction of the proportion of submarine LIPs, a major sink of oxygen (Kump and Barley, 2007), and in an increase in the weathering of emerged felsic material, a major sink of carbon dioxide (e.g. Kramers, 2002; Lowe and Tice, 2004).

2.2.5 Conclusions

The models presented in this study allow the calculation of emerged crustal area as a function of mantle temperature, hypsometry and continental area. Testing three different thermal evolution models, we show that constancy of the continental freeboard (± 200 m) can be achieved if the upper mantle potential temperatures has never been 110-210°C hotter than present. This temperature range is relatively large because freeboard models greatly depend upon thermal evolution models. For constant hypsometry, the area of emerged continental crust would not exceed 12% of the Earth's area by 2.5 Ga. Assuming less efficient mountain building processes in the Archaean further reduces this area to 2-3% of the Earth's area. Given the possibility that 80% of the present-day continental area was already produced by 2.5 Ga, this implies that the continents were mostly flooded throughout the Archaean. Their progressive emergence left in the sedimentological record the footprints of the coupling of a new geochemical reservoir (the felsic continental crust) with previously coupled reservoirs (the mantle and the hydrosphere). Continental emergence resulted in major changes in the Earth's environment, notably by contributing to the rise of atmospheric oxygen.

The models presented in this paper have some limitations. Firstly, there is a poor control of ocean volume over time. For instance, a secular change in the depth of mid-ocean ridges could modify the ocean volume by changing the efficiency of hydration of the oceanic crust (Kasting and Holm, 1992). Secondly, we assume a constant thickness of continental crust over time. The performed Monte Carlo analysis shows that the thickness of the continental crust is the key assumption, and that the continents could have been entirely emerged by 2.5 Ga if the continental crust was 10 km thicker than present. Although, this value is twice that suggested by previous studies Galer and Mezger (1998). Finally, we propose a model assuming isostatic equilibrium, but convective motions in the mantle induce dynamic topography (Husson and Conrad, 2006) and thus small-amplitude changes in sea level over short time scales.

Acknowledgements

The authors wish to thank Steve Galer, Chris Harrison and two anonymous reviewers for their constructive comments, Claude Jaupart for his fruitful editing and Kylie Sedon for polishing the English in the manuscript. N. F. also wishes to acknowledge his Lavoisier grant from the French Ministry of Foreign and European Affairs. This work was partly supported by ARC grant DP0342933, the International Program Development at the University of Sydney and the CNRS RELIEFS program.

2.3 Afterthoughts and extensions

2.3.1 Thickness and density of the oceanic crust

Thickness of the oceanic crust

As stated in section 1.1.2, one particularity of the Archaean rock record is the absence of ophiolites. Archaean plate tectonics are thus essentially theoretical and hard to test. In the models presented in section 2.2, we made the hypothesis that partial melting of a hotter mantle would result in the production of a thicker oceanic crust. While it is based on robust theoretical modelling, this hypothesis is important since the contribution to sea level due to changes in oceanic crustal thickness is the most important of the model (Fig. 2.3). For example, for a mantle 150°C hotter than present the predicted thickness of oceanic crust is $\sim$ 14 km greater than present (Fig. 2.13). This translates in an increase in sea level of 1250 m from Eq. 2.1.

A question to address when assuming that the Archaean oceanic crust was thicker is why no ophiolite was preserved. An explanation to the first order is the absence of continental margins in the Archaean rock record. Since ophiolites are preferentially preserved on continental margins, one preservation bias could account for the other. Moreover, Hoffman and Ranalli (1988) suggested that thick (25 km) Archaean oceanic crust younger than $\sim$ 50 Ma would present a lower ductile layer because of higher temperatures. This would have resulted in the decoupling of the upper and lower oceanic crust, as inferred for present-day continental crust. Hoffman and Ranalli (1988) suggested that this decoupling could have resulted in the delamination of the upper continental crust that could have been obducted, and could have been preserved in some Archaean greenstone belts. As for the lower oceanic crust, it would have been recycled into the mantle. If this mechanism were true, the upper oceanic crust could have been preserved in some places.

Some authors have pointed out that the formation of a thicker oceanic crust would result in an overburden pressure on the diapiric melt column. This increase in pressure would reduce the amount of melt produced at depth and thus constitutes a limit to the total thickness of oceanic crust produced by adiabatic melting (Vlaar and van den Berg, 1991; Korenaga, 2006). Fig. 2.13 shows that for reasonable mantle temperatures, this effect is small compared to uncertainties regarding adiabatic melt productivity and contribution of melt to the oceanic crust (Galer and Mezger, 1998). The Monte Carlo analysis performed in section 2.2.4 also shows that variations in oceanic crustal thickness of $\pm$ 2.5 km have relatively little influence on sea level.

Abbott and Hoffman (1984) argued that because there is no difference between the thickness of the oceanic crust produced at present-day fast spreading ridges (East Pacific Rise, 10-20 cm y^{-1}) compared to that produced at slow spreading ridges (Mid-Atlantic Ridge, 3 cm y^{-1}), there is no reason why the Archaean oceanic crust would be thicker than present-day oceanic crust. However, oceanic crustal thickness is controlled by the temperature at the mid-oceanic ridge and does not depend on spreading rate. If anything, the observation that the thickness of

oceanic crust produced at both of these mid-oceanic ridges is similar shows that melting occurs in near adiabatic conditions in both cases. Furthermore, because the rise of partially molten rocks at mid-oceanic ridges is passive, no correlation is to be expected between the temperature beneath a mid-oceanic ridge and the spreading rate of the ridge. In the case of very slow spreading rate, adiabatic melting does not occur which results in a magma poor mid-oceanic ridge.

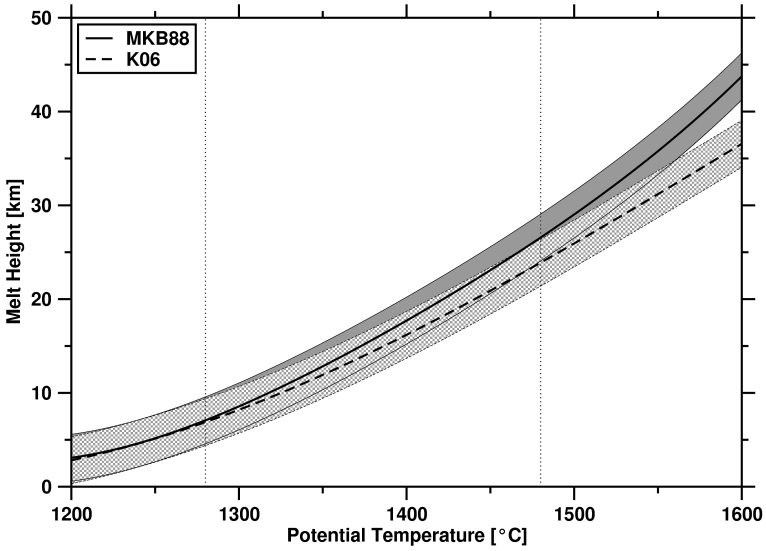

Figure 2.13: Effect of a hotter mantle on the thickness of oceanic crust. The results are shown for two models of adiabatic melting of a peridotitic mantle: McKenzie and Bickle (1988) and Korenaga (2006), allowing for errors of ± 2.5 km (following Galer and Mezger, 1998). Both models are within error of each other for temperature increases of up to 280 °C. Dotted lines: present-day mantle temperature and 200 °C increase in mantle temperature.

Arndt (1983) argued that if plate tectonics were to operate in the Archaean, the oceanic crust could not have been much thicker than at present, because a thick crust is positively buoyant and cannot be subducted. He assumed that because of higher mantle temperatures, the Archaean oceanic crust would have consisted of 50 % komatiite and 50% basalt. This value seems high since komatiites account for less than 15% of Eoarchaean rocks, and less than 6% in the rest of the Archaean. To justify this assumption, Arndt (1983) argued that komatiites erupted in continental domains do not reach the surface but are underplated because of their high density (2700 to 3000 kg m^{-3}). Assuming that in the Archaean, subduction occurred for an age of the ocean floor of 20 Myr and a lithospheric thickness of 40 km, Arndt (1983) calculated that the maximum thickness of the oceanic crust is 7 km if the oceanic lithosphere is to be negatively buoyant. This estimate increases to 9 km if the average age of subduction is 30 Myr. One important limit to this model is that on present-day Earth, the probability of subduction is approximately the same for any age (*e.g.* Sclater et al., 1981). There is thus no *a priori* reason why the average age of subduction would be two to three times lower than present in the Archaean.

Intrinsic density partitioning

The possibility that the composition and thickness of the Archaean oceanic crust was different leads to the concept of intrinsic density partitioning between the oceanic crust and lithospheric mantle (*e.g.* Nisbet and Fowler, 1983). If the potential temperature of the Archaean mantle was much higher than present, then the melt fraction would be greater, the oceanic crust thicker but also more mafic and the underlying mantle would be more depleted and thus lighter. Niu and Batiza (1991) proposed an empirical method, based on experimental data, to calculate the composition of melt produced at mid-oceanic ridges. Hynes (2001) used the results of Niu and Batiza (1991) to calculate the amount of mantle that must be depleted to produce an oceanic crust of known thickness and composition. This parametrisation also allows to calculate the density of the depleted mantle as a function of melt fraction. Since melt fraction is a function of temperature in the models of adiabatic melting of the mantle of McKenzie and Bickle (1988), the parametrisation of Hynes (2001) can readily be incorporated in our model. The evolution of the density of the depleted mantle and of the oceanic crust are shown in Fig. 2.14. For a mantle 200 °C hotter than present, the oceanic crust is 60 kg m^{-3} denser than present and the mantle is 30 kg m^{-3} lighter than present. This increases the ratio of oceanic to mantle density in Eq 2.1 and buffers the effect of a thicker oceanic crust on sea level. For example, the predicted increase in sea level for an oceanic crust 14 km thicker than present is reduced from 1250 m to 900 m. It should be noted that a change in mantle density affects all of the terms in Eq 2.1 so that the change in ridge depth is also buffered.

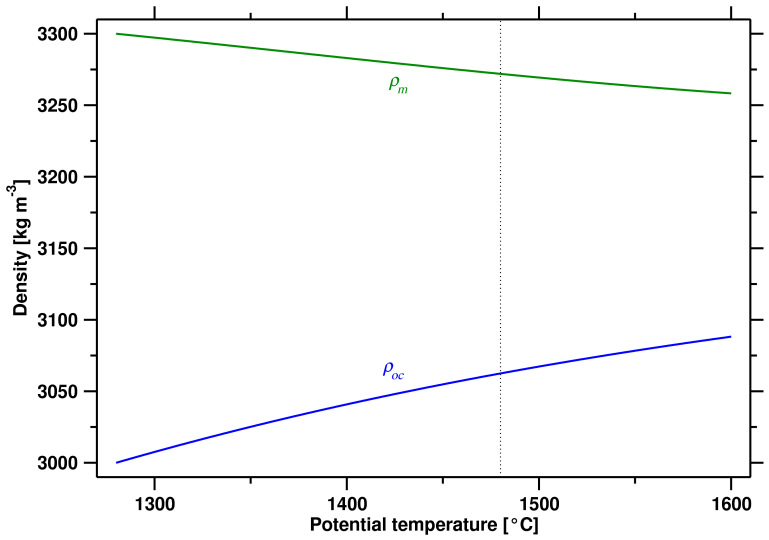

Figure 2.14: Evolution of the density of the oceanic crust (in blue) and of the underlying mantle (in green) as a function of potential temperature, according to the model of Hynes (2001).

The effect of a change in the intrinsic density of the oceanic crust and underlying mantle for the proposed Neoarchaean conditions is shown in Fig. 2.15. A drop in sea level of $\sim$ 200 m and an increase in the area of emerged land of $\sim$ 2% is predicted when the the intrinsic density

change is taken into account. This change is of the same order than the error of ± 200 m in the calculation of sea level associated with the uncertainty of ± 2.5 km in determining the thickness of the oceanic crust.

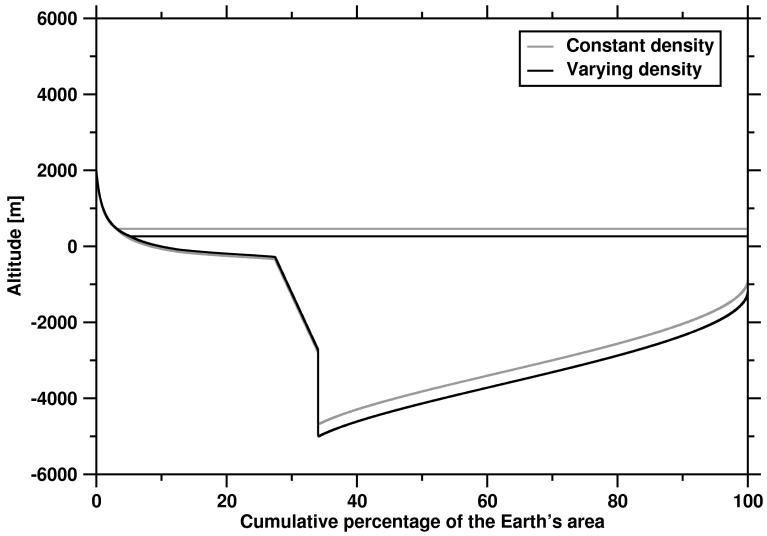

Figure 2.15: Calculated hypsometry, bathymetry and sea level for a late-Archaean configuration ($\sim$ 2.5 Ga, x =0.8, T_p = 1430°C) for the LJ07 model with t_{max} = 180 Ma. The grey lines are for constant densities of the mantle and oceanic crust, and the black lines are for a change in these density as described in Fig. 2.14.

If the change in oceanic crust and lithospheric mantle density can be estimated as a function of mantle temperature, the same is not true of the likely change in continental crust and lithospheric mantle. Flood volcanism on top of continental crust was more extensive in the Archaean, which would have resulted in a higher density of the continental crust. The increase in continental crustal density could potentially have been of the same order than that predicted for the oceanic crust (60 kg m^{-3}). As for the density of the continental root, it depends on the mechanism of root formation (see section 1.3.2). In the plume and arc thickening models, the negative thermal anomaly could be balanced by the chemical anomaly (depletion) from the onset. This is Jordan's "isopycnic" condition for buoyancy (*e.g.* Jordan, 1988). In the model of stacking of oceanic lithosphere, the craton would be negatively buoyant until some eclogitic material is lost to the mantle. In this last model, relative sea level would be high until isostatic re-equilibration. Overall, assuming the continental lithosphere to be neutrally buoyant, the initial density of the root can be assumed to be equal to that of surrounding mantle. Because the mantle cratonic roots are depleted and light, a long term uplift of cratons is expected as the asthenospheric mantle cools down and becomes denser. This long-term uplift was assessed to be of the order of 5 km from regional metamorphism by Galer and Mezger (1998) and is reflected in the present-day thickness of Archaean continental crust that is lower than the mean continental thickness.

In the discussions above, we have seen that even though the prediction of a thicker oceanic crust in the Archaean is theoretical, there is no strong argument that proves it wrong. The

intrinsic density partitioning of the oceanic crust and mantle predicted for higher mantle temperatures would potentially have been offset by a greater density of the continental crust.

2.3.2 Continental crustal thickening and emergence of the continents

Another assumption in the models presented in section 2.2 is the constancy of the thickness of the continental crust through time. This assumption is of importance because sea level is sensitive to the thickness of the continental crust. From Eq. 2.1, an increase of continental thickness of 5 km translates in a sea level drop of about 750 m. The performed Monte Carlo analysis confirms that sea level is sensitive to crustal thickness and that a thicker continental crust in the Archaean would result in lower sea levels. For this reason, previous workers have argued that to satisfy the constant freeboard hypothesis, Archaean continents had to be thicker than present-day continents (Nisbet, 1987; Harrison, 1994; Hynes, 2001).

However, seismological data show that Archaean continental crust is on average thinner than Proterozoic continental crust, not thicker (Durrheim and Mooney, 1994; Artemieva, 2009). According to (Durrheim and Mooney, 1994), Archaean crustal thickness ranges from 27 to 40 km with an average of about 35 km, while Proterozoic crustal thicknesses ranges from 40 to 55 km. Out of the two groups of cratons proposed by Artemieva (2009) and presented in section 1.1.2, the first group displays crustal thicknesses ranging between 32 and 40 km and the second group displays crustal thicknesses ranging between 40 and 50 km. This last range is similar to the range of Proterozoic crustal thicknesses proposed by Artemieva (2009). Galer and Mezger (1998) inferred from the regional metamorphism of ten undisturbed cratons that Archaean continental lithosphere had been uplifted by 5 $\pm$ 2 km since stabilisation. Taking this constraint into account, the average original thickness of Archaean continental crust of Durrheim and Mooney (1994) would be of $\sim$ 40 km, indistinguishable from the average thickness of Precambrian shields and platforms. The first group of Artemieva (2009) would have original thicknesses of 37 to 45 km, slightly thinner than Proterozoic continental crust, while the second group would be 45 to 55 km, within the range of Proterozoic continental crust. Palaeoproterozoic shields also display a relatively thick (140-220 km) and light (3330-3350 kg m^{-3} for all Proterozoic shields) continental lithosphere (Artemieva, 2009). The long-term uplift deduced for Archaean cratons would thus also also affect Proterozoic shields to some extent. The original crustal thickness of cratons from the second group of Artemieva (2009) was thus probably of similar thickness to Proterozoic shields.

Durrheim and Mooney (1994) suggested that the difference between Archaean and Proterozoic crustal thicknesses could be due to the eruption of continental flood basalts (CFBs). Notably, a peak in global magmatic activity at 2.7 Ga $\pm$ 0.05 Ga resulted in the eruption of CFBs 5-15 km thick covering a total area larger than 10^7 km^2 over most, if not all, Archaean cratons. As we shall see in the next chapter, the effect of this "instantaneous" crustal thickening was likely buffered by gravity-driven lower crustal flow. For this reason, we illustrate the minimum thickening of 5 km in Fig 2.16. All other parameters being constant, this thickening

translates into a drop in sea level of $\sim$ 500 m and an increase in the area of emerged land of about 12% of the Earth's surface. An increase in crustal thickness towards the end of the Archaean as suggested by some, but not all, seismological data would thus have significantly contributed to the late-Archaean emergence of the continents.

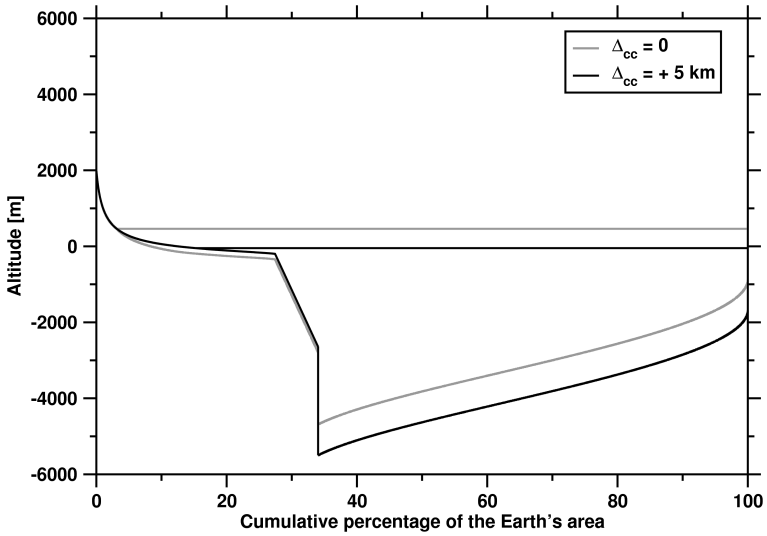

Figure 2.16: Calculated hypsometry, bathymetry and sea level for a late-Archaean configuration ($\sim$ 2.5 Ga, x =0.8, T_p = 1430°C, h_{max} = 3615 m) for the LJ07 model with t_{max} = 180 Ma. The grey lines are for constant crustal thickness and the black lines are for a continental crust 5 km thicker.

2.3.3 Depth of ridgecrests and oceanic volume through time

As briefly discussed in the conclusion of section 2.2, Kasting and Holm (1992) proposed a feedback mechanism between the depth of mid-oceanic ridges and oceanic volume through time. They argued that the penetration depth of hydrothermal processes is smaller for shallower mid-oceanic ridges, resulting in a lower amount of water returned to the mantle by subduction processes. This causes the accumulation of water at the Earth's surface and in turn an increase in the depth of ridgecrests. The present-day depth of fast-spreading mid-oceanic ridges of $\sim$ 2500 m is close to the critical ridge depth of 2400 m from which hydrothermal penetration reaches its optimal value of 5000 m Kasting et al. (2006b). Kasting and Holm (1992) suggested that this was not a coincidence and that the volume of the oceans increased until the optimal ridge depth for hydrothermal penetration was reached.

The models presented in section 2.2 allow to calculate the depth of ridgecrest as a function of mantle temperature and of continental area (Fig. 2.17). For Archaean conditions, ridgecrests are found to be shallower than present for all models. How much shallower depends on the thermal model: the BLT model in which spreading rates are most sensitive to mantle temperature (Fig. 2.5) gives ridgecrests 300 to 700 m shallower than present for Archaean conditions. In contrast, the K06 model that predicts slower spreading rates in the Archaean (Fig. 2.5) gives

ridgecrests 1100 to 2000 m shallower than present for Archaean conditions. The preferred thermal model LJ07 gives ridgecrests 1200-2200 m shallower than present for a constant maximum age of oceanic floor and 800 to 1600 m shallower than present for a maximum age of the oceanic floor of 104 Myr. The calculated depth of Archaean ridgecrests is thus highly dependent on the rate of seafloor spreading.

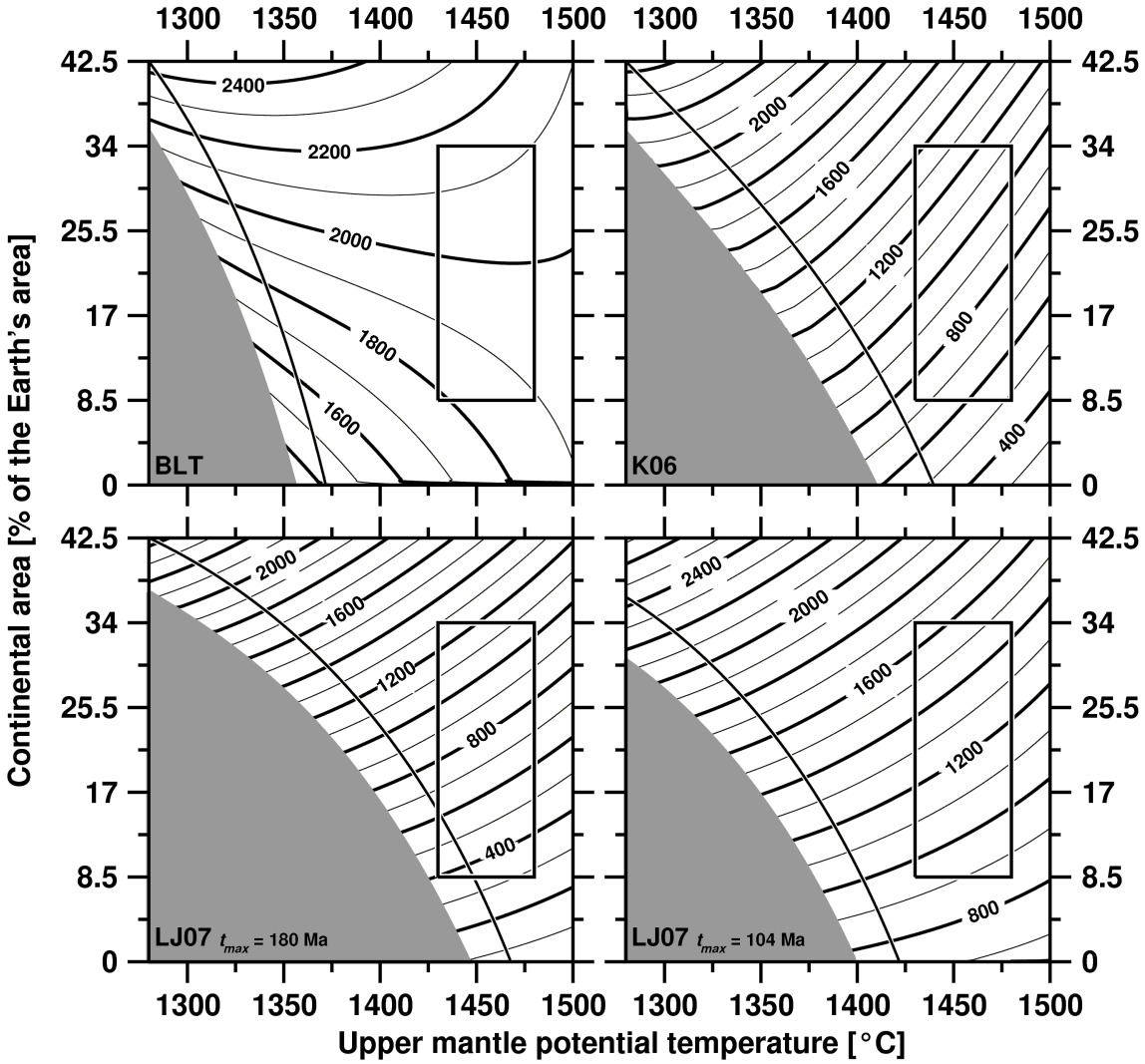

Figure 2.17: Contours of the depth of mid-oceanic ridges (in m) as a function of continental area and mantle temperature for present-day hypsometry. Results are presented for each of the models discussed in chapter 2. The shaded area in each diagram shows the conditions within which the continental slope would emerge. The thick black lines are the contours of constant continental freeboard. The boxes show the range of Archaean conditions (see Fig. 2.7).

Assuming that the subduction of young, hot oceanic crust was more common in the Archaean, several changes in the subduction zone water cycle might have reinforced the feedback mechanism suggested by Kasting and Holm (1992). Hacker et al. (2003b) showed from thermo-petrologic models of subduction zones that the lower seismic zone observed in subduction zones at depths

of up to 50 km within the bending plate is the result of serpentine or chlorite dehydration. Rupke et al. (2004) pointed out that this implies that the shallow ($\sim$ 5 km) penetration depth of sea water might not be the limiting factor for slab hydration (serpentinisation). If this is true, it would largely invalidate the model of Kasting and Holm (1992) in which slab hydration is assumed to depend on hydrothermal penetration. Rupke et al. (2004) proposed that the limiting factor for slab hydration is the depth of the 600°C isotherm, since serpentine is not stable at higher temperatures. Because the depth of the 600°C isotherm depends on the age of the plate and on the potential temperature of the upper mantle, warmer and younger subducting slabs are less hydrated than cold slabs. Moreover, the numerical models of water cycle at subduction zones of Rupke et al. (2004) show that the loss of water of a warm subducting slab to the mantle wedge is greater than that of a cold subducting slab. This implies that less water is returned to the mantle during the subduction of younger and/or warmer slabs. Wyman et al. (2008) built numerical models of subduction zones in which a flat subduction geometry is imposed to inspect the consequences of flat subduction on slab dehydration. While largely illustrative, these models show that the slab would release most of its water to the mantle wedge that is isolated from the mantle in a flat subduction context. If flat subduction was more common in the Archaean, little water would have been returned to the mantle.

If the subduction of hotter, younger slabs was common in the Archaean, the return of water to the mantle would have been reduced because of shallower hydrothermal penetration, lower slab water content and greater water loss during subduction. The depth of the 600°C isotherm in oceanic lithosphere may be the limiting factor for the water content of the slab, rather than the hydrothermal penetration depth. Either model suggests an increasing oceanic volume at the surface of early Earth. This increase is expected to be faster if the oceanic lithosphere is actually hydrated over a thickness of $\sim$ 50 km.

2.3.4 Effect of supercontinents on the area of emerged land

The effect of the formation of a supercontinent on sea level was not discussed in section 2.2. As rigid plates move at the surface of the Earth, continents collide, aggregate to form supercontinents before to break-up. Although the process is transient, the aggregation of supercontinents and their break-up have an impact on sea level. Continental collision leads to higher elevations and thicker continental crust, and to the destruction of continental margins which results in a reduced continental area. Because each of these processes implies a lower sea level, the formation of a supercontinents is expected to trigger an increase in the area of emerged land.

Although the evidence is not unequivocal, supercontinents have been proposed in the Neoarchaean. Bleeker (2003) proposed that two supercratons "Superia" (Superior Province, Baltic Shield, and possibly the Wyoming Craton) and "Slavia" (Slave, Dharwar, Zimbabwe and possibly the Wyoming Craton) existed during the Neoarchaean, and one supercraton, "Vaalbara" (Kaapvaal and Pilbara) existed during the Mesoarchaean. Aspler and Chiarenzelli (1998) proposed two Neoarchaean continents based on Palaeoproterozoic geochronological data: "Zimvaal-

bara" that includes the Zimbabwe, Kaapvaal, Pilbara, and Saõ Francisco cratons and "Kenorland" (first proposed by Williams et al., 1991, who noticed similarities between North American cratons) that consists of Superior and Slave Provinces, Wyoming and North Atlantic cratons and Baltic and Siberian Shield. These reconstructions rely on first order geochronological and stratigraphic similarities between different cratons. The fact that the Wyoming and Zimbabwe cratons are included in different supercratons depending on studies leaves the possibility of a single Neoarchaean continent open.

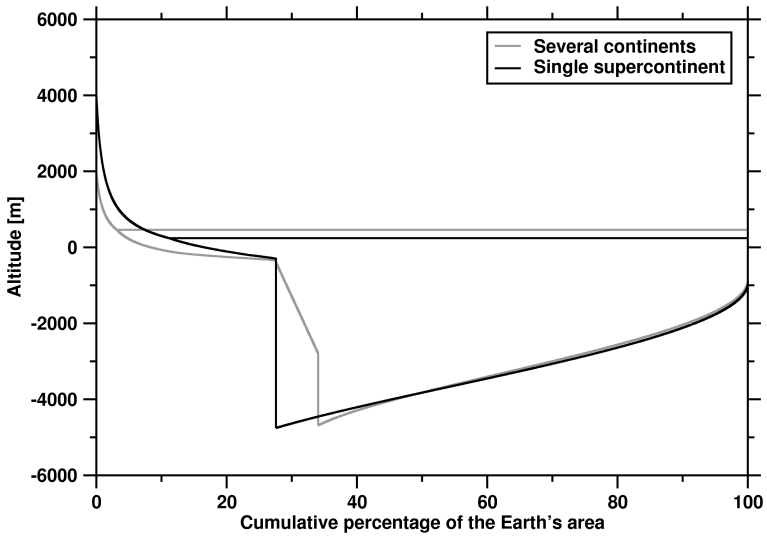

Figure 2.18: Calculated hypsometry, bathymetry and sea level for a late-Archaean configuration ($\sim$ 2.5 Ga, x =0.8, $T_p = 1430^{\circ}$C) for the LJ07 model with $t_{max} = 180$ Ma. The grey lines are for a configuration with several continents and the black lines are for a single supercontinent.

Harrison et al. (1981) proposed a theoretical hypsometric reconstruction for the last supercontinent Pangaea. Assuming that all present-day continents were joined together, they calculate an average elevation of Pangaea. We apply these results to propose a theoretical hypsometric curve for a possible single Archaean supercontinent. In doing this, we assume that the Neoarchaean lithosphere was strong enough to maintain high elevations. The ratio of Kenorland to Archaean maximum elevation ($\sim$ 3600 m, see 2.2.4) is taken equal to the ratio of Pangaea ($\sim$ 1700 m) to present-day maximum elevation (8850 m). This gives a maximum elevation of 6950 m for the Neoarchaean supercontinent. To illustrate an extreme case, we assume continental margins to be completely absent in the supercontinental configuration. This is an over-estimation since some continental margins would be preserved during supercontinental aggregation. Fig. 2.18 shows that the formation of a Neoarchaean supercontinent would result in a drop in sea level of $\sim$ 200 m and an increase in emerged area of 8%. This estimate is a minimum since no change in crustal thickness has been taken into account. Furthermore, 2D and 3D convection numerical models by Coltice et al. (2007) and Coltice et al. (2009) suggest that continental aggregation imposes a reorganisation of convective flow that results in an increase of temperature of up to 100°C below a supercontinent. This would impose a positive dynamic topography on the

supercontinent and result in lower relative sea levels.

The formation of supercratons or of supercontinents in the Archaean would have resulted in larger areas of emerged land and could partially account for the occurrence of clastic sediments observed in the Archaean geological record (Nisbet, 1987, see also sections 1.5 and 1.5). The break-up of these putative supercontinents, however, would have triggered an increase in continental margins and in relative sea-level.

2.4 Conclusion

In this chapter, we identified the mechanisms controlling the secular evolution of sea level. These are the thickness of the oceanic crust, the bathymetry of the ocean floor, and the growth of the continental crust. The thickness of the oceanic crust and seafloor bathymetry both depend on the temperature of the mantle. These thermal mechanisms outbalance the effect of crustal growth so that a constant sea level (freeboard) through time is possible only if the upper mantle never exceeded its present-day value by more than 110-210°C. We also showed that ridgecrests were shallower in the Archaean than at present. Because of a feedback mechanism between ridge depth and oceanic volume, this could have resulted in an increase of the volume of oceans during the first part of the Eoarchaean, until a constant volume of oceans was reached at around 3.8 Ga.

The models presented also allow to estimate the area of emerged land by modelling continental hypsometry. We show that the area of emerged land was less than $\sim 15\%$ of the Earth's surface in the Archaean. Considering that mountain building processes could have been less efficient in the Archaean because the continental crust was hotter, we suggest that the maximum elevation in the hypsometric curve would have been lower than at present. Taking this into account, we show that the area of emerged land could have been reduced to 2-3% of the Earth's surface in the Archaean. Crustal strengthening and/or crustal thickening in the Neoarchaean would have resulted in the emergence of the continents around the Archaean/Proterozoic boundary. In the next chapter, we will focus on the consequences of a hotter crust for its ability to support a load such as a continental flood basalt.

3

Crustal ductility and submerged Archaean continents

Contents

3.1 Characteristics of the deformation of hot continental crust

3.1.1 Ductile continental crust in the Archaean and in the Phanerozoic

We have seen in section 1.2.3 that the occurrence of crustal diapirism at a significant strain rate in the Archaean indicates the deformation of ductile, low viscosity continental crust. Another observation unique to the Archaean is the subaqueous eruption of flood basalts up to 15 km-thick on top of continents. Arndt (1999) underlined that the chemistry of many subaqueous Precambrian magmatic provinces reveals contamination by differentiated material. This advocates for the eruption of these magmatic provinces on top of pre-existing (proto-?) continental crust and for their classification as continental flood basalts (CFBs), and argues against an allochtonous origin of the magmatic provinces such as predicted by the obduction of oceanic crust. Examples of Archaean subaqueous CFBs include the $\sim$ 14 km, 3.49-3.3 Ga Warrawoona Group, Pilbara Craton (Van Kranendonk et al., 2004a), the $\sim$ 5 km-thick, *c.* 2.9 Ga mafic volcanics of the Witch Bay Formation, Steep Rock Group in the Superior Province (Tomlinson et al., 1999), the 12 ± 2 km-thick, 2.72-2.70 Ga tholeiites and komatiites of the Eastern Goldfields, Yilgarn Craton (Barley, 1998), and the 2.77-2.63 Ga, 6.5 km-thick Fortescue Group in the Pilbara Craton (Thorne and Trendall, 2001). The mafic rocks from the Warrawoona Group show little contamination from continental crust (Arndt, 1999) but were emplaced on top of the oldest identified emerged continental block (Buick et al., 1995, see section 1.5).

As discussed in the previous chapter, the fact that thick basaltic piles emplaced on top of continental crust failed to emerge suggests higher sea levels in the Archaean. However, we have seen in section 2.2.4 that in the late-Archaean, continents could have been flooded by $\sim$ 1.1 km of water. This is significantly less than the thickness of the magmatic provinces mentioned above. Even in an extreme case, assuming early crustal growth and a mantle $\sim$ 300 K hotter than present, the maximum sea level change is 6 km (see Tab. 2.1). We shall see in the next chapter that such a large change in sea level is unlikely. It would not anyway explain the subaqueous eruption of CFBs thicker than 6 km. A dynamical process is thus required to explain this observation. One possible mechanism to prevent crustal thickening and to explain the accommodation of thick CFBs is gravity-driven lower crustal flow of a ductile continental crust. Indeed, lower crustal flow is suggested by the flat Moho observed on some Archaean seismic profiles (Mareschal and Jaupart, 2006). The observation of Kump and Barley (2007) that all post-Archaean CFBs are subaerial, as opposed to Archaean CFBs suggests that post-Archaean continental crust was stronger than Archaean continental crust and could sustain the load imposed by thick CFBs.

On present-day Earth, the active deformation of hot continental crust is best defined in Tibet, in the Andean Altiplano and in the Basin and Range province of the western USA. England and McKenzie (1982) suggested from thin sheet modelling that when averaged in space and time, the deformation of the Himalayan belt could be approximated by viscous homogeneous deformation of the continental crust. Royden (1996) proposed that a low viscosity layer under the Tibetan

plateau would explain the absence of surface shortening on the plateau itself, and the presence of a zone of upper crustal extension along the southern edge of the plateau (South Tibetan Detachment System). In this major collisional area, the continental crust is up to $\sim$ 70 km thick. This crustal thickening results in a large radiogenic heat production which translates into elevated Moho temperatures and explains the presence of a low viscosity layer. The South Tibetan Detachment System expresses the accommodation of upper crustal extension, due to gravitational forces, in a convergent regime. To explain the observed crustal thickness of 60 to 65 km under the Altiplano plateau in the the absence of upper crustal shortening, Husson and Sempere (2003) proposed that crustal thickening of the flanking Western and Eastern Cordilleras triggered lower crustal flow that added crustal material to the Altiplano plateau. Finally, Gans (1987) proposed a model in which the middle and lower crust act as a ductile, flowing layer to explain the observations of uniform crustal thicknesses and the absence of Moho relief in the direction of extension across the eastern Basin and Range province. The Basin and Range Province was formed by the collapse of an initially thick continental crust (between 50 and 60 km in the model of Gans, 1987). In this case, high crustal temperatures are explained by the originally thick continental crust and by the high mantle heat flow associated with lithospheric extension.

Sonder et al. (1987) suggested that continental lithospheres with Moho temperature higher than $\sim 700 \pm 100$°C are too weak to support large topographic gradients. On present-day Earth, flow of hot lower continental crust occurs in place where crustal temperatures are anomalously elevated because of crustal thickening associated with orogenies or because of high mantle heat flow associated with lithospheric extension. In the Archaean, when radiogenic heat production was two to four times greater than present, crustal temperatures would have been higher without significant thickening. The temperature of the mantle would also have been greater. What would have been the consequences of higher crustal and mantle temperatures on crustal dynamics and on mountain building processes?

3.1.2 The forces that drive plate tectonics

Harrison (1994) proposed that mountain building would have been greater in the Archaean because of a greater radiogenic heat production within the Earth. His reasoning goes as follows: mountain building is produced by seafloor spreading in continental collisions and at island arcs. Because more radiogenic heat had to be lost from the mantle in the Archaean, seafloor spreading was faster and mountain building was thus greater. This implies that the forces driving plate tectonics, slab pull and the ridge push, were of greater amplitude in the Archaean. This is a big assumption. To the first order, the forces that drive plate tectonics are counter balanced by friction with the mantle. This can be written as

$$F_{rp} + F_{sp} = \mu\, u\,, \tag{3.1}$$

where F_{rp} is the ridge push, F_{sp} is the slab pull, μ is the viscosity of the mantle and u is the spreading rate. Contrary to the statement of Harrison (1994), it is not obvious that spreading rates were faster in the Archaean (Fig. 2.5). Indeed, Korenaga (2006) proposed a model of sluggish plate tectonics for a hotter mantle, and Labrosse and Jaupart (2007) proposed an empirical thermal evolution model because past spreading rates are poorly constrained. As for the viscosity of the mantle, it exponentially depends on mantle temperature T so that $\mu \propto exp(E_a/RT)$, where E_a is an activation energy and R is the gas constant. Because of the high dependency of viscosity on mantle temperature, the right hand side term in Eq. 3.1 will be smaller in the Archaean when the mantle was hotter. Contrary to Harrison (1994), we suggest that the forces that drive plate tectonics were of smaller amplitude in the Archaean, so that mountain building processes were less efficient rather than more efficient.

The estimation of slab pull as a function of mantle temperature is not straightforward. The slab pull depends on the buoyancy of the plate that itself depends on its age. Since spreading rates and the age distribution are not know in the past, the Archaean slab pull cannot be readily quantified. Qualitatively, the subduction of a thick, buoyant oceanic lithosphere would probably result in a smaller amplitude of slab pull compared to the present.

As for the ridge push, it can be written as follows (Turcotte and Schubert, 1982, Eq. 6-405):

$$F_{rp}(t) = g\,\rho_m\,\alpha\,(T_p - T_0)\left[1 + \frac{2}{\pi}\frac{\rho_m \alpha (T_p - T_0)}{\rho_m - \rho_w}\right]\kappa\, t_s, \tag{3.2}$$

where $g = 9.81$ m s^{-2} is the acceleration of the gravity field and other parameters are as defined in Tab. 2.2. This expression is valid for conventional parametrised models in which the subduction potential is estimated from boundary layer theory. In the empirical model of Labrosse and Jaupart (2007), the average ridge push can be calculated from the age distribution as

$$\overline{F_{rp}} = \frac{\int_0^{t_{max}} F_{rp}(t)\frac{dA}{dt}dt}{\int_0^{t_{max}} \frac{dA}{dt}dt}\ . \tag{3.3}$$

The results of calculations of the ridge push, normalised to present-day, as a function of mantle temperature are shown in Fig. 3.1. In the model BLT, the ridge push decreases with mantle temperature since the spreading rate increases with temperature (Fig. 2.5). On the contrary, the ridge push increases with mantle temperature in the model K06 that predicts sluggish plate tectonics for high mantle temperature (Fig. 2.5). In the model LJ07, the average ridge push calculated from Eq. 3.3 is a linear function of mantle temperature since the expression in Eq. 3.2 is integrated over the age of the lithosphere.

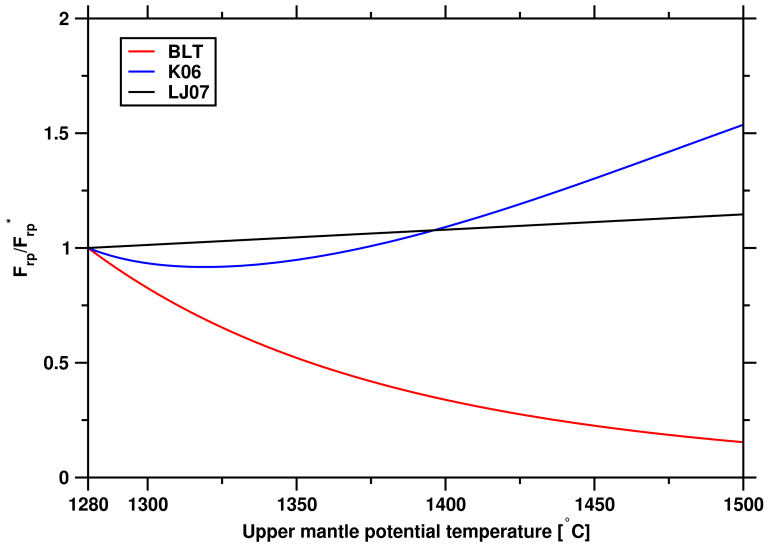

Figure 3.1: Ridge push calculated as a function of mantle temperature for the three thermal evolution described in section 2.2. Results are normalised to present-day.

As expected, the ridge push is most sensitive to mantle temperature in the model BLT in which spreading rate is highly temperature dependent. This model predicts a four fold decrease in ridge push for an increase in mantle temperature of 150°C. For the same increase in mantle temperature, the model K06 predicts a ridge push 20% larger than present, and the model LJ07 a ridge push 10% larger than present. The model BLT results in a thermal catastrophe and can be rejected on this ground. It is thus possible that the ridge push was 10 to 20% larger in the Archaean. Since the forces that drive plate tectonics were overall probably of smaller amplitude in the Archaean than at present, this greater ridge push could have been compensated and exceeded by a lesser slab pull. It is also important to stress that Eq. 3.2 is a simplified calculation of the ridge push. For instance, this calculation does not depend on the thickness of the lithosphere that would have been smaller in the Archaean, because of a hotter mantle. This would tend to decrease the ridge push calculated in the Archaean, and could potentially cancel out the effect of a higher temperature described in Eq. 3.2.

In summary, contrary to the statement of Harrison (1994), it is not obvious that spreading rates were faster in the Archaean, nor that the forces that drive plate tectonics were larger. On the contrary, we argue that a hotter mantle would result in lesser forces driving plate tectonics. Finally, and importantly, the reasoning of Harrison (1994) does not account for expected changes in crustal dynamics for a greater radiogenic heat production in the continental crust.

3.1.3 Importance of crustal temperatures for mountain building processes

We have seen in section 3.1.1 that crustal flow can be associated with thickening of the continental crust on present-day Earth. England and Bickle (1984) argued that crustal thickening as important as observed in present-day Tibet could have occurred in the Archaean. Their

argument is based in the assumption that the exhumation of high-grade metamorphic terranes occurs by erosion following instantaneous thickening. However, as discussed in section 2.2.4, other processes that do not require the thickening of a strong, cold continental crust can result in the exhumation of high metamorphic terranes. Independent constraints on Archaean mountain building, such as palaeoaltimetry proxies, would be needed for the argument to be convincing. However, the preservation of signals related to palaeoaltimetry in terranes that have been exposed to erosion for billion of years is unlikely. Palaeoaltimetry proxies include basalt vesicularity, stomatal density of fossil leaves, terrestrial cosmogenic nuclides and stable isotopes of paleolakes (Clark, 2007). While basalt vesicularity could in theory be applied to the Archaean, fossil leaves are obviously ruled out, cosmogenic nuclides present half-lives (about 1 Myr) considerably too short to be used in the Archaean and original stable isotopic signatures would likely have been overprinted.

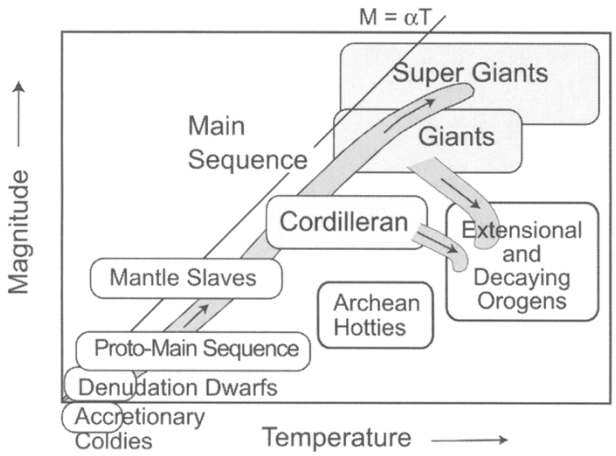

Figure 3.2: Classification of orogens types in a temperature-magnitude diagram. From Beaumont et al. (2006).

Indeed, the critical factor controlling the behaviour of colliding continental lithospheres is their thermal state. Beaumont et al. (2006) proposed a classification of orogens as a function of their temperature and of their magnitude (Fig. 3.2). This classification is inspired by the Hertzsprung-Russell diagram in which the luminosity of star populations is plotted against their surface temperature. In the diagram of Beaumont et al. (2006), the temperature of the orogen represents the excess heat content of the orogen relative to that of undeformed standard continental lithosphere, and the magnitude of the orogen represents the excess crustal or lithospheric thickness. Beaumont et al. (2006) pointed out that because the temperature increases disproportionately faster than the corresponding crustal thickening during continental collision, orogens plot below the line $M = \alpha T$, where M is the magnitude, T the temperature and α is defined for undeformed standard continental lithosphere. Keeping in mind that this diagram is largely qualitative and illustrative, it is worth noting that the magnitude of Archaean orogens proposed in Fig. 3.2 is lower than that of modern orogens. In the Archaean, because of a larger radiogenic heat production, crustal temperatures would increase faster than at present upon thickening.

We shall discuss in the next paragraph how this large crustal temperatures in the Archaean would limit crustal thickening, this is to say the magnitude of the orogen in the definition of Beaumont et al. (2006).

3.1.4 Mountain building processes in the Archaean

Based on the hypothesis of a hotter continental crust in the Archaean, Bailey (1999) proposed a model of gravity-driven continental overflow in which ductile middle and lower continental crust flow over adjacent oceanic basins. However, these considerations are based on potential gravitational energy arguments and remain to be tested in dynamical numerical experiments. Rey and Houseman (2006) compared the collisional behaviour of Phanerozoic and Archaean continental lithospheres predicted by triaxial numerical experiments. The main differences between their reference Phanerozoic and Archaean continental lithospheres are the temperature profile and the density profile: Archaean continental lithosphere is hotter and presents a lighter subcontinental lithospheric mantle. To evaluate the role of gravitational forces in lithospheric deformation, Rey and Houseman (2006) used the ratio of locally variable gravitational stress to lithospheric strength. In the Archaean, lithospheric strength is reduced because of higher crustal temperatures, and the gravitational stress associated with crustal thickening is larger in the upper lithosphere because the lithospheric mantle is lighter. This results in a greater role of gravitational forces for Archaean continental lithosphere compared to Phanerozoic continental lithosphere. Rey and Houseman (2006) concluded that in the Archaean, lateral gravitationally driven crustal flow prevented any significant thickening of the continental lithosphere.

Rey and Coltice (2008) built onto the work of Rey and Houseman (2006) to propose a secular evolution of the plateau elevation reached by a continental lithosphere in a context of ongoing collision. They estimated steady-state continental geotherms for different geological ages using the present-day radiogenic composition of Archaean cratons as reference, and conventional convection parametrisation to estimate the heat flow beneath continents through time. This allowed them to estimate the plateau elevation reached by an orogen as a function of Moho temperature (Fig. 3.3). Their numerical experiments suggest that the lithospheric strengthening that enabled continental lithosphere to support high elevations and ultimately allowed the continents to emerge occurred during the Neoarchaean (Fig. 3.3). The results of Rey and Coltice (2008) were used by Flament et al. (2008) to propose an Archaean orogenic hypsometric curve.

The ductile behaviour of continental crust in hot orogens is expected to result in homogeneous lithospheric deformations distributed over large areas, as opposed to the strain localisation along large scale thrusts observed in cold orogens. This is consistent with the lack of crustal scale thrusts, with the widespread occurrence of craton-scale strike-slip fault, with the observation of regional finite strain fields with similar characteristics over several hundred of kilometres in Archaean terranes (Rey and Houseman, 2006, and references therein), and with the low and homogeneous regional erosion level of 5 ± 2 km recorded across undisturbed Archaean cratons (Galer and Mezger, 1998). Finally, Duclaux et al. (2007) predicted from numerical modelling

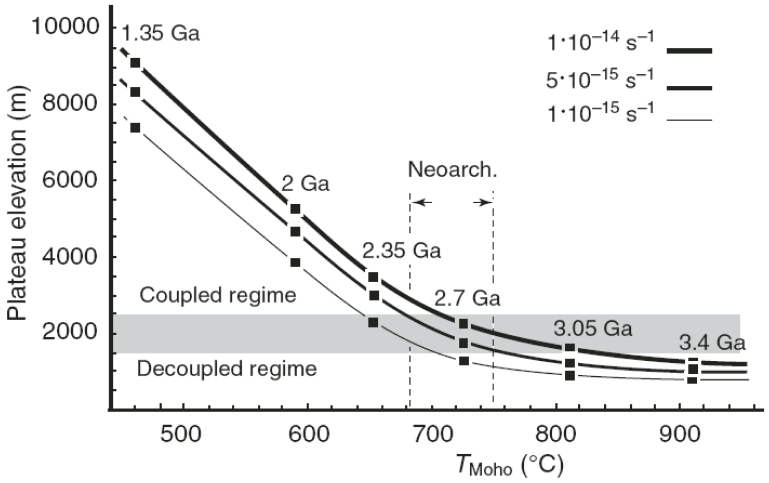

Figure 3.3: Plateau elevation calculated as a function of Moho temperature for a continental lithosphere in a context of ongoing convergence. Results are shown for three convergence rates. From Rey and Coltice (2008).

the existence of a phase of constrictional flow perpendicular to the direction of convergence during the gravitational collapse of hot orogens, and observed structural features associated with this process in the Gawler and Terre Adélie cratons. This constitutes further evidence for hot crustal deformation in the Archaean. It should nevertheless be noted that hot orogens did not occur exclusively in the Archaean but that the change from predominantly hot orogens to predominant cold orogens was likely gradual. For instance, Cagnard et al. (2008) reported both "Archaean-like" (with a prevailing contribution of gravitational forces) and "modern-like" (with strain localisation along thrust systems) orogens from the Palaeoproterozoic, and suggested that the transition from predominant "Archaean-like" orogens to predominant "modern-like" orogens was probably gradual in space and time. Gravitationally driven processes still play an important role in the evolution of modern orogens, and particularly in the final stage of collapse (decaying orogens in Fig. 3.2).

On present-day Earth, the deformation of hot continental crust is essentially associated with transient hot continental geotherms in places where the continental crust is anomalously thick or thin. Continental geotherms would likely have varied in different areas in the Archaean, as reflected by the preserved diversity of Archaean continental lithosphere (Artemieva, 2009, see also section 1.1.2). Nevertheless, Archaean continental geotherms would likely have been hotter on average because of a greater radiogenic heat production. This is illustrated by crustal diapirism and subaqueous continental flood basalts in the Archaean. In this chapter, we will propose a method to evaluate the continental geotherm in the Archaean. This method associates the numerical modelling of a rheological pile to the relaxation time of a continental flood basalt deduced from field observations. A case-study of the Fortescue Group in the East Pilbara Craton will be presented.

3.2 Structure of the Fortescue Group in the East Pilbara Terrane

3.2.1 Overview of the geology of the Pilbara Craton, Western Australia

The Pilbara Craton is one of the best-studied cratons because it is easily accessible, it has suffered relatively little deformation since stabilisation and offers good outcropping conditions. Over a billion year of Archaean geology is recorded with little interruption in the Pilbara Craton, from $\sim$ 3.6 Ga until $\sim$ 2.3 Ga. Low grade ($<$ 500°C, $<$ 0.3 GPa) regional metamorphism affected basalt flows in the Fortescue Group, possibly controlled by burial depth (Smith et al., 1982). In the North Pilbara Craton, metamorphic conditions associated with burial were limited to between 100 and 300°C and 0.05-0.12 GPa (Smith et al., 1982).

Because of this moderate thermal overprinting, the Pilbara Craton has been extensively studied in the quest for early life. Stromatolites were first described in the 3.43 Ga Strelley Pool Chert in the North Pole area by Walter et al. (1980), who suggested they were organo-sedimentary structures built by the activity of micro-organisms. However, Grotzinger and Rothman (1996) pointed out that ancient stromatolites are rarely associated with fossil microbes, and showed analytically that they could be abiotic structures essentially built by chemical precipitation. Schopf and Packer (1987) identified putative microfossils from optical photomicrograph in the $\sim$ 3.4 Ga Apex Basalt and Towers Formation, and Rasmussen (2000) reported further microfossil remains from the $\sim$ 3.2 Ga volcanic massive sulphide Sulphur Spring deposit in the same area. None of these putative fossils are associated with stromatolitic structure, and the obvious concern regarding the antiquity of these microfossils is subsequent contamination. One notable example from the Pilbara are molecular fossils from hydrocarbon-rich shales of the $\sim$ 2.69 Ga Jeerinah Formation and of the Maddina Formation that were proposed to be the earliest biomarkers of Eukaryotes (500 million to one billion year before the widespread appearance of Eukaryotes in the fossil record Brocks et al., 1999), before a reassessment of the evidence by (Rasmussen et al., 2008) who showed that the fossils were younger than peak metamorphism at 2.2 Ga. On the contrary, the microbial origin of the stromatolites of the Tumbiana Formation proposed by Buick (1992), was recently confirmed by the identification of organic globule clusters and aragonite nanocrystals within the thin layers of the stromatolites by Lepot et al. (2008). Because the identification of microfossils is subject to debate, the quest for early life has essentially shifted to the identification of isotopic fractionations due to microbial activity. A recent example from the Pilbara is the identification of sulfur anomalies in the 3.49 Ga Dresser Formation attributed by Philippot et al. (2007) to the activity of sulfur-disproportionating micro-organisms.

The geology of the Pilbara Craton is also spectacular on a structural point of view. The 3.5 to 3.2 Ga East Pilbara Granite Greenstone Terrane (EP) is one of the best preserved examples of Archean dome and basin structures formed by gravity-driven overturn of the crust (see section 1.2.3). These structures are best represented in radiometric images that allow for the representation of surface rocks as a function of their content in radiogenic elements and results in

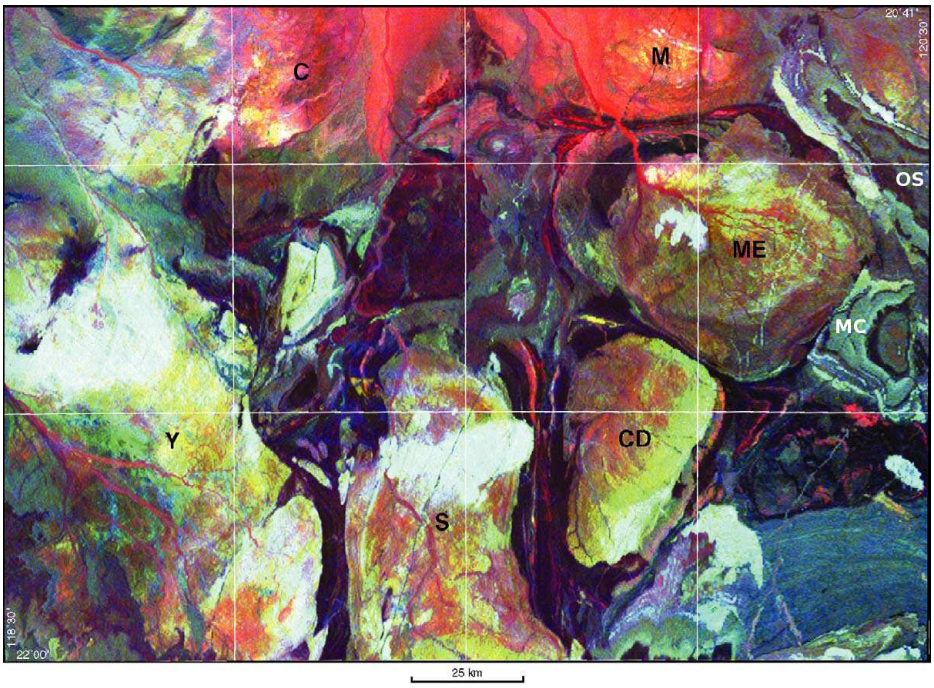

Figure 3.4: Ternary radiometric image of the East Pilbara Granite Greenstone Terrane showing potassium in red, thorium in green and uranium in blue. The dome and basin structure consists of the circular to ovoid granitoid complexes (yellow to orange)and the of the flanking greenstone belts in dark colours, with beds of felsic volcanic rocks as bright yellow to orange bands. The synclinal outliers of the Fortescue Group (in pale brown to beige colours) are preserved between domes, including the bright bullseye pattern defined by the Meentheena Centrocline (MC) and the Oakover Syncline (OS). C: Carlindi, CD: Corunna Downs, M: Muccan, ME: Mount Edgar, S: Shaw, Y: Yule. Figure from Van Kranendonk et al. (2004a).

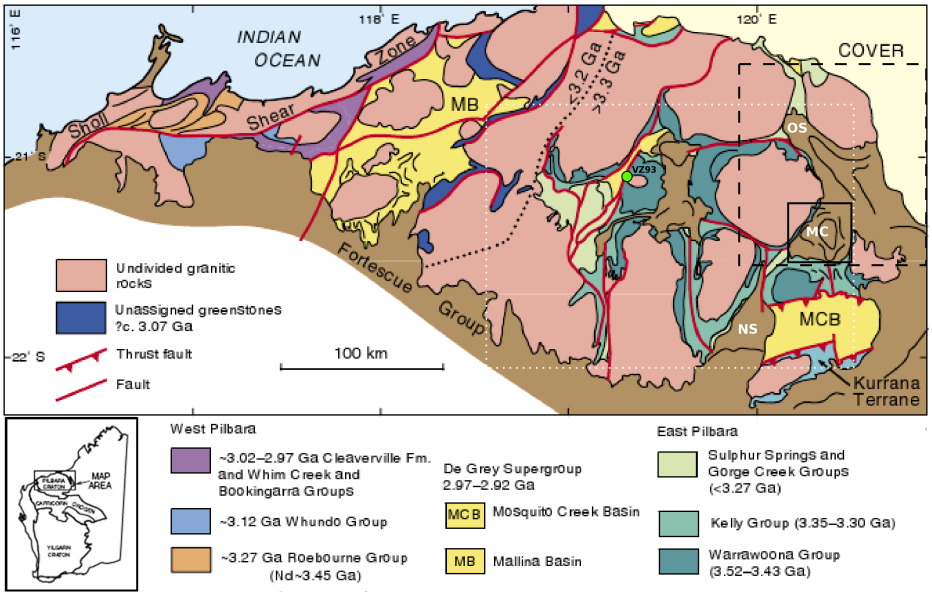

Figure 3.5: Simplified geology of the northern Pilbara Craton showing the main tectonic subdivisions (from Van Kranendonk et al., 2004b). The white dotted rectangle indicates the approximate extent of Fig. 3.4, the plain black rectangle that of Fig. 3.11 and the dashed rectangle that of Fig. 3.6. MC: Meentheena Centrocline, NS: Nullagine Synclinorium, OS: Oakover Syncline.

a sharp contrast between felsic and mafic rocks (Fig. 3.4). In stark contrast, horizontal tectonics possibly dominated from 3.2 Ga in the fault-bounded West Pilbara Granite Greenstone Terrane (WP). Smithies et al. (2007) proposed that the *c.* 3.12 Ga Whundo Group represents the oldest arc-type greenstone and thus the oldest evidence for steep subduction at a convergent margin. The main arguments in favour of a subduction setting for the WP are the observation of enriched geochemical signatures that cannot be attributed to crustal contamination and could thus tentatively be attributed to interaction with a mantle wedge, and the systematic observation of Nd model ages younger than 3.2 Ga in rocks to the west of the dotted line shown in Fig. 3.5 (Smithies et al., 2007). The Pilbara Craton thus constitutes a world-class natural laboratory for the study of early life and early tectonic processes.

3.2.2 General structure of the Fortescue Group in the East Pilbara Terrane

The East Pilbara Granite Greenstone Terrane was formed by repeated melting events that resulted in the depletion of the subcontinental lithosphere, and in the stabilisation of the EP as a stable continent by *c.* 3.2 Ga (Van Kranendonk et al., 2007). The resulting structure of relatively light granitic domes and dense greenstone keels determined the deposition and subsidence of the mafic and felsic volcanic units and associated sedimentary rocks of the 2775-2630 Ma Fortescue Group. Kriewaldt (1964) was the first to point out that the Fortescue Group is preferentially preserved above greenstone keels. Wellman (1999) confirmed this observation by gravity and total magnetic data that showed that up to 3 km out of the 6.5 km of the Fortescue Group are preserved in broad synclines and centroclines in the EP. This structure of broad synclines and especially of centroclines suggests a strong vertical tectonic component and a reactivation of doming and uplift during the deposition of the Fortescue Group (Williams and Bagas, 2007b). Further lines of evidence in favour of this hypothesis include paleocurrent data indicating transport away from granitic complexes (Blake, 1993), strata of the Fortescue Group regionally dipping away from granitic domes (Williams and Bagas, 2007b), sedimentary unconformities within the lower Fortescue Group with steeper bedding close to granitic domes (Van Kranendonk, 2003a), and the observation of ring faulting at the contact between the lower Fortescue Group (Mount Roe Basalt and Hardey Formation) and the Mount Edgar Granitic Complex (Williams and Bagas, 2007b).

However, there is also evidence that the lower Fortescue Group was deposited in an extensional context: in the EP, the *c.* 2772 Ma Black Range Dolerite Suite describes north-northeast oriented dykes (de Vries et al., 2008) which are probable feeders of the Fortescue Group (Lewis et al., 1975) and north-northeast oriented growth faults have been identified in the lower Fortescue Group in the Nullagine Synclinorium (Blake, 1993). In the South Pilbara, west south-west trending growth fault occur during the deposition of the Kylena Formation and of the Tumbiana Formation (2730-2715 Ma de Vries et al., 2008). Two interpretations have been proposed from these observations: a) a "two-stage, two rift" model in which the northeast trending faults in the EP reflect west/northwest - east/southeast extension that was followed by a northeast - south-

west extension stage expressed by a second set of faults oriented northwest - southeast (Blake, 1993; de Vries et al., 2008); b) a single rift model in which the north-easterly trending faults in the EP are coeval of the main northeast - southwest rifting event that resulted in continental breakup (Thorne and Trendall, 2001). Regardless of the preferred rift-model, extension was limited in the EP which had evolved to passive margin by $\sim$ 2750 Ma (Blake, 1993; Thorne and Trendall, 2001). If the interpretation of a passive margin is correct, this would make the Upper Fortescue Group in the East Pilbara Terrane on of the oldest preserved passive margins.

3.2.3 The role of gravitational forces in the formation of the North Oakover Syncline and Meentheena Centrocline

The present study focuses on the structure of the Fortescue Group in the North Oakover Syncline and Meentheena Centrocline (Fig. 3.6).

Relation with the basement

In the Oakover Syncline and in the Meentheena Centrocline, the 2775-2630 Ma volcano-sedimentary rocks of the Fortescue Group unconformably overlie the granite greenstone complex. In some places, such as the eastern edge of the Mont Edgar granitoid complex, units of the lower Fortescue Group are faulted against the granite greenstone complex (Williams and Bagas, 2007b). The age of the greenstone belts ranges from 3469 and 3315 Ma and that of the granitoids between 3315 and 3244 Ma (Williams, 1999b; Williams and Bagas, 2007b). The sedimentary rocks of the De Grey Supergroup that unconformably overly the granite-greenstone complex were deposited between $\sim$ 3020 and 2930 Ma.

We studied the structure of the basement in the Yarrie Tower area (Fig. 3.6). This area was mapped by Williams (1999b) before the stratigraphy of the East Pilbara greenstones was review by Van Kranendonk et al. (2004a), so that the outcropping greenstone (the Yarrie Belt) has not been assigned to a formation yet. A minimum age of the Yarrie Belt is obtained from the Sensitive High-Resolution Ion Microprobe (SHRIMP) U-Pb zircon age of 3438 $\pm$4 Ma of an intrusive granodiorite (Williams, 1999b; Nelson, 1998). This greenstone belt presents a strong linear deformation (Fig. 3.7a) that resembles the deformation of the Warrawoona Syncline (between the Corunna Downs and Mount Edgar granitoid complexes, Fig.3.4) described by Thébaud (2006). In the Warrawoona Syncline, extensive mapping by Thébaud (2006) revealed that the stretching lineation describes a radial pattern oriented towards a central zone in which the lineation is vertical. This is best interpreted as reflecting a sagduction process: the stretching lineation is due to the sinking of the greenstone and the zone where the lineation is vertical is the "sinking centre". Interestingly, a strong argument of Thébaud (2006) in favour of the sagduction model is the observation of extensional quartz vein that are at a high angle to the stretching lineation and rotate along with the stretching lineation so that they are sub-horizontal in the "sinking centre". The simplest explanation of this observation, which requires a single

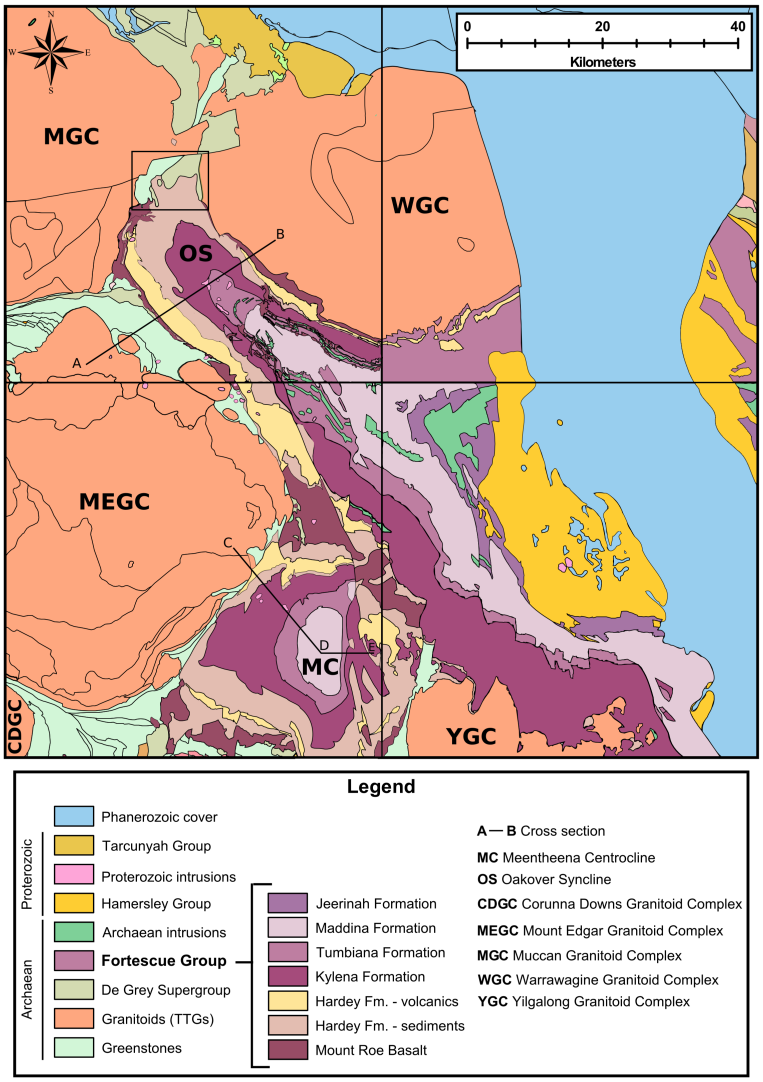

Figure 3.6: Simplified geological map of the study area compiled from the digital 1/100 000$^{\text{th}}$ geological sheets Muccan, Warrawagine, Mount Edgar and Yilgalong available at http://mapserver.doir.wa.gov.au/datacentre/. A-B and C-D-E are the trace of two published cross sections. The plain rectangle shows the Yarrie Tower area.

vertical deformation event, is that the quartz vein are syndeformation. Alternative explanations require multiple events that were not observed in the Warrawoona Syncline (Thébaud, 2006). Extensional quartz veins at a high angle to the stretching lineation were also observed in the Yarrie Tower area (Fig. 3.7b). While extensive mapping of the stretching lineation has not yet been carried out in this area, it is likely that this greenstone underwent a sagduction event during the formation of the adjacent Muccan and Warrawagine granitoid complexes, broadly similar to that described in the Warrawoona Syncline.

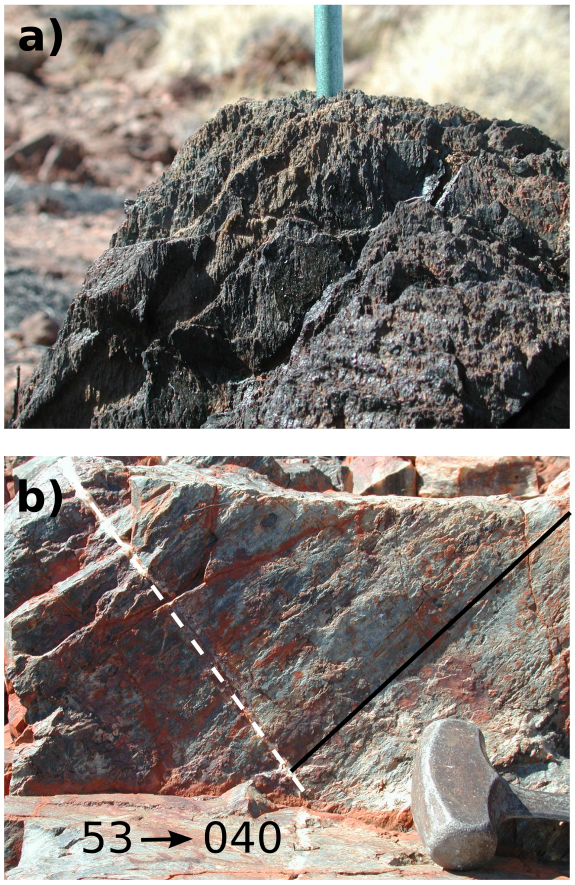

Figure 3.7: Linear deformation of the greenstone in the Yarrie Tower area. a) Vertical lineation in ultramafic basalt. b) Extensional quartz vein (dashed white line) oriented at a high angle to the stretching lineation in chert (plain black line).

Syndepositional deformation of the Fortescue Group

The broad structures of the Oakover Syncline and of the Meentheena Centrocline are shown in Fig. 3.8 on two cross sections from Williams (1999a) and Williams and Bagas (2007a) respectively. These cross sections show the emplacement of the Fortescue Group on top of highly deformed greenstone belts and the unconformable contact between the Fortescue Group and underlying formations. Importantly, these cross sections do not show any faulting associated with the emplacement of the Fortescue Group. The growth faults that have been described

prior to the deposition of the Hardey Formation in the Nullagine Synclinorium (Blake, 1993) and in the Pear Creek Centrocline (Van Kranendonk, 2003a) were also observed locally in the Meentheena Centrocline by Williams and Bagas (2007b) but are absent in the Oakover Syncline. Van Kranendonk (2003a) attributed unconformities in the Pear Creek Formation that overlies the Kylena Formation in the Pear Creek Centrocline to the reactivation of older granitic domes. This implies that deformation by reactivation of older structures went on until at least 2735 Ma in this area. The youngest unconformity that we observed in the Oakover Syncline is an angular unconformity between the *c.* 2766 Ma felsic volcanics of the Hardey Formation and overlying shales (Fig. 3.9a). No markers of syndepositional deformation of the Fortescue Group younger than *c.* 2766 Ma are observed in the Oakover Syncline. Similarly, Williams and Bagas (2007b) concluded that syndepositional deformation of the Fortescue Group did not happen later than $\sim$ 2750 Ma in the Meentheena Centrocline. In the Meentheena Centrocline and Oakover Syncline, the deformation associated with the emplacement of units (Kylena Formation, Tumbiana Formation and Maddina Formation) of cumulative stratigraphic thickness of up to 5500 m remains to be characterised.

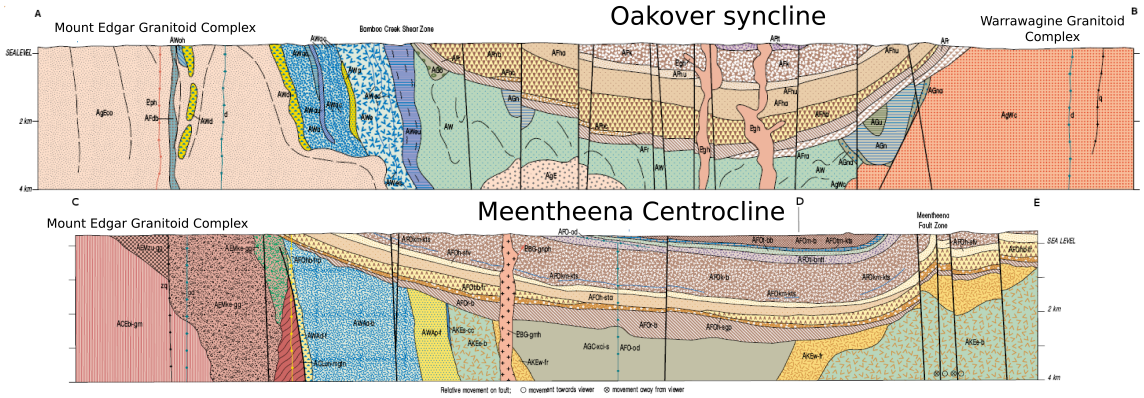

Figure 3.8: Top: cross section of the Oakover Syncline from Williams (1999a). Bottom: cross section of the Meentheena centrocline from Williams and Bagas (2007a).

Assessing the role of gravitational forces in the formation of the Meentheena Centrocline

The role of gravitational forces during a deformation event can be estimated using the Argand ratio AR (Rey and Houseman, 2006), which is derived from the Argand number first proposed by England and McKenzie (1982). The Argand ratio can be defined as

$$AR = \frac{\Delta\,\sigma_{zz}}{\tau(\dot{\epsilon}_0)}\,,$$

where $\Delta\,\sigma_{zz}$ is an estimate of the gravitational stress arising from a crustal thickness or a density contrast, and $\tau(\dot{\epsilon}_0)$ is the stress required to deform the medium for a given strain rate

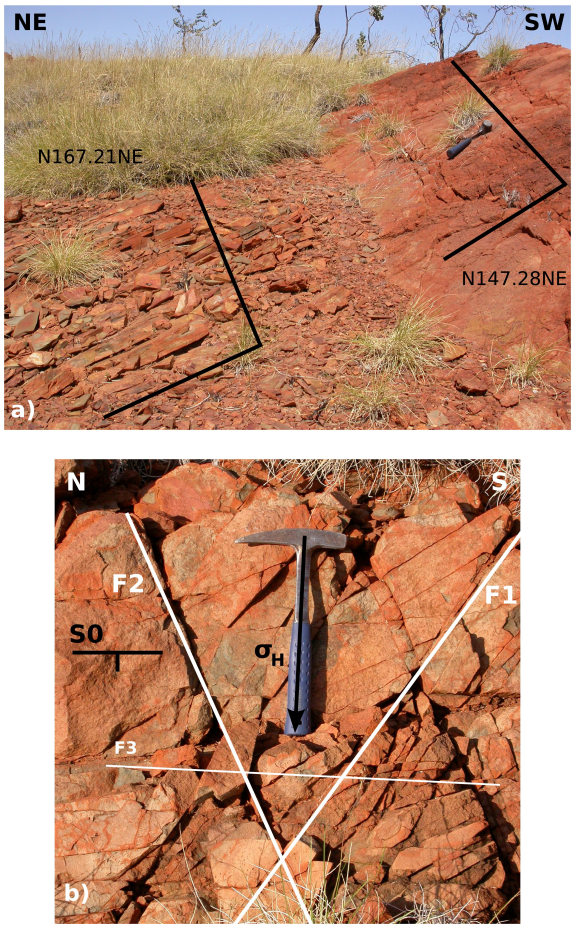

Figure 3.9: a) Angular unconformity between shales from the Hardey Formation and underlying felsic volcanics of the Hardey Formation (Bamboo Creek Member). b) Example of a conjugate fracture pair and inferred orientation of maximum horizontal compressive stress in the Tumbiana Formation at site 30. The set of fractures F3 is pervasive and is attributed to Proterozoic faulting.

$\dot{\epsilon}_0$. Quantitative estimates of the Argand ratio can be obtained from numerical modelling but are impossible to obtain from field observations. The numerator of the Argand ratio can be estimated where gravity data are available to derive a density profile of the continental lithosphere, but neither the stress nor the strain rate are easily retrieved from natural examples, which makes the denominator poorly constrained. However, field observations can allow for the estimation of the orientation of the main axis of paleostress, which indirectly allows for the evaluation of the role of gravitational forces in local to regional deformation events. An example discussed above is the characterisation of the stretching lineation in the Warrawoona Syncline (Thébaud, 2006).

Method

Whereas the Warrawoona Syncline and Yarrie Belt are highly deformed and display a complex structure, structural markers of paleostress syn- to post-depositional of the moderately deformed Upper Fortescue Group are rare. In particular, tension fractures and stylolites are too scarce to be used as a stress marker in the Meentheena Centrocline. The only markers of syn- to post-depositional paleostress that are widespread in the Meentheena Centrocline are fractures, and particularly conjugate fracture pairs. Fig. 3.10 shows the relationship between fractures and main stress axis. The orientation of σ_1 is the bisector of the angle between the azimuth of two conjugate fractures. We will refer to this angle as $\widehat{\text{F1-F2}}$.

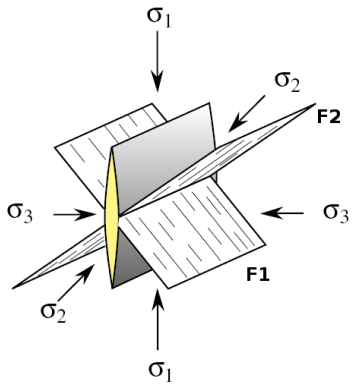

Figure 3.10: Relationship between fractures and main stress axis ($\sigma_1 \geq \sigma_2 \geq \sigma_3$). The thick fracture is a tension fracture and the striated fractures F1 and F2 are conjugate shear fractures. From Nicolas (1984).

To estimate the orientation of principal stress axis of the Upper Fortescue Group, we measured the bedding plane and fractures at 33 sites in the Hardey Formation and in the Tumbiana Formation around the Meentheena Centrocline (Tab. 3.1). The bisector angle between a conjugate fracture pair on a structural surface provide an estimate of the maximum horizontal compressive stress σ_H. The measurements of F1 and F2 at each site were rotated back to the horizontal using the measure of the bedding plane S0. Data for the strike, dip and dip direction of S0, F1 and F2 were averaged at sites where more than one measurement was made. Several measurements were taken radially across the centrocline to assess lateral variability in two areas over which results were then averaged (insets a and b in Tab. 3.1 and Fig. 3.11). All of the

measured fractures were dry, to the exception of the quartz-filled fracture F2 fracture at site 58. The observation of minor to absent offsets between conjugate shear fractures (Fig. 3.9b) suggests an overall moderate deformation.

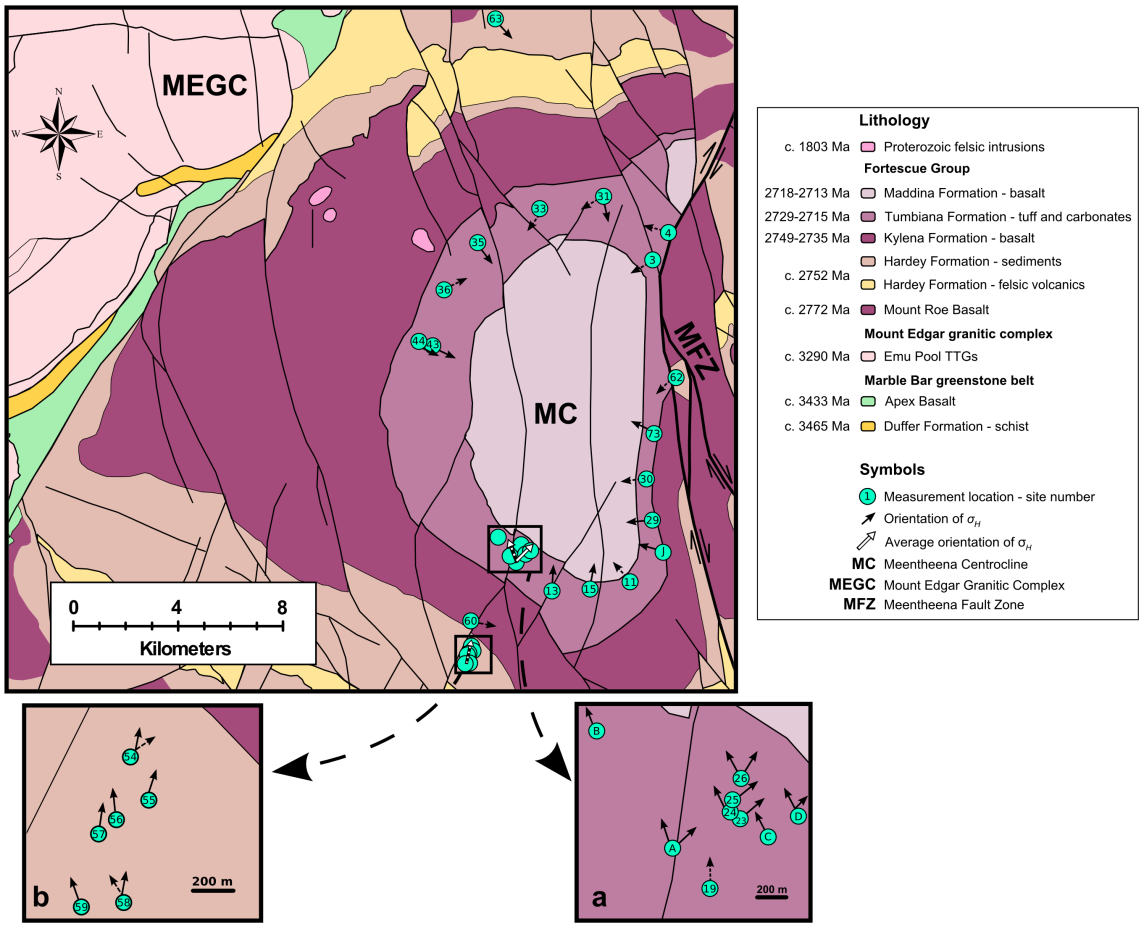

Figure 3.11: Simplified geology of the Meentheena Centrocline compiled from Williams and Bagas (2007a). Arrows indicate σ_H orientations inferred from the data in Tab. 3.1. Large, white arrows are the average orientation of σ_H calculated for each of the two insets. Dashed arrows indicate either high uncertainties or direction of stress consistent with Proterozoic faulting.

Limits of the method

One important limit to the estimation of paleostress directions from conjugate fracture pairs in rocks of Archaean age is their long tectonic history. Multiple deformation events are to be expected in Archaean cratons, and especially at their edges. The Oakover Syncline and Meentheena Centrocline are about 75 km away from the Eastern edge of the Pilbara Craton. Post centrocline faulting is nevertheless observed in the Meentheena Centrocline, where north-northwesterly trending faults such as the Meentheena Fault Zone (see Fig. 3.11) are attributed to far field responses to the 1830-1765 Ma Yapungku Orogeny (Williams and Bagas, 2007b). The measured fractures have to be interpreted in the light of this known deformation event,

and the possibility that some of them are related to other post-centrocline deformation events cannot be excluded. Another limit of the method is that conjugate fracture pairs are not always readily identified. Where more than two sets of fractures occur (*e.g.* at sites 26, 31, 54, 58, A and D), there can be more than one possibility for conjugate fracture pairs and thus for the orientation of σ_H. Multiple measurements at one site or over a small area are helpful to isolate relevant data from noise. Finally, the angle between the orientation of σ_H and the fracture, typically of 30°, varies from $\sim 25°$ to $\sim 40°$. In the present analysis, the angle $\widehat{\text{F1-F2}}$ is most consistent in carbonates (32-35°). At sites 11, 19, 30 and 62, the angle $\widehat{\text{F1-F2}}$ falls outside of the range suggested above. Results for these sites thus have to be taken with care.

Keeping the limits listed above in mind, the inferred orientations of maximum horizontal compressive stress can be used to assess the role of gravitational forces in the formation of the Meentheena Centrocline. If the centrocline was formed by horizontal forces at plate boundaries, the maximum horizontal compressive stress σ_H is expected to be perpendicular to the north-south oriented fold axis. On the contrary, if gravitational forces played an important role in the formation of the Meentheena Centrocline, σ_H is expected to radiate toward the centre of the centrocline.

Table 3.1: Structural data and inferred orientation of the maximum horizontal compressive stress σ_H. The angle $\widehat{\text{F1-F2}}$ and the orientation of σ_H are calculated after rotating the data back to horizontal. The orientation of σ_H is given as an azimuth in degrees, clockwise from the north.

Site #	Lithology	Stratigraphy S0			Fracture F1			Fracture F2			$\widehat{\text{F1-F2}}$	σ_H
		Strike	Dip	Dir.	Strike	Dip	Dir.	Strike	Dip	Dir.		
3	Massive basalt	128	08	SW	085	67	S	037	77	N	43	061
4	Arkositic sandstone	053	07	SE	127	77	N	082	80	N	44	104
11	Sandstone	053	24	NW	124	81	S	153	84	N	33	138
13	Tuff	135	14	NE	044	77	N	117	84	S	76	003
15	Carbonates	102	19	N	041	79	SE	159	84	SW	64	010
29	Lapilli	161	58	W	055	72	SE	094	42	N	75	085
30	Basalt	179	55	W	122	59	NE	069	33	SE	101	083
31	Basaltic sandstone	120	08	SW	024	80	NW	130	84	SW	76	168
								092	85	N	67	059
33	Sandstone	097	04	S	012	74	E	063	79	SE	52	036
35	Basalt	059	13	SE	118	63	NE	173	83	E	58	142
36	Sandstone	040	09	SE	043	76	SE	084	76	S	42	064
43	Basalt	009	17	E	146	82	SW	084	90		62	115
44	Basalt	027	22	E	144	82	SW	084	90		59	115
60	Basalt	138	18	NE	119	68	SW	080	80	SE	39	101
62	Sandstone	016	22	W	62	64	SE	021	66	NE	34	040
63	Siltstone	069	36	SE	170	83	E	118	63	N	52	138
73	Carbonates	006	42	W	126	39	N	085	78	S	70	115
J	Sandstone	179	52	W	105	45	N	077	85	S	56	106
Inset a												
19	Basaltic sandstone	099	21	N	017	87	E	159	88	W	37	179
23	Sandstone	007	11	W	025	90		076	84	S	48	049
24	Basaltic sandstone	132	08	NE	178	90		130	74	SW	48	154
25	-	001	11	W	025	60	W	076	78	S	46	051
26	Sandstone	120	13	N	000	90		062	82	S	62	032
								122	72	SW	59	151
A	Basalt	120	12	N	013	86	E	080	85	S	66	047
								130	62	SW	65	162
B	Carbonate	138	29	NE	014	75	W	125	62	SW	65	159
C	Lapilli	116	23	N	008	80	W	120	56	SW	66	152
D	Sandstone	112	14	NE	008	90		084	78	N	73	045
								113	70	S	75	151
Inset b												
54	Sandstone	132	24	NE	029	82	E	166	90		45	011
								073	66	S	46	056
55	Sandstone	129	18	NE	031	52	SE	170	90		54	018
56	Sandstone	110	34	NE	028	90		145	66	SW	65	174
57	Sandstone	140	23	NE	038	73	W	166	68	W	48	008
58	Sandstone	127	29	NE	034	85	NW	174	64	W	44	010
					126	64	SW				42	147
59	-	130	22	NE	063	86	NW	175	55	E	61	160

Results

The poles to the measured bedding planes are distributed according to a radial pattern on a stereographic projection (Fig. 3.12a), as can be expected for a centroclinal structure. Bedding planes measured on the southwest limb of the centrocline are over-represented on this plot due to the distribution of measurements (Fig. 3.11). The poles to the measured fractures also describe a radial pattern and do not show any preferential orientation (Fig. 3.12b), contrary to what would be expected if the structure had been formed by horizontal forces at plate boundaries. This suggests that the role of forces at plate boundary could have been limited in the formation of the Meentheena Centrocline.

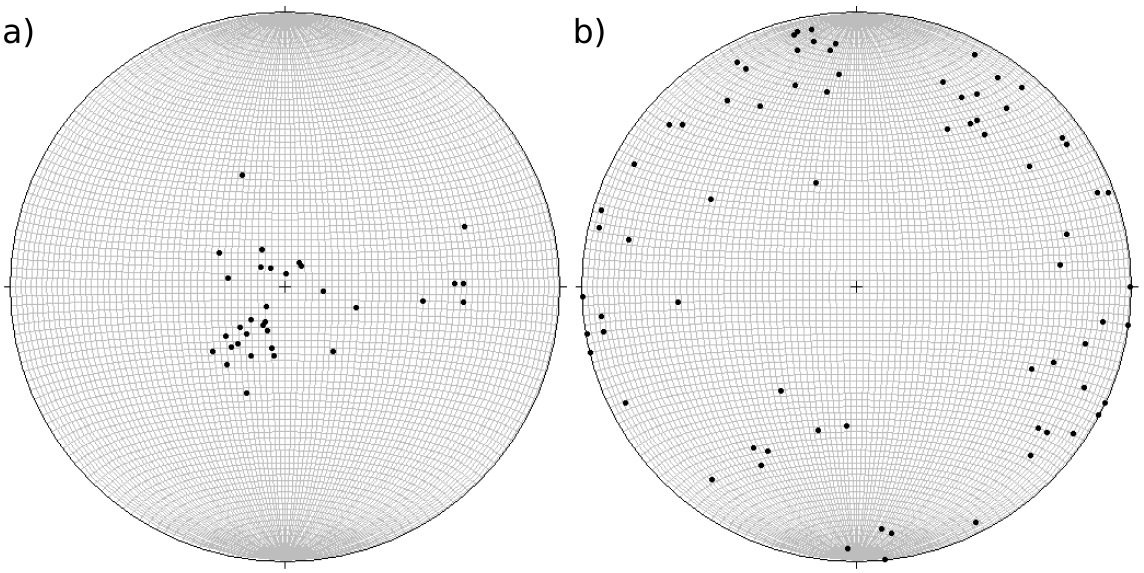

Figure 3.12: Equal area, lower-hemisphere stereographic projection of a) the poles to the bedding planes and b) the poles to the fractures for the data presented in Tab. 3.1.

Moreover, Fig. 3.11 shows that the orientation of the maximum horizontal compressive stress σ_H inferred from the structural data (Tab. 3.1) radiates around the Meentheena Centrocline, suggesting an important contribution of gravitational forces. However, the direction of σ_H does not follow this general radiating pattern at all measurement sites. At sites 3, 4, 31, 33, 36, 60 and 62, the inferred orientation of σ_H is consistent with the observed postdepositional north-northwesterly faulting and can thus be attributed to this faulting. The set of fracture F2 in inset b, oriented N170 (Tab. 3.1), is also consistent with this faulting. The inferred orientation of σ_H (N012, towards the centre of the centrocline) for this area is thus possibly an artifact related to the Yapungku Orogeny. As for the two solutions inferred for the area shown in inset a, the orientation N045 is towards the centre of the centrocline, but the orientation N158 is not consistent with any observed folding or faulting and remains to be explained. It is also worth noting that the well-defined orientation of σ_H on the eastern limb of the Meentheena Centrocline is consistent with subsequent faulting and with both the horizontal tectonics and

vertical tectonics hypothesis. Fewer data were acquired on the western limb of the centrocline, where Proterozoic faulting is less marked. Nevertheless, the inferred orientations of σ_H at sites 11, 13, 15, 35, 43 and 44, and in inset a are only compatible with a preponderant role of gravitational forces.

Conclusion

Overall, the results of the present analysis are consistent with a preponderant role of gravitational forces during the deposition of the Hardey Formation and Tumbiana Formation formation of the Meentheena Centrocline. Of particular importance to this conclusion are the absence of preferential orientation of measured fractures and the orientation of the maximum horizontal compressive stress in the northern and southern parts of the centrocline. This conclusion extends the duration of the role of gravitational forces in the formation of the Meentheena Centrocline from 2775-2750 Ma (Williams and Bagas, 2007b) to at least 2775-2721 Ma, which is the age of a tuff layer in the lower part of the Tumbiana Formation dated by Blake et al. (2004). This long lasting preponderance of radial stress can be readily explained by density differences in the granite-greenstone basement. Denser greenstones would have subsided faster upon deposition of the Fortescue Group which would result in the apparent reactivation of the granitic domes noted by Van Kranendonk (2003a). This reactivation would only be accentuated by the fact that these greenstones, previously deformed during sagduction processes, would likely be weak. Importantly, no important extensional features are observed in the Meentheena Centrocline during the deposition of the Upper Fortescue Group. A mechanism that accounts for the accommodation of the considerable volume of volcano-sedimentary sequence of the Upper Fortescue Group must thus be identified.

3.3 Lower crustal flow and subaqueous Archean Continental Flood Basalts

Foreword

We have seen in section 3.1 that there is substantial evidence for a hotter continental crust in the Archaean. We also discussed the limiting role of gravitational forces in hot orogens. The geological evidence presented in the previous section suggests that gravitational forces played a preponderant role during the deposition of the Fortescue Group. In the following article, we build numerical models to investigate the mode and time of relaxation of a topographic load as a function of the temperature at the base of the continental crust. These numerical experiments show that gravity-driven lower crustal flow occurs for Moho temperatures larger than $\sim$ 550 °C, and that the relaxation time of a topographic anomaly decreases with Moho temperature. Sedimentological observations and geochronological data allow us to independently estimate the relaxation time of the Fortescue Group in the Meentheena Centrocline. This, in turn, allows us to estimate the Moho temperature at the time of deposition of the volcano-sedimentary sequence of the Upper Fortescue Group. This temperature is approximately 200 °C hotter than the current Moho temperature estimated from available heat flow data. There are two main limits to this model. The first limit, inherent to rheological modelling, is that rheological laws constitute a crude simplification of a complex natural system. Rheological laws remain relatively poorly constrained, and rheological parameters are experimentally defined for strain rates several order of magnitude faster than geological strain rates. The second limit is related to the absence of constrain on the contribution of the reactivation of the dense, weak greenstone keel when evaluating the relaxation time of the Fortescue Group. This reactivation would tend to decrease the relaxation time which would result in an over-estimation of the Moho Temperature. However, numerical experiments in which a weak zone simulating the greenstone keel was incorporated did not yield significantly different relaxation times.

In the absence of extensional features, lower crustal flow of hot continental crust is thus a possible mechanism to account for the accommodation of the Upper Fortescue Group in the Meentheena Centrocline. More generally, gravitationally-driven lower crustal flow, or possibly continental overflow as proposed by Bailey (1999), would contribute to maintaining thick continental flood basalts below sea level, which partly explains Arndt's (1999) observation of common subaqueous flood volcanism in the Precambrian.

The following is a manuscript entitled *Lower crustal flow and subaqueous Archean Continental Flood Basalts* by Nicolas Flament, Patrice Rey, Nicolas Coltice, Gilles Dromart and Nicolas Olivier submitted to *Geology*.

Abstract

Potentially higher sea levels do not fully explain why subaqueous flood volcanism on top of continental crust was common throughout the Archean. One possible way of maintaining basaltic piles several kilometers thick below sea level is via gravity-driven lower crustal flow of hot continental crust. In this paper, we run numerical experiments to determine the relaxation time of a topographic load emplaced on continental crust as a function of Moho temperature. We use a visco-plastic model in which the viscosity depends on temperature. We apply the results of these models to the Fortescue Group, in the Pilbara Craton. Data regarding the eruption time and stratigraphic thickness of the Maddina Formation basalts, together with sedimentary structures pointing to shallow initial and final depth of emplacement, constrain the relaxation time for this section of the Fortescue Group continental flood basalts to between 0.75 and 2 Myr. According to our modeling results this translates to a Moho temperature range of 610 to 690°C for continental crust 40 km thick (580 to 665°C for continental crust 30 km thick). This is significantly higher than the present-day Moho temperature range of 400 to 500°C for Archean cratons, suggesting that the cooling of the studied continental lithosphere was approximately 200°C over 2.72 Ga. The observation that many Archean continental flood basalts failed to emerge despite their thickness suggests that gravity-driven lower crustal flow of hot continental crust was an efficient process that maintained continents below sea level throughout the Archean.

Keywords: Archean, Large Igneous Province, Continental Flood Basalt, crustal flow, continental geotherm.

3.3.1 Introduction

The rapid eruption of large amounts of mafic flood volcanics has formed Large Igneous Provinces (LIPs), including Continental Flood Basalts (CFBs), throughout geological times (Prokoph et al., 2004). Archean CFBs typically consist of 5 to 15 km thick piles dominated by mafic volcanics, and many cover surface areas larger than 100,000 km^2 (De Wit and Ashwal, 1997). Interestingly, 80% of Archean LIPs erupted in subaqueous environments, whereas only 20% of post-Archean LIPs are subaqueous and all post-Archean CFBs are subaerial (Kump and Barley, 2007). This implies that many Archean CFBs that erupted on top of continental crust failed to emerge despite their thickness. Higher sea levels in the Archean do not fully explain immersed continental crust since the maximum amplitude of sea level variation is of the order of 1 km (Flament et al., 2008). Thus, tectonic processes other than eustatism that led to the subaqueous eruption of thick Archean CFBs need to be identified.

In this paper, we investigate the characteristic relaxation time to remove thickness contrast following the emplacement of a topographic load, modeling a CFB, as a function of continental geotherm. Two-dimensional numerical experiments using the particle-in-cell finite-element code Ellipsis (Moresi et al., 2003) show that the relaxation of the topography occurs via lower crustal

flow. For temperature-dependent viscosity, the characteristic relaxation time decreases with Moho temperature. Constraining the characteristic relaxation time of the Fortescue CFB, East Pilbara Terrane, using field data, allows us to estimate the Moho temperature at the time of eruption. Data on the eruption time (2718-2713 Ma) and the stratigraphic thickness ($\sim$ 600 m) of the lower Maddina Formation, together with sedimentary structures pointing to shallow initial and final depths of emplacement (respectively 10 m and 0 m), constrain the relaxation time to between 0.75 and 2 Myr for this section of the Fortescue CFB. According to our numerical results, this relaxation time implies a Moho temperature range at time of emplacement of 610 to 690 °C for continental crust 40 km thick (580 to 665 °C for crust 30 km thick). These results are compatible with conservative estimates of Neoarchean Moho temperatures of between 680 and 750 °C for continental crust 40km thick (Rey and Coltice, 2008). They are also significantly higher than the present-day Moho temperature of Neoarchean cratons of 430 $\pm$ 100 °C (Artemieva, 2006), suggesting a cooling of the studied continental lithosphere by $\sim$ 200 °C since 2.7 Ga.

3.3.2 Model

To investigate the thermal-mechanical response of a lithospheric section following the emplacement of a CFB, we designed a 2D Cartesian model in which the CFB is modeled as a plateau which is emplaced instantaneously on a laterally homogeneous continental lithosphere.
As shown in Fig. 3.13, the models are 800 km wide and 100 km deep. A continental crust 40 km thick sits on top of the uppermost 40 km of the mantle. Because of the symmetry of the problem, only one half of the CFB is considered. The spatial resolution of the models is 520 m. We consider CFBs of half-width 150 km and of thickness 3, 6, 9 and 12 km. The density of the CFB is conservatively set to 2840 kg m^{-3} (Fig. 3.13), as volcanic provinces can consist of up to 50% sediments.

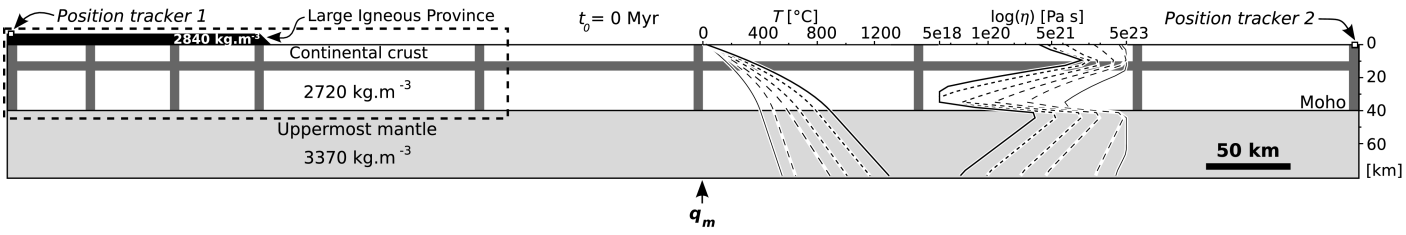

Figure 3.13: Geometry, material densities, continental geotherms, viscosity profiles and Lagrangian particles (position trackers) used in the models. The thick dark-grey lines in the continental crust are strain markers. The area within the dashed frame is shown in Fig. 3.14. See text for the definition of parameters.

Rheological model

We adopt a visco-plastic rheological model, combining frictional flow and temperature-dependent viscosity (supplementary material, section 3.3.7). Frictional flow is described using the Coulomb

criteria (Moresi and Solomatov, 1998), and we further implement a strain softening law (supplementary material, section 3.3.7). The temperature-dependent viscosity follows the Frank-Kamanetskii approximation (e.g. Solomatov and Moresi, 1996):

$$\eta = b \exp(-\gamma\ T)\ , \tag{3.4}$$

where T is the temperature, b the reference viscosity and $\gamma = Q/RT_p^2$ the viscosity range over the experienced temperature range, with Q being the activation enthalpy, R the gas constant and T_p the potential temperature of the mantle at the base of the lithosphere. The range of viscosities is limited to $5\times\ 10^{18}$-$5\times\ 10^{23}$ Pa s to reduce calculation time. All boundaries in the models are free-slip. Our visco-plastic approximation is valid to the first order since elastic processes can be neglected as the wavelength of the CFB (300 km) is greater than the elastic thickness of the continental lithosphere ($\sim$ 50km), and because the characteristic relaxation time of the considered topographic loads are much larger than the Maxwell time for the continental lithosphere ($<$ 1 kyr). Our rheological model reproduces characteristic stress profiles for a given strain rate.

Thermal model

The calculation of the continental geotherm mainly depends on crustal radiogenic heat production and mantle heat flow. In this study, the distribution of radiogenic elements in the continental crust is assumed to be homogeneous and the heat production of the mantle is neglected. The Archean crustal heat production is calculated using the present-day concentrations of U, Th and K proposed by Taylor and McLennan (1995) for Archean cratons. The use of present-day cratons as crustal reference is conservative since the enriched Archean upper continental crust is likely to have been eroded over time (Galer and Mezger, 1998) and the warmest part of Archean continents would have been more readily recycled into the mantle (Gurnis and Davies, 1986). As for the mantle heat flow, it varies between a present-day value conservatively set to 12 mW m^{-2} (Jaupart and Mareschal, 1999) and 32 mW m^{-2} (supplementary material, section 3.3.7). The surface temperature is set to 20 °C. We determine a series of six geotherms for which the Moho temperature ranges between 400 °C and 900 °C (Fig. 3.13).

3.3.3 Results

Following the loading, gravitational readjustment of the lithosphere occurs through creep flow mostly in the lower continental crust (Fig. 3.14). For Moho temperatures larger than $\sim$ 550°C, deep crustal flow is localized to a channel characterized by a Poiseuille-like velocity profile (Fig. 3.14). The thickness of this channel increases from 10 to 15km for increasingly hot geotherms.

In our numerical experiments, the subsidence of the CFB with respect to the surrounding continental crust is determined by tracking the vertical position of two distant Lagrangian particles

(Fig. 3.13). The subsidence of the CFB follows an exponential evolution over time, and we determine the relaxation time by fitting the subsidence according to:

$$w = w_0 \exp(-t/\tau),$$

where w is the elevation after a time t, w_0 is the initial elevation and τ is the characteristic relaxation time.

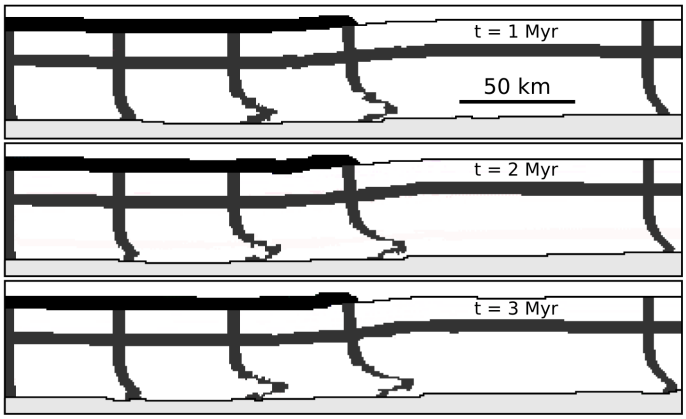

Figure 3.14: Graphical output showing the intensity of the lower crustal flow at $t \approx 1$ Myr, $t \approx 2$ Myr and $t \approx 3$ Myr for a CFB 6 km thick and a Moho temperature of ~ 680°C.

The relaxation time is expected to depend on the density of the load ρ_{CFB}, on the viscosity of the flowing crust η_{cc} and on the wavelength of the topographic anomaly λ (McKenzie and Jackson, 2002). Indeed, a series of numerical experiments for different densities of the CFB, all other parameters being constant, allows us to determine that the relaxation time is proportional to $1/\rho_{CFB}$. The same test run for different half-widths of the CFB shows that the relaxation time initially increases with λ until it reaches a near-constant value. This threshold occurs at $\lambda \approx 100$ km for a Moho temperature of ~ 400°C and at $\lambda \approx 150$ km for a Moho temperature of ~ 680°C. The non-dependency of relaxation time on λ at large wavelength indicates pure shear of the whole modeled lithosphere (McKenzie and Jackson, 2002). Four series of experiments using the computed continental geotherms and different CFB thicknesses confirm that the relaxation time does not depend on the initial thickness of the load (Kruse et al., 1991, Fig. 3.15). In addition, we observe a negative exponential relationship between relaxation time and Moho temperature (Fig. 3.15). This is due to the linear dependency of the relaxation time on the viscosity which itself depends on temperature (Eq. 3.4). Fitting an exponential model to the results of the four series of models described above gives an exponential constant close to half of the exponential constant in the Frank-Kamanetskii approximation ($\gamma_{cc}/2$). Two additional series of models, for a different γ_{cc} in Eq. 3.4 and for a different crustal thickness (i.e. a different series of geotherms) give the same exponential constant (Fig. 3.15). This suggests that the effective viscosity of the modeled lithosphere during the relaxation of the topographic load is an average viscosity between the viscosity of the fast-deforming lower continental crust and the

larger effective viscosity of the slow-deforming upper crust and upper mantle. The consistency of the fitted exponential constant for different rheological laws and continental geotherms suggests that the relationship can be inverted to estimate the Moho temperature for a known relaxation time.

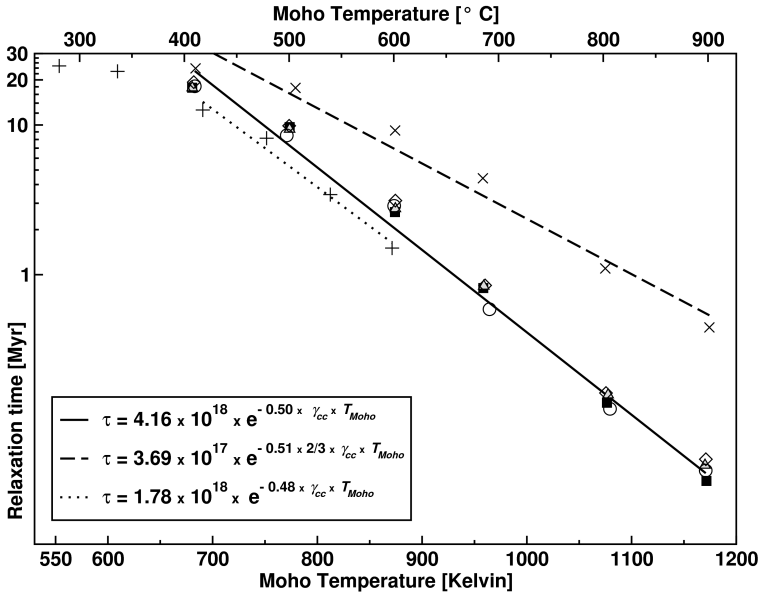

Figure 3.15: Relaxation time as a function of temperature at the base of the crust. Results are presented for: reference parameters and a thickness of the CFB of 12 km (empty circles), 9 km (empty diamonds), 6 km (gray triangles), 3 km (black squares); a thickness of the CFB of 6km and: $\gamma = 2/3\ \gamma_{cc}$ in Eq. 3.4 (crosses), a continental crust 30 km thick (plus symbols). Results of the exponential fits are shown.

Finally, the initial maximum velocity in the channel depends exponentially on the temperature at the base of the crust. This velocity reaches 0.7 cm yr^{-1} for the hottest geotherm and for a 12 km thick CFB. For the coldest studied geotherm, the maximum velocity is two orders of magnitude lower and the relaxation time is two orders of magnitude longer.

3.3.4 Case-study: Fortescue Group, Pilbara Craton

Our two-dimensional numerical experiments suggest that information on the subsidence history of a CFB of known thickness would constrain the Moho temperature at the time of eruption. Archean CFBs are well-suited to apply the model because many erupted in subaqueous environments (Arndt, 1999; Kump and Barley, 2007), allowing us to estimate the initial and final depth of eruption from the depositional facies of associated sedimentary rocks. In the Pilbara Craton, the 6.5 km thick Fortescue Group consists of $\sim$ 50% volcanic rocks and $\sim$ 50% sedimentary rocks (Thorne and Trendall, 2001). The age of the group is well constrained to 2775-2630 Ma (Thorne and Trendall, 2001, and references therein). Syn-depositional faulting in the lower Fortescue Group indicates a continental rifting origin in the southern part of the Pilbara Craton (Blake, 1993; Thorne and Trendall, 2001). The absence of syn-depositional faulting later than

$\sim$ 2750 Ma in the northern part of the craton is interpreted as the evolution from rifted margin to passive margin (Blake, 1993). There is abundant evidence for subaqueous sedimentation and volcanism throughout the Fortescue Group (Thorne and Trendall, 2001). In particular, in the Meentheena Centrocline and in the Nullagine Synclinorium, north Pilbara, stromatolite-bearing shallow-water (0 to 10 m deep, Fig. 3.16) sedimentary rocks of the Mopoke, Meentheena and Kuruna Members alternate with the effusive volcanics of the Kylena Formation Mingah Member and Maddina Formation (Blake et al., 2004; Williams and Bagas, 2007b). This alternation suggests that the erupting basalts remained close to sea level. The datation of three felsic tuffs allows us to constrain the deposition time of the Maddina Formation basalts between 3 and 8 Myr (Blake et al., 2004, Fig. 3.16d). Applying these data to our model: initial depth of 10 ± 5 m (wave-dominated shore), final depth of 0 ± 5 m (marginal flood plain), total thickness of 500 to 600 m ($\pm$ 50 m) and deposition time of 3 to 8 Myr ($\pm$ 1 Myr) gives a relaxation time between 0.75 ± 0.4 and 2 ± 0.6 Myr.

The thickness of the crust in the Pilbara Craton in the Archean must have been between the present-day crustal thickness of 30 km (Drummond, 1985) and a maximum value of 40 km that accounts for erosion as suggested by regional metamorphism (Smith et al., 1982). Considering a continental crust 40 km thick, our models imply that the Moho temperature at the time of eruption of the Maddina Formation basalts was between 610 ± 25 and 690 ± 50 °C (Fig. 3.15). The Moho temperature range for a crust 30 km thick is between 580 ± 25 and 665 ± 50 °C (Fig. 3.15). The former temperature estimate is consistent with the Moho temperature of $\sim$ 685 °C computed for a 2.75 Ga continental crust 40 km thick and a mantle heat flow of 26 mW m^{-2} (Fig. 3.13 and supplementary information). The proposed Moho temperature ranges translate from Eq. 3.4 in minimum lower crustal viscosities between 4.3 10^{18} and 3.2 10^{19} Pa s for continental crust 40 km thick and between 8 10^{18} and 6.8 10^{19} Pa s for crust 30 km thick.

3.3.5 Discussion

Our calculation of characteristic relaxation times from geological data is valid for a constant eustatic sea level. This approximation is correct to the first order since a change in eustatic sea level of 500 to 600 m over 3 to 8 Myr is highly unlikely with regard to Phanerozoic rates of sea level change (e.g. Müller et al., 2008). Changes in relative sea level due to forces at plate boundaries can also safely be ruled out for the East Pilbara Terrane between 2721Ma and 2713 Ma, since no growth faults are observed in the upper crust. In addition, the CFB is assumed to have erupted instantaneously. Our conclusions are thus valid for finite emplacement times similar to relaxation times. This is true of Archean CFBs emplaced over a period of the order of 1 Myr similar to the estimated characteristic relaxation time for Neoarchean continental crust.

Both the Moho temperature range ($\sim$ 610-690 °C at 2.72 Ga) and deformation mechanism proposed in this study are consistent with numerical modeling of Archean orogens in which thickening of the continental crust is impeded by gravity-driven crustal flow (Rey and Houseman,

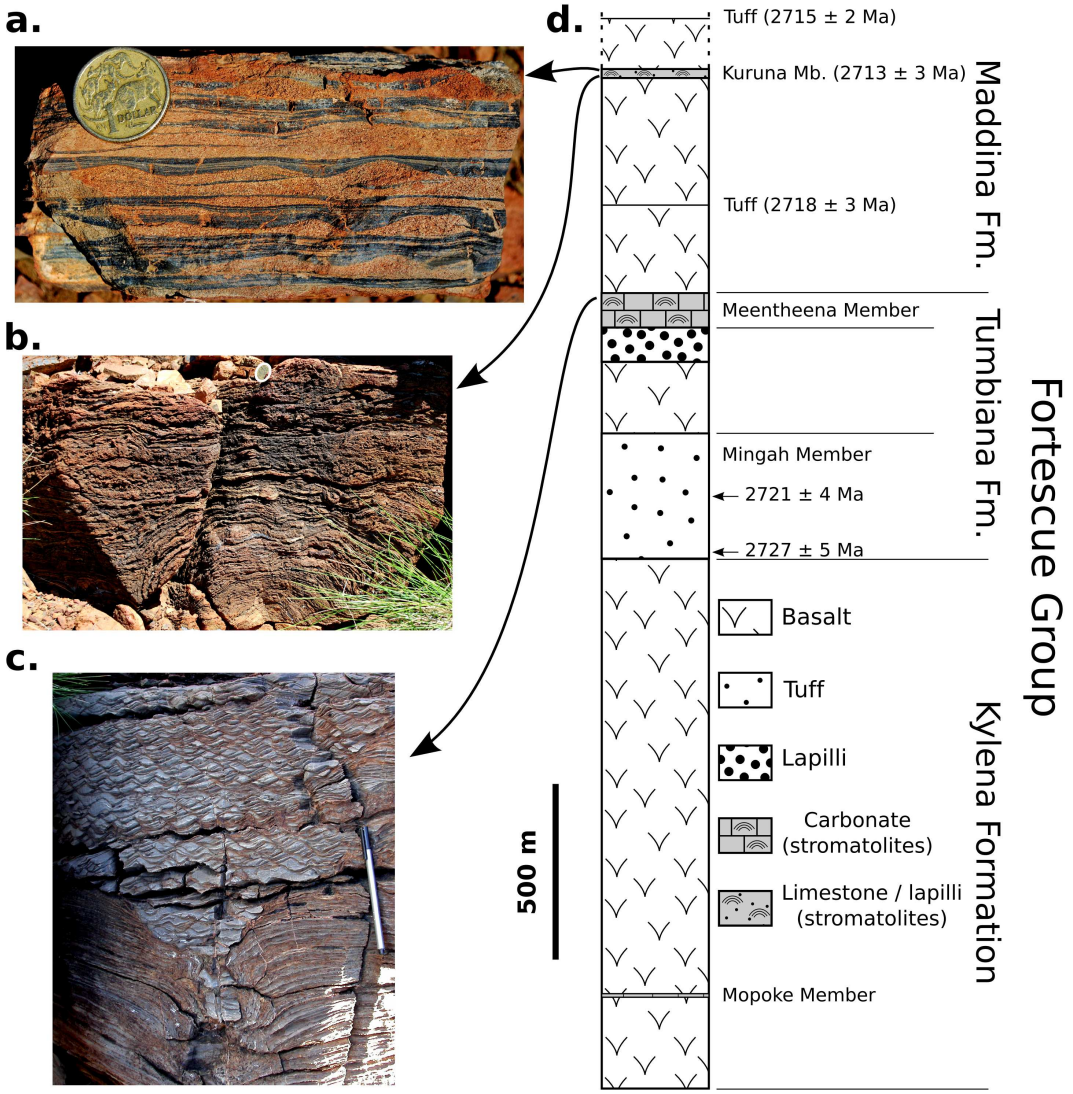

Figure 3.16: Lithologies of the upper Fortescue Group in the Meentheena Centrocline. The pictures illustrate shallow-water facies: a. wavy bedding (mudstone-sandstone interlayers) with laminated, rippled sand sheets indicating an overbank and floodplain depositional environments; b. Domal to tabular stromatolitic crusts. Diameter of the coin in a. and b.: 25 mm; c. Laterally-linked stromatolites underlying wave-ripple laminae. Length of pen: 16 cm. d. Simplified stratigraphic column. The thicknesses are from Williams and Bagas (2007b) and the geochronological data (approximate position) are from the nearby Nullagine Synclinorium (Blake et al., 2004). The dashed section of the Maddina Formation is not exposed in the Meentheena Centrocline.

2006; Rey and Coltice, 2008). They are also compatible with the results of Sonder et al. (1987) which suggest that continental lithospheres with Moho Temperature higher than $\sim 700 \pm 100$ °C cannot support large topographic gradients. However, the Moho temperature of ~ 500 °C computed for a radiogenic heat production calculated at 2.75 Ga and assuming a present-day mantle heat flow of 12 mW m^{-3} is well below the Moho temperature range deduced from our modeling and field data. This suggests that a time-independent mantle heat flow under continents (Lenardic and Kaula, 1995) is difficult to reconcile with the geological record. Our Moho temperature estimates at the time of eruption are also significantly hotter than the present-day temperature at 50 km depth of $\sim 430 \pm 98$ °C inferred from surface heat flow data for Archean cratons of age between 3.0 Ga and 2.5Ga (Artemieva, 2006). The present-day surface heat flow for the Pilbara Craton is 43 ± 3 mW m^{-2} ($n = 4$; Cull, 1982), which according to our thermal model gives a present-day Moho temperature of 485 °C for continental crust 40 km thick (390 °C for crust 30 km thick). This result suggests a cooling of the Pilbara continental lithosphere by ~ 200 °C since 2.72 Ga.

Flament et al. (2008) argued that Neoarchean continents were mostly flooded by up to ~ 1.1 km of water. Hence, subaqueous Archean CFBs that include sections thicker than ~ 1.1 km erupted over a few million years were possibly kept below sea level by gravity-driven crustal flow. Such CFB sections include the 3467-3465 Ma, > 4-km-thick lower Warrawoona Group, Pilbara Craton (Van Kranendonk et al., 2004a); the ~ 2713 Ma, 6.5-km-thick thick intrusive Stillwater complex in the Wyoming Province (McCallum, 1996); the ~ 2709 Ma, 4-km-thick Platberg and Klipriviersberg basalts of the Ventersdorp Group in the Kaapvaal Craton (Armstrong et al., 1991); the ~ 2708 Ma, 3 km-thick komatiites of the Kurnalpi terrane, Eastern Goldfields in the Yilgarn Craton (Kositcin et al., 2008); and the $\sim$ 2505-2501 Ma, $\sim$ 7-km-thick Strelna Group in the eastern Baltic Shield (Amelin et al., 1995). These examples suggest that gravity-driven lower crustal flow contributed to maintain continents below sea level throughout the Archean.

3.3.6 Conclusion

Knowledge of the eruption time, the stratigraphic thickness, and the initial and final elevation of a CFB allows us to constrain the Moho temperature of the continental crust at the time of eruption. To do this, we use numerical models to estimate the relaxation time of a topographic load by gravity-driven crustal flow, as a function of Moho temperature. Applied to the upper Fortescue Group in the East Pilbara Terrane, the model gives a relaxation time of 0.75 to 2 Myr, which translates into a Moho temperature at the time of eruption of 610 to 690 °C for continental crust 40 km thick or 580 to 665 °C for crust 30 km thick. These temperature estimates are significantly higher than the present-day Moho temperature of Archean cratons, suggesting a cooling of the studied continental lithosphere of $\sim$ 200°C over 2720 Myr. The observation that many subaqueous Archean CFB include sections thicker than ~ 1 km erupted over a few million years suggests that gravity-driven crustal flow was a key process that maintained Archean continents below sea level.

3.3.7 Supplementary information

Table 3.2: List of parameters used in the models.

Parameter [a]	Meaning	Value(s)	Unit
(a) Mechanical parameters			
β	Ratio of $f(0)/f(\epsilon_0)$	0.2	
ϵ_0	Strain weakening term	0.5	
ρ_{atm}	Atmospheric density	2.5	kg m^{-3}
σ_{cc}	Crustal maximum yield stress	250	MPa
σ_m	Mantelic maximum yield stress	500	MPa
ϕ_{cc}	Crustal internal angle of friction	15	°
ϕ_m	Mantelic internal angle of friction	25	°
b_{atm}	Atmospheric pre-exponential constant	7.5×10^{18}	Pa s
b_{cc}	Crustal pre-exponential constant	1.48×10^{29}	Pa s
b_m	Mantelic pre-exponential constant	1.19×10^{28}	Pa s
C_{cc}	Crustal cohesion	10	MPa
C_m	Mantelic cohesion	200	MPa
d_{cc}	Crustal thickness range	30-40	km
d_{CFB}	Thickness range for the CFB	3-12	km
g	acceleration of gravity field	9.81	m s^{-2}
Q_{atm}	Atmospheric activation enthalpy	0	kJ mol^{-1}
Q_{cc}	Crustal activation enthalpy	550	kJ mol^{-1}
Q_m	Mantelic activation enthalpy	280	kJ mol^{-1}
R	Gas constant	8.3145	J mol^{-1} K^{-1}
T_p	Upper mantle potential temperature	1330	°C
(b) Thermal parameters			
α_m	Mantelic coefficient of thermal expansion	2.8×10^{-5}	K^{-1}
κ	Thermal diffusivity	0.9×10^{-6}	m^2 s^{-1}
C_p	Heat capacity	1000	J kg^{-1} K^{-1}
H_{cc}	crustal heat production	see Tab. 2	μW m^{-3}
q_m	basal mantle heat flux	see Tab. 2	mW m^{-2}

[a] Non-listed values for the CFB are taken equal to crustal values.

Rheological model

To implement strain softening (O'Neill et al., 2006), the Coulomb criteria is described by:

$$\sigma_s = (C + \tan(\phi)\,\sigma_n) \times f(\epsilon)\ ,$$

where σ_s is the shear stress , C is the coefficient of cohesion of the material at atmospheric pressure, ϕ is the angle of internal friction, σ_n is the stress normal to the failure plane approximated by the lithostatic pressure (Moresi and Solomatov, 1998) and

$$f(\epsilon) = 1 - (1-\beta)\frac{\epsilon}{\epsilon_0}\ , \tag{3.5}$$

where ϵ is the strain, ϵ_0 is the strain weakening term and β is the ratio of $f(0)/f(\epsilon_0)$. Values for these parameters are given in Tab. 3.2.

Thermal model

The crustal heat production is calculated back in time using:

$$H = \Sigma_i \alpha^i C_0^i H^i \exp\left(\frac{a \ln(2)}{\tau_{1/2}^i}\right), \tag{3.6}$$

where i is a radioactive element amongst U^{238}, U^{235}, Th^{232} and K^{40} , α^i is the natural proportion of the radioactive element, C_0^i is the concentration of the element, H^i is rate of heat release of the element, a is the age for which the radiogenic heat production is calculated and $\tau_{1/2}^i$ is the half-life of the element. Values for the concentrations are taken from Taylor and McLennan (1995) and values for other parameters in Eq. 3.6 are taken from Turcotte and Schubert (2002). The radiogenic heat production, mantle heat flow and Moho temperature for the geotherms used in the models are given in Tab. 3.3.

Table 3.3: Thermal parameters used for the calculation of continental geotherms.

Age [a] Ga	H_{cc} μW m^{-3}	q_m mW m^{-2}	d_{cc} km	T_{Moho} °C
1.65	0.69	12.0	40	404
			30	267
2.75	0.98	12.0	40	496
			30	322
2.30	0.84	23.0	40	598
			30	406
2.75	0.98	26.0	40	682
			30	460
3.25	1.19	29.5	40	797
			30	535
3.60	1.39	32.0	40	896
			30	598

[a] To compute radiogenic heat production.

Numerical model

An atmospheric layer is required to implement topographic anomalies in Ellipsis. We model this atmosphere as a compressible low-density and low-viscosity material (Tab. 3.2). All other materials are considered incompressible.

3.4 Reflection on the depositional environment of the Kylena and Tumbiana Formations

There is an ongoing debate regarding the depositional environment of the formations of the Upper Fortescue Group, and especially the Tumbiana Formation: some authors have proposed that the carbonates of the Tumbiana Formation (Meentheena Member) are of lacustrine origin (*e.g.* Buick, 1992; Bolhar and Van Kranendonk, 2007) whereas others interpreted them as deposited in a marine setting (Thorne and Trendall, 2001; Sakurai et al., 2005). The conclusions of the models developed in the previous section are valid for both depositional environments, since a change in water depth of $\sim$ 600 m requires a geodynamical explanation in both settings. Nevertheless, new sedimentological and geochemical data were acquired on the Tumbiana and Kylena Formation that are relevant to this debate. Awramik and Buchheim (2009) recently reviewed the arguments in favour of the lacustrine and of the marine model, and proposed new arguments in favour of the lacustrine model. They concluded that while "there is no single line of evidence that unequivocally establishes a lacustrine origin [...], multiple lines of evidence are collectively consistent with a lacustrine origin" for the Meentheena Member. For an exhaustive list of these arguments, the reader is referred to Awramik and Buchheim (2009). In the next section, we focus on two arguments that have been used in favour of the lacustrine model: rare earth element and yttrium (REY) patterns from Bolhar and Van Kranendonk (2007), and the absence of asymmetrical ripples that would suggest unidirectional flow and thus possibly tidal activity. We show that both of these arguments cannot be used against a marine setting for the Meentheena and Mopoke Members.

3.4.1 A reappraisal of the evidence evidence based on rare earth element and yttrium (REY) analysis

In seawater, rare earth elements (REE) occur mostly in the 3+ oxidation state and exhibit gently decreasing ionic radii of their solvated trivalent cations with increasing atomic number. The close similarities in the ionic radii of the REE lead to a chemical coherence of the entire group since the ionic radius is a key characteristic in the chemical properties of ionic species (German and Elderfield, 1990). REE patterns in the marine environment thus exhibit progressive variations in abundance across the series. Elderfield et al. (1988) identified variations in the relative abundance of REEs in modern oceans reflecting the composition of the source (river input, aeolian transport and hydrothermal vents), interaction with the bio-geochemical cycle and the effects of advective transport linked to water depth. Webb and Kamber (2000) proposed a proxy for modern shallow seawater interacting with the biosphere from the Heron Reef off the east coast of Australia. The identification of a similar REY pattern in 3.4 Ga stromatolites from the Strelley Pool Chert in the Pilbara Craton was used by Van Kranendonk et al. (2003b) as evidence for the biogenicity of these stromatolites, and for a marine sedimentary environment. One notable difference between the samples from the Strelley Pool Chert and that from

Heron Reef is the absence of negative Ce-anomaly in the former. Since negative Ce-anomalies arise from the oxidation of Ce in aqueous environments from the solvated 3+ state to insoluble Ce(IV) (German and Elderfield, 1990), the absence of Ce-anomaly in Archaean stromatolites is readily explained by their formation under low concentrations of free oxygen. It has indeed been proposed that the Archaean atmosphere was essentially devoid of oxygen (*e.g.* Holland, 1999). We will discuss this point in more details in further sections.

Johannesson et al. (2006) cautioned against the use of REY patterns in palaeoenvironmental reconstructions. They showed that groundwaters from Central México are statistically indistinguishable from modern seawater, and concluded that REY data should be completed by Nd isotopic data to be used as an argument in palaeoenvironmental reconstructions. However, in a recent study, Bolhar and Van Kranendonk (2007) compared the REE relative abundance of eight stromatolitic samples from four formations (Kylena, Tumbiana, Maddina and Jeerinah) of the Fortescue Group with the seawater proxy of Webb and Kamber (2000) and with an algal stromatolite from an Eocene (56-34 Ma) anoxic lacustrine deposit (the Green River Formation in the western United States). Bolhar and Van Kranendonk (2007) concluded from that the analysed samples were "deposited in either a lacustrine setting, or a shallow lagoonal setting with a dominant riverine input". The main arguments of Bolhar and Van Kranendonk (2007) in favour of this conclusion are the absence of La and Gd anomalies and the low Y/Ho ratio of their analysed samples. Positive La and Gd anomalies and elevated Y/Ho ratios have been proposed to constitute an indicator for derivation of the REE from seawater (Bau and Dulski, 1996; Kamber et al., 2004).
In the present study, we report new data from the Mopoke Member of the Kylena Formation (four samples) and from the Meentheena Member of the Tumbiana Formation (nine samples) in the Meentheena Centrocline and in the Oakover Syncline. These two members have been proposed to represent similar shallow depositional settings (Williams and Bagas, 2007b). Our data are mostly similar to that of Bolhar and Van Kranendonk (2007). However, following Kamber and Webb (2001), we propose that the lack of La and Gd anomaly and the low Y/Ho of the Fortescue carbonates is best explained by a high detritic input. We conclude that while a distinction between a marine and a lacustrine setting cannot be made based on REY data, the analysed stromatolites were deposited in a shallow environment under high detritic input.

Samples and sampling strategy

Two silicified carbonates containing microbial laminations were sampled from the Mopoke Member of the Kylena Formation (Figs. 3.17 and 3.18). One columnar stromatolite (B15B), one domal stromatolite (B20H) and a sample bearing microbial laminations (B20F) were selected from the Meentheena Member of the Tumbiana Formation. Two stromatolites from the Mopoke Member and six stromatolites from the Meentheena Member from Olivier et al. (in prep.) are included in the study (Tab. 3.5). The samples labeled MP come from the same site as sample

BC19, sample MC27 from the same site as the samples labeled B20 (Fig. 3.17) and the samples labeled CS were collected along a section in the Tumbiana Formation in the southwest part of the Meentheena Centrocline, located in the inset a of Fig. 3.11. The number in the name of samples labled CS refers to the distance in metres from the base of the section.

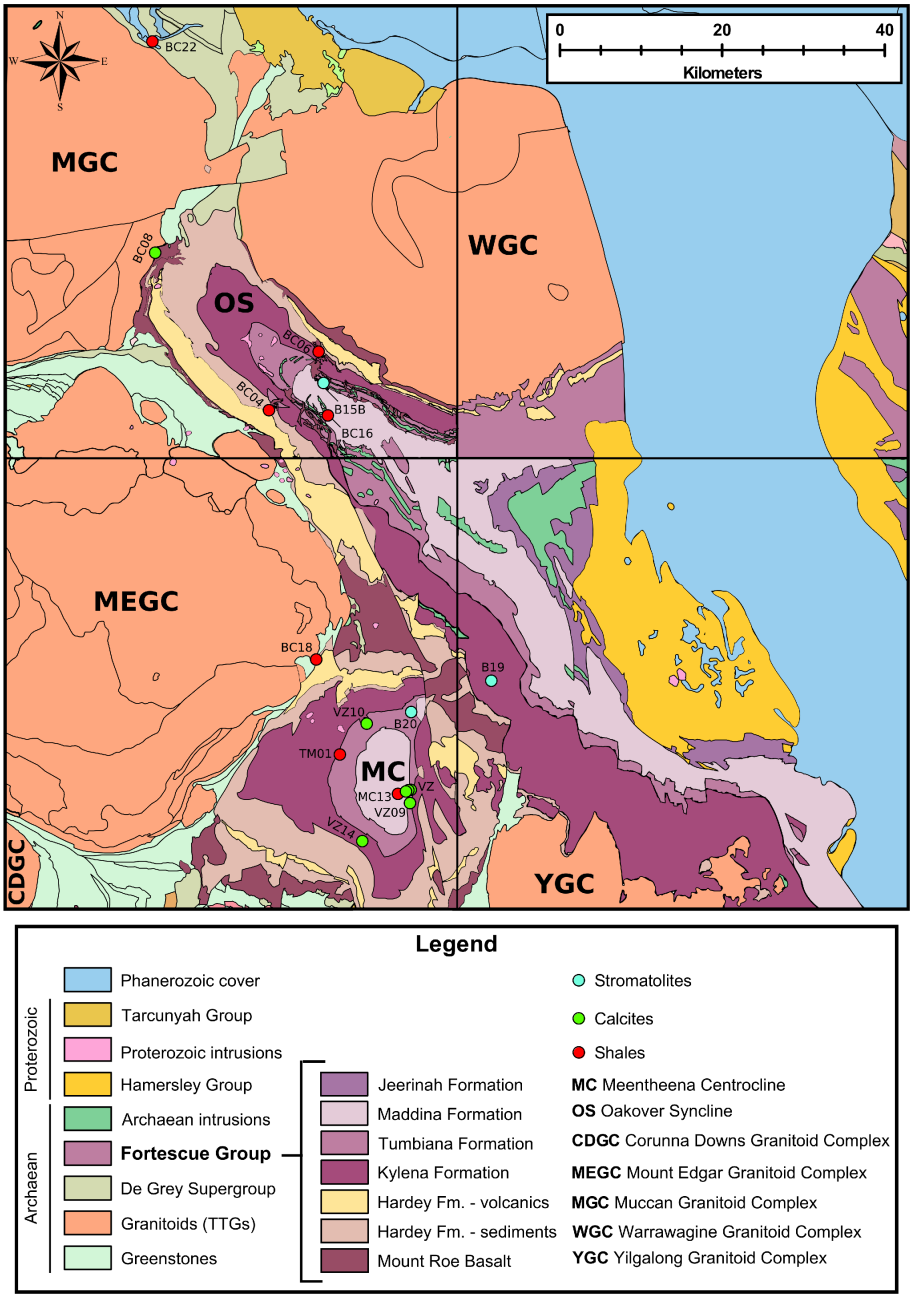

Figure 3.17: Simplified geological map of the study area showing sampling sites. At site VZ, from right to left: VZ01 and VZ04, VZ77, VZ78. Map compiled from the digital 1/100 000th geological sheets Muccan, Warrawagine, Mount Edgar and Yilgalong available at http://mapserver.doir.wa.gov.au/datacentre/.

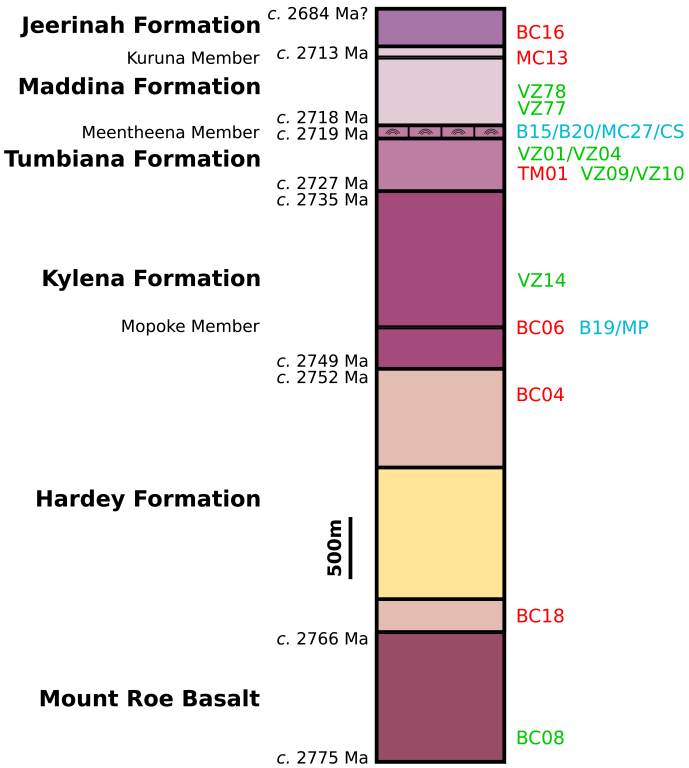

Figure 3.18: Simplified stratigraphic column of the Fortescue Group in the study area (Fig. 3.17). Thicknesses and ages are taken from Williams and Bagas (2007b) and Williams (1999b). Sample labels are reported on the right hand side (stratigraphic position is approximate). The colour code is the same as in Fig. 3.17. Samples BC22 and VZ93 are from units older than the Fortescue Group and are thus not shown.

Methods

Whole rock samples were cut using a diamond rocksaw and cubes of unaltered material were selected for crushing using a tungsten carbide mill. Depending on the amount of material available, between 25 and 85 g of powder were obtained. These samples were then split using an aluminium sample splitter. 5 g of subsample were analysed for their content in major elements at the University of New South Wales by routine X-ray spectrographic analysis following the method of Norrish and Hutton (1969). Approximately 100 mg of the same subsample were weighed accurately for routine ICPMS trace element analysis undertaken at GEMOC at Macquarie University, Australia. For the samples from (Olivier et al., in prep.), stromatolitic laminae were selected from polished slabs under binocular lenses in order to avoid detrital sediments. These samples were then prepared following the method described in Olivier and Boyet (2006) and were analysed for trace elements at ENS Lyon, France.

Results

Major elements

The data in Tab. 3.4 show that the analysed stromatolites consistently contain 36-42 wt.% CaO and 20-25 wt.% SiO_2. The relatively low contents in MgO, MnO and FeO suggest that dolomite and ankerite are minor components of the rock, consistently with electron microscopy analyses on drill core samples that show that Tumbiana carbonates consist of 90% calcite with minor amounts of dolomite and calcite (Thomazo et al., 2009).

Table 3.4: Content in major elements (in weight percentage of oxides) of the analysed stromatolites.

Oxide wt.%	B19A	B19B	B20F	B20H	B15B
SiO_2	22.5	25.17	24.16	25.23	19.93
TiO_2	0.14	0.09	0.15	0.22	0.15
Al_2O_3	1.81	0.85	2.07	2.05	1.77
Fe_2O_3	2.09	0.93	2.88	3.5	4.12
MnO	0.16	0.11	0.35	0.47	0.55
MgO	0.98	0.52	1.08	0.97	1.03
CaO	38.99	39.23	37.54	36.26	41.27
Na_2O	0.09	BLD[a]	BLD	0.22	0.6
K_2O	0.39	0.21	0.16	0.08	0.12
P_2O_5	0.03	0.03	0.03	0.05	0.03
SO_3	0.4	0.02	BLD	0.03	0.14
L.O.I. [b]	31.58	31.85	30.78	29.88	29.36
Total	99.16	98.91	99.17	98.97	99.06
$CaCO_3$	71.17	71.86	68.89	66.83	71.3

[a] BLD: below level of detection (< 0.01%)
[b] LOI: loss on ignition at 1,050°C

The maximum content of the samples in $CaCO_3$ (assuming that the loss on ignition represents the carbon in calcite) ranges between 67 and 72 wt.% (Tab. 3.4). Raman spectroscopy analyses at ENS Lyon on stromatolite B20F showed that the sample contains fine-grained sediments as expected from its content in SiO_2 and Al_2O_3, and amorphous carbon (*i.e.* organic matter). The total organic content (TOC) of 14 drill core stromatolite samples analysed by Thomazo et al. (2009) ranges between 0.06 and 0.43wt.% with an average of 0.13±0.1wt.%. The TOC is likely to be higher in surface samples that are more exposed to contamination by organic matter.

Rare earth elements and yttrium (REY)

The trace element data of the analysed stromatolites are shown in Tab. 3.5 and the PAAS-normalised (Post-Archaean average Australian Shale; Taylor and McLennan, 1985) REY patterns are shown in Fig. 3.19. PAAS is chosen as a standard to be consistent with previous investigations on Archaean stromatolites (Kamber and Webb, 2001; Van Kranendonk et al., 2003b; Kamber et al., 2004; Bolhar and Van Kranendonk, 2007) despite the fact it is a composite of 23 analyses of shales younger than the Archaean.

Table 3.5: Concentrations in rare earth elements and yttrium (in part per million) of the analysed stromatolites. The REE anomalies used in Fig. 3.20 are also shown.

ppm	Kylena Formation				Tumbiana Formation								
	B19A	B19B	MP01[a]	MP02[a]	B20F	B20H	B15B	MC27[a]	CS46[a]	CS58[a]	CS78[a]	CS85[a]	CS93[a]
Y	6.11	4.45	5.08	3.63	6.25	8.09	8.12	2.73	2.84	1.87	6.17	12.39	10.08
La	4.54	4.09	4.96	5.18	6.19	8.28	7.58	2.66	2.73	1.96	6.60	11.13	7.72
Ce	7.72	7.13	9.33	10.34	11.56	13.86	12.67	5.01	4.97	3.63	11.97	21.52	14.69
Pr	0.93	0.85	0.98	1.18	1.41	1.61	1.46	0.55	0.57	0.43	1.36	2.42	1.75
Nd	3.33	3.17	3.89	4.23	5.34	5.94	5.26	2.31	2.29	1.63	5.49	9.53	7.39
Sm	0.73	0.62	0.72	0.75	1.15	1.21	1.07	0.50	0.46	0.31	1.18	1.91	1.66
Eu	0.2	0.16	0.18	0.17	0.35	0.38	0.24	0.19	0.18	0.19	0.28	0.54	0.46
Gd	0.78	0.65	0.83	0.78	1.19	1.25	1.16	0.59	0.52	0.40	1.39	2.10	1.93
Tb	0.13	0.11	0.13	0.10	0.19	0.2	0.18	0.08	0.08	0.06	0.22	0.34	0.31
Dy	0.78	0.66	0.78	0.64	1.14	1.12	1.04	0.53	0.44	0.33	1.40	2.09	1.69
Ho	0.18	0.15	0.17	0.14	0.24	0.25	0.23	0.09	0.10	0.08	0.29	0.46	0.37
Er	0.53	0.46	0.47	0.41	0.68	0.71	0.66	0.30	0.29	0.23	0.82	1.32	0.95
Yb	0.5	0.44	0.52	0.51	0.59	0.64	0.6	0.24	0.26	0.22	0.72	1.38	0.80
Lu	0.08	0.07	0.06	0.07	0.09	0.1	0.09	0.05	0.04	0.03	0.11	0.22	0.12
La/La^{*} [b]	1.34	1.3	1.06	1.08	1.25	1.31	1.3	1.11	1.19	1.21	1.18	1.1	1.19
Ce/Ce^{*} [c]	0.86	0.88	0.97	0.96	0.9	0.87	0.87	0.95	0.91	0.91	0.92	0.95	0.92
Pr/Pr^{*} [d]	1.04	1.02	0.92	1.01	1.02	1.01	1.01	0.92	0.96	1	0.95	0.96	0.95
Gd/Gd^{*} [e]	1.09	1.07	1.03	1.44	1.06	1.04	1.09	1.55	0.97	1.12	1.19	1.12	0.98
Y/Ho	34.64	29.18	29.38	26.54	25.53	32.64	35.52	28.78	27.64	24.25	21.35	27.2	27.6

[a] Data from Olivier et al. (in prep.).
[b] $La/La^{*} = \frac{La_P}{2Ce_P - Pr_P}$ where the subscript $_P$ designs PAAS-normalised values
[c] $Ce/Ce^{*} = \frac{Ce_P}{0.5(La_P + Pr_P)}$
[d] $Pr/Pr^{*} = \frac{Pr_P}{0.5(Ce_P + Nd_P)}$
[e] $Gd/Gd^{*} = \frac{Gd_P}{2Tb_P - Dy_P}$

All samples are depleted in REEs compared to PAAS (Fig. 3.19). Samples from the Mopoke Member are uniform in their REE content ($\Sigma REE = 22.5$ ppm $\pm$ 1.8) whereas the REE content ranges between 9.5 and 55 ppm for samples from the Meentheena Member ($\Sigma REE = 27.4$ ppm $\pm$ 12.8). Since the absolute content of REEs does not systematically decrease with the SiO_2 content of the samples, the variations in REE abundance may be attributed to the proportions of organic C-rich, fine-grained laminated calcite to organic C-poor, coarse-grained cements (Kamber and Webb, 2001). This can however not be verified in this study since the TOC of the samples was not analysed. Samples CS78, CS85 and CS93, toward the top of the section of Olivier et al. (in prep.), are less depleted in REE than samples CS46 and CS58, toward the bottom of the section. This possibly reflects a variable importance of diagenetic processes.

The REY patterns in Fig. 3.19 are slightly enriched in middle rare earth elements (MREE) to HREE with $Pr/Yb_{PAAS} = 0.67 \pm 0.08$, $Pr/Sm_{PAAS} = 0.81 \pm 0.09$ and $Sm/Yb_{PAAS} = 0.83 \pm 0.13$. The bell-shaped REY pattern of sample CS93 is possibly due diagenesis since modelling of the partitioning of REE between water and apatite by Reynard et al. (1999) suggests that bell-shaped REY patterns in biogenic fossil apatites are due to extensive diagenesis. This constitutes a warning regarding the diagenesis of the analysed samples. Most of the samples present positive Eu-anomalies, with $Eu/EU^{*} = 1.12 \pm 0.1$ for the Kylena Formation and $Eu/EU^{*} = 1.45 \pm 0.45$ for the Tumbiana Formation. Samples MP01, MP02, B15B and CS78 do not present a significant

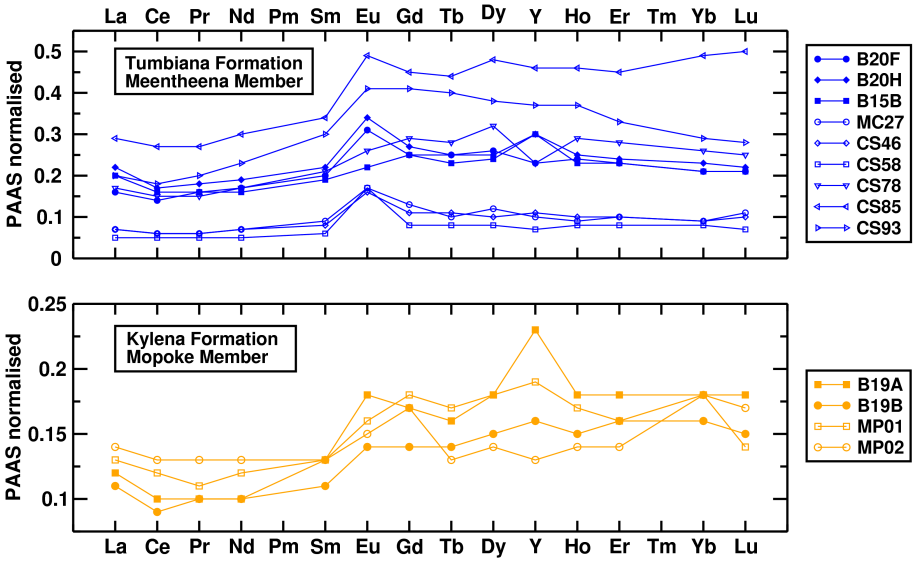

Figure 3.19: Rare earth element and yttrium (REY) patterns for the analysed stromatolites. Open symbols denote data from Olivier et al. (in prep.).

Eu-anomaly, and samples MP02 and CS78 further present a slight deficiency of Y in relation to neighbouring REE. Y/Ho ratios cluster at 28.5 ± 4 with slightly lower values for the samples from Olivier et al. (in prep.) (26.6 ± 2.6 compared to 31.5 ± 4.1). La displays a slight positive anomaly ($La/La^* = 1.2 \pm 0.1$) with again slightly lower values for the samples from Olivier et al. (in prep.) (1.14 ± 0.06 compared to 1.3 ± 0.03). Ce and Gd display no significant anomaly (to the exception of samples MP02 and MC27 for Gd anomaly with respectively 1.44 and 1.55). For the sake of consistency, all anomalies are calculated in the same way as in Bolhar and Van Kranendonk (2007) (see Tab. 3.5).

Comparison with trace element data on Archaean and Phanerozoic stromatolites

Fig. 3.20 summarises the main arguments used by Bolhar and Van Kranendonk (2007) (see their Fig. 8) to discriminate between a marine and a lacustrine setting for the Fortescue carbonates. The average REY patterns for each formation are compared in Fig. 3.20a with the results of Bolhar and Van Kranendonk (2007), with the sample from the Green River Formation, used by Bolhar and Van Kranendonk (2007) as a proxy for modern anoxic lakes, and with average patterns for the Holocene Heron Reef (Webb and Kamber, 2000) and for the 3.4 Ga stromatolites from the Strelley Pool Chert (Van Kranendonk et al., 2003b). Our average for the Tumbiana Formation ($n = 8$) is similar to that of Bolhar and Van Kranendonk (2007) ($n = 3$) for its contents in HREE but contains more LREE and MREE. Compared to the sample of Bolhar and Van Kranendonk (2007), our average for the Kylena Formation ($n = 4$) contains slightly more REE and displays a flatter pattern with no depletion in HREE. The depletion in HREE of the Kylena sample of Bolhar and Van Kranendonk (2007) is conspicuous and remains to be explained. Overall, our REY patterns are broadly similar to that of the sample from the

Green River Formation. The main differences are the slightly negative La-anomaly displayed by the sample from the Green River Formation and the positive Eu anomaly displayed by the Fortescue carbonates. In sharp contrast, our average REY patterns strongly differ from the proxy for modern sea water of Webb and Kamber (2000) and from the of 3.4 Ga stromatolites from the Strelley Pool Chert (Van Kranendonk et al., 2003b). These latter patterns display higher Y/Ho, stronger La-anomalies and are more LREE-depleted.

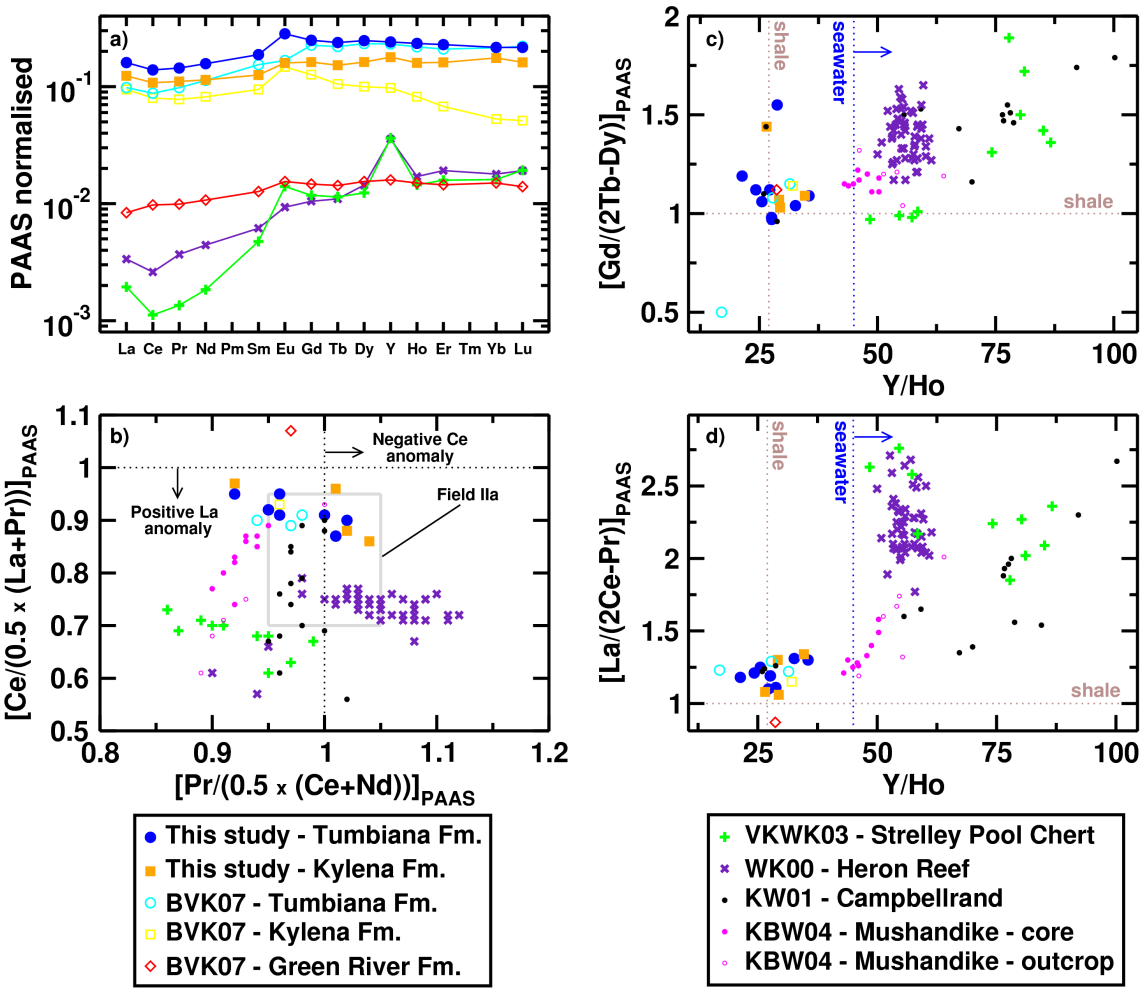

Figure 3.20: a) Average rare earth element and yttrium (REY) patterns; b) discrimination between La and Ce anomalies using a plot of shale-normalised Ce/Ce* vs. Pr/Pr*. The field IIa is from Bau and Dulski (1996); c) discrimination between marine and non-marine sediments using a plot of shale-normalised Gd/Gd* vs. Y/Ho; d) same as c) for La/La*. BVK07: Bolhar and Van Kranendonk (2007); VKWK03: Van Kranendonk et al. (2003b); WK00: Webb and Kamber (2000); KW01: Kamber and Webb (2001); KBW04: Kamber et al. (2004).

Fig. 3.20b is a plot of the Ce-anomaly versus the Pr-anomaly for the samples shown in Fig. 3.20a, along with data on Archaean stromatolites from the 2.52 Ga Campbellrand carbonate platform, South Africa (Kamber and Webb, 2001) and from the *c.* 2.84 Ga Mushandike stromatolitic limestones, Zimbabwe (Kamber et al., 2004). Samples that display a negative Ce-anomaly plot in the bottom right quadrant while samples that display a positive La-anomaly plot in the bottom

left quadrant (Bau and Dulski, 1996). The field IIa of Bau and Dulski (1996) that indicates analytically insignificant Ce anomaly but positive La anomaly is also shown in Fig. 3.20b. Most samples from the Kylena and Tumbiana Formations plot within the field IIa of Bau and Dulski (1996) with $0.92 < Pr/Pr^{*} < 1.04$ and $0.86 < Ce/Ce^{*} < 0.95$ (Fig. 3.20b). This indicates the absence of negative Ce anomaly and the presence of a positive La anomaly. The Fortescue carbonates thus seem to present a positive La anomaly, contrary to the statement of Bolhar and Van Kranendonk (2007).

Fig 3.20c and d respectively show Gd and La anomaly as a function of Y/Ho. These plots show that in terms of Y/Ho, stromatolites from the Tumbiana and Kylena Formations (Y/Ho<30) are clearly distinct from modern seawater (Y/Ho>45) and from other plotted Archaean stromatolites (Y/Ho>42), to the notable exception of the three shallowest samples from the Campbellrand carbonate platform (Kamber and Webb, 2001). These three samples were not plotted in Fig. 8 of Bolhar and Van Kranendonk (2007). Overall, Gd and La anomalies are weaker for the Fortescue carbonates compared to other samples. One sample from the Tumbiana Formation from (Bolhar and Van Kranendonk, 2007) displays a low Gd anomaly and samples MP02 and MC27 display high Gd anomalies. Other samples have Gd anomalies of 1.07 ± 0.06 and plot close to the sample from the Green River Formation and to shallow samples from the Campbellrand carbonate platform (Kamber and Webb, 2001). La anomalies are similar for the three shallow Campbellrand samples and for the Fortescue samples, whereas the sample from the Green River Formation does not display a positive La anomaly.

Discussion

Bolhar and Van Kranendonk (2007) focused on the differences in La, Gd anomalies and Y/Ho ratio between the Fortescue samples and the Strelley Pool Chert samples that are *interpreted* as seawater derivatives to conclude that Fortescue samples are not of marine origin. However, contamination of the analysed sediments by detrital or terrigenous material is another possible explanation for the data. This is the explanation put forward by Kamber and Webb (2001) to explain the different signature in Y/Ho and La anomaly of their three analysed samples from sedimentologically shallower environments. Kamber and Webb (2001) used mixing calculations between a shale end-member and a microbialite end-member that showed that contamination by a few percent of sedimentary material results in a drop in Y/Ho and La anomaly. They concluded that their three shallower samples had been deposited in an environment with greater detritic input compared to deeper samples. In this regard, it is worth noting that the data plotted in each of Fig 3.20c and d describe general trends from high Y/Ho and elevated anomaly towards shale values. The Fortescue samples, the three shallow Campbellrand samples and the sample from the Green River Formation are the only ones to plot close to the shale cross-hairs. Importantly, the only stromatolites reported from the Green River Formation occur in a unit deposited in < 10 m water depth (Keighley et al., 2003), possibly with high detritic input. The absence of La and Gd anomaly and the low Y/Ho content of the sample from the Green River Formation

could thus reflect a high detritic or terrigenous input rather than a lacustrine signature. In this regard, one may simply conclude that the Fortescue samples were exposed to relatively high detritic or terrigenous input, possibly in a shallow environment. This is consistent with the SiO_2 content of the samples (Tab. 3.4) suggesting detrital quartz is an important component of the samples, and with sedimentary structures pointing to shallow depth for the Tumbiana Formation (Flament et al., 2009). However, the samples from Olivier et al. (in prep.) that were selected to avoid detrital sediments present lower Y/Ho and positive La anomalies, contrary to what would be expected from the mixing calculations of Kamber and Webb (2001). This could indicate that the stromatolitic laminae were formed in equilibrium with water of terrigenous signature. Alternatively, very fine sediments could be incorporated between stromatolitic laminae during the formation of the algal build-up. To the first order, stromatolitic structures can be thought of as resulting from the competition between upward phototropic growth and lateral growth from sedimentary input (Batchelor et al., 2005). Columnar stromatolites form in environments with little sedimentary input, whereas algal mats form in environments with high sedimentary input. In this regard, it is worth noting that the analysed microbial mat (sample B20F) displays lower Y/Ho and La anomaly than domal (sample B20H) and columnar (sample B15B) stromatolitic buildups (Tab. 3.5). Such considerations should also probably be included when using REY patterns to assess the origin of Archaean stromatolites.

3.4.2 Non-ubiquitous unidirectional flow suggested by asymmetric ripples

Another argument of Awramik and Buchheim (2009) in favour of a lacustrine depositional setting for the Meentheena Member is the absence of asymmetric ripples that would indicate unidirectional flow and could thus reflect the effect of tides. As noted by Awramik and Buchheim (2009), the absence of asymmetric ripples is not a definitive argument against a marine setting since they would not be expected in a tideless or microtidal epeiric sea. Furthermore, Fig. 3.21 shows trains of asymmetric ripple marks identified by Olivier et al. (in prep.) at depths of 79 and 123 m in the diamond drillcore PDP1 recovered in the northern part of the Meentheena Centrocline as part of the Pilbara Drilling Project (Van Kranendonk et al., 2006). Similar structures also occur at a depth of 88 m in the drillcore (not shown). While they are not ubiquitous, asymmetric ripples do occur in the Meentheena Member. The argument of the absence of asymmetric ripples against a marine setting does thus not hold.

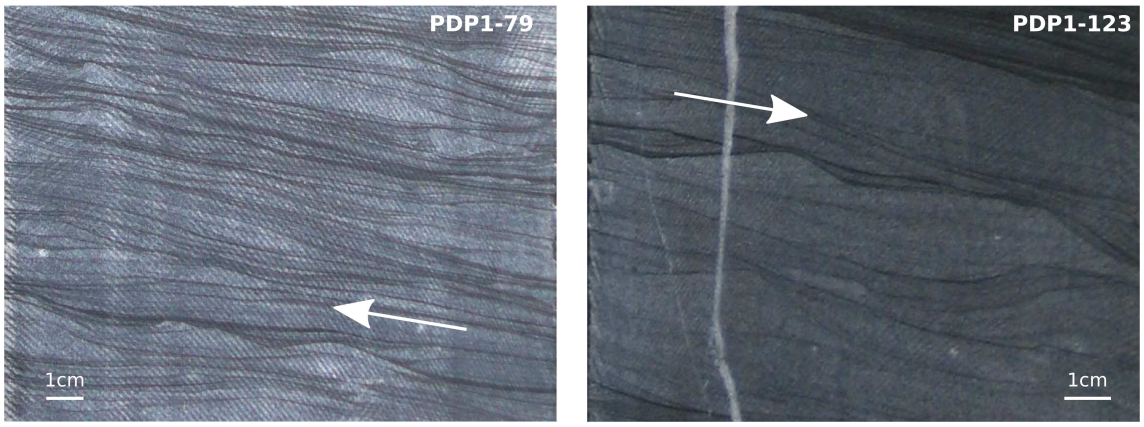

Figure 3.21: Centimetre-scale asymmetric ripples from drillcore PDP1. Numbers refer to the depth within the drillcore. Arrows indicate the inferred flow direction. Scale is approximate.

3.4.3 Conclusion and future work

The controversy regarding the depositional environment of the Upper Fortescue Group holds because no definitive argument allows for a clear, definitive distinction between a marine or a lacustrine setting. We showed that rare earth element data from the Fortescue Group do not uniquevocally point to a lacustrine or lagoonal, contrary to the conclusion of Bolhar and Van Kranendonk (2007). Instead, these data show that the carbonates of the Mopoke Member and of the Meentheena Member were deposited in a shallow setting (< 10 m) with relatively high detritic input. This is in agreement with the shallow depositional depth deduced from the occurrence of mud cracks in the Meentheena and Mopoke Members, and of flat pebbles in the Meentheena member (see Fig. 3.16 for more shallow depth sedimentological structures) and reinforces the modelling results obtained therein. Furthermore, we reported asymmetric ripple marks from drillcore PDP1 while Awramik and Buchheim (2009) argued that no asymmetric ripples occurred in the Meentheena Centrocline. Unidirectional flow did occur during the deposition of the Meentheena Member, but this observation does not unequivocally argue in favour of a marine setting. The fact that two of the arguments in favour of a lacustrine model are inconclusive illustrates the need for a strong, definitive argument. Soon to be released strontium and neodymium isotopic data, combined with an integrated geochemical and sedimentological study of the Tumbiana Formation (Olivier et al., in prep.), will help to better characterise the depositional environment of the Mopoke Member (Kylena Formation) and Meentheena Member (Tumbiana Formation) in the East Pilbara Terrane.

3.5 Conclusion

In this chapter, we proposed a method to evaluate Archaean continental geotherm. Numerical modelling shows that lower crustal flow of ductile, hot continental crust can explain the rapid relaxation of topographic anomalies such as continental flood basalts. These models can predict the relaxation time as a function of Moho temperature. Sedimentological observations and geochronological data can be used to infer a relaxation time from natural example. This in turn allows to estimate the Moho temperature at the time of deposition of the sediments. Applied to the Upper Fortescue Group in the Meentheena Centrocline, this method suggests that in the Pilbara Craton, the Moho temperature has cooled by 200 $\pm$ 100°C since 2.7 Ga. This predicted cooling of the continental crust is consistent with the preservation of ductile features such as crustal diapirism in Archaean continental crust. The estimated temperature range is large due to uncertainties in the determination of the relaxation time from field data and to the lack of strong constraints regarding the rheological model and the reactivation of the dome and basin structure. Lower crustal flow is a plausible mechanism to explain the accommodation of the Upper Fortescue sequence in the absence of upper crustal extension in the East Pilbara Terrane. Together with the higher sea levels predicted in the previous chapter, gravity-driven lower crustal flow fully explain the widespread occurrence of subaqueous flood magmatism in the Precambrian.

4

Crustal growth, emerged land area, and consequences for the composition of the oceans

Contents

4.1 Interactions of the continental crust with the mantle and with the exosphere

We have seen in previous chapters that in the long term, sea level is controlled by the cooling of the mantle and by the strengthening of the continental lithosphere. In the present chapter, we build onto our models to further investigate the interactions between the mantle, the continental crust and the exosphere (oceans and atmosphere) that are summarised in Fig 4.1. The effects of mantle temperature, continental area and hypsometry on sea level, emerged area and ridge depth were the object of chapters 2 and 3. In chapter 2, continental area and mantle temperature were treated as independent parameters. However, Spohn and Breuer (1993) pointed out that crustal growth has an effect on mantle temperature since the continents preferentially incorporate radiogenic elements as they grow, and impose a thermal insulation on the mantle (Fig. 4.1). The mantle would have been more radiogenic prior to the extraction of the continental crust, which implies higher mantle temperature early in Earth's history (Spohn and Breuer, 1993), and the thermal insulation imposed by the continents results in a slower cooling of the mantle (Grigné and Labrosse, 2001). We shall further discuss these effects in the next sections, and incorporate them in our models to quantify their consequences for the evolution of sea level and emerged land surface.

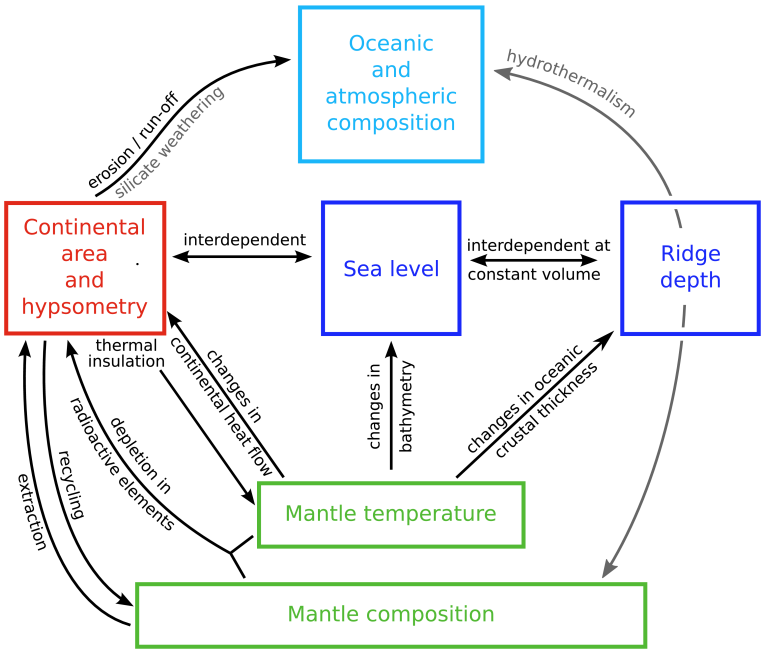

Figure 4.1: Flowchart representing the interactions between the variables discussed in the present chapter. Grey arrows and text denote processes that are not quantified in the present study and will be qualitatively discussed in chapter 5.

Another effect of the continents on the composition of the mantle is due to the growth of the continental crust, that is the difference between the extraction of felsic silicates from the mantle

and their recycling into the mantle (Fig. 4.1). Recycling of continental crust can notably occur by subduction of sediments (*e.g.* Fyfe, 1978; Reymer and Schubert, 1984) and by delamination of lower continental crust. Rudnick (1995) pointed out that the andesitic bulk composition of the continental crust is more evolved than expected from the dominantly basaltic magmatism that is responsible for present-day crustal growth processes. One possible model to explain this discrepancy is the delamination of the more mafic lower crust into the mantle (Rudnick, 1995). In this model, multiple melting events would result in the rise of differentiated, relatively light melt, and in the accumulation of a less differentiated, dense residue in the lower crust. This residue could be recycled into the mantle by delamination. Such processes could be identified from geochemical anomalies Rudnick (1995) but would be difficult to quantify.

The accretion of island arcs has been proposed as a likely process of crustal addition because island arcs magmatism is of andesitic composition, similar to that of the bulk continental crust (*e.g.* Reymer and Schubert, 1984; Taylor and McLennan, 1985). However, andesitic suites are relatively rare in Archaean volcanic sequences ($11 \pm 6\%$ of supracrustal rocks older than 3.5 Ga compared to $19 \pm 16\%$ for supracrustal rocks younger than 542 Ma; Condie, 1993), so that crustal additions in the Archaean could not be accounted for by this process. Taylor and McLennan (1985) suggested that arc volcanism accretion was efficient only during the post-Archaean. Thus, other extraction processes must be called for to explain the formation of the differentiated Archaean tonalite-trondhjemite-granodiorite (TTG) series. One problem regarding the formation of TTGs is the lack of constrain regarding the depth of melting of their source Rudnick (1995). In a hot subduction model, the source of TTGs could either be the lower crust, the subducting slab or the mantle wedge Rudnick (1995). Thus, evidence for the formation of TTGs by subduction processes is far from compelling. Other possible crustal addition processes possibly responsible for the formation of Archaean TTGs include intraplate magmatism related to plume volcanism Rudnick (1995), the accretion of buoyant oceanic plateaus differentiated by melting processes related to their accretion, and the remelting of thick basaltic piles (Albarède, 1998b) followed by partial convective overturn of the crust as in the sagduction model (*e.g.* McGregor, 1951, see also section 1.2.3). The complexity of crustal extraction and recycling processes is part of the reason why the continental growth curve is poorly constrained. We shall further discuss the problem of crustal growth in the present chapter.

Finally, Fig 4.1 shows that the continental crust regulates the composition of the oceans and of the atmosphere by weathering and erosion processes. These processes are closely related, since the rate of physical and chemical weathering processes constitute the ultimate limit on erosion rates Hay (1998). In a way, erosion can be seen as the transport of previously weathered geological material. Weathering processes are of importance to the evolution of the atmosphere since silicate weathering is a sink of atmospheric oxygen and of atmospheric carbon dioxide (*e.g.* Hay, 1998). Thus, secular changes in the rate of silicate weathering, related to emerged land surface, are important to Archaean climate modelling, as shown for example in the models of Godderis and Veizer (2000) and of Sleep and Zahnle (2001). Finally, the efficiency of erosion

processes regulates the sedimentary run-off from the continents to the oceans and is thus of importance to the composition of the oceans. For instance, the evolution of the strontium isotope signature of marine carbonates is thought to reflect changes in the relative contribution of the radiogenic continents compared to that of the depleted mantle to the composition of the oceans (*e.g.* Shields and Veizer, 2002). We will further discuss the regulation of the composition of the oceans and of the atmosphere by weathering and erosion processes in the following sections. We first focus on the effect of crustal growth on mantle temperature.

4.1.1 Effect of the continental lithosphere on mantle temperature

As shown in Fig. 4.1, the thermal evolution of the Earth is closely linked to that of the extraction and growth of the continental crust. Since the continental crust preferentially concentrates radiogenic elements, the early mantle was less depleted in radiogenic elements when the volume of the continents was smaller. Spohn and Breuer (1993) pointed out that this progressive depletion of the mantle implies that the mantle was more radiogenic and thus hotter in the past. This effect enhances the higher radiogenic heat production in the past due to radiogenic decay. Thermal evolution models by Grigné and Labrosse (2001) suggest that an initially non-depleted mantle would have been $\sim$ 120°C hotter than a depleted mantle at 4.5 Ga. Furthermore, the lower average present-day heat flow in continental areas (65 mW m^{-2}) compared to the oceanic areas ($\sim$ 100 mW m^{-2} Pollack et al, 1993) suggests that oceans are more efficient than continents at evacuating internal heat. As they grow, continents would thus act as a thermal insulator with respect to the mantle, and efficient heat loss would occur over an increasingly smaller oceanic area. This thermal blanketing effects of continents on thermal evolution models was studied by Spohn and Breuer (1993), and later by Grigné and Labrosse (2001) who considered perfectly insulating continents. Grigné and Labrosse (2001) showed that continental insulation results in predicted mantle temperatures between 30 and 100°C hotter, depending on crustal growth models. Grigné and Labrosse (2001) further suggested that to account for the observed present-day oceanic heat flow, crustal growth must have begun before 3 Ga and reached steady-state by 1.5 Ga. Considering continents as perfect thermal insulators is a useful end-member to understand their thermal blanketing effect, but this is probably an overestimation. In a recent review of the thermal budget of the Earth, Jaupart et al. (2007) suggested that out of the total heat flow from continental areas of 14 TW, the crustal radiogenic heat flow is between 6 and 7 TW and the lithospheric radiogenic heat flow is between 0.25 and 1 TW. This leaves between 6 and 7 TW as a total non-radiogenic continental heat flow, which translates into an average reduced continental heat flow (that is the mantle heat flow below continents) between 27.7 and 32.3 mW m^{-3}, less than a third of the averaged oceanic heat flow (Pollack et al, 1993). Thus, continents are efficient insulators rather than perfect insulators. Nevertheless, keeping in mind that the mantle has probably not cooled by more than 200-300°C since the Archaean (see section 1.2.1), the effects of the continents on mantle temperature (100°C due to thermal blanketing and 120°C due to mantle depletion) are considerable. Finally, the presence

of continents also has an impact on plate tectonics. Indeed, it is not clear whether plate tectonics could operate at all in the absence of continents. Tackley (2000) used a strongly temperature-dependent viscosity combined with plastic behaviour above a given yield stress to obtain self-consistent plate tectonics in mantle convection models. Grigné and Tackley (2005) showed that the introduction of rigid continents in such mantle convection models stabilises the regime in plate tectonics mode, with no reversal to stagnant-lid regime, and also allows to obtain more realistic subduction geometries. Labrosse and Jaupart (2007) also pointed out that the observed present-day triangular seafloor age distribution, which reflects an equal probability of subduction of seafloor of any given age, could be imposed by the presence of unsubductable continents. Labrosse and Jaupart (2007) proposed that the seafloor age distribution would be rectangular on a continent-free Earth, which would modify the total oceanic heat flow of the Earth and thus the temperature of the mantle. This effect will be incorporated in the models presented in the present chapter.

4.1.2 Effect of the continental crust on the composition of the atmosphere and of the oceans

The effect of a change in the efficiency of weathering and erosion processes on the composition of the atmosphere and of the oceans can be illustrated from the recent example of the collision between Indian and Asia (Fig. 4.2). Kent and Muttoni (2008) attributed the observed increase in the amount of cherts in deep-sea sediments from $\sim$ 65 Ma to an increase in silicate weathering (Fig. 4.2a). The increase in the $^{87}Sr/^{86}Sr$ of marine foraminifera (used as a proxy for the oceanic $^{87}Sr/^{86}Sr$) from $\sim$ 40 Ma (Fig. 4.2a) also indicates an enhanced contribution of a radiogenic, continental source. Interestingly, there is a $\sim$ 10 Myr long lag between the peak in the amount of cherts in deep-sea sediments and the increase of $^{87}Sr/^{86}Sr$ suggesting that these proxies of chemical weathering could react on different time scales. While a difference of $\sim$ 10 Myr is relevant on short time scales such as in the example of the collision between India and Asia, it is less important to the study of secular trends.

Fig. 4.2b shows the climatic consequences of the formation of the Himalayas. The $\delta^{18}O$ of benthic foraminifera is used as a proxy for seawater, with lower values indicating higher temperatures. Fig. 4.2b shows that seawater temperature peaked at around 50 Ma and decreased from then on. As for the partial atmospheric pressure of CO_2 (pCO_2), deduced from several proxies including alkenones and leaf stomata (Kent and Muttoni, 2008, and references therein), it possibly decreased from $\sim$ 2000 ppm at 50 Ma to $\sim$ 250 ppm at 10 Ma. However, it should be noted that the data on CO_2 proxies are more scarce and present larger uncertainties when going back in time. Kent and Muttoni (2008) proposed that the increase in seawater temperature at the beginning of the collision between India and Asia was due to the release of CO_2 from subduction of carbonate-rich sediments deposited on the Thethyan seafloor. In this scenario, silicate weathering became the dominating climatic control after the closing of the Thetys at around 50 Ma.

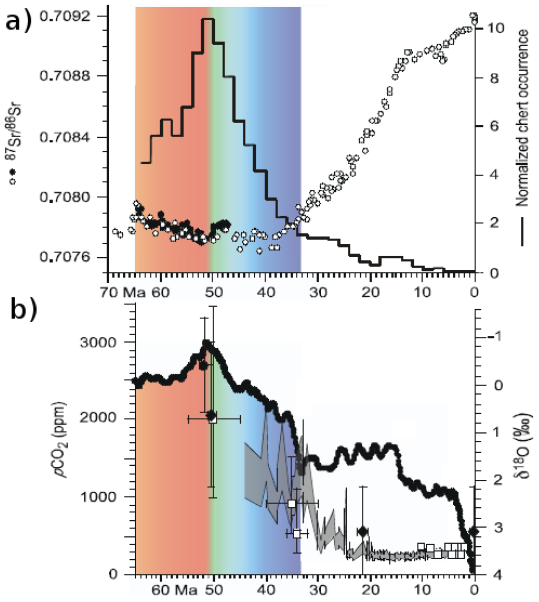

Figure 4.2: Consequences of the formation of the Himalayan mountain belt on the composition of the oceans and of the atmosphere (red and blue areas indicate the timing of collision between India and Asia). a) Strontium isotopic ratios ($^{87}Sr/^{86}Sr$) of marine foraminifera (circles) and chert occurrences in deep-sea sediments (histogram). b) Benthic foraminiferal oxygen isotope synthesis (black curve) and estimates of atmospheric concentrations of CO_2 based on several indicators (shaded curve, filled circle, filled diamonds and open circles). Figure from Kent and Muttoni (2008).

On short time scales, the climatic consequences of the formation of the Himalayas appear to be complex. However, enhanced erosion and silicate weathering are the dominating effect in the long-term, which was probably associated with the establishment of the present glacial climate (Raymo and Ruddiman, 1992). On even longer time scales, the increase of weathering and erosion processes associated with the secular increase in the area of emerged land (Flament et al., 2008) and in the elevation of mountain belts (Rey and Coltice, 2008) would thus exert a first-order control on the composition of the atmosphere and of the oceans. Sleep and Zahnle (2001) proposed a model for the long-term carbon dioxide cycle in which they assumed a constant continental area. In this model, the long-term carbon cycle is controlled by the mantle, and Sleep and Zahnle (2001) concluded that the Archaean climate would have been cool unless a greenhouse gas other than carbon dioxide was concentrated in the atmosphere. Taking the effect of a reduced continental area as predicted by our models would probably affect this conclusion. Indeed, similar modelling by Godderis and Veizer (2000) shows that an increasing continental area with time results in an increase in silicate weathering and in continental carbonate deposition, that are two sinks of carbon dioxide with respect to the atmosphere. This suggests that the Archaean pCO_2 could have been higher than proposed by Sleep and Zahnle (2001). However, as we shall discuss in a later section, the model of Godderis and Veizer (2000) assumes a constant continental freeboard so that the area of emerged land is still overestimated in this model.

4.1.3 Contrast between crustal growth models

We saw in section 1.4.1 that many contrasted crustal growth models have been proposed over the years. These models can be divided in two main categories, including delayed crustal growth models that propose a significant extraction of juvenile continental crust from the mantle during the Neoarchaean (*e.g.* Veizer and Jansen, 1979; Taylor and McLennan, 1985), in stark contrast of early crustal growth models that propose an early extraction of felsic material and a balance between extraction and recycling processes over the last $\sim$ 3.8 Ga (*e.g.* Fyfe, 1978; Armstrong, 1981). In this subsection, we propose an overview of the geochemical proxies used to build crustal growth models from each category.

Delayed crustal growth models

Evolution of the trace element composition of shales as a proxy for crustal growth

Taylor and McLennan (1985) studied the time evolution of the trace element composition of fine-grained sediments, and especially that of black shales, used as a proxy for the composition of the upper continental crust. Rare earth elements (REE), Th and Sc are particularly suited to this analysis because they are largely immobile during the processes of erosion, transport and sedimentation. The analysis of Taylor and McLennan (1985) revealed changes in several geochemical indexes, some of which are shown in Fig. 4.3. Archaean fine-grained sediments do not display a negative Eu anomaly (Eu/Eu^*), contrary to post-Archaean fined-grained sediments, and they display lower ΣLREE/ΣHREE and Th/Sc than post-Archaean sediments (Fig. 4.3). Negative Eu anomalies in sedimentary rocks, and thus in the upper continental crust, reflect chemical fractionation within the continental crust and particularly the production of potassium-rich, differentiated granitic rocks that display negative Eu anomalies. Th is an incompatible element whereas Sc is compatible, and LREEs are incompatible with respect to HREEs. Thus, ratios of ΣLREE to ΣHREE and of Th to Sc are used as an index of chemical differentiation. Elevated ΣLREE/ΣHREE and Th/Sc ratios indicate an enrichment in incompatible elements with respect to compatible elements and thus reflects differentiated material.

The trends in Eu anomaly, ΣLREE/ΣHREE and Th/Sc in (Fig. 4.3) all suggest that the upper continental crust was less differentiated (*i.e.* more mafic) in the Archaean than in the post-Archaean. Based on these observations, Taylor and McLennan (1985) proposed a crustal growth model characterised by a period of juvenile crustal extraction towards the end of the Archaean (Fig. 1.9).

Evolution of the oceanic $^{87}Sr/^{86}Sr$ as a proxy for crustal growth

Since the trace element composition of fine-grained sediments recorded the appearance of the differentiated continental crust in the late Archaean, a synchronous change is to be expected in the composition of the oceans. We saw in section 4.1.2 that the $^{87}Sr/^{86}Sr$ of marine carbonates is used as a proxy of the oceanic $^{87}Sr/^{86}Sr$. Changes in oceanic $^{87}Sr/^{86}Sr$ reflect changes in the

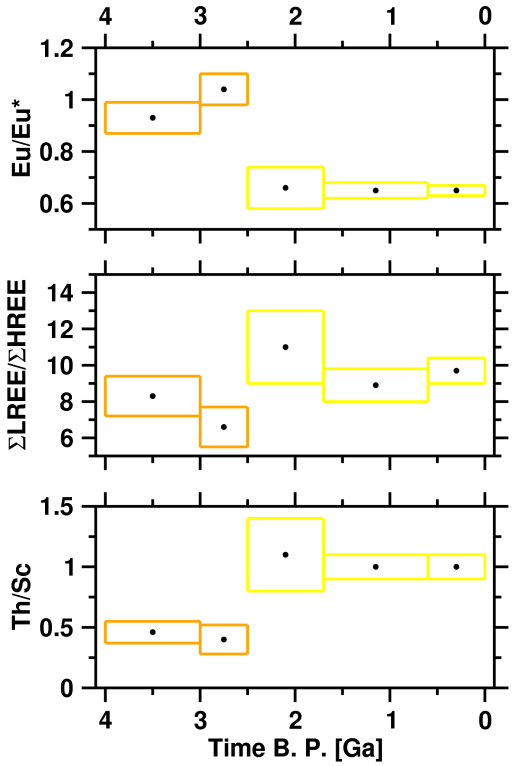

Figure 4.3: Time averages of geochemical indexes in fine-grained sediments (from Taylor and McLennan, 1985). All three geochemical indexes display a shift at the Archaean/Proterozoic boundary.

relative contributions of the continental versus mantle chemical reservoirs to ocean composition. A compilation of strontium isotopic signature in marine carbonates through time reveals that the oceanic $^{87}Sr/^{86}Sr$ ratio increases over time (see Fig. 4.4). This increase in $^{87}Sr/^{86}Sr$ reflects the increasing contribution of a radiogenic source, *i.e* of the continental crust to the composition of the oceans. Based on this geochemical proxy, Veizer and Jansen (1979) proposed a "late" continental growth curve that is broadly similar to that of Taylor and McLennan (1985). There are however several problems in using the "oceanic" $^{87}Sr/^{86}Sr$ as a proxy for crustal growth. Firstly, the best *maximum* estimate of "oceanic" $^{87}Sr/^{86}Sr$ is assumed to be given by the least radiogenic value at any given time on the basis that "postdepositional alteration *nearly* always causes an increase in $^{87}Sr/^{86}Sr$" (Shields and Veizer, 2002). Thus, the shift in oceanic $^{87}Sr/^{86}Sr$ from mantle-derived $^{87}Sr/^{86}Sr$ observed at $\sim$ 2.8 Ga (Fig. 4.4) could be an artifact due to postdepositional alteration. Moreover, this change in oceanic $^{87}Sr/^{86}Sr$ is poorly constrained because $^{87}Sr/^{86}Sr$ data on marine carbonates are scarce between $\sim$ 2.8 Ga and $\sim$ 2 Ga.

The age distribution of minerals and continents as a proxy for crustal growth

Other progressive, delayed crustal growth models are based on the age distribution of minerals and continents. Gastil (1960) was the first to point out that the age distribution of preserved mineral describes peaks. Condie (1998) and Condie (2000) proposed an episodic crustal growth model based on the observation of peaks in the U-Pb crystallisation age of zircons in continental

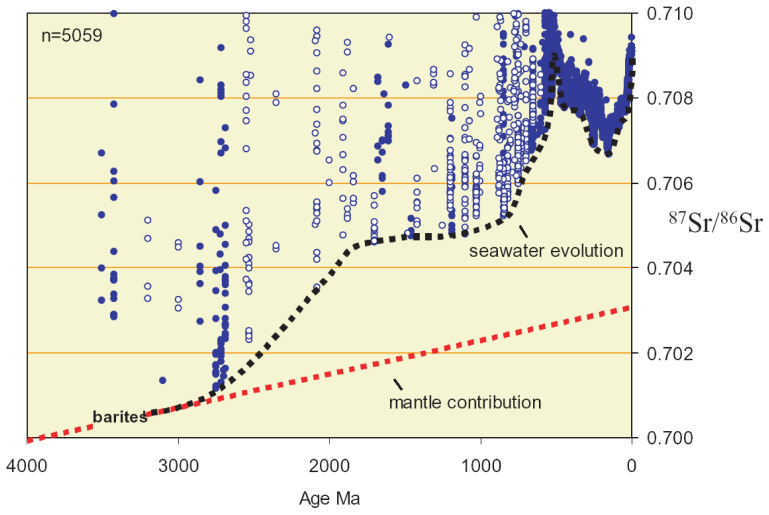

Figure 4.4: Evolution of the oceanic $^{87}Sr/^{86}Sr$ as recorded from marine carbonates. Open circles denote poorly dated samples (uncertainty greater than ± 50 Ma). Figure from Shields and Veizer (2002).

crust. This crustal growth model is based on the observation of peaks in the age distribution at 2.7, 1.9, and 1.2 Ga. The biggest assumptions in this model is that these zircons are juvenile, and that the crystallisation ages were not disturbed by subsequent processes. Indeed, subsequent thermal events would favour chemical diffusion and could thus possibly shift the U-Pb signal towards younger ages. The juvenile character of zircons can be estimated from their $\delta^{18}O$ signature. Zircons formed in I-type granites (granite formed by the remelting of a magma) display an oxygen isotope signature close to that of the mantle ($\sim$ 5‰ VSMOW), whereas zircons formed in S-type granites (granite formed by the partial melting of a sedimentary source that has interacted with the Earth's surface) display higher $\delta^{18}O$ values. In an integrated study of the U-Pb, oxygen and Lu-Hf isotope compositions of detrital zircons from Palaeozoic sedimentary rocks that accumulated along the palaeo-Pacific margin of the former Gondwana supercontinent, Kemp et al. (2006) showed that the Hf model age of juvenile zircons, which indicates the age of extraction from the mantle, can be more than one billion of years older than the U-Pb crystallisation age of the same mineral. This suggests that reworking of the continental crust is an important process during which the U-Pb crystallisation age of zircons can be reset. Thus, crustal growth models based on the sole U-Pb age distribution of zircons should be considered with caution. Another bias in crustal growth models based on the age of preserved continental crust is that the increasingly large dataset on Archaean rocks and minerals tends to shift the model towards larger crustal fractions for ancient times.

Early crustal growth models

In sharp contrast to the delayed and episodic crustal growth model, Armstrong (1981, 1991) advocated for a constant volume of continental crust at the surface of the Earth through time. Fyfe (1978) even proposed a model in which the volume of continental crust was greater at the

surface of the Earth in the Archaean, which implies that recycling processes must have been more efficient than extraction processes since the Archaean. The model of Fyfe (1978) was based on a mass balance between accretion and recycling processes at subduction zones. However, as discussed at the beginning of this section, extraction processes are probably not limited to arc magmatism (Rudnick, 1995; Albarède, 1998b). The following is an overview of the geochemical proxies consistent with early crustal growth models.

Evolution of Nb/U in basalts as a proxy for mantle depletion

The extraction of the continental crust and its preservation at the Earth's surface must have depleted the mantle in incompatible elements that preferentially incorporate the melt fraction. A useful geochemical proxy to track the secular evolution of this depletion is the Nb/U ratio. Hofmann et al. (1986) showed that Nb and U have similar partition coefficients during the partial melting process that produces mid-ocean ridge basalts and oceanic island basalts. However, U is incompatible and is preferentially incorporated in the continental crust so that Nb/U is 9.7 in the continental crust (Rudnick and Fountain, 1995) compared to 32.4 in the primitive mantle (McDonough and Sun, 1995) and to 47 for modern mid-ocean ridge basalts and oceanic island basalts (Hofmann et al., 1986). Basaltic and komatiitic suites from the Yilgarn Craton (Nb/U of up to 47 at 2.7 Ga; Sylvester et al., 1997), from the Superior Province (Nb/U of up to 50 at 2.9 Ga; Kerrich et al., 1999) and from the Kaapvaal Craton (Nb/U = 43 at 3.5 Ga; Campbell, 2003) display Nb/U ratios similar to that of modern mid-ocean ridge basalts and oceanic island basalts, suggesting that the mantle was possibly depleted by extraction of the continental crust as early as 3.5 Ga. Campbell (2003) recently proposed an early crustal growth curve from available and new Nb/U data on basalt-komatiite suites.

^{142}Nd anomalies, Hf anomalies, and the early differentiation of the silicate Earth

The absence of a primitive mantle signature in basalts younger than 3.5 Ga suggests that the differentiation of the silicate Earth could have started in the Hadaean. In the absence of rocks older than $\sim$ 4 Ga, the short-lived radiochronometer ^{146}Sm-^{142}Nd (half-life of 103 Myr) constitutes a powerful tool to investigate the differentiation of the early Earth. The identification of a positive ^{142}Nd anomaly in rocks from the 3.8 Ga Isua greenstone belt in West Greenland (Boyet et al., 2003; Caro et al., 2003) suggests that crustal extraction occurred before ^{146}Sm was extinct, within the first $\sim$ 500 Myr of Earth's history. Boyet et al. (2003) and Caro et al. (2003) independently proposed a major geochemical differentiation within the first 150 Myr of the silicate Earth from geochemical modelling. Finally, the hafnium isotopic composition of zircons older than 4 Ga from Jack Hills, Yilgarn Craton, Western Australia (Blichert-Toft and Albarède, 2008; Harrison et al, 2008) indicates that the parent granite of these zircons was more radiogenic than the primitive undepleted mantle. This again points to an early extraction of continental material, and implies that crustal growth started earlier than $\sim$ 4 Ga, and possibly as early as 4.5 Ga.

It appears from this overview of crustal growth models that delayed crustal growth models are based on crustal geochemical proxies whereas early crustal growth models are based on mantle geochemical proxies. Rey and Coltice (2008) pointed out that the continental crust appeared in the geochemical record due to the strengthening of the continental lithosphere during the Neoarchaean. Flament et al. (2008) further suggested that the continental crust was largely flooded in the Archaean. Thus, the continental crust could have been largely isolated from the atmosphere and from the oceans in the Archaean because weathering and erosion processes occurred over less elevated surface and over a smaller land area. This would have delayed the appearance of the continental crust in the surface geochemical record, even if it had been extracted from the mantle early in Earth's history.

In this chapter, we propose a model that allows for the investigation of the effect of contrasted crustal growth end-members on the evolution of mantle temperature, sea level, ridge depth, emerged land area, and their impact on the evolution of Earth's external envelopes (the hydrosphere, atmosphere and biosphere). Models have been proposed that investigate the role of crustal growth on mantle temperature (*e.g.* Spohn and Breuer, 1993; Grigné and Labrosse, 2001; Labrosse and Jaupart, 2007) and on the composition of the oceans and of the atmosphere (*e.g.* Godderis and Veizer, 2000; Sleep and Zahnle, 2001), but to our knowledge this study is the first to propose an integrated model from the mantle, to the crust, to the surface. The strength of this approach is that it permits the investigation of the effect of one parameter, the growth of the continents, on both surface and interior processes (Fig. 4.1). The limit of this approach is that hypotheses have to be made at different levels. Nevertheless, the structure of the model imposes that hypotheses must be consistent at all levels.

Our modelling results suggest that crustal growth regulates the evolution of mantle temperature, with early crustal growth models predicting mantle temperatures at $\sim$ 3.5 Ga 60 to 90°C hotter than delayed crustal growth models. This, in turn, has an effect on the evolution of secular sea level that is largely controlled by mantle temperature, as well as crustal growth. Despite the predicted differences in sea level, early and delayed crustal growth models consistently predict a similar area of emerged land of less than $\sim$ 4% of the Earth's surface in the Archaean. Using these results in a geochemical box model that allows for the calculation of the evolution of $^{87}Sr/^{86}Sr$ in the mantle, continental crust and oceans, we show that early crustal growth models as indicated by geochemical proxies from the mantle are consistent with surface geochemical proxies when the effect of a reduced emerged land area and of a lower maximum continental elevation are taken into account.

4.2 An integrated model, from the mantle to the surface

The integrated model used in this study is described in Fig. 4.5. The crustal fraction, calculated for contrasted crustal growth models, is an input to the calculation of mantle temperature from the thermal evolution model of Labrosse and Jaupart (2007). The mantle heat flow beneath

continents that is an output of the thermal model is used along with the radiogenic continental heat production to calculate the plateau elevation from the models of Rey and Coltice (2008). The maximum continental elevation is deduced from the plateau elevation using the shape of the continental hypsometry proposed in Flament et al. (2008). Mantle temperature, crustal fraction and continental hypsometry are used as inputs to calculate sea level, emerged land area and ridge depth as in Flament et al. (2008). Finally, the emerged area and continental hypsometry are used to calculate the sedimentary run-off from continents to oceans in a geochemical box model that allows for the calculation of oceanic $^{87}Sr/^{86}Sr$. For comparison, this last calculation is also done under the conventional assumption of a constant freeboard (dashed arrow in Fig. 4.5). In this section, we present this integrated model in more details.

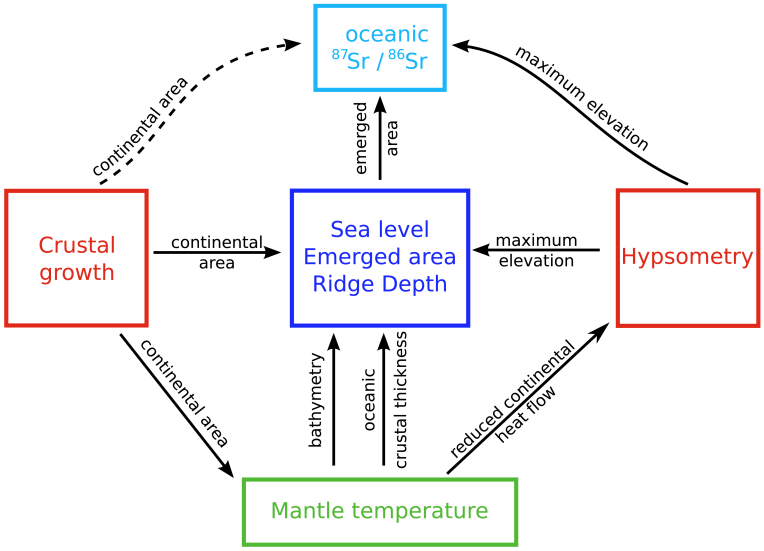

Figure 4.5: Schematic description of the model used in this study. Arrows indicate inputs and boxes indicate the variables and parameters of the model. Mantle temperature is calculated as in Labrosse and Jaupart (2007), continental hypsometry is calculated from the results of Rey and Coltice (2008) and sea level, emerged area of land and ridge depth are calculated as in Flament et al. (2008).

4.2.1 Crustal growth end-members

We have seen in the previous section that the growth of continents is far from consensual. In order to investigate the consequences of contrasted crustal growth models on mantle temperature, we adopt the same sigmoidal formulation as Grigné and Labrosse (2001) and Labrosse and Jaupart (2007) for the fraction of continents formed with respect to the present-day, hereafter referred to as crustal fraction

$$f(t) = \frac{1}{1 + \exp(-(t + t_1)/t_2)} \ , \tag{4.1}$$

where the time t is set to 0 at present and is negative in the past, and t_1 and t_2 are two time constants. This model imposes a single crustal growth stage centered on time t_1 and of duration t_2. We propose to use four end-members out of the crustal growth models presented

in section 1.4.1 and discussed in more details in section 4.1.3. These end-members include a constant growth model (*i.e* a sigmoid in which steady-state has not been reached yet), hereafter referred to as CGM, somewhat similar to that of Hurley and Rand (1969) but with crustal growth starting at 4.5 Ga; a Neoarchaean crustal growth model, hereafter referred to as NGM, broadly similar to that of Taylor and McLennan (1985) and of Veizer and Jansen (1979); an early crustal growth model, hereafter referred to as EGM, similar to that proposed by Armstrong (1981); and a model in which crustal recycling has been more important than crustal additions over the last 3.5 Ga (Fig. 4.6). This last model, hereafter referred to as RM, is an exaggeration of the model of Fyfe (1978). In order to obtain a larger crustal fraction in the past as predicted by the model of Fyfe (1978), we used an arbitrary function in which Eq. 4.1 is timed by a decreasing exponential function so that $f_{rec} = f(t) \times \exp(t/\tau)$, with $\tau = 10$ Ga.

Table 4.1: Time constants used in Eq. 4.1 for the crustal growth models shown in Fig. 4.6.

Model	t_1 (yrs)	t_2 (yrs)
Neoarchaean (NGM)	2.5×10^9	2×10^8
Early (EGM)	3.8×10^9	1×10^8
Recycling (RM)	2.5×10^9	1×10^8

Together, the four proposed models cover most of the range of published crustal growth curves (see Fig. 1.9) to the exception of the "crustal preservation curve" of Hurley and Rand (1969) in which only the preserved material is taken into account. However, with the accumulation of data on Hadaean zircons and Eoarchaean rocks (*e.g.* Harrison, 2009, and section 1.4.1) over forty years since the work of Hurley and Rand (1969), the "crustal preservation curve" has progressively shifted towards older ages.

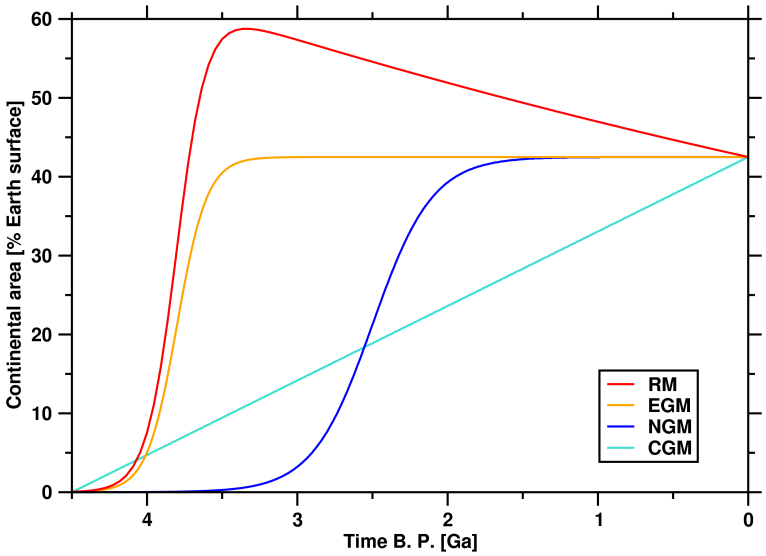

Figure 4.6: Crustal growth models used in the present study.

4.2.2 Modelling the thermal evolution of the Earth as a function of crustal growth

The four crustal growth curves shown in Fig. 4.6 allow us to investigate the consequences of contrasted crustal growth models on mantle temperature. In order to do so, we must adopt a thermal evolution model, as discussed in sections 1.2.2 and 2.2.2. We use the empirical thermal evolution model of Labrosse and Jaupart (2007) that is a plate tectonics model based on the observed seafloor age distribution. The strength of this model is that it accounts for the observation that oceanic lithosphere can subduct independently of its age. The drawback is that there is no physical model as yet that gives a relationship between mantle temperature and maximum age of the oceanic lithosphere.

Calculations of the evolution of mantle temperature are based on the global heat balance for the Earth, which can be written as

$$MC_p \frac{\mathrm{d}T_m}{\mathrm{d}t} = -Q_{tot} + \sum_i H_i e^{-t/\tau_i} \,, \tag{4.2}$$

where M is the mass of the Earth, C_p is the heat capacity, T_m is the mantle potential temperature and Q_{tot} is the total heat loss of the Earth that can be separated in an oceanic heat loss Q_{oc} and a continental heat loss Q_{cont}. Each radioactive isotope i generates heat at a present-day rate H_i, exponentially increasing in the past with a decay time scale τ_i.

It is important to keep in mind that there are relatively large uncertainties in the global heat balance for the Earth. In a recent review of the subject, Jaupart et al. (2007) proposed that the total heat loss of the Earth is 46 ± 3 TW and the total radioactive heat production of the bulk silicate Earth (mantle and continental crust) of 20 ± 3 TW. The next greatest heat source is the heat from the core that accounts for ∼ 8 TW of the total heat budget, with a large range of possible values of between 5 and 13 TW (Jaupart et al., 2007). Overall, the present cooling of the Earth as reviewed by Jaupart et al. (2007) is 18 TW, with a large range of possible values between 8 and 29 TW. This translates in a present-day rate of cooling of 118 K Gyr^{-1} with a range of possible values of between 53 and 190 K Gyr^{-1}. These uncertainties are intrinsic to thermal evolution models and partly explain why the thermal evolution of the Earth is relatively poorly constrained. Keeping these limits in mind, we propose thermal evolution models of the mantle based on the empirical thermal model of Labrosse and Jaupart (2007) in the following.

In the parametrisation of Labrosse and Jaupart (2007), the cooling of the core is taken into account by using an average heat capacity C_p that accounts for the thermal evolution of the core and for the isentropic temperature gradient in the mantle. Its value is listed in Tab. 4.2, along with other parameters relevant to the calculation.

For a given seafloor age distribution, the oceanic heat loss can be written as

$$Q_{oc} = \frac{A_{oc}\, k\, \lambda}{\sqrt{\pi\, \kappa\, t_{max}}}\, T_m \tag{4.3}$$

where A_{oc} is the total oceanic area, k is the thermal conductivity, λ is a seafloor age distribution factor, κ is the thermal diffusivity and t_{max} is the maximum age of subduction of the oceanic lithosphere. The seafloor age distribution factor is equal to 2 for a rectangular age distribution of seafloor, and to 8/3 for a triangular age distribution of seafloor (Labrosse and Jaupart, 2007).

Table 4.2: Input parameters for calculations of mantle temperature (from Labrosse and Jaupart, 2007)

Parameter	Value	Unit
k	3.15	W m^{-1} K^{-1}
κ	8 10^{-7}	m^2 s^{-1}
A_{oc}	3.09 10^{14}	m^2
A_{cc}	2.01 10^{14}	m^2
t_{max}	180	Ma
C_P	1200	J kg^{-1} K^{-1}
M	6 10^{24}	kg

The heat balance of the mantle, relevant to the calculation of the evolution of mantle temperature, can be written as follow to take crustal growth into account:

$$MC_p\frac{\mathrm{d}T_m}{\mathrm{d}t} = -\frac{(A_{oc}+A_{cc}(1-f))\,k\,\lambda(f)}{\sqrt{\pi\,\kappa\,t_{max}}}\,T_m - f\,Q_{cont} + \sum_i (H_{oi}+(1-f)\,H_{ci})\,e^{-t/\tau_i}, \quad (4.4)$$

where f is the crustal fraction, A_{cc} is the present-day continental area and Q_{cont} is the present-day total continental heat flow below the continents (also called reduced continental heat flow), set to 7 TW as discussed in section 4.1.1. H_{oi} is the present-day radioactive heat production of the depleted mantle, derived from a bulk silicate Earth model based on the composition of CI chondrites, which gives $H_{oi} \approx 12.4$ TW (Labrosse and Jaupart, 2007). H_{ci} is the present-day radioactive heat production of the continental crust, also set to 7 TW as discussed in section 4.1.1. The thickness of the continental crust is assumed to be constant so that the crustal fraction f represents the total continental area with respect to the present, as in Flament et al. (2008). Finally, the maximum age of subduction t_{max} is assumed to be constant in the present calculations. A shorter t_{max} would imply a reduced heat loss and, because of the large radioactive heat production in the mantle, would lead to high temperatures that are not in agreement with petrological and rheological constraints (Labrosse and Jaupart, 2007; Jaupart et al., 2007).

It appears from Eq. 4.4 that crustal growth acts in four ways on the thermal evolution of the mantle. Firstly, the oceanic area changes so that oceanic heat flow occurs over a larger area in the past. This implies a greater heat loss and thus lower mantle temperatures for small crustal fractions f (*e.g.* Grigné and Labrosse, 2001). Secondly, the continents are not perfect thermal insulators but account for a non-radiogenic heat flow Q_{cont}that depends on continental area, so that the reduced continental heat flow is assumed to be constant through time, as was first proposed from numerical convection modelling by Lenardic and Kaula (1995). Thirdly, the

seafloor age distribution factor varies with crustal fraction according to $\lambda(f) = 2+2/3\,f$, so that the age distribution is rectangular when there are no continents and triangular for present-day continental area. This effect implies a reduced oceanic heat loss for small crustal fractions and is thus opposite to the first effect. Finally, the last term of Eq. 4.4 expresses the depletion of the mantle in radiogenic elements with crustal growth. A non-depleted mantle in the past implies higher heat production and thus higher mantle temperatures. Eq. 4.4 is solved numerically for the four crustal growth curves shown in Fig. 4.6 using the numerical code of Labrosse and Jaupart (2007).

4.2.3 Modelling the evolution of the maximum continental elevation

We saw in the previous chapter that the Archaean continental crust was probably hotter than present-day "average" continental crust. Gravitationally-driven crustal flow maintained thick continental flood basalts below sea level and prevented significant magmatic crustal thickening. Thin sheet modelling by Rey and Coltice (2008) suggests that the plateau elevation reached by a continental lithosphere is limited to $\sim$ 2000 m for Moho temperatures larger than $\sim$ 700°C (Fig. 3.3), compared to 5500 m for present-day Tibet (Molnar et al., 1993). The relationship between plateau elevation and Moho temperature is non-linear, with a marked increase in plateau elevation for temperatures lower than $\sim$ 700°C (Fig. 3.3; Rey and Coltice, 2008), due to the rapid strengthening of the lithospheric mantle. To include an estimation of plateau elevation in the present models, we fit the results of the most conservative model (strain rate of 1×10^{-14} s^{-1}) of Rey and Coltice (2008) using a power-law (Fig. 4.7). The elevation of the Tibetan plateau is assumed to be the maximum for the plateau elevation at all times. The plateau elevation can then be calculated from Moho temperature.

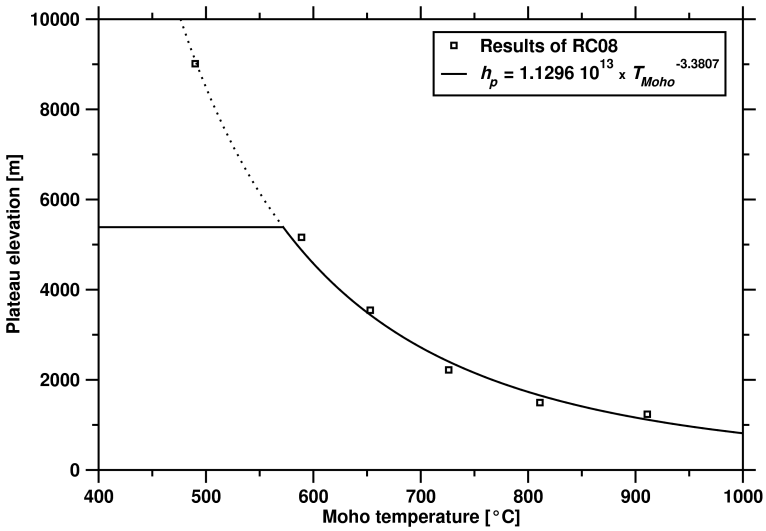

Figure 4.7: Secular evolution of plateau elevation as a function of Moho temperature from Rey and Coltice (2008). The present-day plateau elevation is assumed to be the maximum (horizontal straight line).

The plateau elevation is the steady-state elevation in a context of ongoing convergence and is not relevant to the calculation of the hypsometric curve that reflects dynamic processes. The maximum elevation relevant to the hypsometric is that of the dynamically supported elevation. For instance, the dynamically supported elevation of Mount Everest is 8850 m, in comparison to the elevation of the Tibetan plateau of 5500 m. For a given plateau elevation, the dynamically supported maximum elevation is calculated from the shape of the hypsometric curve given in Flament et al. (2008) (Eq. 2.6). For example, a plateau elevation of 2000 m gives a dynamically supported maximum elevation of $\sim$ 3400 m. In doing this, we assume that mountain building processes represent a steady-state situation. However, even though they are dynamically required on a plate tectonics Earth, mountain building processes are transient (see section 2.1). In a quiescent period marked by the absence of orogens, mountain belts would be eroded down so that the hypsometry would be similar to the anorogenic end-member proposed in Flament et al. (2008) for which the maximum elevation is lower (Fig. 2.9). In this regard, the calculated maximum elevation is an upper limit at all times.

To calculate the Moho temperature, we use a simple one-dimensional heat steady-state conduction model. Under these assumptions, the energy conservation can be written as

$$0 = k \frac{\mathrm{d}^2 T}{d z^2} + \rho_{cc} H \,, \tag{4.5}$$

where k is the thermal conductivity, T is the temperature, z is the depth, ρ_{cc} is the density of the continental crust and $H = H_{ci}/f\, A_{cc}\, z_{cc}\, \rho_{cc}$ is the heat production per unit mass, that depends on time similarly to H_{ci} (see Eq. 4.4). f is the crustal fraction, and A_{cc} and z_{cc} are respectively the area and the thickness of the continental crust. The values of the parameters relevant to the calculation are listed in Tab. 4.3.

Solving Eq. 4.5 for the Moho temperature with knowledge of the mantle heat flux at the base of the continental crust $q_m = Q_{cont}/f\, A_{cc}$ and of the surface temperature T_0 gives

$$T_{Moho} = T_0 + \frac{q_m}{k} z_{cc} + \frac{\rho_{cc} H}{2\, k} z_{cc}^2 \,. \tag{4.6}$$

Table 4.3: Input parameters for the calculation of Moho temperature.

Parameter	Value	Unit
A_{cc}	2.01 10^{14}	m^2
k	2.5	W m^{-1} K^{-1}
q_m	33	mW m^{-2}
T_0	20	°C
z_{cc}	40	km
ρ_{cc}	2820	kg m^{-3}

The calculation of Moho temperature from Eq. 4.6 taking H_{ci} and Q_{cont} from the thermal

evolution models presented in the previous section gives a Moho temperature of $\sim$ 1000°C at 2.7 Ga. This temperature estimate is much larger than that of 610 to 690°C proposed by Flament et al. (2009) for the Pilbara Craton at 2.7 Ga, based on field observations and numerical modelling. This is due to the high value of the mantle heat flow ($\sim$ 33 mW m^{-2}), almost three times as high as the mantle heat flow of 12 mW m^{-2} proposed by Jaupart and Mareschal (1999) for the Canadian Shield. The value of $\sim$ 33 mW m^{-2} is used in the present model in order to be consistent with the output of the thermal evolution model.

To counter-balance the high heat flow under the continents, we build an *ad hoc* conservative model for the radiogenic heat production. Firstly, we assume that heat producing elements are distributed in the 40-km-thick continental crust according to

$$H(z) = H_0 \exp(-z/h_r), \tag{4.7}$$

where H_0 is the surface heat production, z is the depth and h_r is the characteristic thickness of a layer enriched in heat producing elements. It is important to stress that an exponential vertical distribution of radiogenic elements is not systematically observed in Archaean cratons (Jaupart and Mareschal, 1999). However, homogeneously distributed radioelements yield high Moho temperatures, in excess of $\sim$ 1000°C, for a large mantle heat flow. This model would predict low plateau elevations throughout Earth's history, which is not consistent with the observed present-day elevations of the Tibet and Altiplano plateaus. Secondly, the total radiogenic heat production in the continental crust described by Eq. 4.7 is set to be equal to that of a homogeneous continental crust using the concentrations in U, Th and K of present-day Archaean cratons of Taylor and McLennan (1995). This implies that the following calculations of Moho temperatures are only valid for cratons, as in Flament et al. (2009) and in Rey and Coltice (2008). Thirdly, the characteristic thickness of the enriched heat producing layer h_r is assumed to linearly decrease with time from 20 km at 4.5 Ga to $\sim$ 9 km at 2 Ga. This accentuates the decrease of Moho temperature with time predicted from the decrease in radiogenic heat production. While the use of a linear law is arbitrary, this change in the thickness of the heat producing layer can be seen as reflecting the re-distribution of radiogenic elements from a possibly homogeneous early continental crust (Mareschal and Jaupart, 2006).

The solution of the energy conservation (Eq. 4.5) with the distribution of radioactive elements given in Eq. 4.7 is

$$T_{Moho} = T_0 + \frac{q_m}{k} z_{cc} + \frac{\rho_{cc} H_0 h_r^2}{k} \left(1 - e^{-z_{cc}/h_r}\right) . \tag{4.8}$$

The time evolution of cratonic Moho temperature using the *ad hoc* thermal model is shown in Fig. 4.8a. The calculated present-day Moho temperature is $\sim$ 460°C, which is consistent with the temperature at 50 km depth of $\sim$ 430 $\pm$ 98 °C inferred from surface heat flow data for Neoarchaean cratons (Artemieva, 2006), and the calculated Moho temperature at 2.7 Ga is $\sim$ 645°C, which falls within the range of estimates for the Pilbara Craton (Flament et al., 2009). The secular evolution of the plateau elevation is calculated from the secular evolution of the Moho

temperature (Fig. 4.8b). At $\sim$ 2 Ga, an Archaean craton in a context of ongoing convergence would give a plateau elevation similar to that of present-day Tibet. Comparison with the modelling results of Rey and Coltice (2008) shows that the model used in the present study is conservative.

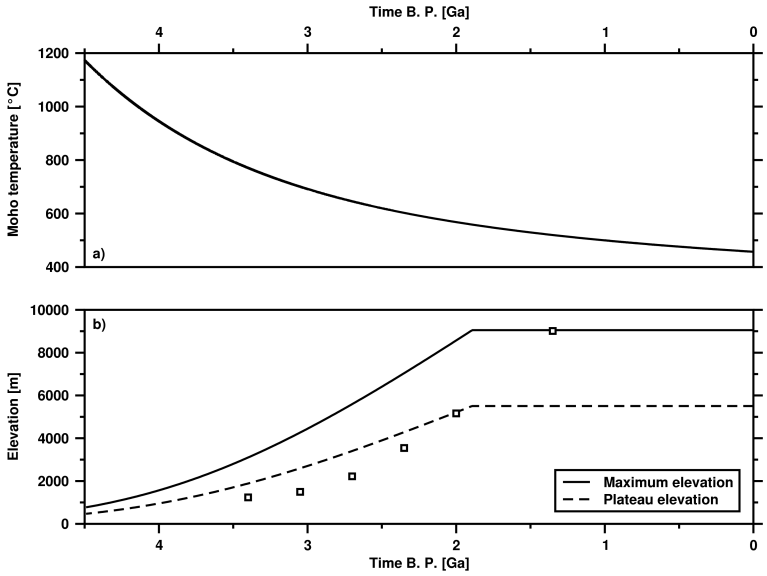

Figure 4.8: Secular evolution of Moho temperature and plateau elevation. a) Secular evolution of the Moho temperature. See text for details regarding the thermal model used for the calculation. b) Secular evolution of the plateau elevation (dashed curve) and maximum continental elevation (plain curve). Plateau elevation values from Rey and Coltice (2008) are shown as empty black squares for comparison.

The thermal model described above, while largely arbitrary, gives a conservative estimate of the evolution of Moho temperature. It should be stressed that this Moho temperature is calculated for a steady state continental lithosphere, which constitutes an important assumption. Indeed, the present-day continental crust, for which surface heat flow varies between 50 and 120 mW m^{-2} depending on tectonic setting (Artemieva, 2009), cannot be described by a steady-state or average continental geotherm. A large range of continental geotherms were probably also represented in the Archaean, as suggested by the observed differences in the crustal and lithospheric thickness of Archaean cratons (Artemieva, 2009).

4.2.4 Modelling the evolution of sea level and area of emerged land

We use the model described in Flament et al. (2008) - see section 2.2.2 - to calculate the evolution of sea level and area of emerged land as a function of mantle temperature, crustal fraction and hypsometry. The two main assumptions of this model are a constant oceanic volume and a constant thickness of the continental crust. This model also allows for the calculation of the depth of ridgecrests through time that will be discussed in chapter 5.

4.2.5 Modelling the evolution of the oceanic $^{87}Sr/^{86}Sr$

In order to estimate the evolution of $^{87}Sr/^{86}Sr$ in the mantle, the oceans an the continental crust for different crustal growth curves, we built a chemical box model following the formulation of Albarède (1998a). In this formulation, the mass conservation of a reservoir i is written as

$$\frac{dM_i}{dt} = \sum^{j\neq i} Q_{j\to i} - \sum^{j\neq i} Q_{i\to j}\,, \tag{4.9}$$

where M_i is the mass of box i, t is the time and $Q_{i\to j}$ is the mass flux from box i to box j. The concentration C_i^k of the element k in the box i can vary by (a) output or input fluxes, (b) dilution, (c) radioactive decay and (d) production from parent element. This balance is expressed by

$$\frac{dC_i^k}{dt} = -\left(\lambda^k + \frac{\sum^{j\neq i} Q_{j\to i} - \sum^{j\neq i} Q_{i\to j}}{M_i} + \frac{\sum^{j\neq i} Q_{i\to j}K_{i\to j}^k}{M_i}\right) C_i^k + \frac{\sum^{j\neq i} Q_{j\to i}K_{j\to i}^k}{M_i} C_j^k + \lambda^{k-1}C_i^{k-1}\,, \tag{4.10}$$

where $K_{i\to j}^k$ is the enrichment factor due to the fractionation of element k upon transfer from box i to j. The element k is produced by the parent $k-1$ and produces the daughter element $k+1$ with radioactive decay constants respectively λ^{k-1} and λ^k.

We consider the isotopic system that includes the stable isotope ^{86}Sr, the radioactive parent ^{87}Rb that decays to the daughter element ^{87}Sr with a constant $\lambda^{^{87}Rb} = 1.42 \times 10^{-11}$ yr^{-1}, in a box model that consists of three reservoirs, namely the mantle (M), the continental crust (CC) and the oceans (OC) (Fig. 4.9). The initial isotopic ratios of rubidium and strontium in the mantle ($^{87}Rb/^{86}Sr = 0.085$ and $^{87}Sr/^{86}Sr = 0.699$) are taken from Zindler and Hart (1986).

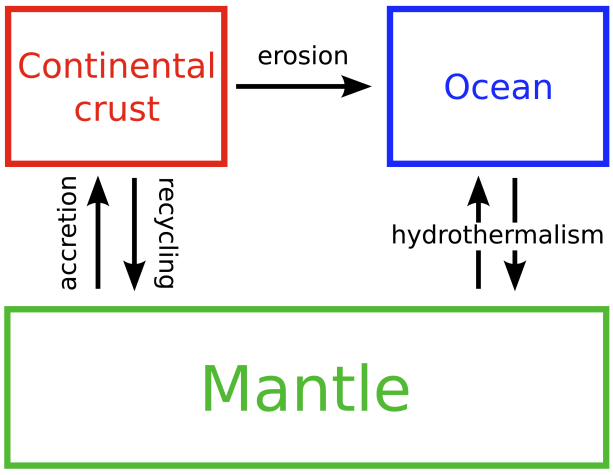

Figure 4.9: Schematic description of the model. Each box represents a reservoir and each arrow represents a flux.

The mass flux from the mantle to the continental crust is described by crustal accretion, which is written as

$$Q_{M\rightarrow CC} = M_{CC}(t) = M^*_{CC}\ f(t)\,,$$

where $f(t)$ is the crustal fraction given by Eq. 4.1 and M^*_{CC} is the present-day continental mass (Tab. 4.4). Rb and Sr are incompatible elements that are preferentially enriched into the melt fraction upon melting, which is translated by two enrichment factors $K^{Rb}_{M\rightarrow CC}$ and $K^{Sr}_{M\rightarrow CC}$. The flux opposite to crustal accretion is the recycling of continental crust back into the mantle, expressed as a fraction of recycled continental crust f_{recy} with respect to total extracted continental crust, so that

$$Q_{CC\rightarrow M} = M_{CC}(t)\, f_{recy}.$$

The total amount of continental crust extracted from the mantle is the sum of $f(0)$ and f_{recy}.

Table 4.4: Mass of each of the three reservoirs. The mass of the continental crust is for the present-day.

Reservoir	M	CC	OC
Mass [10^{21}kg]	4000	26	1.4

The flux of strontium from the continents to the oceans is written as

$$Q^{Sr}_{CC\rightarrow OC} \propto Q^{Sr}_r\ A\ Y\,, \tag{4.11}$$

where Q^{Sr}_r is the present-day river strontium flux to the oceans taken as $2.5{\times}10^9$ kg yr^{-1} from Goddéris and François (2000), A is the emerged area with respect to present day emerged area and Y is the continental sedimentary yield, also called run-off, with respect to present day sedimentary yield. The term $A\,Y$ varies between 0 and 1. A is taken equal to the crustal fraction f in models that assume a constant freeboard, and equal to the emerged fraction of continents with respect to present-day emerged area f_{emer} in other models. Based on data regarding the sedimentary yield and the maximum elevation in the drainage basin of 280 rivers from Milliman and Syvitski (1992), Hay (1998) proposed an empirical model in which the sedimentary yield exponentially depends on the maximum elevation of the drainage basin. Following this empirical model, we estimate the runoff compared to present-day as $Y = e^{\alpha\ (h_{max}-h_{eve})}$, where α was determined as 0.002 by Hay (1998), h_{max} is the maximum continental elevation in the hypsometric curve and h_{eve} is the elevation of Mount Everest. The oceans are assumed to be in steady-state with regard to strontium concentration, which implies that the sedimentary flux of strontium onto the seafloor is equal to the river flux of strontium to the oceans.

The flux of strontium between the mantle and the oceans is assumed to be in steady-state, and is written as

$$Q^{Sr}_{M\rightarrow OC} = Q^{Sr}_{OC\rightarrow M} = Q^{Sr}_{hy}\,, \tag{4.12}$$

where Q_{hy}^{Sr} is the present-day total strontium hydrothermal flux (hydrothermal exchange at mid-oceanic ridges and seafloor weathering away from the ridge) taken as $1.5{\times}10^9$ kg yr^{-1} from Goddéris and François (2000).

The enrichment factors $K_{M\rightarrow CC}^{Rb}$ and $K_{M\rightarrow CC}^{Sr}$ are adjusted in order to obtain the present-day concentration of Sr in the continental crust (320 ± 46 ppm; Rudnick and Gao, 2003). In doing this, we assume that the concentration of the mantle in Sr is 70% of the primitive undepleted mantle of McDonough and Sun (1995) (19.9 ppm) to account for a hidden enriched mantle reservoir. The existence of a hidden enriched mantle reservoir is needed to explain the discrepancy between the geochemical composition of mid-ocean-ridge basalts (MORBs) and that of ocean island basalts (OIBs) (Hofmann, 1997). The source of MORBs is shallower than that of OIBs that probably are the product of deep mantle plumes, and OIBs are overall enriched in incompatible elements with respect to MORBs (Hofmann, 1997). This has led to several hypothesis regarding the enriched mantle reservoir over the years. Hofmann (1997) was a proponent of two-layer mantle convection, in which the upper mantle is depleted and the largely isolated lower mantle is enriched. However, Coltice and Ricard (1999) showed from box geochemical models dynamically similar to whole-mantle convection that whole-mantle convection could account for the geochemical data if the lowermost layer of the mantle, called the D" layer, was enriched in incompatible elements through the recycling of subducted crust. Finally, Labrosse et al. (2007) proposed that the D" layer could represent a slowly crystallising dense layer at the base of the mantle that would have remained isolated from the rest of the mantle and would thus be a candidate for a hidden, enriched mantle reservoir. Our assumption that the concentration of the mantle in Sr is 70% of the primitive undepleted mantle is consistent with the results of Coltice and Ricard (1999) who suggested that the D" layer could contain up to a third of Earth's radiogenic elements.

Table 4.5: Enrichment factors and fraction of recycled continental crust.

Parameter	Value
$K_{M\rightarrow CC}^{Rb}$	215
$K_{M\rightarrow CC}^{Sr}$	27
f_{recy} (NGM)	0.57
f_{recy} (EGM)	1.09

The fraction of recycled continental crust f_{recy} is adjusted so that the present-day $^{87}Sr/^{86}Sr$ of the oceans is 0.709 (Shields and Veizer, 2002), that of the continents approximately 0.712 and that of the depleted mantle approximately 0.7025 (Workman and Hart, 2005). Values for all adjusted parameters are shown in Tab. 4.5. To account for the observed crustal and oceanic $^{87}Sr/^{86}Sr$, the fraction of recycled continental crust is twice as much for model EGM than for model NGM. This can be explained as follows. ^{87}Rb is incompatible and preferentially incorporated in the continental crust. Early in Earth's history, the mantle was richer in ^{87}Rb

because little decay to ^{87}Sr had occurred. Thus, the extraction of continental crust from the mantle early in Earth's history, as predicted by model EGM, would have resulted in a highly radiogenic continental crust, and in turn in highly radiogenic oceans. A high fraction of recycled continental crust buffers this effect over time and allows to obtain the present-day observed values of ^{87}Sr/^{86}Sr in the continents and in the oceans.

4.3 Influence of crustal growth models on the evolution of mantle temperature, sea level, area of emerged land and oceanic ^{87}Sr/ ^{86}Sr

The integrated model described in the previous section permits to investigate the effect of crustal growth models on the evolution of mantle temperature, sea level, area of emerged land and oceanic ^{87}Sr/^{86}Sr.

4.3.1 Effect of crustal growth models on mantle temperature

The thermal evolution models computed for the four proposed crustal growth end-members are shown in Fig. 4.10 along with the rheological constraint for the onset of solid-state convection. Jaupart et al. (2007) proposed that the onset of solid-state convection occurs at a crystal fraction of $\sim$ 60%. They concluded from recent phase diagrams of rocks from the mantle that the temperature threshold for the onset of solid-state convection is 200 $\pm$ 100 °C hotter than present. The uppermost value of a mantle temperature 300 °C hotter than present is shown in Fig. 4.10.

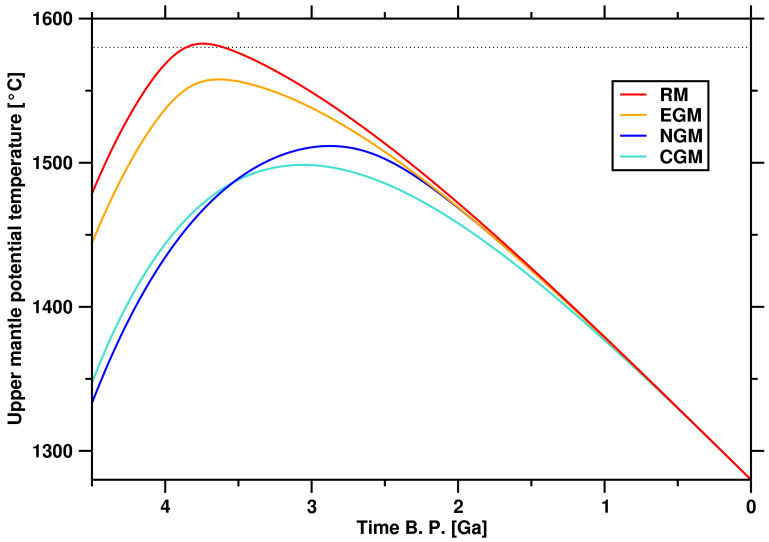

Figure 4.10: Thermal evolution models computed for the four crustal growth models shown in Fig. 4.6. The dotted line shows a mantle temperature 300°C hotter than present.

All of the models display an early warming period that is due to a larger heat production from

radiogenic elements than heat loss. This reflects the smaller variation in heat loss compared to the variation in heat production predicted in the thermal evolution model of Labrosse and Jaupart (2007). The duration of the early warming period depends on crustal growth models. Maximum mantle temperature is reached at $\sim$ 3.7 Ga for early crustal growth models (models EGM and RM), whereas it is reached at $\sim$ 3 Ga for delayed crustal growth models (models CGM and NGM). The age at which the maximum mantle temperature is reached is essentially controlled by the seafloor age distribution factor that is greater for larger continental areas. All models are in agreement with the uppermost temperature threshold for the onset of solid-state convection and predict an early warming phase. Thus, these models predict relatively cool mantle temperatures for the early Earth and are hard to reconcile with a probable early magma ocean stage. An early magma ocean stage is expected to have occurred since the gravitational energy liberated by accretion could have been large enough to entirely melt the outer 1000 km of the Earth's mantle (Kaula, 1979). An early cooling period, that is not accounted for by the models, would be required to be consistent with an early magma ocean stage. For this reason, Labrosse and Jaupart (2007) stressed that their modelling results were valid from the present until the thermal equilibrium. This period extends to $\sim$ 3.7 Ga for early crustal growth models and to $\sim$ 3 Ga for delayed crustal growth models.

One effect of the continents is to reduce heat loss because of the smaller oceanic area and of the insulating effect of continents. Early crustal growth models result in a smaller heat loss until $\sim$ 3.8 Ga and thus in larger mantle temperatures. This effect is important since early crustal growth models predict mantle temperatures 270 to 300°C greater than present, whereas delayed crustal growth models predict mantle temperatures 220 to 230°C hotter than present. Thus, delayed crustal growth models are consistent with a temperature threshold for the onset of solid-state convection of 200°C as suggested by Jaupart et al. (2007) whereas early crustal growth models are not. All models are consistent with a temperature threshold extended to the upper limit of 300°C.

4.3.2 Effect of crustal growth models on sea level

Having determined the evolution of mantle temperature, crustal fraction and maximum elevation, we calculate the evolution of sea level and emerged land area using the model of Flament et al. (2008). The two main hypotheses of this model are that the volume of oceans and the thickness of the continental crust are assumed to be constant. Four situations can occur for a given set of parameters in which a) the continents are partially flooded ; b) the continents are entirely flooded; c) the continents are entirely emerged; and d) the mid-oceanic ridges emerge. Model calculations are only valid for partially flooded continents. Situations b), c) and d) constitute limits of the model and the calculation (going back in time) stops if any of these situations occurs. For this reason, some of the evolution models presented in the following do not span the whole of Earth's history.

Flament et al. (2008) showed that the evolution of sea level is mainly controlled by that of mantle temperature. In this respect, it is worth noting that the maximum calculated sea levels at $\sim$ 3.5 Ga for models EGM and RM, and at $\sim$ 2.9 Ga for model CGM (Fig. 4.11) are imposed by the respective maximum mantle temperature (Fig. 4.10 and section 4.3.1). In model NGM, the pulse in crustal growth between 3 and 2 Ga results in an increase in sea level so that the maximum sea level is offset compared to the maximum mantle temperature. This increase in emerged area for a pulse in crustal growth is also consistent with the results of Flament et al. (2008) who showed that emerged area closely depends on crustal fraction for small continental fractions (section 2.2.3 and Fig. 2.8). The important early increase in sea level for early crustal growth models reflects both crustal growth and the early warming period observed in the thermal evolution models.

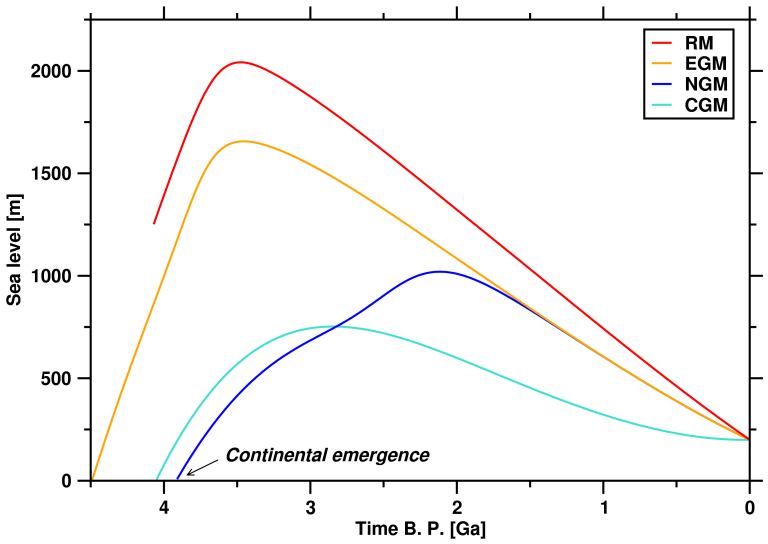

Figure 4.11: Secular evolution of sea level for the four proposed crustal growth models. The reference is the edge of the continental shelf so that present-day sea level is 200 m.

One important difference between the results presented in Fig. 4.11 and that of Flament et al. (2008) is that the continental crust plays a role in regulating mantle temperature in the present models. In Flament et al. (2008), sea level and emerged land surface were estimated for a given mantle temperature and crustal fraction consistent with proposed Archaean conditions but independent with respect to one another. However, we showed in the previous section that there is a strong feedback between crustal fraction and mantle temperature so that these parameters cannot be considered independent. The high sea levels predicted for large continental areas are enhanced by the fact that large continental areas early in Earth's history result in higher mantle temperature, and thus in higher sea levels, so that the effect of crustal growth on mantle temperature imposes a positive feedback on sea level. Fig. 4.11 shows that early crustal growth models predict a maximum amplitude of sea level change between $\sim$ 1450 m (model EGM) and $\sim$ 1850 m (model RM), which is significantly larger than the sea level change of between $\sim$ 550 m

(model CGM) and ∼ 800 m (model NGM) predicted for delayed crustal growth models. Note that the smallest amplitude of sea level change calculated for model CGM is ∼ 550 m, about twice the amplitude of Phanerozoic sea level change (Miller et al., 2005). The hypothesis of constant continental freeboard is thus difficult to reconcile with any of the proposed crustal growth end-members that cover the range of all published crustal growth models, to the exception of the outdated preservation model of Hurley and Rand (1969). Entirely emerged continents, due to a large oceanic reservoir, are predicted for the delayed crustal growth models at ∼ 4 Ga for small continental fraction (< 0.1) and relatively low temperature (∼ 150°C greater than present). This complete emergence of continents is important to discuss since it constitutes a limit to our calculation. However, we have seen in the previous section that results for the delayed crustal growth models are valid until the maximum mantle temperature predicted at approximately 3 Ga. Thus, the continental emergence predicted at ∼ 4 Ga for delayed crustal growth models is hypothetical.

4.3.3 Effect of crustal growth models on the area of emerged land

Fig. 4.12 shows the secular evolution of the area of emerged continental crust for all models. Importantly, the predicted area of emerged continental crust is similar for all crustal growth models, despite the differences of ∼ 1 km in calculated sea level between early and late crustal growth models. The area of emerged land is intrinsically small for delayed crustal growth models that predict small continental fractions in the Archaean. In contrast, early crustal growth models predict large continental fractions in the Archaean that result in high sea levels and thus in largely flooded continents. As a consequence, the predicted emerged area is broadly similar for early and delayed crustal growth models.

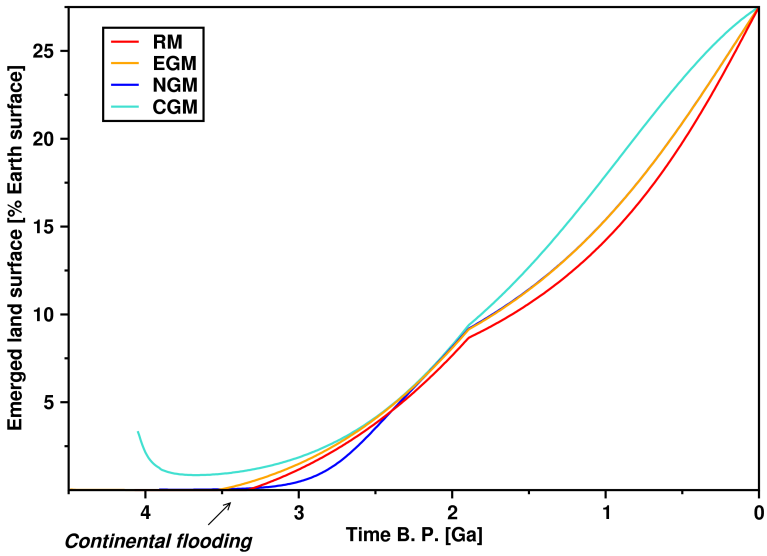

Figure 4.12: Secular evolution of the area of emerged land. Note that the results are similar for all models despite differences in sea level (Fig. 4.11).

Between 2 and 2.5 Ga, the calculated emerged area is similar for all models, and the emerged area at 2.5 Ga is less than $\sim$ 4% of the Earth's surface for all models. This estimation is slightly larger than that of Flament et al. (2008) who proposed an area of emerged land of less than 3% of the Earth's surface in the Archaean. This is because in Flament et al. (2008) the maximum continental elevation in the Archaean orogenic end-member for continental hypsometry was assumed to be constant and of $\sim$ 3600 m, whereas it increases from $\sim$ 1700 m at 3.5 Ga to $\sim$ 6400 m at 2.5 Ga in the present models (Fig 4.8b).

Model CGM predicts a slightly larger area of emerged land than other models in the post-Archaean despite a smaller continental fraction (Fig. 4.6). This is because model CGM predicts a smaller continental area than other models, which results in a lower sea level and thus in a larger area of emerged land. Moreover, still due to a reduced continental area, model CGM predicts slightly lower mantle temperatures between 2.5 and 1.5 Ga, which also results in a lower sea level. In contrast, model RM predicts larger continental areas than other models, which results in higher sea levels and thus in a smaller area of emerged land.

Model NGM predicts a smaller area of emerged land than other models between 2.5 Ga and 3.5 Ga because of a reduced continental fraction compared to other models. Model CGM predicts a larger area of emerged land than other models between $\sim$ 3 and $\sim$ 4 Ga because of significantly lower mantle temperatures compared to early crustal growth models, and a significantly larger crustal fraction than model NGM. The early decrease in area of emerged land for model CGM is due to the early warming added to an increasing crustal fraction. However, it is important to remember that results are speculative for ages older than 3 Ga for the delayed crustal growth models, so that this early decrease in area of emerged land is largely speculative.

Near-complete continental flooding is predicted between $\sim$ 3.3 and 3.5 Ga for models RM, EGM and NGM. The calculations remain valid as long as sea level does not exceed the maximum continental elevation, which is true for the presented models. This explains why calculations do not stop between $\sim$ 3.3 and 3.5 Ga for models RM, EGM and NGM. The prediction of entirely flooded continents (*water world*) is somewhat at odd with the geological record. Indeed, we discussed in sections 1.5 and 2.2.4 that there is geological evidence for emerged land in the Archaean rock record. The most direct argument is the identification of an angular unconformity at $\sim$ 3.5 Ga within the Warrawoona Group, Pilbara Craton (Buick et al., 1995). Moreover, the presence of clastic sediments in the Archaean rock record (Nisbet, 1987) definitely indicates that some land was emerged. However, these clastic sediments represent a more local provenance than their modern equivalent (Sircombe et al., 2001), which suggests smaller draining areas and thus smaller emerged land areas. Finally, the δ^{18}O signature of Hadaean zircons from Jack Hills, Yilgarn Craton, interpreted to reflect the presence of clay minerals in their source (Mojzsis et al., 2001; Wilde et al. , 2001), could indicate emerged land as early as $\sim$ 4.3 Ga - assuming these clay minerals formed at the Earth's surface.

The progressive continental emergence from 3.5 Ga predicted by our models (and notably model EGM) is compatible with the observation of an angular unconformity in the Pilbara Craton at

3.5 Ga (Buick et al., 1995). Moreover, emerged continents in the Archaean could reflect transient low sea level associated with the dynamic topography imposed by a mantle plume, or with the formation of a supercontinent or of a supercraton (section 2.3.4). In addition, we have assumed a constant volume of oceans in the present models. A possibly reduced volume of oceans before $\sim$ 3.8 Ga (Kasting and Holm, 1992, see also sections 1.4.2 and 2.3.3) would result in a larger area of emerged land. Furthermore, the steady-state *ad hoc* thermal model that we built does not account for the probable variability of Archaean continental geotherms in time and space. Thus, the continental geotherm could have been cooler in certain places, resulting in locally higher elevations. Indeed, continental emergence was likely progressive since cratonisation did not occur simultaneously for all cratons. The predicted reduced emerged land area can thus be reconciled with the geological record for models EGM and RM that predict large continental areas from 3.8 Ga. However, model NGM predicts that less than 10% of the Earth's surface was covered by continents 3.5 Ga ago, dropping to 0% at 3.8 Ga, and cannot be reconciled with the observation of emerged land possibly as early as 4.3 Ga.

4.3.4 Effect of crustal growth models on oceanic $^{87}Sr/^{86}Sr$

The geochemical model presented in section 4.2.5 allows for the calculation of evolution of the $^{87}Sr/^{86}Sr$ of the mantle, oceanic crust and seawater as a function of emerged area and maximum continental elevation. In the following, we compare the results of this model for two crustal growth models, including a late crustal growth model (model NGM, similar to that of Taylor and McLennan, 1985; Veizer and Jansen, 1979) and an early crustal growth model (model EGM, similar to that of Armstrong, 1981, 1991).

Fig. 4.13a shows the results obtained for each crustal growth model, assuming that the area of emerged land is equal to the crustal fraction in Eq. 4.11, which is the conventional assumption in modelling the evolution of oceanic $^{87}Sr/^{86}Sr$ (Veizer and Jansen, 1979; Godderis and Veizer, 2000). It is important to note that this assumption implies a constant continental freeboard, which is consistent neither with the observation of common subaqueous flood volcanism in the Archaean (Arndt, 1999; Kump and Barley, 2007), nor with numerical freeboard models (Flament et al., 2008). The data compiled from the $^{87}Sr/^{86}Sr$ of marine carbonates by Shields and Veizer (2002) are also plotted in Fig. 4.13. This figure shows that the delayed continental growth model displays a better fit to the data, and especially reproduces the shift of the oceanic reservoir from the mantle reservoir at $\sim$ 2.8 Ga. In contrast, model EGM predicts an oceanic reservoir significantly more radiogenic than suggested by the data, and a shift between oceanic and mantle reservoirs at $\sim$ 4 Ga that is not observed in the data. This argument that advocates for delayed crustal growth has been used to discriminate between crustal growth models (Veizer and Jansen, 1979; Godderis and Veizer, 2000).

However, the results presented in Fig. 4.13a are only valid for a constant freeboard and a constant hypsometry. These are conventional assumptions, but we have shown in chapter 2 and in this chapter that the constant freeboard hypothesis is not valid. Moreover, our results

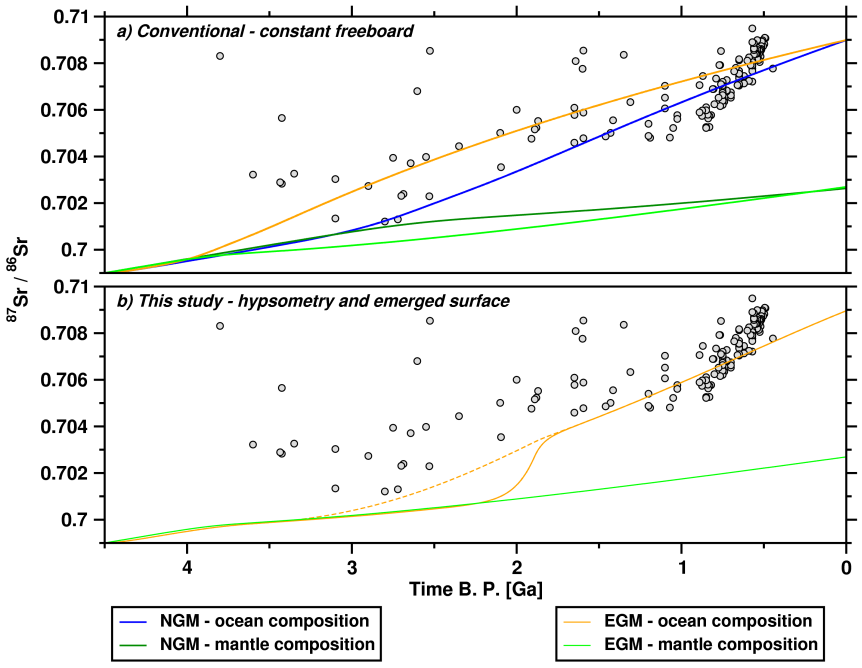

Figure 4.13: Evolution of the $^{87}Sr/^{86}Sr$ of seawater and of the mantle for a) Neoarchaean (NGM) and early (EGM) crustal growth models, for constant hypsometry and constant freeboard; b) model EGM, taking the emerged area from Fig. 4.12, for a constant maximum continental elevation (dashed curve) and using the evolution of maximum continental elevation shown in Fig. 4.8b (plain curve). Grey circles are $^{87}Sr/^{86}Sr$ data on marine carbonates from Shields and Veizer (2002).

from chapter 3, in agreement with the results of Rey and Coltice (2008), suggest that Archaean continental lithospheres could not sustain an important load so that the Archaean maximum continental elevation was probably lower than the elevation of Mount Everest. Thus, there is no reason to assume a constant freeboard and a constant hypsometry in models of the evolution of the composition of the atmosphere and of the oceans.

Fig. 4.13b shows the results of the calculation of $^{87}Sr/^{86}Sr$ taking the emerged area predicted for model EGM (Fig. 4.12) instead of the total continental area. A reduced area of emerged land results in a reduced flux from the continents to the oceans (Eq. 4.11) so that the oceans are less radiogenic. It is clear from Fig. 4.13b (orange dashed curve) that a secular change in the area of emerged land delays the contribution of the continents to the composition of the oceans. Indeed, the result of this calculation is very close to that for model NGM assuming constant freeboard (Fig. 4.13a). The effect of a change in the maximum continental elevation as predicted by our models (Fig. 4.8) is also shown in Fig. 4.13b. A reduced maximum continental elevation also results in a reduced flux from the continents to the oceans (Eq. 4.11), but in this case the change is exponential, as opposed to the linear contribution of emerged land area. The results of a calculation taking both effects of a reduced area of emerged land and a lower maximum continental elevation (Fig. 4.13b, orange plain curve) show that the composition of the oceans would remain controlled by the mantle until the late-Archaean lithospheric strengthening (Rey and Coltice, 2008) that resulted in increased continental erosion. The shift in oceanic $^{87}Sr/^{86}Sr$

at $\sim$ 2 Ga predicted by this model (Fig. 4.13b) is delayed by $\sim$ 800 Myr compared to the shift observed in the data (Fig. 4.4). This could be due to the fact that the thermal model built for the purpose of the present study does not account for the likely variability in Archaean continental geotherms, as discussed in section 4.3.3. Lower Moho temperatures and/or transient effects could result in an earlier shift of the predicted oceanic $^{87}Sr/^{86}Sr$. Ultimately, a model could be proposed in which maximum continental elevation would be adjusted to match the trend described by the data, including the second shift observed between $\sim$ 1000 and 500 Ma ago. This second shift reflects elevated rates of erosion associated with transient enhanced mountain building, possibly in relation with the aggregation, break-up and dispersal of the supercontinent Rodinia (Powell et al, 1993). However, there is no point in overfitting the strontium isotope data on marine carbonates since they present large uncertainties.

4.4 Reconciling early crustal growth models with surface geochemical proxies

4.4.1 Evolution of the oceanic $^{87}Sr/^{86}Sr$

The modelling results presented in the previous section (Fig. 4.13) show that the early crustal growth model is consistent with the evolution of oceanic $^{87}Sr/^{86}Sr$ when a reduced area of emerged land and a lower maximum continental elevation are taken into account. The increase in continental elevations and the increase in emerged land area in the Neoarchaean resulted in more important sedimentary yields from the continents to the oceans, which enhanced the contribution of the continents to the composition of the oceans, particularly in radiogenic strontium. A progressive continental emergence provides an alternative explanation for the strontium isotope data on marine carbonates. The evolution of $^{87}Sr/^{86}Sr$ in marine carbonates does not reflect an increase in continental volume, but an increase in weathering and erosion processes. Thus, oceanic $^{87}Sr/^{86}Sr$ is not a geochemical proxy of crustal growth but rather a geochemical proxy of the flux of the felsic continents to the oceans (Rey and Coltice, 2008; Flament et al., 2008). The crustal growth model that was proposed by Veizer and Jansen (1979) to account for these data was based on the unrealistic assumptions of a constant freeboard and continental elevation. However, our modelling results show that this crustal growth model is not needed to account for the data. In the next section, we turn to another geochemical proxy of delayed crustal growth models by proposing a study of the trace element composition of fine-grained sediments from the Pilbara Craton, with implications for crustal differentiation.

4.4.2 Tracking the emergence of the continental crust in the Pilbara Craton

Taylor and McLennan (1985) proposed that the observed changes in the trace element composition of fine-grained sediments towards the end of the Archaean reflect the formation of juvenile continental crust (section 4.1.3). There are several problems with this interpretation. First, it

should be noted that the data in Fig. 4.3 are averaged over periods longer than 500 Myr, implying that variations over shorter timescales are averaged out. Moreover, Harrison (2009) suggested that the observed higher Th/Sc in post-Archaean sediments could reflect lesser vertical mixing in a compositionally stratified continental crust rather than a fundamentally different crustal composition. Furthermore, Condie (1993) pointed out that Taylor and McLennan (1985) compared greenstone-type sediments from the Archean with cratonic sediments in the post-Archean, implying that the data themselves could be biased. To avoid this bias, Condie (1993) compared the evolution of the composition of shales only from cratonic or passive margin successions. This buffered the changes observed by Taylor and McLennan (1985) at the Archaean/Proterozoic boundary. In particular, the Eu anomaly of Archaean and post-Archaean shales are within error of each other in the analysis of Condie (1993). Thus, the data of Taylor and McLennan (1985) do not only contain a temporal signal, but also a environmental signal linked to the tectonic setting of the analysed sediments. The temporal signal itself might be more complex than proposed by Taylor and McLennan (1985) since Hawkesworth and Kemp (2006) suggested from the Hf model age and δ^{18}O of sedimentary and igneous zircons that it may take up to a billion years for newly formed continental crust to dominate the sedimentary record. Finally, and importantly, fine-grained sediments reflect the composition of the emerged continental crust. If the fraction of emerged continental crust was reduced, as suggested by our models, and because a large fraction of the continents were covered by subaqueous greenstone belts, a significant fraction of differentiated continental crust could have existed without being recorded in the sedimentary record. Thus, the evolution of the trace element composition of fine grained sediments may not constrain crustal growth.

Nevertheless, the trace element composition of fine-grained sediments can be used to track the appearance of a differentiated reservoir at the Earth's surface. In the following, we report new trace element data on fine-grained sediments from the East Pilbara Craton. We have seen in section 3.2.1 that the Pilbara Craton presents an almost continuous record of over a billion year of Archaean geology. In particular, the continuous sedimentary record of the Mount Bruce Supergroup spans more than 320 Myr (from 2772 Ma until 2449 Ma; Trendall et al., 2004) across the Archaean/Proterozoic boundary. The felsic lavas, zircons and tuff units of the Fortescue Group (Arndt et al., 1991; Wingate, 1999; Blake et al., 2004; Trendall et al., 2004) are particularly well established. Together with the availability of geological maps at the scale of 1/100 000$^{\text{th}}$, this makes it possible to study the evolution of geochemical proxies in the trace element composition of fine-grained sediments of the Fortescue Group on a regional scale and at a high temporal frequency. The present study from the Pilbara Craton includes seven new samples that are temporally well constrained. In the future, this regional study could be integrated in a more global study to track environmental changes at the Archaean/Proterozoic boundary at high temporal frequency.

Samples and sampling strategy

Fine-grained sedimentary units occur in all of the formations of the Fortescue Group to the exception of the Mount Roe Basalt. Seven outcrop fine-grained sediments were sampled in the Oakover Syncline and in the Meentheena Centrocline (Figs. 3.17 and 3.18). They consist of one shale sample from the $<$ 3235 Ma Gorge Creek Group, two shale samples from the Hardey Formation, one sample of black silicified shale from the Mopoke Member of the Kylena Formation, one sample from the Tumbiana Formation, one sample of black silicified shale from the Kuruna Member of the Maddina Formation and one sample of argilite from the Jeerinah Formation (Figs. 3.17 and 3.18).

Methods

The samples were prepared and analysed for major and trace elements using the methods described in section 3.4.1.

Results

Major elements

The concentrations in major elements of the analysed fine grained sediments are shown in Tab. 4.6. Samples BC06, MC13 and BC16 are significantly richer in silica than the average Archaean shale of Condie (1993). The average composition of the other samples is similar to that of the average Archaean shale of Condie (1993).

Table 4.6: Content in major elements (in weight percentage of oxides) of the analysed fine-grained sediments. The standard deviation (1σ) is given in brackets.

Oxide wt.%	Samples							Averages			
	BC22	BC04	BC18	BC06	TM01	MC13	BC16	All	SiO_2 rich	Other	Archaean[a]
SiO_2	56.67	57.23	59.74	74.36	67.83	87.4	80.51	69.11 (12.09)	80.76 (6.52)	60.37 (5.15)	60.95
TiO_2	0.78	1.12	1.02	0.36	0.95	0.49	0.46	0.74 (0.3)	0.44 (0.07)	0.97 (0.14)	0.62
Al_2O_3	18.44	21.08	17.19	6.01	10.91	4.71	9.37	12.53 (6.4)	6.7 (2.4)	16.91 (4.31)	17.5
Fe_2O_3	9.31	7.49	10.16	8.18	6.63	1.23	3.49	6.64 (3.21)	4.3 (3.55)	8.4 (1.62)	7.53
MnO	0.06	0.03	0.07	0.08	0.05	0.01	0.02	0.05 (0.03)	0.04 (0.04)	0.05 (0.02)	-
MgO	5.07	2.18	2.92	3.94	4.97	0.22	1.13	2.92 (1.87)	1.76 (1.94)	3.79 (1.46)	3.88
CaO	0.2	0.13	0.13	1.82	2.54	1.51	0.1	0.92 (1.02)	1.14 (0.92)	0.75 (1.19)	0.64
Na_2O	0.02	0.01	0.01	0	2.89	1.35	0.14	0.63 (1.11)	0.5 (0.74)	0.73 (1.44)	0.68
K_2O	3.24	5.77	3.44	0.5	0.29	1.13	2.26	2.38 (1.95)	1.3 (0.89)	3.19 (2.25)	3.07
P_2O_5	0.07	0.13	0.11	0.07	0.28	0.66	0.04	0.19 (0.22)	0.26 (0.35)	0.15 (0.09)	0.1
SO_3	BLD [b]	BLD	BLD	0.5	BLD	0.09	BLD	0.08 (0.19)	0.2 (0.27)	-	-
L.O.I. [c]	5.6	4.8	4.63	3.96	3.68	0.65	2.9	3.75 (1.62)	2.5 (1.69)	4.68 (0.79)	-
Total	99.45	99.96	99.42	99.74	101.01	99.44	100.43	99.92 (0.6)	99.87 (0.51)	99.96 (0.74)	94.97

$\longrightarrow$ samples ordered according to their stratigraphic position

[a] From Condie (1993)
[b] BLD: below level of detection ($<$ 0.01%)
[c] LOI: loss on ignition at 1,050°C

Rare earth elements and Y (REY), Sc and Th

Sample concentrations in rare earth elements, Sc, Y and Th are shown in Tab. 4.7, and chondrite-normalised and PAAS-normalised rare earth element and yttrium (REY) diagrams are shown in Fig. 4.14. All samples are enriched in REE with respect to chondrite CI (values for the chondrite are taken from McDonough and Sun, 1995). The samples that are not anomalously rich in SiO_2 present characteristic shale REE patterns with a negative slope that reflects enrichment in light REE (LREE) compared to heavy REE (HREE), and a negative Eu anomaly. The samples with high SiO_2 are characterized by a La_N/Yb_N of 4-6.5, whereas other samples are characterized by high La_N/Yb_N (≥ 8.4) which is consistent with Archaean shale REE patterns. All samples, except SiO_2-rich sample BC06, are rich in rare earth elements (> 120 ppm) and present a slightly negative to negative Eu-anomaly. Sample BC06 contains less rare earth elements (37 ppm) and presents a slightly positive Eu-anomaly of 1.26. The negative Eu-anomaly is strongest for SiO_2-rich samples BC16 and MC13 (respectively 0.48 and 0.65), whereas it ranges between 0.68 and 0.78 for other samples.

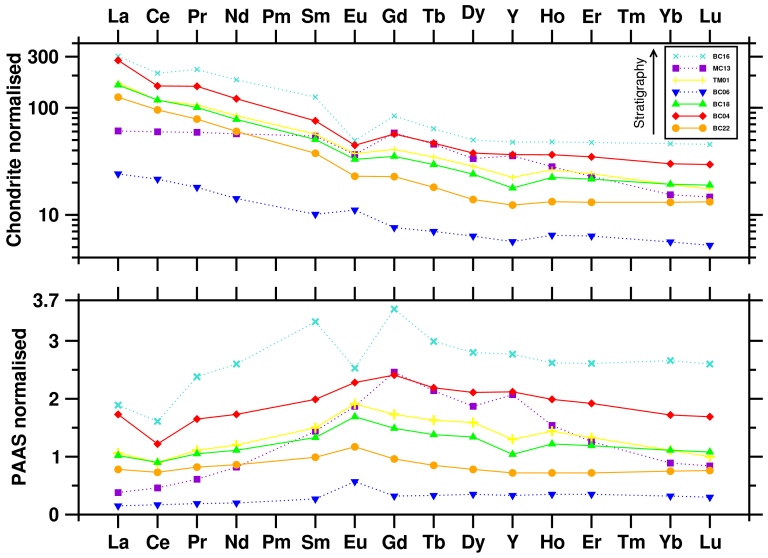

Figure 4.14: Rare earth element and yttrium (REY) patterns for the analysed fine-grained samples. The dotted lines are for SiO_2-rich samples.

All the samples that are not SiO_2-rich present patterns of similar shape (Fig 4.14). Sample MC13 is clearly different to other samples since it presents no fractionation of LREE in a chondrite-normalised diagram and a bell-shaped pattern in a PAAS-normalised diagram. Sample BC16 presents a negative Eu-anomaly PAAS normalised contrary to all other samples. As for the abundances of Sc and Th, they are quite variable in the analysed samples with Sc $= 18.62 \pm 9.12$ ppm, Th $= 7.68 \pm 6.15$ ppm and Th/Sc $= 0.44 \pm 0.33$ (uncertainties are given as 1σ). Sample BC04 is particularly rich in Th (19.82 ppm).

Table 4.7: Concentrations in rare earth elements, Sc, Y and Th (in part per million) of the analysed fine-grained sediments. The geochemical indexes plotted in Fig 4.15 are also shown.

ppm	BC22	BC04	BC18	BC06	TM01	MC13	BC16
Sc	29.12	21.34	24.73	7.76	27.39	10.22	9.75
Y	19.37	57.3	27.96	8.83	35.12	55.81	74.8
La	29.74	65.64	38.62	5.72	40.43	14.39	71.81
Ce	58.53	97.96	72.29	13.21	71.77	36.52	128.93
Pr	7.28	14.72	9.33	1.68	9.85	5.47	21.14
Nd	27.48	55.5	35.55	6.49	38.52	26.1	83.33
Sm	5.57	11.17	7.47	1.5	8.39	8.05	18.64
Eu	1.29	2.51	1.86	0.62	2.1	2.06	2.78
Gd	4.53	11.32	7	1.51	8.13	11.57	16.67
Tb	0.65	1.69	1.06	0.25	1.25	1.65	2.3
Dy	3.42	9.29	5.9	1.56	7	8.24	12.3
Ho	0.72	1.99	1.22	0.35	1.44	1.54	2.62
Er	2.1	5.57	3.45	1.02	3.87	3.66	7.58
Yb	2.11	4.83	3.11	0.9	3.09	2.48	7.44
Lu	0.33	0.73	0.47	0.13	0.43	0.36	1.12
Th	7.45	19.82	9.27	2.5	4.24	1.61	8.84
ΣREE	145.27	283.94	188.76	36.6	197.64	123.56	376.98
Eu/Eu^{*} [a]	0.78	0.68	0.78	1.26	0.78	0.65	0.48
ΣLREE/ΣHREE	7.71	6.29	6.4	3.57	5.89	2.74	6.1
Th/Sc	0.26	0.93	0.37	0.32	0.15	0.16	0.91

⟶ samples ordered according to their stratigraphic position

[a] $Eu/Eu^{*} = \frac{Eu_N}{\sqrt{Sm_N \times Gd_N}}$ where the subscript $_N$ designs chondrite-normalised values

Discussion

Fig. 4.15 shows the same geochemical indexes than Fig. 4.3 for fine-grained sediments from the Pilbara Craton. Data from the present-study are plotted along with data available from the Pilbara Craton (McLennan and Taylor, 1983; Sugitani, 2006).

SiO_2-rich samples left aside, Eu/Eu^{*} displays a smooth decrease from 1 to 0.7 between 3.33 and 2.73 Ga. The absence of negative Eu anomaly in samples older than 3 Ga is consistent with the results of Taylor and McLennan (1985). However, samples ranging from 3 to 2.5 Ga are consistent with the cratonic shales of Condie (1993) rather than with the greenstone-derived shales of Taylor and McLennan (1985). ΣLREE/ΣHREE also displays a decrease from 9.4 to 6.2 between 3.33 and 2.73 Ga. However, Th/Sc does not show any systematic variation along the stratigraphy of the Pilbara Craton.

The decrease in Eu/Eu^{*} and ΣLREE/ΣHREE from 3.33 to 2.73 Ga possibly reflects the progressive appearance of differentiated rocks in the Pilbara Craton. This could be attributed to the progressive unroofing of the granitic batholiths observed in the East Pilbara Terrane (Fig. 3.4). Two models have been proposed for the formation of the granite-greenstone East Pilbara Terrane, including the sagduction model presented in section 1.2.3 and a metamorphic core complex model (Zegers et al., 2001). In both of these models, the granitic batholiths are formed by melting of the lower continental crust. It is worth noting that the smooth decrease observed in the Eu/Eu^{*} and ΣLREE/ΣHREE for the fine-grained sediments in the Pilbara is particularly consistent with the sagduction model that predicts crustal diapirism from $\sim$ 3.3 Ga (Fig. 1.5). Thus, the data presented herein illustrate that the trace element composition of fine-grained sediments could reflect crustal differentiation rather than crustal growth, as acknowledged by McLennan et al. (2006).

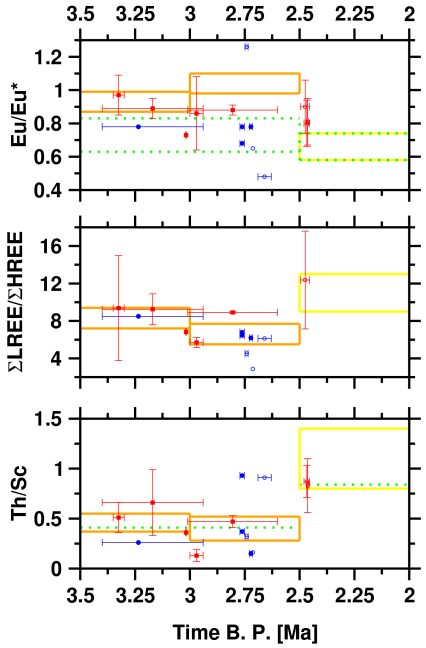

Figure 4.15: Temporal variation of three geochemical indexes in fine-grained sediments from the Pilbara Craton. Blue circles: present study (open circles denote SiO_2-rich samples); red squares: published data from McLennan and Taylor (1983); Sugitani (2006) and data from the on line geochemistry database of the Geological Survey of Western Australia available at http://geochem.doir.wa.gov.au/geochem/. The orange and yellow rectangles are averages for Archaean and Palaeoproterozoic black shales from Taylor and McLennan (1985). The green dotted boxes and lines are averages for cratonic and passive margin shales from Condie (1993).

Conclusion and future work

The evolution of the trace element composition of fine-grained sediments from the East Pilbara Craton reflects the progressive unroofing of differentiated, felsic diapirs. While consistent with the results of Taylor and McLennan (1985), we suggest that our data could reflect crustal differentiation rather than crustal growth. The analysis above was limited to three of the many geochemical indexes suggested by Taylor and McLennan (1985). A detailed study of the absolute abundances in Ni and Cr, and of the elemental ratios Co/Th, Cr/Th, Zr/Y and K/Rb of the samples would help to further constrain the relative importance of TTGs and komatiites (mafic volcanics) in their source, and to assess the degree of metasomatism they were exposed to (Condie, 1993). Finally, soon to be released isotopic strontium and neodymium data should allow to estimate a model age for the source of the samples. To date, the best geochemical method to discriminate between crustal growth and crustal reworking is the integrated study of the U-Pb, oxygen and Lu-Hf isotope compositions of detrital zircons proposed by Kemp et al. (2006). This type of data would certainly be worth acquiring in the Pilbara Craton.

4.5 Conclusion

The model developed in this study allows for the investigation of the influence of crustal growth models on mantle temperature, emerged land area and oceanic $^{87}Sr/^{86}Sr$. Our results suggest that because of the thermal insulation imposed by continents on the mantle, early crustal models result in higher mantle temperature. Since both elevated mantle temperatures and large crustal fractions trigger high sea level, early crustal growth models predict higher sea levels in the Archaean. However, our models suggest that the emerged land area does not depend on crustal growth models and was reduced to less than 5% of the Earth's in the Archaean. Continental flooding is predicted at around 3.5 Ga for all models except the constant growth model. In the case of delayed crustal growth model that predict very reduced crustal fractions before 3.5 Ga, continental flooding could be hard to reconcile with geological data suggesting some land was emerged in the Archaean. In the case of early crustal growth models, a local change in relative sea level or hypsometry could account for emerged land in the Archaean. However, delayed crustal growth models cannot easily be reconciled with geological observations that suggest some land was emerged in the Archaean.

Our models reconcile early crustal growth models with the evolution of the oceanic $^{87}Sr/^{86}Sr$ as recorded by marine carbonates when a reduced emerged area and a lower continental elevation are accounted for. Thus, a delayed crustal growth model is not needed to account for the observed trend in oceanic $^{87}Sr/^{86}Sr$. As for the trace element composition of fine-grained sediments, it might reflect crustal growth processes, but also crustal differentiation and crustal reworking processes. The composition of fine-grained sediments is a proxy for the average composition of the emerged upper continental crust that suggests that the upper continental crust was more mafic in the Archaean. We suggest that the delayed appearance of the differentiated crust in surface geochemical proxies reflects the emergence of the continental crust rather than its extraction from the mantle. Until the Neoarchaean, the continental crust was largely covered by thick subaqueous greenstone covers and was thus an isolated geochemical reservoir. The Neoarchaean strengthening of the continental lithosphere, added to the secular increase in emerged land area, resulted in the appearance of the differentiated continental crust in the sedimentological record, with first order consequences for the evolution of Earth's exogenic envelopes.

5

Consequences for Earth's exogenic envelopes

Contents

The enrichment of oceans in radiogenic strontium discussed in the previous chapter is an example of the consequences of continental emergence for the Earth's exogenic envelopes. In the present chapter, we qualitatively discuss further consequences of the secular increase in the depth of rigecrests and in the surface of emerged land predicted by our models for the evolution of the composition of the oceans and of the atmosphere, and for the evolution of early life.

5.1 Consequences of the secular deepening of ridgecrests

The depth of ridgecrests is of importance to interactions between the oceanic lithosphere and the hydrosphere, and it could have a role in the evolution of oceanic volume since shallower ridgecrests in the past, as predicted by our models, could imply shallower hydrothermal penetration and thus a smaller return of water to the mantle at subduction zones (section 2.3.3; Kasting and Holm, 1992). Kasting et al. (2006b) further suggested that a secular change in the depth of ridgecrests could explain the trend observed in δ^{18}O of marine carbonates (Fig. 5.2). This would imply that the δ^{18}O of marine carbonates, and possibly of marine cherts, may not be a relevant proxy of the evolution of the temperature of the oceans, as proposed by Knauth and Lowe (2003),Knauth et al. (2006), and Robert and Chaussidon (2006). The depth of ridgecrests also imposes thermodynamic constraints on putative early deep ecosystems. Mid-oceanic ridges have been proposed to be an ideal environment (*ecological niche*) for the development of early hyperthermophiles (Nisbet and Sleep, 2001) and/or piezophile organisms. Finally, ridge emergence is important to discuss since it would result in the direct release of volcanic gases into the atmosphere, which would result in the accumulation of carbon dioxide in the atmosphere, possibly balanced out by the emergence of easily weathered basaltic material.
In this section, we present the evolution of the depth of ridgecrests predicted by the model presented in section 4.2, and we qualitatively discuss the implications of these modelling results.

5.1.1 Effect of crustal growth models on the depth of ridgecrests

Fig 5.1 shows the secular evolution of the depth of ridgecrests calculated for the four crustal growth models proposed in section 4.2.1. Consistently with the results presented in section 2.3.3, ridgecrests are predicted to be shallower in the past than at present for all models. Interestingly, the evolution of the depth of ridgecrests appears to be anticorrelated to crustal growth, contrary to the evolution of sea level that essentially reflects the evolution of mantle temperature. This result suggests that a proxy for the evolution of ridgecrest depth could potentially be used to constrain crustal growth, with the important limitation that the present-day depth of ridgecrests displays a large range between 2500 and 3500 m. Kitajima et al. (2001) proposed from a petrographic study and thermodynamic calculations that the $\sim$ 3.5 Ga greenstone complex at North Pole in the Pilbara Craton was emplaced under a water column of $\sim$ 1.6 km. They interpreted this greenstone complex as an ophiolite and concluded that Archaean mid-oceanic ridges were approximately 1 km shallower than present. This estimate fits the result of model

RM (Fig. 5.1) that predicts a ridge depth of ∼ 1550 m at 3.5 Ga. However, the North Pole greenstone complex is not an ophiolite, but rather a continental flood basalt (CFB) related to a mantle plume event (Van Kranendonk et al., 2007). Thus, the result of Kitajima et al. (2001) suggests that the CFB at North Pole was emplaced under a ∼ 1.6 km-thick water column, which adds up to the evidence for flooded continents in the Eoarchaean predicted by the models of Flament et al. (2008).

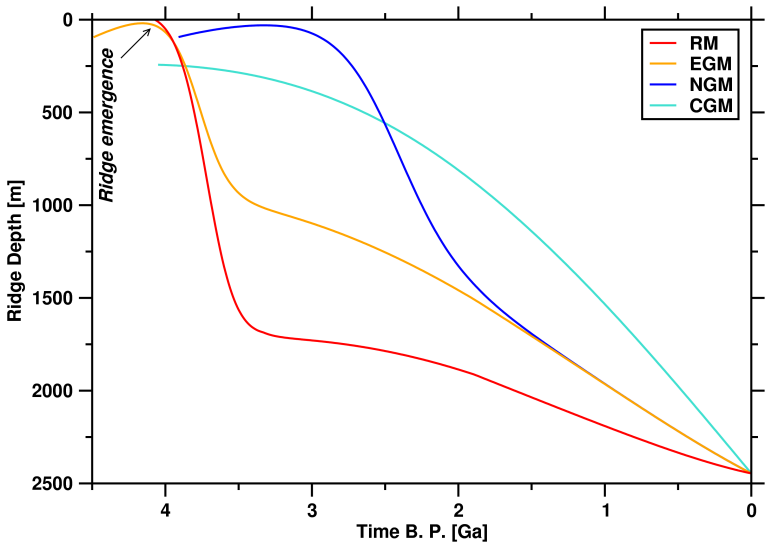

Figure 5.1: Secular evolution of the depth of ridgecrests for the four proposed crustal growth models.

Regarding our modelling results, early crustal growth models predict ridgecrests significantly less shallow than progressive crustal growth models because a larger continental surface results in a reduced area of oceans and thus in higher sea level, and because a higher mantle temperature results in a smoother bathymetry and thus in a lower oceanic volume below ridgecrests. At 2.5 Ga, ridgecrests are between ∼ 660 m (model RM) and ∼ 1200 m (model EGM) shallower than present for early crustal growth models compared to ∼ 1900 m shallower than present for delayed crustal growth models.

Interestingly, the depth of ridgecrests is relatively constant for all models between ∼ 3 and 3.5 Ga, which implies that changes in sea level are counterbalanced by the sum of changes in the volume of water above continents and in the volume of water below ridgecrest. For model NGM, the ridgecrest is only ∼ 75 m deep during this time interval (for which the validity of delayed crustal growth models is less certain, as discussed in section 4.3.1), and ridgecrest deepening starts from 3 Ga due to the decrease in mantle temperature and the increase in crustal fraction predicted by this model. Ridgecrest emergence occurs when the volume of the reservoir below the ridge is large enough to hold the entire oceanic volume. In the present models, ridge emergence occurs for model RM at ∼ 4.1 Ga for small crustal fraction (∼ 0.1) and for mantle temperature ∼ 300°C larger than present, which result in a large surface of oceans with sufficiently marked bathymetry (∼ 1 km, Fig. 2.4) to store the entire oceanic volume. It is

worth noting that ridgecrest emergence is predicted earlier than 3.7 Ga, period for which early crustal growth models are more speculative because they predict an early warming of the mantle that could be difficult to reconcile with the possibility of an early magma ocean that would on the contrary require an early cooling period (section 4.3.1).

5.1.2 Oxygen isotopic composition of seawater, hot Archaean oceans, and ridgecrest depth

We have discussed the secular trend described by oceanic $^{87}Sr/^{86}Sr$ in section 4.3.4. The evolution of the isotopic composition of marine carbonates in oxygen, used as a proxy for the composition of seawater, also displays a secular trend of increasing $\delta^{18}O$ since the Archaean (Fig. 5.2) for which many explanations have been proposed over the years (see Jaffrés et al., 2007, for a recent review). Possible explanations include hot Archaean oceans (up to 70°C; Knauth and Lowe, 2003; Robert and Chaussidon, 2006), the alteration of the initial oxygen isotopic composition of Archaean carbonates by diagenesis and/or metamorphism (*e.g.* Knauth and Kennedy, 2009), and a change in the oxygen composition of seawater itself over time (Walker and Lohmann, 1989; Shields and Veizer, 2002; Kasting et al., 2006a,b; Jaffrés et al., 2007).

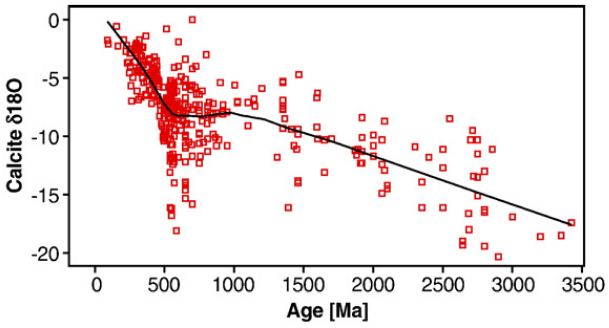

Figure 5.2: Average oxygen isotopic composition of marine carbonates deposited over the past 3.8 Ga. Data are from Veizer et al. (1999) and Shields and Veizer (2002). The solid line represents a least-squares fit to the data. Figure from Jaffrés et al. (2007).

Two further arguments in favour of hot Archaean oceans come from the evolution of the isotopic composition of cherts that displays secular increasing trends in $\delta^{18}O$ (Knauth and Lowe, 1978) and in $\delta^{30}Si$ (Robert and Chaussidon, 2006). Robert and Chaussidon (2006) argued that the $\delta^{30}Si$ of cherts is controlled by the difference between the temperature of the oceans and that of hydrothermal fluids and interpreted the trend of $\delta^{30}Si$ in cherts as a decrease in the temperature of seawater. A counter-argument is that the trend could instead reflect an increase in the global mean temperature of hydrothermal alteration (Jaffrés et al., 2007). Moreover, the time and space coverage of the analysed cherts is sparse, and it is not clear whether all of the analysed cherts were formed in open marine environments (Jaffrés et al., 2007).
We acquired $\delta^{13}C$ and $\delta^{18}O$ data on stromatolites and hydrothermal calcites from the East Pilbara Craton to evaluate the possibility of hotter Archaean oceans. These data are presented

in appendix A. $\delta^{13}C$ values do not display any significant fractionations, with values ranging between −4.5 and 1.9‰ VPDB. Oxygen isotopes are more fractionated with values between −21.7 and −13.3‰ VPDB, consistently with previously published data. We noted that the $\delta^{18}O$ data are statistically similar for our stromatolite samples and hydrothermal calcite samples, implying either low temperature hydrothermal activity, or alteration of the initial oxygen isotopic composition of our samples. However, without knowledge of the equilibrium $\delta^{18}O$ of the water these stromatolites and calcites were formed in, it is not possible to use oxygen isotopes as a proxy of palaeotemperature. This is particularly true of the Tumbiana Formation, since the equilibrium $\delta^{18}O$ would be close to 0‰ VSMOW for seawater whereas the average $\delta^{18}O$ of modern lakes is 20.6‰ VSMOW (Mook, 2001). Finally, diagenesis and metamorphism would probably result in a lighter oxygen isotopic composition (Knauth and Kennedy, 2009, see also appendix A) that could explain the similar signature of the analysed stromatolites and hydrothermal calcites. In this respect, we note that our surface samples are less depleted in ^{18}O than the core samples of Thomazo et al. (2009). Thus, some alteration processes could result in an enrichment rather than a depletion in ^{18}O. While unconclusive as yet, this isotopic study undelines the difficulty in deciphering the ^{18}O record of marine carbonates.

An alternative explanation to the trend in the global data on marine carbonates is that the $\delta^{18}O$ of seawater itself has changed over time. Kasting et al. (2006b) proposed a model in which the oxygen composition of seawater is controlled by the depth of ridgecrests. The reasoning of Kasting et al. (2006b) can be summarised as follows. Present-day ridgecrests are at least 2.5 km and at such depths, hydrothermal processes occur in a superconvective regime. This results in deep hydrothermal penetration (Kasting and Holm, 1992) and in high-temperature water-rock interactions over a large region. These interactions result in the transfer of ^{18}O from the oceanic crust to seawater, explaining why modern seawater is relatively rich in ^{18}O (Kasting et al., 2006a). If mid-oceanic ridges were shallower in the past, the maximum hydrothermal penetration depth would have been shallower (as first suggested by Walker and Lohmann, 1989), resulting in a relative depletion of seawater in ^{18}O. Indeed, our modelling results show that ridgecrests were shallower in the past. For the preferred early crustal growth model (EGM), the depth of ridgecrests is $\sim$ 1250 m at 2.5 Ga and of $\sim$ 950 m at 3.5 Ga, compared to 2500 m at present (Fig. 5.1). Coupling our model that predicts the evolution of the depth of ridgecrests to the model of Kasting et al. (2006b) would allow for the calculation of the secular evolution of the $\delta^{18}O$ of seawater. Building onto the model of Kasting et al. (2006b), Jaffrés et al. (2007) showed that the observed trend of seawater $\delta^{18}O$ could be reproduced by incorporating an estimation of the depth of ridgecrests. However, Jaffrés et al. (2007) used a conventional parametrised model that predicts a 10-fold decrease in spreading rate since 3.5 Ga to evaluate changes in the depth of the ridge. As discussed previously, the link is tame between mantle temperature and spreading rate so that the model used by Jaffrés et al. (2007) is not realistic. Nevertheless, their model allows for a qualitative understanding of the process. If the evolution of seawater $\delta^{18}O$ is actually due to the secular change in the depth of ridgecrests, the data could be used to constrain

a model coupling the model presented in chapter 4 to the model of Kasting et al. (2006b). This could allow for the discrimination between early and delayed crustal growth models that predict a contrasted evolution of mid-oceanic ridges through time (Fig. 5.1). However, as in the case of the evolution of strontium isotope signature of seawater, the main limit to use oceanic oxygen isotopes as a constraint on geodynamic models are the uncertainties associated to the data.

5.1.3 Climatic consequences of changes in the depth of ridgecrests

Shallower ridgecrests in the Archaean would also have had climatic consequences. If shallower ridgecrests result in shallower hydrothermal penetration as suggested by Kasting et al. (2006b), this could have resulted in an increase in the concentration in carbon dioxide of the oceans, because hydrothermal processes incorporate carbon in the oceanic crust. Carbonatisation of the oceanic crust can occur at different temperatures. Cold hydrothermal alteration results in the formation of carbonate veins (Alt and Teagle, 1999), and hot alteration in the incorporation of carbon in the oceanic crust through rock-water interaction (Sleep and Zahnle, 2001). We do not discuss cold hydrothermal activity away from the ridge, since the model of Kasting et al. (2006b) is only valid for high temperature hydrothermal activity. Sleep and Zahnle (2001) proposed a model in which hydorthermal processes were more efficient in the Archaean because of faster rates of crustal production as predicted by conventional parametrised convection models. Sleep and Zahnle (2001) concluded that the efficient carbonatisation of the oceanic crust through high temperature metamorphism would have buffered the oceanic CO_2, and in turn would have maintained cold conditions at the surface of the Earth because of the equilibrium between atmospheric and oceanic CO_2 levels. However, conventional parametrised convection models predict unrealistically high spreading rates in the past so that the models of Sleep and Zahnle (2001) possibly predict unrealistically efficient hydrothermal processes. Moreover, a less efficient high-temperature hydrothermal activity for shallower ridgecrests would result in less efficient carbonatisation of the oceanic crust. This effect would likely alter the conclusion of Sleep and Zahnle (2001) that Archaean climates were cool, and is important to include in future models of the long term carbon cycle.

Our modelling results suggest that in the extreme, for small crustal fraction (~ 0.1) and high mantle temperature (~ 300°C hotter than present), ridgecrests could emerge. The predicted ridge emergence for model RM should be taken with caution since it occurs during the early warming of the thermal model, period for which the modelling results are more speculative. Ridgecrest emergence would result in the degassing of volcanic gases, including greenhouse gases such as carbon dioxide, directly into the atmosphere. This in turn would potentially result in an increase of atmospheric temperatures. On the other hand, ridgecrest emergence would imply an increase in the emerged area of easily weathered basaltic material, which would constitute a major sink of carbon dioxide. The weathering effect occurs over a longer time scale, but it could in the long term counterbalance, and possibly exceed, the effect of a degassing directly into the atmosphere on geological timescales.

5.1.4 Are mid-oceanic ridges a favourable habitat for early life?

Mid-oceanic ridges could also constitute a favourable habitat for early biotopes that require (a) stability, (b) protection from UV radiation and (c) a source of energy for bio-chemical reactions. The stability criteria would likely be met by mid-oceanic ridges provided their depth did not vary too rapidly. Protection from UV radiation would be necessary in the absence of an ozone layer. As we shall discuss in the next section, it is possible that the Archaean atmosphere was essentially devoid of oxygen. Goldblatt et al. (2006) suggested that an ozone layer can only form once atmospheric concentration of oxygen reaches 10^{-5} PAL, where PAL is the present atmospheric level of oxygen (21%). The Archaean atmosphere possibly contained oxygen concentrations lower than 10^{-5} PAL, in which case there would have been no ozone layer in the upper atmosphere. This, in turn, would have implied a less efficient shielding from UV radiation which would have impeded the development of early life since UV radiation alters the structure of organic molecules, including DNA. On early Earth, this absence of a protective ozone layer would to a certain extent be compensated by the reduced UV radiation of the "faint" young Sun, $\sim$ 25% compared to present (Newman and Rood, 1977). However, this effect would be less pronounced in the late Archaean since the luminosity of the Sun increases over time. Early biotopes at mid-oceanic ridges would have been protected from UV radiation if the overlying water column was thick enough. Finally, hydrothermal vents at mid-oceanic ridges would have provided a source of energy for biochemical reactions. Nisbet and Sleep (2001) proposed that hyperthermophile methanogens and sulfate reducers would have been adapted to mid-oceanic ridges from the earliest Archaean on.

Our modelling results for the preferred early crustal growth model suggest that the depth of ridgecrests was of $\sim$ 950 m by 3.5 Ga, progressively increasing to $\sim$ 1250 m by 2.5 Ga. In this scenario, mid-oceanic ridges would have been a favourable habitat for early life from 3.5 Ga. The rapid increase in ridgecrest from 4 Ga to 3.5 Ga is due to the early warming predicted by the thermal model and is thus speculative. It follows that mid-oceanic ridges could have been a favourable habitat for early life before 3.5 Ga.

5.2 Consequences of the rise of the continents

The emergence of a differentiated reservoir as recorded by the change in the trace element composition of fine-grained sediments at the Archaean/Proterozoic boundary and by the enrichment of oceans in ^{87}Sr from $\sim$ 2.8 Ga would also have had major consequences for the composition of the oceans and of the atmosphere. In particular, it has been proposed that the atmosphere was essentially devoid of oxygen in the Archaean, before its oxidation around the Archaean/Proterozoic boundary. This event is referred to as the "great oxidation event" (GOE). In the following, we give an overview of the geological evidence for the GOE, and we then discuss the potential contribution of the rise of the continents to the oxidation of the atmosphere.

5.2.1 The great oxidation event

Many lines of geological evidence suggest that the atmosphere could have been reducing in the Archaean, including the widespread occurrence of banded iron formations (BIFs) and the lack of oxidised red beds in the Archaean rock record. Banded iron formations are characterised by a centimetre to millimetre scale layering in which iron is present alternatively in reduced and oxidised form. While the formation of BIFs remains largely poorly understood, this layering suggests rapid changes in oceanic oxygen levels. Red beds are formed by the oxidation of iron in surface rocks and indicate the presence of atmospheric oxygen. Thus, the absence of red beds in the Archaean rock record likely indicates a reducing atmosphere. However, the geological evidence in favour of a reducing Archaean atmosphere is not clear cut and there is an ongoing debate on the oxidising state of the Archaean atmosphere and oceans.

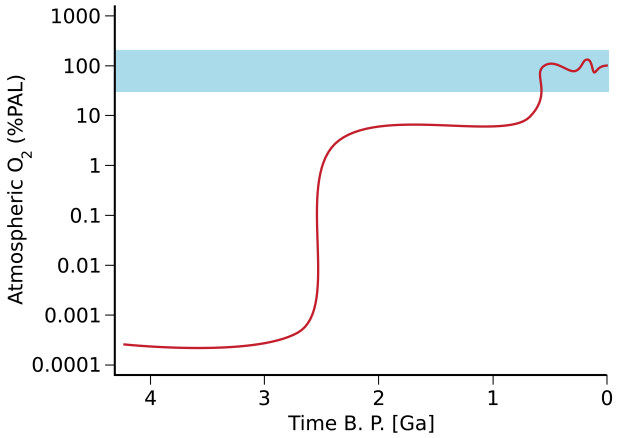

Figure 5.3: Two proposed models for the evolution of atmospheric concentration in oxygen. The red curve (from Kump, 2008) displays an sharp increase from 5×10^{-6} PAL to 5×10^{-2} PAL at $\sim$ 2.45 Ga that is the great oxidation event. In sharp contrast, the light blue area represents an oxygen level within 50% of present day throughout Earth's history, which is the preferred model of Ohmoto (1996).

Fig. 5.3 illustrates the sharp contrast between models of the evolution of atmospheric oxygen levels. On the one hand, the followers of Holland (1999) are proponents of the great oxidation event, whereas the followers of Ohmoto (1996) are proponents of nearly constant levels of atmospheric levels. Farquhar et al. (2000) reported mass-independent fraction of sulphur (MIF-S) isotopes that are considered as the "smoking gun" for the rise of atmospheric oxygen. Usually, discrimination between isotopes during geo(bio)chemical processes is a function of their mass. The processes that result in the mass-independent fractionation of sulphur are thought to be restricted to gas-phase photochemical reactions in the upper atmosphere. Such reactions occur on present-day Earth, but MIF-S anomalies are rapidly homogenised in an oxidising atmosphere. Farquhar et al. (2000) proposed that such fractionations would have been preserved in an oxygen-devoid atmosphere, implying that the MIF-S signature they reported in rocks older than 2090 Ma reflected a reducing atmosphere. Many studies based on the MIF-S signature of Archaean rocks followed and Bekker et al. (2004) proposed that the rise of atmospheric oxygen

occurred between 2.45 and 2.32 Ga. A recent multiple isotopic study (for the elements C, O and S) of pristine samples from a diamond drillcore through the Tumbiana Formation, Pilbara Craton, suggests that MIF-S anomalies can also be caused by the activity of methanotrophs (Thomazo et al., 2009). Thus, some authors will probably argue that MIF-S anomalies are not necessarily due to photochemical reaction in the upper atmosphere. However, Thomazo et al. (2009) argued that the preservation of the MIF-S anomalies they reported requires low level of atmospheric oxygen. While there are more proponents of the great oxidation event, the debate is still going. Hoashi et al. (2009) reported pristine haematite from a drillcore in the 3.46 Ga Marble Bar Chert, Pilbara Craton, which they interpreted as evidence for the formation of this chert in an oxygenated water body. If this interpretation is correct, this finding implies that at least some intermediate and deep ocean regions were oxidised in the Eoarchaean, since the Marble Bar Chert is thought to have formed in deep seawater (Dromart et al., 2008).

5.2.2 The oxygen cycle

To investigate the possible consequences of our modelling results for the oxidation of the atmosphere, we must evaluate the sources and sinks of atmospheric oxygen. Contrary to our quantitative modelling of the evolution of oceanic $^{87}Sr/^{86}Sr$ (section 4.3.4), we discuss the consequences of continental emergence on atmospheric oxygen qualitatively. Campbell and Allen (2008) suggested that a change in the production rate of atmospheric O_2 is the most likely cause of the oxidation of the atmosphere because the oxidation state of the mantle has probably remained constant over time. They proposed a simplified cycle for dioxygen that is shown in Fig. 5.4. It appears from this cycle that atmospheric oxygen is mainly produced by photosynthesis, so that ultimately, the origin of atmospheric oxygen is biotic. The link is thus narrow between the evolution of early life and that of the atmosphere. The reaction of photosynthesis can be written as follows

$$CO_2 + H_2O \rightleftarrows CH_2O + O_2\,, \tag{5.1}$$

and the back-reaction is aerobic respiration. A rise in atmospheric oxygen occurs if the products of the reaction do not back-react. On geological timescales, this would be due to the burial of organic carbon. Other sinks of oxygen are the oxidation of volcanic gases such as H_2, SO_2, H_2S and CO, the oxidation of pyrite during weathering processes (Fig. 5.4), and the oxidation of reduced C and S gases during burial diagenesis and metamorphism (Campbell and Allen, 2008).

5.2.3 Enhanced erosion and the availability of nutrients and the evolution of early life

It is likely that photosynthetic cyanobacteria had evolved by the late-Archaean. While the proposed evidence of $\sim$ 2.7 Ga molecular biomarkers of Eukaryotes (Brocks et al., 1999) has been reassessed by Rasmussen et al. (2008), Lepot et al. (2008) identified aragonite nanocrystals, prob-

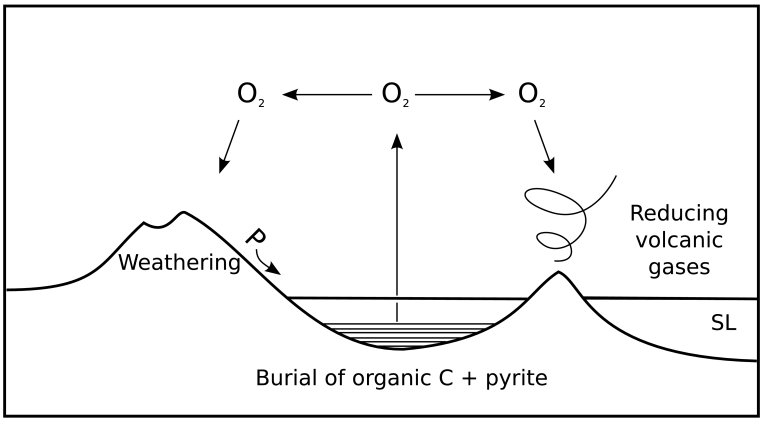

Figure 5.4: Schematic dioxygen cycle showing the main sources and sinks. From Campbell and Allen (2008).

ably of biogenic origin, in pristine drillcore stromatolitic samples from the Tumbiana Formation. This suggests that the stromatolites of the Tumbiana Formation are of biogenic origin and by extension, because modern stromatolites are associated with photosynthetic micro-organisms, this finding also indirectly suggests that photosynthetic micro-organisms had evolved by 2.7 Ga.

We have seen in section 4.3.4 that the sedimentary yield from the continents to the oceans is a function of maximum continental elevation and of emerged land surface (Eq. 4.11), and that continental emergence is probably responsible for the enrichment of oceans in ^{87}Sr. Similarly, the input to the oceans of other elements concentrated in the continental crust would increase because of continental emergence. Of importance to life are nutrients, amongst which figures the element phosphorus, necessary not only to form the phosphate-desoxyribose backbone of deoxyribonucleic acid (DNA), but also to form the three phosphate groups of the molecule adenosine triphosphate (ATP) involved in intracellular energy transfers. Phosphorus is thus crucial not only to store genetical information, which allows the replication of living organisms, but also to transfer energy through living organisms. It is worth noting that phosphorus is about ten times more concentrated in the continental crust (870 ppm, Rudnick and Fountain, 1995) than in the primitive upper mantle (90 ppm, McDonough and Sun, 1995), and that the concentration of present-day and Archaean continental crust are similar (Rudnick and Fountain, 1995). Because of an increase in weathering and erosion processes, continental emergence would thus result in an increased availability of phosphorus, particularly at river outlets. Planctonic micro-organisms would thrive because of this increase in nutrient availability, similarly to the algae that thrive on phosphorus rich fertilisers and form algae blooms at river outlets in cultivated areas on modern Earth. This increase in biomass and bioactivity (also referred to as increase of primary productivity) would result in an increase of the rate of production of oxygen and would thus favour the oxidation of the atmosphere. In the extreme, oxygen levels can reach a toxic limit in the ocean, which would result in mass extinction of photosynthetic micro-organisms and thus decrease the rate of dioxygen production.

5.2.4 Palaeoproterozoic enlargement of continental platforms

Photosynthetic micro-organisms are particularly adapted to continental platforms, where both light and nutrients are abundant (*e.g.* Nisbet and Sleep, 2001). The oceanic layer in which enough light is available, called the photic zone, is approximately 100 m deep on modern Earth. In the absence of a UV-shielding ozone layer, the photic zone would probably be deeper in the Archaean. This effect would be buffered by the fainter light emitted by the Sun (Newman and Rood, 1977). In a review of the Precambrian sedimentary record, Eriksson et al. (2005) suggested that there was an enlargement of epereic passive margin basins between 2.6 and 2.4 Ga. Our modelling results, that suggest a late-Archaean continental emergence and largely flooded continents (sections 2.2 and 2.3), are consistent with this observation.

This enlargement of shallow seas would not only have favoured the development of photosynthetic micro-organisms, but it would also have promoted sedimentation and subsidence processes. This would have resulted in a net increase of oxygen in the atmosphere through the enhanced production of dioxygen by photosynthetic micro-organisms and through the burial of reduced carbon and of pyrite. Campbell and Allen (2008) proposed a model in which they explain increases in atmospheric by the formation of supercontinents. Supercontinents result in higher elevation so that the run-off from continents to oceans increases. However, as discussed in section 2.3.4, the amount of continental margins is reduced in a supercontinental configuration. While the sedimentary yield to the oceans would increase, the reduction of the total area of continental margins would not favour the burial of reduced carbon and pyrite so that the net contribution of supercontinental aggregation to atmospheric oxidation might be less important than argued by Campbell and Allen (2008). Regarding the secular evolution of atmospheric oxygen, our modelling results suggest a late-Archaean increase in the area of emerged land, in the maximum continental elevation and in the area of epereic seas. All of these environmental changes could have contributed to the oxidation of the atmosphere.

5.2.5 Emergence of continental flood basalts

As discussed at length in the present contribution, a concomitant effect of the emergence of the continents is the emergence of continental flood basalts. Holland (2002) pointed out that submarine volcanism is less reducing than subaerial volcanism. Kump and Barley (2007) revisited the database of Prokoph et al. (2004) of large igneous provinces through time and classified each province as subaerial or submarine . While this method is largely qualitative - for instance Kump and Barley (2007) classified the basalts from the Fortescue Group as subaerial when we have seen in chapter 3 that this group is largely subaqueous - it suggests that (at most) 20% of Archaean large igneous provinces erupted subaerially, in contrast to 80% of post-Archaean large igneous provinces and the totality of post-Archaean continental flood basalts. Based on the model of Holland (2002), Kump and Barley (2007) argued that this shift from predominantly subaqueous to predominantly subaerial flood volcanism towards the Archaean/Proterozoic boundary would

have decreased the rate of oxygen consumption by reducing volcanic gases and thus promoted the oxidation of the atmosphere. The observation of more common subaqueous flood volcanism has been used in the present study as an argument for flooded continents in the Archaean, and our modelling results are consistent with this observation. Thus, it is possible that the emergence of continental flood basalts contributed to the oxidation of the atmosphere. However, the main weakness of the model of Kump and Barley (2007) is that it does not account for the most important subaqueous volcanic process that are mid-oceanic ridges. As discussed in section 5.1.2, it is possible that the intake of oxygen at mid-oceanic ridges was less important because of shallower hydrothermal penetration. In this regard, model NGM that predicts a deepening of ridgecrests from $\sim$ 75 m to $\sim$ 1500 m between 3 Ga and 2 Ga (Fig.5.1) could result in an important increase in hydrothermal penetration, possibly contributing to the great oxidation event.

5.2.6 Emergence of the continents and increased weathering processes

The processes discussed above would all contribute to the oxidation of the atmosphere. On the other hand, the emergence of the continents and the increase in continental elevations would also result in enhanced silicate weathering processes that would decrease the amount of oxygen in the atmosphere (Fig. 5.4). Enhanced silicate weathering would also consume carbon dioxide so that this process might not significantly affect the partial pressure of atmospheric oxygen. It would however decrease the absolute amount of oxygen in the atmosphere. It is worth noting that since the atmosphere is oxidant at present, the rate of additions of oxygen by life must have exceeded the rate of subtraction of oxygen in the long term.

One consequence of the *water world* predicted by our models is that because of less efficient weathering processes atmospheric levels in carbon dioxide would not be buffered, which could result in the accumulation of carbon dioxide in the atmosphere (Walker, 1985), sometimes referred to as runaway greenhouse. However, the trace element composition of shales indicates that the emerged surface essentially consisted of mafic rocks in the Archaean. Since mafic rocks are easily weathered, they consume more carbon dioxide than felsic rocks, which would buffer the predicted runaway greenhouse. Nevertheless, high levels of atmospheric carbon dioxide might be needed to account for the possibility of hot Archaean oceans, since modelling by Sleep and Zahnle (2001), assuming a constant continental surface, suggests cool Archaean climates.

5.3 Conclusion

We have seen in this chapter that our models predict a secular deepening of mid-oceanic ridges that is anticorrelated to crustal growth. Early crustal growth models predict mid-oceanic ridges between 660 and 1200 m shallower than present at 2.5 Ga, whereas delayed crustal growth models predict mid-oceanic $\sim$ 2 km shallower than present in the Archaean. Shallower ridgecrests in the Archaean have several implications. Firstly, they could account for the evolution of the δ^{18}O of marine carbonates, since a shallower hydrothermal penetration would result in limited water-rock exchange in the past that could explain the observed trend of increasing depletion in ^{18}O of marine carbonates back in geological times. Furthermore, shallower hydrothermal penetration would result in a decrease of the carbonatisation of the oceanic crust, which would trigger the accumulation of carbon dioxide in the oceans and in the atmosphere. This would have contributed to hot Archaean climates. Finally, ridgecrests could have been a suitable habitat for early life since the early crustal growth models predict mid-oceanic ridges constantly deeper than 1 km in the Archaean. This environment would thus have been stable and shielded from UV radiation by a deep water column.

As for the change in the area of emerged land predicted by our models, it could have contributed to the great oxidation event proposed at $\sim$ 2.45 Ga. The emergence of the continents would have resulted in an increased input of phosphorus to the ocean which would have enhanced the primary productivity of photosynthetic organisms, and thus their rate of oxygen production. An increase in the amount of continental platforms, corollary of the increase in emerged area predicted by our models, would have resulted in greater rates of sedimentation. This would have favoured the burial of reduced carbon and pyrite, and thus decreased their rate of oxidation. Finally, the emergence of continents could have been associated with a decrease in subaqueous volcanism, that is more reducing than subaerial volcanism. The associated decrease in oxidation of volcanic gases could also have contributed to the oxidation of the atmosphere. The three effects listed above would have been buffered by the increase in the efficiency of weathering processes expected for a larger emerged area. Ultimately, the main source of oxygen for the atmosphere are photosynthetic organisms. Thus, the present-day oxidising state of the atmosphere indicates that sources of oxygen must have exceeded sinks of atmospheric oxygen in the long term.

6

Conclusion and future work

6.1 Conclusion

The Archaean rock record proves difficult to decipher since it is fragmentary, biased, and has been exposed to subsequent geological processes for over half of Earth's history. Nevertheless, several independent petrological, geochemical and rheological constraints indicate that in the Archaean, the upper mantle was 200 ± 100°C hotter than at present. Moreover, the Archaean continental crust preserved unique diapiric structures associated with the deformation of hot, ductile continental crust. This suggests that overall, the Archaean continental crust was hotter than present-day continental crust. Another salient feature of the Archaean rock record is the common occurrence of subaqueous flood volcanism emplaced on top of continents, which suggests higher sea levels in the Archaean.

In the long term, sea level is controlled by changes in a) the isostatic equilibrium between continents and oceans, b) oceanic bathymetry, c) continental area, and d) continental hypsometry. We developed a physical model in which the bathymetry and isostatic equilibrium between oceans and continents are a function of mantle temperature. The second parameter of this model is the continental area. The numerical results of this model suggest that less than 15% of the Earth's surface was emerged in the Archaean, which represents approximately half of the present-day land area. Furthermore, it is likely that the Archaean continental lithosphere could not sustain elevations as high as present-day continental lithosphere, because it was hotter and thus weaker. Taking this effect into account, our results show that less than 3% of the Earth's surface, which approximately represents the area of the South American continent, was emerged in the Archaean. This result is consistent with widespread subaqueous continental flood basalts in the Archaean.

We studied the 2775-2630 Ma Fortescue continental flood basalt in the East Pilbara Craton, Western Australia. Sedimentological and structural field observations are consistent with a flexural emplacement of this 6.5 km-thick volcano-sedimentary pile. To investigate the effect of the eruption of continental flood basalts, we built a thermo-mechanical model of a continental lithosphere in which the basaltic pile is treated as a topographic load. Our results suggest that the relaxation of the topographic load can occur via gravity-driven lower crustal flow at elevated crustal temperatures, and that the characteristic relaxation time depends on Moho temperature. Our field observations, together with published geochronological and heat flow data, allowed us to constrain the relaxation time of the Fortescue Group and to infer a cooling of the continental crust of 200°C over 2.7 Ga in the Pilbara Craton. This result supports the idea of a hotter continental crust in the Archaean. It is also consistent with the limitation of Archaean continental elevations by gravity-driven lower crustal flow, to the difference that in the case of continental flood basalts, crustal thickening can occur in the absence of horizontal forces at plate boundaries.

The least constrained and most debated parameter relevant to the long-term evolution of sea level is the evolution of continental area through geological times (crustal growth). In a synthesis,

we built an integrated model that allows for the investigation of the influence of contrasted crustal growth models on mantle temperature, sea level, emerged land area, ridge depth and oceanic composition in $^{87}Sr/^{86}Sr$. This model includes the effect of the Neoarchaean increase in maximum continental elevation due to the strengthening of the continental lithosphere. The results of this model suggest that the emerged land area does not depend on crustal growth models, and that it was less than 5% of the Earth's surface in the Archaean, dropping to approximately 0% (*continental flooding*) at $\sim$ 3.5 Ga. Before 3.5 Ga, emerged land would have been associated with transient low relative sea level, either because of regional dynamic topography for example due to the formation of a supercontinent, or because of locally cooler crustal temperatures. Our modelling results also reconcile early crustal growth models with the evolution of oceanic $^{87}Sr/^{86}Sr$, when a reduced area of emerged land and a lower maximum continental elevation are taken into account. This result suggests that there may be no need for delayed crustal growth models. Instead, we suggest that erosion and weathering of the continental crust were limited in the Archaean because the continental crust was largely covered by subaqueous basaltic piles. The delayed appearance of the differentiated continental crust in the surface geochemical record is due to the secular increase in the surface of emerged land and to the Neoarchaean strengthening of the continental lithosphere.

The appearance of the differentiated continental crust at the surface of the Earth would also have resulted in an increased input of phosphorus to the oceans. Because phosphorus is a nutrient, this would have enhanced the primary productivity of photosynthetic organisms and thus their rate of oxygen production. The enlargement of continental platforms, corollary of continental emergence, would have favoured the sedimentation of reduced carbon and of pyrite, and thus decreased the rate of their respective oxidation. Thus, it is possible that the emergence of the continents could have contributed to the great oxidation event of the atmosphere at the Archaean/Proterozoic boundary. A secular deepening of ridgecrests as predicted by our models would also have had consequences for the composition of the oceans and of the atmosphere. The corollary secular increase in the depth of hydrothermal penetration could account for the observed secular enrichment of the oceans in ^{18}O. For shallower ridges, less efficient high-temperature hydrothermal processes would also imply a decrease in the carbonatisation of the oceanic crust, and thus possibly greater amounts of carbon dioxide in the atmosphere. Finally, ridgecrests are predicted to be approximately 1 km deep throughout the Archaean for early crustal growth models, which would make them a suitable habitat, sheltered from UV radiation, for the evolution of early hyperthermophile micro-organisms.

6.2 Future work

The method presented in chapter 3.1 to evaluate the thermal state of a continental lithosphere from field observations and numerical models could be applied to continental flood basalts of different ages. This could allow for the constraint of the evolution of the thermal state of the lithosphere. Post-Archaean continental flood basalts are subaerial, but there are potentially more palaeoaltimetry proxies in recent times, including the stomatal density of fossil leaves, terrestrial cosmogenic nuclides and stable isotopes of palaeolakes (Clark, 2007). The only palaeoaltimetry proxies adapted to the Archaean are basalt vesicularity and sedimentary environments of subaqueous continental flood basalts. In the Phanerozoic, when more palaeoaltimetry proxies are available, relaxation times are expected to be of more than 20 Myr, so that changes in elevation could be difficult to track. The method is best suited for subaqueous Archaean continental flood basalts, which still leaves numerous case-study opportunities, as pointed out in section 3.3.
Another outlook of the work presented in this contribution is the coupling of the model described in chapter 4, that allows for the calculation of the depth of ridgecrests, to the models of Kasting et al. (2006b) that allows for the calculation of the δ^{18}O of seawater as a function of the depth of ridgecrests. If the secular evolution in oceanic δ^{18}O is due to a change in the depth of ridgecrests as suggested by Kasting et al. (2006b), the results of such a coupled model could be used to discriminate between early and delayed crustal growth models that predict a very contrasted evolution of the depth of ridgecrests.
Finally, we have shown that the secular deepening of ridgecrests and the enlargement of emerged land surface predicted by our models would have important climatic consequences. The evolution of the depth of ridgecrests and of the area of emerged land are both relevant to the long-term carbon dioxide cycle. Integrating our modelling results to climate models similar to that of Sleep and Zahnle (2001) would potentially give interesting insights into the Archaean climate. The use of the predicted area of emerged land as input for global climate models, taking into account the changes in silicate weathering processes and in albedo imposed by a reduced land surface, is also promising for future work.

A

Stable isotope data on carbonates from the East Pilbara craton

Contents

The carbonates and cherts from the Tumbiana Formation are amongst the most depleted in ^{18}O of the geological record (Knauth et al., 2006). In this section, we report new $\delta^{18}O$ and $\delta^{13}C$ data from five stromatolites and nine hydrothermal calcites from the East Pilbara Terrane and compare them to published data.

A.1 Samples and sampling strategy

The analysed stromatolites are the same as in section 3.4.1. In addition, nine calcite samples were collected from hydrothermal vents, including eight along the stratigraphy of the Fortescue Group (Figs. 3.17 and 3.18), and one (VZ93) from the 3470-3458 Ma Apex basalt (Fig. 3.5).

A.2 Methods

The preparation of the stromatolite samples was described in section 3.4.1. The calcite samples for which enough material was available were prepared following the method described in section 3.4.1. Samples VZ01, VZ09, VZ10 and VZ93 were not crushed prior to analysis because material was scarce for these samples.
The $\delta^{18}O$ and $\delta^{13}C$ values of the carbonate fraction of the samples were determined from a few milligrams of subsample at CSIRO by Environmental Isotopes Pty Ltd. Carbonates were analysed in individual reaction vessels using 100% phosphoric acid at 25°C. The samples were reacted overnight and CO_2 produced from the reaction of calcite was extracted using a gas syringe and analyzed by injection into a He stream, and separated from other gases by GC attached to a Finnigan 252 mass spectrometer using a Conflo III. The mass spectrometer is calibrated against the international standard VPDB (Vienna Peedee belemnite) which is defined by the International Atomic Energy Agency as standard IAEA-NBS 19 ($\delta^{13}C = +1.95‰$ VPDB; $\delta^{18}O = -2.20‰$ VPDB; Coplen et al., 2006). Replicate analysis of the standard calcites is generally better than ± 0.1‰ VPDB for C and O. The analyses were corrected using standards NBS 22 ($\delta^{13}C = -30.03‰$ VPDB; Coplen et al., 2006).

A.3 Results

Values are reported in Tab. A.1 in permil (‰) using the δ notation relative to VPDB:

$$\delta^{18}O = \left(\frac{\left(\frac{^{18}O}{^{16}O}\right)_{sample}}{\left(\frac{^{18}O}{^{16}O}\right)_{standard}} - 1 \right) 1000$$

and

$$\delta^{13}C = \left(\frac{\left(\frac{^{13}C}{^{12}C}\right)_{sample}}{\left(\frac{^{13}C}{^{12}C}\right)_{standard}} - 1 \right) 1000.$$

Variations from the standard may be positive or negative, negative δ values reflecting fractionation of the light isotope into the analysed sample compared to the standard.

Table A.1: Oxygen and carbon isotopic composition (in ‰ VPDB) of the analysed calcites and stromatolites.

‰ VPDB	Stromatolites					Calcites								
	B19A	B19B	B20F	B20H	B15B	VZ93	BC08	VZ14	VZ09	VZ10	VZ01	VZ04	VZ77	VZ78
δ^{13}C	-0.1	1.9	1.0	-4.5	-0.5	0.2	-2.0	-0.5	-2.0	-1.2	-0.2	-0.7	-0.2	-2.1
δ^{18}O	-19.1	-15.3	-14.1	-15.1	-15.4	-17.9	-21.7	-17.0	-16.7	-16.3	-14.9	-13.3	-14.3	-18.3
⟶ samples ordered according to their stratigraphic position														

The measured δ^{13}C obtained on stromatolites from the Kylena and Tumbiana Formations are statistically identical (Fig. A.1a). δ^{13}C ranges between -0.1 and 1.9‰ and averages at 0.9 ± 1.4‰ for the Kylena Formation, and it ranges between -4.5 and 1‰ with an average of -1.8 ± 2.5‰ for the Tumbiana Formation. The carbon isotope signature of our samples from the Tumbiana Formation are consistent with previously published data (Fig. A.1a). The δ^{13}C measured on hydrothermal calcites is similar to that of stromatolites and previously published data, with values of -0.5‰ for the Kylena Formation, -1 ± 0.8‰ for the Tumbiana Formation and -1 ± 1.2‰ for the other calcites from the East Pilbara Terrane.

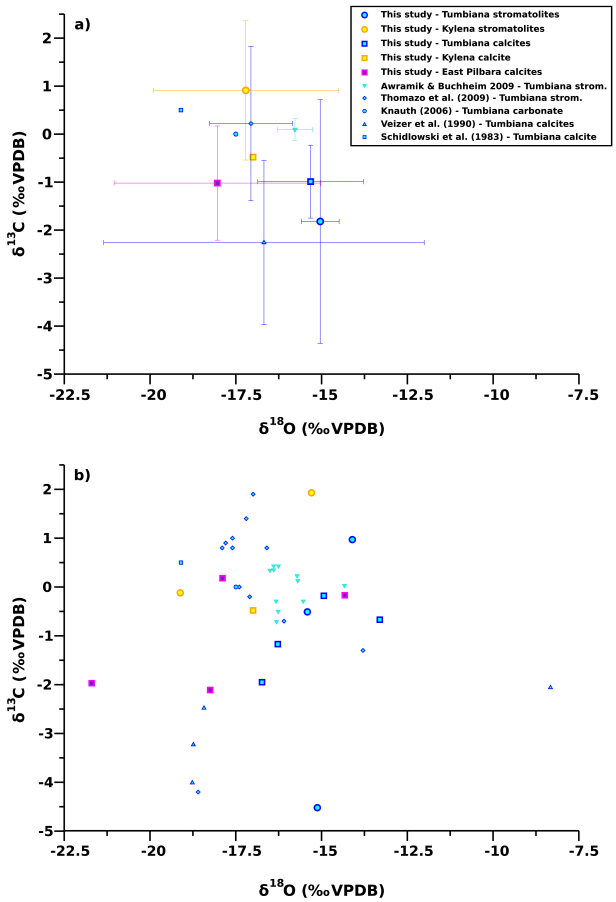

Figure A.1: Stable isotopes in East Pilbara Archaean carbonates. a) averages and error bars (1σ); b) individual samples. Data are shown for the present study and for previous studies of the Tumbiana Formation.

δ^{18}O values are statistically identical between stromatolites from the Kylena (-17.2 ± 2.7‰) and Tumbiana (-15 ± 0.5‰) Formations (Fig. A.1a). However, our outcrop stromatolitic samples from the Tumbiana Formation appear less depleted in ^{18}O than the drill core stromatolitic samples of Thomazo et al. (2009) that average at -17 ± 1.2‰. Importantly, the δ^{18}O measured on hydrothermal calcites is similar to that of stromatolites and previously published data, with values of -17‰ for the Kylena Formation, -15.3 ± 1.5‰ for the Tumbiana Formation and -18 ± 3‰ for the other calcites from the East Pilbara Terrane. Finally, no firm correlation between δ^{18}O and δ^{13}C appears from the data (Fig. A.1b).

A.4 Comparison with published stable isotope data from the Tumbiana Formation

The most important result from the present study is probably that the δ^{18}O of hydrothermal calcites is identical to that of stromatolites. If the oxygen isotope data are used as a palaeotemperature proxy, this would imply that the hydrothermal calcites were formed from the circulation of fluids at the same temperature than the water in which the stromatolites were formed. Three main hypotheses are possible to explain this: a) the hydrothermal calcites and stromatolites were formed in the same hot seawater (or lake water). This hypothesis implies low hydrothermal temperatures for the sampled hydrothermal vents, including one ∼1.7 b.y older than the Tumbiana Formation; b) the hydrothermal calcites and stromatolites were formed in equilibrium with seawater (or lake water) depleted in ^{18}O compared to present-day seawater; c) the initial oxygen isotopic composition of all the samples was altered by subsequent diagenesis and/or metamorphism.

Fig. A.2 shows that carbonates from the East Pilbara Terrane do not differ from other pre-850 Ma carbonates. The lithification arrow in Fig. A.2 shows the trend described by primary Cenozoic carbonates lithified in equilibrium with increasing amounts of meteoric water depleted in ^{18}O due to evaporation and in ^{13}C due to the incorporation of light (δ^{13}C < -20‰) organic material (Knauth and Kennedy, 2009). The alteration arrows show the expected trend due to the recrystallisation of the rock and isotopic re-equilibration with higher temperature fluids. This process lowers the δ^{18}O of the rock at nearly constant δ^{13}C (Knauth and Kennedy, 2009). It appears from Fig. A.2 that marine carbonates older than 850 Ma do not show significant negative ^{13}C values. Knauth and Kennedy (2009) interpreted this as reflecting a lighter coastal phytomass. The presence of a consequent coastal phytomass, depleted in ^{13}C (with δ^{13}C < −20‰ VSMOW), results in the depletion of meteoric water that is only seen in the diagenesis of marine carbonates younger than ∼ 850 Ma (Knauth and Kennedy, 2009). As for the strongly negative δ^{18}O values, Knauth and Kennedy (2009) explained them by the longer exposition of older samples to metamorphism. However, our surface stromatolitic samples from the Tumbiana Formation display less negative δ^{18}O than the core samples of Thomazo et al. (2009). Assuming that the core samples are pristine, this implies that the original signature of

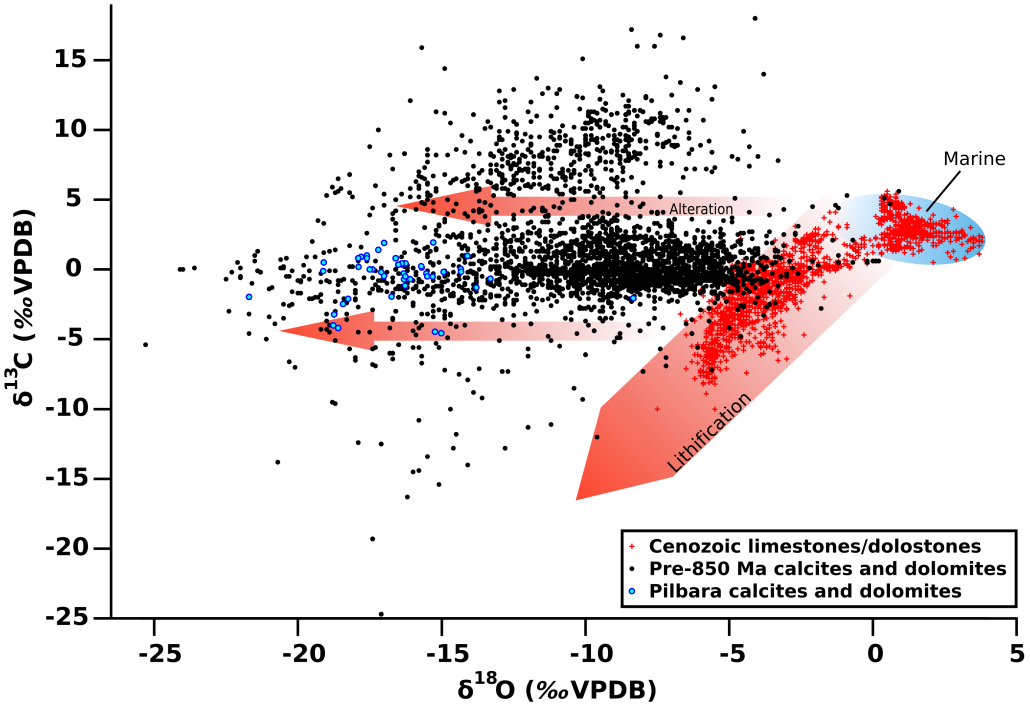

Figure A.2: Stable isotopes in primary Cenozoic (last 65.5 Ma) limestones and dolostones (red plus symbols) and in all marine calcites and dolomites older than 850 Ma (black dots). Data from Fig. A.1b are reported for comparison (blue circles). The blue area shows modern seawater. The red arrows describe the trends described by lithification and alteration processes. Figure from Knauth and Kennedy (2009).

our samples could have been isotopically lighter, and progressively enriched in ^{18}O by subsequent alteration. This variation is opposite to that described by the alteration arrow in Fig. A.2, illustrating the difficulty to interpret stable isotope data of Archaean terranes. It is not yet clear whether the similar ^{18}O content of hydrothermal calcites and stromatolites observed in our data reflects the original isotopic signature or the alteration of the initial oxygen isotopic composition.

A.5 Conclusion and future work

The stable isotope data presented in this study are similar for samples of different ages (ranging from 3470 to 2713 Ma) and lithology (stromatolites and hydrothermal calcites). This implies either that the hydrothermal calcites formed in equilibrium with the same fluid (sea or lake water) as the stromatolites, or that the original signature of all the samples was altered by posterior metamorphism. This question remains unresolved as yet because of the many processes affecting the oxygen isotope signature of carbonates. This isotopic dataset is to be completed by $^{87}Sr/^{86}Sr$ data in the near future to track the evolution of the $^{87}Sr/^{86}Sr$ of marine carbonates (section 4.1.3; Shields and Veizer, 2002) at high temporal frequency.

Bibliography

Abbott, D. H., and Hoffman, S. E., 1984. Archaean plate tectonics revisited 1: Heat flow, spreading rate, and the age of subducting oceanic lithosphere and their effects on the origin and evolution of continents. Tectonics 3, 429–448.

Abbott, D., Burgess, L., Longhi, J. and Smith, W. H. F., 1994. An empirical thermal history of the Earh's upper mantle. J. Geophys. Res. 99, 13835–13850.

Albarède, F., 1998a. Time-dependent models of U-Th-He and K-Ar evolution and the layering of mantle convection, Chemical Geology 145, 413–429.

Albarède, F., 1998b. The growth of continental crust. Tectonophysics 296, 1–14.

Allègre, C. J., Jaupart, C., 1985. Continental tectonics and continental kinetics. Earth Planet. Sci. Lett. 74, 171–186.

Alt, J. C., and Teagle, D. A. H., 1999. Uptake of carbon during alteration of oceanic crust, Geochim. Cosmochim. Acta, 63, 1527–1535.

Amelin, Y. V., Heaman, L. M., and Semenov, V. S., 1995. U-Pb geochronology of layered mafic intrusions in the eastern Baltic Shield: Implications for the timing and duration of Paleoproterozoic continental rifting. Precambrian Res. 75, 31–46.

Armstrong R. L., 1981. Radiogenic isotopes: the case for crustal recycling on a near-steady-state no-continental-growth Earth. Philos. Trans. R. Soc. London Ser. A 301, 443–471.

Armstrong R. L., 1991. The persistent myth of crustal growth. Aust. J. Earth Sci. 38, 613–630.

Armstrong, R. A., Compston, W., Retief, E. A., Williams, I. S., and Welke, H. J., 1991. Zircon ion microprobe studies bearing on the age and evolution of the Witwatersrand triad. Precambrian Res. 53, 243–266.

Arndt, N. T., 1983. Role of a thin, komatiite-rich oceanic crust in the Archean plate-tectonic process. Geology 11, 372–375.

Arndt, N. T., Nelson, D. R., Compston, W., Trendall, A. F. and Thorne A. M., 1991. The age of the Fortescue Group, Hamersley Basin, Western Australia, from ion microprobe zircon U-Pb results. Aust. J. Earth Sci. 38, 261–281.

Arndt, N. T., Ginibre, C., Chauvel, C., Albarède, F., Cheadle, M., Herzberg, C., Jenner, G., and Lahaye, Y., 1998. Were komatiites wet? Geology 26 (8), 739–742.

Arndt, N. T., 1999. Why was flood volcanism on submerged continental platforms so common in the Precambrian? Precambrian Res. 97 (3-4), 155–164.

Arndt, N. T., Coltice, N., Helmstaedt, H. and Gregoire, M., 2009. Origin of Archean subcontinental lithospheric mantle: Some petrological constraints. Lithos 109, 61–71.

Artemieva, I. M., 2006. Global 1°× 1° thermal model TC1 for the continental lithosphere: Implications for lithosphere secular evolution. Tectonophysics 416, 245–277.

Artemieva, I. M., 2009. The continental lithosphere: Reconciling thermal, seismic, and petrologic data. Lithos 109, 23–46.

Aspler, L. B., and Chiarenzelli J. R., 1998. Two Neoarchean supercontinents? Evidence from the Paleoproterozoic. Sediment. Geol. 120, 75–104.

Awramik, S. M., Buchheim, H. P., 2009. A giant, late Archean lake system: the Meentheena Member (Tumbiana Formation; Fortescue Group), Western Australia, Precambrian Res., doi:10.1016/j.precamres.2009.07.005.

Bailey, R. C., 1999. Gravity-driven continental overflow and Archaean tectonics. Nature, 398, 413–415.

Barker, F., and Arth, J. G., 1976. Generation of trondhjemitic-tonalitic liquids and Archean bimodal trondhjemite-basalt suites. Geology 4, 596–600.

Barley, M. E., Krapez, B., Groves, D. I., and Kerrich, R., 1998. The Late Archaean bonanza: metallogenic and environmental consequences of the interaction between mantle plumes, lithospheric tectonics and global cyclicity. Precambrian Res. 91, 65–90.

Batchelor, M. T., Burne, R. V., Henry, B. I., and Slatyer, T., 2005. Statistical physics and stromatolite growth: new perspectives on an ancient dilemma. Physica A 350, 6–11.

Bau, M., and Dulski, P., 1996. Distribution of yttrium and rare-earth elements in the Penge and Kuruman iron-formations, Transvaal Supergroup, South Africa. Precambrian Res. 79, 37–55.

Beaumont, C., Nguyen, M. H., Jamieson, R. A., and Ellis, S., 2006. Crustal flow modes in large hot orogens. In: Law, R. D., Searle, M. P., and Godin, L. (Eds.), Channel flow, ductile extrusion and exhumation in continental collision zones. Geol. Soc., London, Spec. Pub. 268, 91–145.

Bekker, A., Holland, H. D., Wang, P. L., Rumble, D., Stein, H. J, Hannah, J. L., Coetzee, L. L., and Beukes, N. J., 2004. Dating the rise of atmospheric oxygen. Nature 427, 117–120.

Berry, A. J., Danyushevsky, L. V., ONeill, H. St. C., Newville, M., and Sutton, S. R., 2008. Oxidation state of iron in komatiitic melt inclusions indicates hot Archaean mantle. Nature 455, 960–963.

Bickle, M. J., 1978. Heat loss from the Earth: A constraint on Archaean tectonics from the relation between geothermal gradients and the rate of plate production. Earth Planet. Sci. Lett. 40, 301–315.

Bickle, M. J., Nisbet, E. G., Martin, A., 1994. Archean greenstone belts are not oceanic crust, J. Geol., 102, 121–138.

Blake, T. S., 1993. Late Archaean crustal extension, sedimentary basin formation, flood basalt volcanism and continental rifting: the Nullagine and Mount Jope Supersequences, Western Australia. Precambrian Res. 60, 185–241.

Blake, T. S., Buick, R., Brown, S. J. A., and Barley, M. E., 2004. Geochronology of a Late Archaean flood basalt province in the Pilbara Craton, Australia: constraints on basin evolution, volcanic and sedimentary accumulation, and continental drift rates. Precambrian Res. 133, 143–173.

Bleeker, W., 2002. Archaean tectonics: a review, with illustrations from the Slave craton. Geol. Soc., London, Spec. Pub. 199 (1), 151–181.

Bleeker, W., 2003.The late Archean record: a puzzle in ca. 35 pieces. Lithos 71, 99–134.

Blichert-Toft J., and Albarède F., 2008. Hafnium isotopes in Jack Hills zircons and the formation of the Hadean crust. Earth Planet. Sci. Lett. 265, 686–702.

Bolhar, R., and Van Kranendonk, M. J., 2007. A non-marine depositional setting for the northern Fortescue Group, Pilbara Craton, inferred from trace element geochemistry of stromatolitic carbonates. Precambrian Res. 155, 229–250.

Bose, K., and Ganguly, J., 1995. Experimental and theoretical studies of the stabilities of talc, antigorite and phase A at high pressures with applications to subduction processes. Earth Planet. Sc. Lett. 136, 109–121.

Bouhallier, H., Chardon, D. and Choukroune, P., 1995. Strain patterns in Archaean dome-and-basin structures: The Dharwar craton (Karnataka, South India). Earth Planet. Sc. Lett. 135 (1-4), 57–75.

Bowen, G. J., and Wilkinson, B., 2002. Spatial distribution of δ^{18}O in meteoric precipitation. Geology 30, 315–318.

Bowring, S. A., and Williams, I. S., 1999. Priscoan (4.004.03 Ga) orthogneisses from northwestern Canada. Contrib. Mineral. Petrol. 134, 3–16.

Boyd, F. R., 1989. Compositional distinction between oceanic and cratonic lithosphere, Earth Planet. Sc. Lett. 96, 15–26.

Boyet, M., Blichert-Toft, J., Rosing, M., Storey, M., Telouk, P., and Albarède, F., 2003. ^{142}Nd evidence for early Earth differentiation. Earth Planet. Sci. Lett. 214, 427–442.

Boyet, M., and Carlson, R. W., 2006. A new geochemical model for the Earth's mantle inferred from ^{146}Sm-^{142}Nd systematics. Earth Planet. Sci. Lett. 250, 254-268.

Brocks, J. J., Logan, G. A., Buick, R., and Summons, R. E., 1999. Archean Molecular Fossils and the Early Rise of Eukaryotes. Science 285, 1033–1036.

Buick, R., 1992. The Antiquity of Oxygenic Photosynthesis: Evidence from Stromatolites in Sulphate-Deficient Archaean Lakes. Science 255, 74–77.

Buick, R., Thornett, J. R., McNaughton, N., Smith, J. B., Barley, M. E. and Savage, M., 1995. Nature 375 (6532), 574–577.

Cagnard, F., Gapais, D., and Barbey, P., 2008. Transition between "Archaean-type" to "Modern-type" orogenic belts: insights from Palaeoproterozoic times. Geophys. Res. Abstracts 10, EGU2008-A-07341.

Campbell, I. H., and Hill, R. I., 1988. A two-stage model for the formation of the granite-greenstone terrains of the Kalgoorlie-Norseman area, Western Australia, Earth Planet. Sc. Lett. 90, 11–25.

Campbell, I. H., 2003. Constraints on continental growth models from Nb/U ratios in the 3.5 Ga Barberton and other Archaean basalt-komatiite suites. Am. J. Sci. 303 (4), 319–351.

Campbell, I. H. and Allen, C. M., 2008. Formation of supercontinents linked to increases in atmospheric oxygen. Nat. Geosci. 1, 554–558.

Caro G., Bourdon B., Birck J. L., and Moorbath S., 2003. ^{146}Sm-^{142}Nd evidence from Isua metamorphosed sediments for early differentiation of the Earths mantle. Nature 423, 428–432.

Carlson, R. W., Pearson, D. G. and James, D. E., 2005. Physical, chemical, and chronological characteristics of continental mantle, Rev. Geophys., 43, RG1001, doi:10.1029/2004RG000156.

Catuneanu, O., Martins-Neto, M. A., and Eriksson, P. G., 2005. Precambrian sequence stratigraphy. Sediment. Geol. 176, 67–95.

Christensen, M. I., Mooney, W. D., 1995. Seismic velocity structure and composition of the continental-crust - a global view. J Geophys. Res.-Sol. Ea. 100 (B6), 9761–9788.

Christensen, U. R., 1985. Thermal evolution models for the Earth, J. Geophys. Res. 90, 2995–3007.

Clark, M. K., 2007. The significance of paleotopography. Rev. Mineral. Geochem. 66, 1–21.

Cogné, J.-P., Humler, E., 2004. Temporal variation of oceanic spreading and crustal production rates during the last 180 My. Earth Planet. Sc. Lett. 227 (3-4), 427–439.

Collins, W. J., van Kranendonk M. J. and Teyssier, C., 1998. Partial convective overturn of Archaean crust in the east Pilbara Craton, Western Australia: driving mechanisms and tectonic implications. J. Struct. Geol. 20 (9-10), 1405–1424.

Coltice N., and Ricard, Y., 1999. Geochemical observations and one layer mantle convection. Earth Planet. Sc. Lett. 174, 125–137.

Coltice, N., Phillips, B. R., Bertrand, H., Ricard, Y., and Rey, P. F., 2007. Global warming of the mantle at the origin of ood basalts over supercontinents. Geology 35, 391–394.

Coltice, N., Bertrand, H., Rey, P., Jourdan, F., Phillips, B. R., and Ricard Y., 2009. Global warming of the mantle beneath continents back to the Archaean. Gondwana Res. 15, 254–266.

Coltice, N., Marty, B., and Yokochi, R., 2009b. Xenon isotope constraints on the thermal evolution of the early Earth. Chem. Geol. 266, 4–9.

Condie, K. C., 1993. Chemical composition and evolution of the upper continental crust: Contrasting results from surface samples and shales. Chem. Geol. 104, 1–37.

Condie, K. C., 1998. Episodic continental growth and supercontinents: a mantle avalanche connection? Earth Planet. Sc. Lett. 163, 97–108.

Condie, K. C., 2000. Episodic continental growth models: afterthoughts and extensions. Tectonophysics 322 (1-2), 153–162.

Condie, K. C., and Benn, K., 2006. Archean geodynamics: Similar to or different from modern geodynamics? In: Benn, K., Mareschal, J. -C., and Condie, K. C. (Eds.): Archean geodynamics and environments: AGU Geophys. Monogr. 164, Washington DC, 47–59.

Condie, K. C., and Kröner, A., 2008. When did plate tectonics begin? Evidence from the geologic record. In: Condie, K. C., and Pease, V. (Eds.): When did plate tectonics begin on planet Earth? GSA special paper 440, 281–294.

Coplen, T. B., Brand, W. A., Gehre, M., Gröning, M., Meijer, H. A. J., Toman, B., and Verkouteren, R. M., 2006. New guidelines for δ^{13}C measurements. Anal. Chem. 78, 2439-2441.

Cull, J. P., 1982. An appraisal of Australian heat-flow data. Bur. Min. Resour. J. Aust. Geol. Geoph. 7, 11–21.

Davies, G. F., 1980. Thermal histories of convective Earth models and constraints on radiogenic heat-production in the Earth. J. Geophys. Res. 85 (NB5), 2517–2530.

Davies, G. F., 1993. Conjectures on the thermal and tectonic evolution of the Earth. Lithos 30, 281–289.

Delor C. A., Burg J. P. and Clarke G., 1991. Relations diapirisme-métamorphisme dans la Province du Pilbara (Australie Occidentale) : implications pour les régimes thermiques et tectoniques à l'Archéen. CR Acad. Sci. Paris 312, 257–263.

de Vries, S. T., Pryer, L. L., and Fry, N., 2008. Evolution of Neoarchaean and Proterozoic basins of Australia. Precambrian Res. 166, 39–53.

De Wit, M. J., and Ashwal, L. D., 1997. Greenstone belts: Oxford Mono. Geol. Geoph., 35. Oxford, Clarendon Press, 809 p.

De Wit, M. J., 1998. On Archean granites, greenstones, cratons and tectonics: does the evidence demand a verdict? Precambrian Res. 91, 181–226.

Dixon, J. M., Summers, J. M., 1983. Patterns of total and incremental strain in subsiding troughs: experimental centrifuged models of inter-diapir synclines. Can. J. Earth Sci. 20 (12), 1843–1861.

Dromart, G., Coltice, N., Flament, N., Olivier, N., and Rey, P. F., 2008. Deep-water environments for the putative Early Archean life: Chert units depositional facies, Warrawoona Group, Western Australia. Eos Trans. AGU 89, Fall Meet. Suppl., Abstract V13B-2118.

Drummond, B. J., 1985. Seismic P-wave anisotropy in the subcrustal lithosphere of north-west Australia, Geophys. J. Roy. Astr. S. 81, 497–519.

Duclaux, G., Rey, P., Guillot, S., and Ménot, R.-P., 2007. Orogen-parallel flow during continental convergence: Numerical experiments and Archean field examples. Geology 35, 715–718.

Raymond Durrheim, R. J., and Mooney, W. D., 1994. Evolution of the Precambrian Lithosphere: Seismological and geochemical constraints. J. Geophys. Res. 99, 15359–15374.

Elderfield, H., Whitfield, M., Burton, J. D., Bacon, M. P., and Liss, P. S., 1988. The oceanic chemistry of the rare-earth elements. Philos. T. R. Soc. A 325, 105–126.

England, P., and McKenzie, D., 1982. A thin viscous sheet model for continental deformation. Geophys. J. R. Astr. Soc. 70, 295–321.

England, P. and Bickle, M., 1984. Continental thermal and tectonic regimes during the Archean. J. Geol. 92 (4), 353–367.

Eriksson, K. A. and Fedo, C. M, 1994. Archean synrift and stable-shelf sedimentary successions. In: Condie, K. C. (Ed.), Archean crustal evolution, Developments in Precambrian geology (11). Elsevier, 171–204.

Eriksson, P. G., 1999. Sea level changes and the continental freeboard concept: general principles and application to the Precambrian. Precambrian Res. 97, 143–154.

Eriksson, P. G., Catuneanu, O., Sarkar, S., Tirsgaard, H., 2005. Patterns of sedimentation in the Precambrian. Sediment. Geol. 176 (1-2), 17–42.

Eriksson, P. G., Banerjee, S., Catuneanu, O., Sarkar, S., Bumby, A. J. and Mtimkulu, M. N., 2007. Prime controls on ArchaeanPalaeoproterozoic sedimentation: Change over time. Gondwana Res. 12, 550–559.

Farquhar, J., Bao, H., and Thiemens, M., 2000. Atmospheric influence of Earth's earliest sulfur cycle. Science 289, 756–758.

Flament, N., Coltice, N., and Rey, P. F., 2008. A case for late-Archaean continental emergence from thermal evolution models and hypsometry. Earth Planet. Sc. Lett. 275, 326–336.

Flament, N., Rey, P. F., Coltice, N., Dromart, G., and Olivier, N., 2009. Lower crustal flow and subaqueous Archean Continental Flood Basalts. *Submitted to Geology.*

Furnes, H., de Wit, M., Staudigel, H., Rosing, M. and Muehlenbachs, K., 2007. A Vestige of Earth's Oldest Ophiolite. Science 315, 1704–1707.

Fyfe W. S., 1978. The evolution of the Earths crust: modern plate tectonics to ancient hot spot tectonics? Chem. Geol. 23, 89–114.

Galer, S. J. G., 1991. Interrelationships between continental freeboard, tectonics and mantle temperature. Earth Planet. Sc. Lett. 105 (1-3), 214–228.

Galer, S. J. G., Mezger, K., 1998. Metamorphism, denudation and sea level in the Archean and cooling of the Earth. Precambrian Res. 92 (4), 389–412.

Gans, P. B., 1987. An open-system, two-layer crustal stretching model for the eastern Great Basin. Tectonics 6, 1–12.

Gastil, G., 1960. The distribution of mineral dates in time and space. Am. J. Sci. 258, 1–35.

German, C. R., and Elderfield, H., 1990. Application of the Ce anomaly as a paleoredox indicator: The ground rules. Paleoceanography 5, 823–833.

Goddéris, Y., and François, L. M., 1995. The Cenozoic evolution of the strontium and carbon cycles: relative importance of continental erosion and mantle exchanges. Chemical Geology 126, 169–190.

Godderis, Y., and Veizer, J., 2000. Tectonic control of chemical and isotopic composition of ancient oceans: the impact of continental growth. Am. J. Sci. 300, 434–461.

Goldblatt, C., Lenton, T. M. and Watson, A. J., 2006. Bistability of atmospheric oxygen and the Great Oxidation. Nature 443, 683–686.

Goodwin, A. M. , and Smith, I. E. M., 1980. Chemical discontinuities in Archean metavolcanic terrains and the development of Archean crust. Precambrian Res. 10, 301–311,

Green, D. H., Nicholls, I. A., Viljoen, M. and Viljoen, R., 1975. Experimental demonstration of the existence of peridotitic liquids in earliest Archean magmatism. Geology 3 (1), 11–14.

Grigné, C., and Labrosse, S., 2001. Effects of continents on Earth cooling: thermal blanketing and depletion in radioactive elements. Geophys. Res. Lett. 28, 2707–2710.

Grigné, C., and Tackley, P. J., 2005. Plate tectonics is enhanced by continents. Eos Trans. AGU, 86(52), Fall Meet. Suppl., Abstract T13F-08.

Grotzinger, J. P. and Rothman, D. H., 1996, An abiotic model for stromatolite morphogenesis. Nature 383, 423–425.

Grove, T. L., Parman, S. W., 2004. Thermal evolution of the Earth as recorded by komatiites. Earth Planet. Sc. Lett. 219 (3-4), 173–187.

Gurnis, M., and Davies, G. F., 1986. Apparent episodic crustal growth arising from a smoothly evolving mantle. Geology 14, 396–399.

Gutscher, M. -A., Spakman, W., Bijwaard, H., and Engdahl, E. R., 2000. Geodynamics of flat subduction: Seismicity and tomographic constraints from the Andean margin, Tectonics, 19, 814–833.

Hacker, B. D., Peacock, S. M., Abers, G. A.,and Holloway, S. D., 2003b. Subduction factory 2. Are intermediate-depth earthquakes in subducting slabs linked to metamorphic dehydration reactions? J. Geophys. Res. 108, doi:10.1029/2001JB001129.

Hamilton, W. B., 1998. Archean magmatism and deformation were not products of plate tectonics. Precambrian Res. 91, 143–179.

Haq, B. U., Hardenbol, J. and Vail, P. R., 1987. Chronology of fluctuating sea levels since the Triassic. Science 235 (4793), 1156–1167.

Hargraves, R. B., 1976. Precambrian geologic history. Science 193 (4251), 363–371.

Harnois, L., 1988. The CIW index: A new chemical index of weathering. Sediment. Geol. 55, 319–322.

Harrison, C.G.A., Brass, G.W., Saltzman, E., Sloan II, J., Southam, J. and Whitman, J.M., 1981. Sea level variations, global sedimentation rates and the hypsographic curve. Earth Planet. Sc. Lett. 54 (1), 1–16.

Harrison, C.G.A., 1994. Rates of continental erosion and mountain building. Geol. Rundsch. 83, 431–447.

Harrison, C. G. A., 1999. Constraints on ocean volume change since the Archean. Geophys. Res. Lett. 26 (13), 1913–1916.

Harrison T. M., Schmitt A. K., McCulloch M. T., and Lovera O. M., 2008. Early ($\geq$ 4.5 Ga) formation of terrestrial crust: Lu-Hf, δ^{18}O, and Ti thermometry results for Hadean zircons. Earth Planet. Sci. Lett. 268, 476–486.

Harrison, T. M., 2009. The Hadean Crust: Evidence from $>$ 4 Ga Zircons. Annu. Rev. Earth Planet. Sci. 37,479–505.

Hawkesworth, C. J. and Kemp, A. I. S., 2006. Evolution of the continental crust. Nature 443 (7113), 811–817.

Hay, W. W., 1998. Detrital sediment fluxes from continents to oceans. Chem. Geol. 145, 287-323.

Hays, J. D., and Pitman III, W. C., 1973. Lithospheric plate motion, sea level changes and climatic and ecological consequences. Nature 246, 18–22.

Helmstaedt, H., and Schulze, D. J., 1989. Southern African kimberlites and their mantle sample: implications for Archaean tectonics and lithosphere evolution. In: Ross et al. (Eds.), Kimberlites and related Rocks: proceedings of the Fourth International Kimberlite Conference, Perth, 1986., Geol. Soc. Australia Special Publication 14, 358–368.

Hickman, A. H., 2004. Two contrasting granitegreenstone terranes in the Pilbara Craton, Australia: evidence for vertical and horizontal tectonic regimes prior to 2900 Ma. Precambrian Res. 131, 153-172.

Hoashi, M., Bevacqua, D. C., Otake, T., Watanabe, Y., Hickman, A. H., Utsunomiya, S., and Ohmoto, H., 2009. Primary haematite formation in an oxygenated sea 3.46 billion years ago. Nat. Geosci. 2, 301–306

Hoffman, P. F. and Ranalli, G., 1988. Archean oceanic flake tectonics. Geophys. Res. Lett. 15, 1077–1080.

Hofmann, A. W., Jochum, K. P., Seufert, M., and White, W. M., 1986. Nb and Pb in oceanic basalts; new constraints on mantle evolution: Earth and Planetary Science Letters, v. 79, p. 3345.

Hofmann, A. W., 1997. Mantle geochemistry: the message from oceanic volcanism. Nature 385, 219–229.

Holland, H. D., 2002. Volcanic gases, black smokers, and the great oxidation event. Geochim. Cosmochim. Ac. 66, 3811–3826.

Holland, H. D., 1999. When did the Earths atmosphere become oxic? A reply. Geochem. News 100, 20–22.

Hurley, P. M, Hughes, H., Pinson, W. H., Fairbairn, H. W., and Faure, G., 1962. Radiogenic strontium-87 model of continent formation. J. Geophys. Res. 67, 5315–5334.

Hurley P. M., and Rand J. R., 1969. Pre-drift continental nuclei. Science 164, 1229–1242.

Husson, L., and Sempere, T., 2003. Thickening the Altiplano crust by gravity-driven crustal channel flow. Geophys. Res. Lett. 30, doi:10.1029/2002GL016877.

Husson, L. and Conrad, C. P., 2006. Tectonic velocities, dynamic topography, and relative sea level. Geophys. Res. Lett. 33 (18), L18303.

Hynes, A., 2001. Freeboard revisited: continental growth, crustal thickness change and Earth's thermal efficiency. Earth Planet. Sc. Lett. 185 (1-2), 161–172.

Hynes, A., 2008. Effects of a warmer mantle on the characteristics of Archean passive margins. In: Condie, K. C., and Pease, V. (Eds.): When did plate tectonics begin on planet Earth? GSA special paper 440, 149–156.

Intergovernmental Panel on Climate Change, 2007. Climate Change 2007: Synthesis Report - Summary for Policymakers. 22 p.

Jaffrés, J. B. D., Shields, G. A., and Wallmann, K., 2007. The oxygen isotope evolution of seawater: a critical review of a long-standing controversy and an improved geological water cycle model for the past 3.4 billion years. Earth-Sci. Rev. 83, 83–122.

Jaupart, C., and Mareschal, J. -C., 1999. The thermal structure and thickness of continental roots. Lithos 48, 93–114.

Jaupart, C., Labrosse, S., Mareschal, J-C., 2007. Temperatures, heat and energy in the mantle of the Earth, in: Bercovici, D. and Schubert, G. (Eds.), Treatise on geophysics, vol. 7: Mantle dynamics. Elsevier-Pergamon.

Johannesson, K. H., Hawkins Jr., D. L., and Cortés, A., 2006. Do Archean chemical sediments record ancient seawater rare earth element patterns? Geochim. Cosmochim. Ac. 70, 871–890.

Jordan, T. H., 1988. Structure and formation of the continental tectosphere. Journ. Petrol.: Special Lithosphere Issue, 11–37.

Kamber, B. S. and Webb, G. E., 2001. The geochemistry of late Archaean microbial carbonate: Implications for ocean chemistry and continental erosion history. Geochim. Cosmochim. Ac. 65, 2509–2525.

Kamber, B. S., Bolhar, R., and Webb, G. E., 2004. Geochemistry of late Archaean stromatolites from Zimbabwe: evidence for microbial life in restricted epicontinental seas. Precambrian Res. 132, 379-399.

Kasting, J. F., Holm, N. G., 1992. What determines the volume of the oceans? Earth Planet. Sc. Lett. 109 (3-4), 507–515.

Kasting, J. F., and Howard, M. T., 2006a. Atmospheric composition and climate on the early Earth. Phil. Trans. R. Soc. B 361, 1733–1742.

Kasting, J. F., Howard, M. T., Wallmann, K., Veizer, J., Shields, G., and Jaffrés, J., 2006b. Paleoclimates, ocean depth, and the oxygen isotopic composition of seawater. Earth Planet. Sc. Lett. 252, 82–93.

Kato, Y., Yamaguchi, K. E., and Ohmoto, H., 2006. Rare earth elements in Precambrian banded iron formations: Secular changes of Ce and Eu anomalies and evolution of atmospheric oxygen. In: Kesler, S. E., and Ohmoto, H., Eds., Evolution of Early Earths Atmosphere, Hydrosphere, and BiosphereConstraints from Ore Deposits: GSA Memoir 198, 269–289.

Kaufman, P. S., and Royden, L. H., 1994. Lower crustal flow in an extensional setting: Constraints from the Halloran Hills region, eastern Mojave Desert, California. J. Geoph. Res.-Sol. Ea. 99, 15,723–15,739.

Kaula, W. M., 1979. Thermal evolution of Earth and Moon growing by planetesimal impacts. J. Geoph. Res. 84, 999–1008.

Keighley, D., Flint, S., Howell, J. and Moscariello, A., 2003. Sequence stratigraphy in lacustrine basins: A model for part of the Green River Formation (Eocene), Southwest Uinta Basin, Utah, U. S. A. J. Sediment. Res. 73, 987–1006.

Kemp, A. I. S., Hawkesworth, C. J., Paterson, B. A. and Kinny, P. D., 2006. Episodic growth of the Gondwana supercontinent from hafnium and oxygen isotopes in zircon. Nature 439 (7076), 580–583.

Kent, D. V., and Muttoni, G., 2008. Equatorial convergence of India and early Cenozoic climate trends. P. Natl. Acad. Sci. USA 105, 16065–16070.

Kerrich, R. , Wyman, D., Hollings, P., and Polat, A., 1999. Variability of Nb/U and Th/La in 3.0 to 2.7 Ga Superior Province ocean plateau basalts: implications for the timing of continental growth and lithosphere recycling. Earth Planet. Sc. Lett. 168, 101–115.

Kitajima, K., Maruyama, S., Utsunomiya, S., and Liou, J. G., 2001. Seafloor hydrothermal alteration at an Archaean mid-ocean ridge. J. Metamorph. Geol. 19, 583–599.

Knauth, L. P., and Lowe, D. R., 1978. Oxygen isotope geochemistry of cherts from the Onverwacht Group (3.4 billion years), Transvaal, South Africa, with implications for secular variations in the isotopic composition of cherts, Earth Planet. Sc. Lett. 41, 209–222.

Knauth, L. P., and Lowe, D. R., 2003. High Archean climatic temperature inferred from oxygen isotope geochemistry of cherts in the 3.5 Ga Swaziland Supergroup, South Africa. GSA Bulletin 115, 566–580.

Knauth, L. P., Awramik, S. M., and Buchheim, H. P., 2006. Isotope geochemistry of 2.7 Ga chert and carbonate, Tumbiana Formation, Australia: implications for late Archean climatic temperatures and early evolution of life. Philadelphia Annual Meeting 2006, GSA Abstracts with Programs, Vol. 38, No. 7, p. 394.

Knauth, L. P., and Kennedy, M. J., 2009. The late Precambrian greening of the Earth. Nature 460, 728–732.

Konstantinovskii, A. A., 2003. Epochs of Diamond Placer Formation in the Precambrian and Phanerozoic. Lithol. Miner. Resour. 38, 530–546.

Korenaga, J., 2006. Archean geodynamics and the thermal evolution of Earth. In: Benn, K., Mareschal, J. -C., and Condie, K. C. (Eds.): Archean geodynamics and environments: AGU Geophys. Monogr. 164, Washington DC, 7–32.

Kositcin, N., Brown, S. J. A., Barley, M. E., Krapež, B., Cassidy, K. F., Champion, D. C., 2008. SHRIMP U-Pb zircon age constraints on the Late Archaean tectonostratigraphic architecture of the Eastern Goldfields Superterrane, Yilgarn Craton, Western Australia. Precambrian Res. 161, 5–33.

Kramers, J. D., 2002. Global modelling of continent formation and destruction through geological time and implications for CO2 drawdown in the Archaean Eon. Geol. Soc., Lond., Spec. Pub. 199 (1), 259–274.

Kriewaldt, M., 1964. The Fortescue Group of the Roebourne region, North-West Division: Geol. Surv. West. Aust., Annual Report 1963, 30–34.

Kruse, S., McNutt, M., Phipps-Morgan, J., Royden, L., and Wernicke, B., 1991. Lithospheric extension near Lake Mead, Nevada: A model for ductile flow in the lower crust. J. Geoph. Res.-Sol. Ea. 96, 4435–4456.

Kump, L. R. and Barley, M. E, 2007. Increased subaerial volcanism and the rise of atmospheric oxygen 2.5 billion years ago. Nature 448 (7157), 1033–1036.

Kump, L. R., 2008. The rise of atmospheric oxygen. Nature 451 (7176), 277–278.

Kusky T. M. and Kidd W. S. F., 1992. Remnants of an Archean oceanic plateau, Belingwe greenstone belt, Zimbabwe. Geology 20, 43–46

Labrosse, S., Jaupart, C., 2007. Thermal evolution of the Earth: Secular changes and fluctuations of plate characteristics. Earth Planet. Sc. Lett. 260 (3-4), 465–481.

Labrosse, S., Hernlund, J. W., and Coltice, N., 2007. A crystallizing dense magma ocean at the base of the Earths mantle. Nature 450, 866–869.

Lee, C. -T. A., 2006. Geochemical/petrologic constraints on the origin of cratonic mantle. In: Benn, K., Mareschal, J. -C., and Condie, K. C. (Eds.): Archean geodynamics and environments: AGU Geophys. Monogr. 164, Washington DC, 89–114.

Lenardic, A., and Kaula, W. M., 1995. Mantle dynamics and the heat flow into the Earth's continents. Nature 378, 709–711.

Lepot, K., Benzerara, K., Brown Jr., G. E. and Philippot, P., 2008. Microbially inuenced formation of 2,724-million-year-old stromatolites. Nat. Geosci. 1, 118–121.

Lewis, J. D., Rosman, K. R. J., and de Laeter, J. R., 1975. The age and metamorphic effects of the Black Range dolerite dyke: Geol. Surv. West. Aust., Annual Report 1974, 80–88.

Lowe, D. R., 1994. Archean greenstone-related sedimentary rocks. In: Condie, K. C. (Ed.), Archean crustal evolution, Developments in Precambrian geology (11). Amsterdam, Elsevier, 121–169.

Lowe, D. R. and Tice, M. M., 2004. Geologic evidence for Archean atmospheric and climatic evolution: Fluctuating levels of CO2, CH4, and O2 with an overriding tectonic control. Geology 32 (6), 493–496.

Mareschal, J.- C., and West, G. F., 1980. A model for Archean tectonism. Part 2. Numerical models of vertical tectonism in greenstone belts. Can. J. Earth Sci., 17, 60–71.

Mareschal, J.- C., and Jaupart, C., 2006. Archean thermal regime and stabilization of the cratons. In: Benn, K., Mareschal, J. -C., and Condie, K. C. (Eds.): Archean geodynamics and environments: AGU Geophys. Monogr. 164, Washington DC, 61–732.

Marty, B., and Yokochi, R., 2006. Water in the Early Earth. Reviews Mineral. Geochem. 62, pp. 421–450.

McCallum, I. S., 1996. The Stillwater Complex. In: Cawthorn, R. G. (Ed.), Layered intrusions. Amsterdam, Elsevier, 441–483.

McDonough, W. F. and Sun, S. -s., 1995. The composition of the Earth. Chem. Geol. 120, 223–253.

McGregor, A. M., 1951. Some milestones in the Precambrian of Southern Rhodesia. Trans. Geol. Soc. S. Afr. 54, 27–70.

McKenzie, D., 1984. The generation and compaction of partially molten rock. J. Petrol. 25 (3), 713–765.

McKenzie, D., Bickle, M. J., 1988. The volume and composition of melt generated by extension of the lithosphere. J. Petrol. 29 (3), 625–679.

McKenzie, D., and Jackson, J., 2002. Conditions for flow in the continental crust. Tectonics 21, 1055, doi:10.1029/2002TC001394.

McLennan, S. M., Taylor, S. R., 1980. Th and U in sedimentary rocks: crustal evolution and sedimentary recycling. Nature 285 (5767), 621–624.

McLennan, S. M., Taylor, S. R., 1983. Continental freeboard, sedimentation rates and growth of continental crust. Nature 306 (5939), 169–172.

McLennan, S. M., Taylor, S. R. and Hemming, S. R., 2006. Composition, differentiation and evolution of the continental crust: constraints from sedimentary rocks and heat flow. In: Brown, M. and Rushmer, T. (Eds.), Evolution and differentiation of the continental crust, Cambridge, 92–134.

Menneken, M., Nemchin, A. A., Geisler, T., Pidgeon, R. T., and Wilde S. A., 2007. Hadean diamonds in zircon from Jack Hills, Western Australia. Nature 448, 917–920.

Michaut, C., and Jaupart, C., 2007. Secular cooling and thermal structure of continental lithosphere. Earth Planet. Sc. Lett. 257, 83–96.

Miller, K. G., Kominz, M. A., Browning, J. V., Wright, J. D., Mountain, G. S., Katz, M. E., Sugarman, P. J., Cramer, B. S.,Christie-Blick, N. and Pekar, S. F., 2005. The Phanerozoic record of global sea-level change. Science 310 (5752), 1293–1298.

Milliman, J. D. and Syvitski, J. P. M., 1992. Geomorphic/tectonic control of sediment discharge to the ocean: The importance of small mountainous rivers. J. Geol. 100, 525–544.

Mojzsis, S. J., Harrison, T. M., and Pidgeon, R. T., 2001. Oxygen-isotope evidence from ancient zircons for liquid water at the Earth's surface 4,300 Myr ago. Nature 409, 178–181.

Molnar, P., England, P. and Martinod, J., 1993. Mantle dynamics, uplift of the Tibetan plateau, and the Indian monsoon. Rev. Geophys. 31, 357–396.

Mook, W. G., 2001. Natural abundance of the stable isotopes of C, O and H. In: Mook, W.G. (Ed.), Environmental Isotopes in the Hydrological Cycle. Iaea Reports and Technical Documents, Vienna.

Moorbath, S., 1977. Ages, isotopes and evolution of Precambrian continental crust. Chem. Geol. 20, 151–187.

Moresi, L., and Solomatov, V., 1998. Mantle convection with a brittle lithosphere: thoughts on the global tectonic styles of the Earth and Venus. Geoph. J. Int. 133, 669–682.

Moresi, L., Dufour, F., and MẗHlhaus, H. -B., 2003. A Lagrangian integration point finite element method for large deformation modeling of viscoelastic geomaterials. J Comput. Phys. 184, 476–497.

Müller, R. D., Sdrolias, M., Gaina, C., Steinberger, B., and Heine, C., 2008. Long-term sea-level fluctuations driven by ocean basin dynamics. Science 319, 1357–1362.

Nisbet, E. G., and Fowler, C. M. R., 1983. Model for Archean plate tectonics. Geology 11, 376–379.

Nisbet, E. G., 1987. The young Earth: an introduction to Archaean geology, pp. 151–162. Allen & Unwin, Boston, 402 p.

Nisbet, E. G., Cheadle, M. J., Arndt, N. T., Bickle, M. J., 1993. Constraining the potential temperature of the Archaean mantle: A review of the evidence from komatiites. Lithos 30 (3-4), 291–307.

Nisbet, E. G., Sleep, N. H., 2001. The habitat and nature of early life. Nature 409 (6823), 1083–1091.

Niu, Y. and Batiza, R., 1991. An empirical method for calculating melt compositions produced beneath mid-ocean ridges: application for axis and off-axis (seamounts) melting. J. Geophys. Res. 96, 21,753–21,777.

Norrish, K., and Hutton, J. T., 1969. An accurate X-ray spectrographic method for the analysis of a wide range of geological samples. Geochim. Cosmochim. Ac. 33, 431–453.

Nutman, A. P, and Friend, C. R. L., 2007. Comment on "A vestige of Earth's oldest ophiolite". Science 318, 746.

Nelson, D. R., 1998, Compilation of SHRIMP U-Pb zircon geochronology data, 1997. West. Aust. Geol. Surv. Record I998/2, 242 p.

Newman, M. J., and Rood, R. T., 1977. Implications of Solar Evolution for the Earth's Early Atmosphere. Science 198, 1035–1037. title = Implications of Solar Evolution for the Earth's Early Atmosphere,

Nicolas, A., 1984. Principes de tectonique. Masson, Paris, 196 p.

Ohmoto, H., 1996. Evidence in pre-2.2 Ga paleosols for the early evolution of atmospheric oxygen and terrestrial biota. Geology 24, 1135–1138.

Olivier, N., and Boyet, M., 2006. Rare earth and trace elements of microbialites in Upper Jurassic coral- and sponge-microbialite reefs. Chemical Geology 230, 105–123.

Olivier, N., et al., in prep. Integrated sedimentological and geochemical study of the Tumbiana Formation, Fortescue Group, in the East Pilbara Craton, Western Australia.

ONeil, J., Carlson, R. W., Francis, D. and Stevenson R. K., 2008. Neodymium-142 evidence for Hadean mafic crust. Science 321, 1828–1831.

O'Neill, C. ,Moresi, L., Müller, D., Albert, R. and Dufour, F., 2006. Ellipsis 3D: A particle-in-cell finite-element hybrid code for modelling mantle convection and lithospheric deformation. Comput. Geosc. 32 (10), 1769–1779.

Parman, S. W., Dann, J. C., Grove, T. L., and de Wit, M. J., 1997. Emplacement conditions of komatiite magmas from the 3.49 Ga Komati Formation, Barberton Greenstone Belt, South Africa, Earth Planet. Sc. Lett. 150, 303–323.

Parsons, B., 1982. Causes and consequences of the relation between area and age of the ocean-floor. J. Geophys. Res. 87, 289–302.

Patchett, P. J., Kouvo, O. Hedge, C. E. and Tatsumoto, M., 1981. Evolution of continental crust and mantle heterogeneity: evidence from Hf isotopes. Contrib. Mineral. Petr. 78, 279–297.

Pearson, D. G., and Wittig, N., 2008. Formation of Archaean continental lithosphere and its diamonds: the root of the problem. J. Geol. Soc. London 165, 894–914.

Philippot, P., Van Zuilen, M., Lepot, K., Thomazo, C., Farquhar, J., and Van Kranendonk, M. J., 2007. Early Archaean microorganisms preferred elemental sulfur, not sulfate. Science 317, 1534–1537.

Pollack, H. N., Hurter S. J., and Johnson J. R., 1993. Heat ow from the earths interior: analysis of the global data set. Rev. Geophys. 31, 267–280.

Polat, A., Hofmann, A. W., Munker, C., Regelous, M., and Appel, P. W. U. 2003. Contrasting geochemical patterns in the 3.7-3.8 Ga pillow basalt cores and rims, Isua greenstone belt, Southwest Greenland: implications for postmagmatic alteration processes, Geochim. Cosmochim. Ac. 67, 2003, 441–457.

Powell, C. M. A., Li, Z. X., McElhinny, M. W., Meert, J. G., and Park, J. K., 1993. Paleomagnetic constraints on timing of the Neoproterozoic breakup of Rodinia and the Cambrian formation of Gondwana. Geology 21, 889–892.

Prokoph, A., Ernst, R. E., and Buchan, K. L., 2004. Timeseries analysis of Large Igneous Provinces: 3500 Ma to present. Journal Geol. 112, 1–22.

Rasmussen, B., 2000. Filamentous microfossils in a 3,235-million-year-old volcanogenic massive sulphide deposit. Nature 405, 676–679.

Rasmussen, B., Fletcher, I. R., Brocks, J. J., and Kilburn, M. R., 2008. Reassessing the first appearance of eukaryotes and cyanobacteria. Nature 455, 1101–1104.

Rasmussen, B., Blake, T. S., Fletcher, I. R., and Kilburn, M. R., 2009. Evidence for microbial life in synsedimentary cavities from 2.75 Ga terrestrial environments. Geology 37, 423–426.

Raymo, M. E., and Ruddiman, W. F., 1992. Tectonic forcing of late Cenozoic climate. Nature 359, 117–122.

Rey, P. F., Philippot, P., and Thébaud, N., 2003. Contribution of mantle plumes, crustal thickening and greenstone blanketing to the 2.75-2.65 Ga global crisis. Precambrian Res. 127, 43–60.

Rey, P. F., Houseman, G., 2006. Lithospheric scale gravitational flow: the impact of body forces on orogenic processes from Archaean to Phanerozoic. In: Buiter, S. J. H, and Schreurs, G. (Eds.), Analogue and numerical modelling of crustal-scale processes. Geol. Soc., Lond., Spec. Pub. 253 (1), 153–167.

Rey, P. F. and Coltice N., 2008. Neoarchean strengthening of the lithosphere and the coupling of the Earth's geochemical reservoirs. Geology 36, 635–638.

Reymer, A., Schubert, G., 1984. Phanerozoic addition rates to the continental-crust and crustal growth. Tectonics 3 (1), 63–77.

Reynard, B., Lecuyer, C., and Grandjean, P., 1999. Crystal-chemical controls on rare-earth element concentrations in fossil biogenic apatites and implications for paleoenvironmental reconstructions. Chem. Geol. 155, 233–241.

Rino, S., Komiya, T., Windley, B. F., Katayama, I., Motoki, A., Hirata, T., 2004. Major episodic increases of continental crustal growth determined from zircon ages of river sands; implications for mantle overturns in the early Precambrian. Phys. Earth Plan. Int. 146 (1-2), 369–394.

Robert, F., and Chaussidon, M., 2006. A palaeotemperature curve for the Precambrian oceans based on silicon isotopes in cherts. Nature 443, 969–972.

Rowley, D. B., 2002. Rate of plate creation and destruction: 180 Ma to present. Geol. Soc. Am. Bull. 114, 927–933.

Royden, L., 1996. Coupling and decoupling of crust and mantle in convergent orogens: Implications for strain partitioning in the crust. J. Geophys. Res. 101, 17,679–17,705.

Rudnick, R. L., 1995. Making continental crust, Nature 378 (6557), 571–578.

Rudnick, R. L. and Fountain, D. M., 1995. Nature and composition of the continental crust: a lower crustal perspective. Rev. Geophys. 33, 267–309.

Rudnick, R. L. and Gao, S., 2003. Composition of the continental crust. In: Rudnick, R. L., Holland, H. D., and Turekian K. K. (Eds.), Treatise on geochemistry 3, 1–64.

Rüpke, L. H., Phipps Morgan, J., Hort, M., and Connolly, J. A. D., 2004. Serpentine and the subduction zone water cycle. Earth Planet. Sc. Lett. 223, 17–34.

Sakurai, R., Ito, M., Ueno, Y., Kitajima, K., and Maruyama, S., 2005. Facies architecture and sequence-stratigraphic features of the Tumbiana Formation in the Pilbara Craton, northwestern Australia: Implications for depositional environments of oxygenic stromatolites during the Late Archean. Precambrian Res. 138, 255-273.

Schopf, J. W., and Packer, B. M., 1987. Early Archean (3.3-Billion to 3.5-Billion-Year-Old) Microfossils from Warrawoona Group, Australia. Science 237, 70–73.

Sclater, J. G. and Parsons, B. and Jaupart, C.,1981. Oceans and continents: Similarities and differences in the mechanisms of heat loss. J. Geophys. Res. 86, 11535–11552.

Schidlowski, M., Hayes, J. M., and Kaplan, I. R., 1983. Isotopic inferences of ancient biochemistries: Carbon, sulfur, hydrogen, and nitrogen. In: Schopf, J.W. (Ed.), Earth's Earliest Biosphere: Its Origin and Evolution. Princeton Univ. Press, Princeton.

Schubert, G., Reymer, A. P. S., 1985. Continental volume and freeboard through geological time. Nature 316 (6026), 336–339.

Shields, G., Veizer, J., 2002. Precambrian marine carbonate isotope database: Version 1.1. Geochem. Geophy. Geosy. 3, 1031.

Sircombe, K. N. Bleeker, W. and Stern, R. A., 2001. Detrital zircon geochronology and grain-size analysis of a 2800 Ma Mesoarchean proto-cratonic cover succession, Slave Province, Canada. Earth Planet. Sc. Lett. 189 (3-4), 207–220.

Sleep, N. H. and Windley, B. F., 1982. Archean plate-tectonics - constraints and inferences. J. Geol. 90 (4), 363–379.

Sleep, N. H., and Zahnle, K., 2001. Carbon dioxide cycling and implications for climate on ancient Earth. J. Geophys. Res. 106, 1373–1399.

Smith, R. E., Perdrix, J. L., and Parks, T. C., 1982. Burial metamorphism in the Hamersley Basin, Western Australia. J. Petrol. 23, 75–102.

Smithies, R. H.,Van Kranendonk, M. J., and Champion, D.C., 2007. The Mesoarchean emergence of modern-style subduction, Gondwana Res. 11, 50–68.

Solomatov, V. S., and Moresi, L. -N., 1996. Three regimes of mantle convection with non-Newtonian viscosity and stagnant lid convection on the terrestrial planets: Geophys. Res. Lett. 24, 1907–1910.

Solomatov, V. S., 2000. Fluid dynamics of a terrestrial magma ocean. In: Canup, R. M., and Righter, K. (Eds), Origin of the Earth and Moon, Tucson: University of Arizona Press., p. 323–338.

Sonder, L. J., England, P. C., Wernicke, B. P., and Christiansen, R. L., 1987. A physical model for Cenozoic extension of the western North America. In: Coward, M. P., Dewey, J. F., and Hancock, P. L. (Eds.), Continental extensional tectonics: Geol. Soc., Lond., Spec. Pub. 28, p. 187–201.

Southam, J. R., Hay, W. W., 1981. Global sedimentary mass balance and sea level changes, In: Emiliani, C. (Ed.), The Sea, v. 7, the Oceanic Lithosphere. Wiley-Interscience, New York, 1617–1684.

Spohn, T., and Breuer, D., 1993. Mantle differentiation through continental crust growth and recycling and the thermal evolution of the Earth. In: Takahashi, E., Jeanloz, R., and R. Rudie (Eds.), Evolution of the Earth and planets. AGU Geophys. Monogr., Washington DC, 55–71.

Sramek, O., Ricard, Y. and Bercovici, D., 2007. Simultaneous melting and compaction in deformable two-phase media. Geophys. J. Int. 168 (3), 964–982.

Stachel, T., and Harris, J. W., 2008. The origin of cratonic diamonds Constraints from mineral inclusions. Ore Geol. Rev. 34, 5–32.

Strahler, A. N., 1952. Hypsometric (area-altitude) analysis of erosional topography. Geol. Soc. Am. Bull. 63 (11), 1117–1142.

Sugitani, K., Yamashita, F., Nagaoka, T., Yamamoto, K., Minami, M., Mimura, K., and Suzuki, K., 2006. Geochemistry and sedimentary petrology of Archean clastic sedimentary rocks at Mt. Goldsworthy, Pilbara Craton, Western Australia: Evidence for the early evolution of continental crust and hydrothermal alteration. Precambrian Res. 147, 124–147.

Sylvester, P. J., Campbell, I. H. and Bowyer, D. A., 1997. Niobium/Uranium evidence for early formation of the continental crust. Science 275, 521–523.

Tackley, P. J., 2000. Mantle convection and plate tectonics: Toward an integrated physical and chemical theory. Science 288, 2002-2007.

Taylor, S. R. and McLennan, S. M., 1985. The continental crust: its composition and evolution. Blackwell Scientific Publications, 328 p.

Taylor, S. R., and McLennan, S. M., 1995. The geochemical evolution of the continental crust. Rev. Geophys. 33, 241–265.

Thébaud, N., 2006. De la caractérisation des fluides aurifères par rayonnement synchrotron à la géodynamique archéenne : Etude des interactions fluides-roches dans un point triple de foliation archéen (Le synclinal de Warrawoona, Australie Occidentale). Thèse de doctorat de lUniversité de Paris 6, 280 p.

Thomazo, C., Ader, M., Farquhar, J., and Philippot, P., 2009. Methanotrophs regulated atmospheric sulfur isotope anomalies during the Mesoarchean (Tumbiana Formation, Western Australia). Earth Planet. Sc. Lett. 279, 65–75.

Thorne, A. M., and Trendall, A. F., 2001. Geology of the Fortescue Group, Pilbara Craton, Western Australia: West. Aust. Geol. Surv. Bull. 144, 249 p.

Tomlinson, K. Y., Hughes, D. J., Thurston, P. C., and Hall, R. P., 1999. Plume magmatism and crustal growth at 2.9 to 3.0 Ga in the Steep Rock and Lumby Lake area, Western Superior Province. Lithos 46, 103–136.

Trendall, A. F., Compston, W., Nelson, D. R., De Laeter, J. R., and Bennett V. C., 2004. SHRIMP zircon ages constraining the depositional chronology of the Hamersley Group, Western Australia. Aust. J. Earth Sci. 51, 621–644.

Turcotte, D. L., and Burke, K., 1978. Global sea-level change s and the thermal structure of the Earth. Earth Planet. Sc. Lett. 41, 341–346.

Turcotte, D. L., and Schubert, G., 1982. Geodynamics: Applications of continuum physics to geological problems. Wiley, J. & Sons Inc., New York, 450 p.

Turcotte, D. L., and Schubert, G., 2002. Geodynamics, second edition: Cambridge University Press, 456 p.

Upadhyay, D., Scherer, E. E., and Mezger, K. ^{142}Nd evidence for an enriched Hadean reservoir in cratonic roots. Nature 459, 1118–1121.

U.S. Department of Commerce, National Oceanic and Atmospheric Administration, National Geophysical Data Center, 2006.
URL http://www.ngdc.noaa.gov/mgg/fliers/06mgg01.html

Vail, P. R., Mitchum, R. M., Todd, R. G., Widmier, J. M., Thompson III, S., Sangree, J. B., Bubb, J. N., Hatlelid, W. G., 1977. Seismic stratigraphy and global changes of sea level. Am. Assoc. Petrol. Geol. Mem. 26, 49–212.

Valley, J., Lackey, J., Cavosie, A., Clechenko, C., Spicuzza, M., Basei, M., Bindeman, I., Ferreira, V., Sial, A., King, E., Peck, W., Sinha, A. and Wei, C., 2005. 4.4 billion years of crustal maturation: oxygen isotope ratios of magmatic zircon. Contrib. Mineral. Pet. 150 (6), 561–580.

Van Kranendonk, M. J., 2003a. Stratigraphic and tectonic signicance of eight local unconformities in the Fortescue Group, Pear Creek Centrocline, Pilbara Craton, Western Australia. Geol. Surv. West. Aust., Annual Review 2001-02, 70–79.

Van Kranendonk, M. J., Webb, G. E., and Kamber, B. S., 2003b. Geological and trace element evidence for a marine sedimentary environment of deposition and biogenicity of 3.45 Ga stromatolitic carbonates in the Pilbara Craton, and support for a reducing Archaean ocean. Geobiology 1, 91–108.

Van Kranendonk, M. J., Collins, W. J., Hickman, A., Pawley , M. J., 2004a. Critical tests of vertical vs. horizontal tectonic models for the Archaean East Pilbara GraniteGreenstone Terrane, Pilbara Craton, Western Australia. Precambrian Res. 131, 173–211.

Van Kranendonk, M. J., Smithies, R. H., Hickman, A. H., Bagas, L., Williams, I. R., and Farrell, T. R., 2004b. Event stratigraphy applied to 700 million years of Archaean crustal evolution, Pilbara Craton, Western Australia. Geol. Surv. West. Aust., Annual Review 2003-04, 49–61.

Van Kranendonk, M. J., Philippot, P., Lepot, K., 2006. The Pilbara drilling project: c. 2.72 Ga Tumbiana Formation and c. 3.49 Ga Dresser Formation, Pilbara Craton, Western Australia. Geol. Surv. West. Aust. 2006. 25p.

Van Kranendonk, M. J., Smithies, R. H., Hickman, A. H., and Champion, D. C., 2007. Review: secular tectonic evolution of Archean continental crust: interplay between horizontal and vertical processes in the formation of the Pilbara Craton, Australia. Terra Nova 19, 1–38.

Vearncombe, S., Barley, M. E., Groves, D. I., McNaughton, N. J., Mikucki, E. J., and Vearncombe, J. R., 1995. 3.26 Ga black smoker-type mineralization in the Strelley Belt, Pilbara Craton, Western Australia. J. Geol. Soc. London 52, 587–590.

Veizer, J. and Compston, W., 1976. $^{87}Sr/^{86}Sr$ in Precambrian carbonates as an index of crustal evolution. Geochim. Cosmochim. Ac. 40, 905-914.

Veizer, J. and Jansen, S. L., 1979. Basement and sedimentary recycling and continental evolution. J. Geol. 87, 341–370.

Veizer, J., Clayton,R. N., Hinton, R. W., Von Brunn, V., Mason, T. R., Buck, S. G., and Hoefs, J., 1990. Geochemistry of Precambrian carbonates: 3-shelf seas and non-marine environments of the Archean. Geochim. Cosmochim. Ac. 54, 2717–2729.

Veizer, J., Ala, D., Azmy, K., Bruckschen, P., Buhl, D., Bruhn, F., Carden, G. A. F., Diener, A., Ebneth, S., Godderis, Y., Jasper, T., Korte, C., Pawellek, F., Podlaha, O., and Strauss, H., 1999. $^{87}Sr/^{86}Sr$, $\delta^{13}C$ and $\delta^{18}O$ evolution of Phanerozoic seawater, Chem. Geol., 161, 59–88.

Viljoen, M. J. and Viljoen, R. P., 1969. Evidence for the existence of a mobile extrusive peridotitic magma from the Komati Formation of the Onverwacht Group. In: Upper Mantle Project. Geol. Soc. S. Afr. Spec. Publ. 3, 87–112.

Vine, F. J., 1966. Spreading of the ocean floor: New evidence. Science 154, 1405–1415.

Vlaar, N. J. and van den Berg, A. P., 1991. Continental evolution and archaeo-sea-levels, in: Sabadini, R. and Lambeck, K. and Boschi, E. (Eds.), Glacial Isostasy, Sea-Level and Mantle Rheology. pp. 637-662.

Vlaar, N. J., van Keken, P. E. and van den Berg, A. P., 1994. Cooling of the Earth in the Archaean: Consequences of pressure-release melting in a hotter mantle. Earth Planet. Sci. Lett. 121, 1–18.

Vlaar, N. J., 2000. Continental emergence and growth on a cooling earth. Tectonophysics 322 (1-2), 191–202.

Walker, J. C. G., 1985. Carbon dioxide on the early Earth. Orig. Life Evol. Biosph. 16, 117–127.

Walker, J. C. G., and Lohmann, K. C., 1989. Why the oxygen isotopic composition of sea water changes with time. Geophys. Res. Lett. 4, 323–326.

Walter, M. R., Buick, R., and Dunlop, J. S. R., 1980. Stromatolites 3,400-3,500 Myr old from the North Pole area, Western Australia. Nature 284, 443–445.

Wasserburg, G. J., MacDonald, G. J. F., Hoyle, F., and Fowler W. A., 1964. Relative contributions of uranium, thorium, and potassium to heat production in the Earth. Science, 143, 465–467.

Webb, A. and Kamber, B. S., 2000. Rare earth elements in Holocene reefal microbialites: A new shallow seawater proxy. Geochim. Cosmochim. Ac. 64, 1557–1565.

Wellman, P., 1999. Interpretation of regional gephysics of the Pilbara Craton, northwest Australia. Australian Geological Survey Organisation, Record 1999/4.

West, G. F., Mareschal, J. C., 1979. A model for Archean tectonism. Part 1. The thermal conditions. Can. J. Earth Sci. 16, 1942–1950.

White, R. S., McKenzie, D. and Onions, R. K., 1992. Oceanic crustal thickness from seismic measurements and rare-earth element inversions. J Geophys. Res.-Sol. Ea. 97, 19683–19715.

Wilde, S. A., Valley, J. W., Peck, W. H., and Graham, C. M., 2001. Evidence from detrital zircons for the existence of continental crust and oceans on the Earth 4.4 Gyr ago. Nature 409, 175–178.

Wilks, M. E. and Nisbet E. G., 1985. Archaean stromatolites from the Steep Rock Group, northwestern Ontario, Canada. Can. J. Earth Sci. 22, 792-799.

Harold Williams, H., Hoffman, P. F., Lewry, J. F., Monger, J. W. H. and Rivers, T., 1991. Anatomy of North America: thematic geologic portrayals of the continent. Tectonophysics 187, 117–134.

Williams, I. R., 1999. Muccan, WA Sheet 2956. Geol. Surv. West. Aust., 1:100 000 Geological Series. URL http://mapserver.doir.wa.gov.au/datacentre/

Williams, I. R., 1999. Geology of the Muccan 1:100 000 sheet. Geol. Surv. West. Aust., 1:100 000 Geological Series Explanatory Notes, 39 p.

Williams, I. R. and Bagas, L., 2007. Mount Edgar, WA Sheet 2955. Geol. Surv. West. Aust., 1:100 000 Geological Series. URL http://mapserver.doir.wa.gov.au/datacentre/

Williams, I. R. and Bagas, L., 2007b. Geology of the Mount Edgar 1:100 000 sheet. Geol. Surv. West. Aust., 1:100 000 Geological Series Explanatory Notes, 62 p.

Wilson, J. T., 1965. Evidence from Ocean Islands Suggesting Movement in the Earth. Philos. T. R. Soc. A 258, 145–167.

Windley, B. F., 1977. Timing of continental growth and emergence. Nature 270 (5636), 426–428.

Wingate, M. T. D., 1999. Ion microprobe baddeleyite and zircon ages for Late Archaean mafic dykes of the Pilbara Craton, Western Australia. Aust. J. Earth Sci. 46, 493–500.

Wise, D. U., 1974. Continental margins, freeboard and the volumes of continents and oceans through time. In: Burk, C.A. and Drake, C.L. (Eds.), The Geology of Continental Margins. Springer, New York, pp. 87–108.

Workman, R. K., and Hart, S. R., 2005. Major and trace element composition of the depleted MORB mantle (DMM). Earth Planet. Sci. Lett. 231, 53–72.

Wyman,D. A., O'neill, C., and Ayer, J. A., 2008. Evidence for modern-style subduction to 3.1 Ga: A plateau-adakite-gold (diamond) association. In: Condie, K. C., and Pease, V. (Eds.), When did plate tectonics begin on planet Earth? GSA Special Paper 440, 129–148.

Zegers, T. E., Nelson, D. R., Wijbrans, J. R., and White, S. H., 2001. SHRIMP U-Pb zircon dating of Archean core complex formation and pancratonic strike-slip deformation in the East Pilbara Granite-Greenstone Terrain. Tectonics 20, 883–908.

Zindler, A., and Hart, S., 1986. Chemical geodynamics. Annu. Rev. Earth Planet. Sci. 14, 493–571.

Author: Nicolas Flament
Title: Secular cooling of the solid Earth, emergence of the continents, and evolution of Earth's external envelopes
Advisors: Nicolas Coltice and Patrice Rey
Place and date of defence: 9 December 2009 at Ecole Normale Supérieure de Lyon

---

Abstract

The secular cooling of the mantle and of the continental lithosphere trigger an increase in the area of emerged land. The corollary increase in weathering and erosion processes has major consequences for the evolution of Earth's external envelopes.

We developed a physical model to evaluate the area of emerged land as a function of mantle temperature, continental area, and of the distribution of continental elevations. Our numerical results show that less than 15% of Earth's surface consisted of emerged land by the end of the Archaean. This is consistent with many geological and geochemical observations.

To estimate the secular cooling of the continental lithosphere, we combined thermo-mechanical models with field observations. Our results, constrained by geological data, suggest that the Moho temperature has decreased by $\sim 200°C$ over 2.7 Ga in the Pilbara Craton.

To evaluate the effect of continental growth on the evolution of the area of emerged land, we developed a model based on published thermal evolution models. Our results suggest that the area of emerged land was less than 5% of Earth's surface in the Archaean, and that it does not depend on crustal growth. This allows to reconcile the evolution of oceanic $^{87}Sr/^{86}Sr$ with early crustal growth models.

Continents are enriched in phosphorus, which is essential to the biosphere. The emergence of the continents would thus have triggered an increase in the production of oxygen by photosynthetic micro-organisms, possibly contributing to the oxidation of the atmosphere 2.4 Ga ago.

Keywords

Archaean; continental emergence; freeboard; continental growth; hypsometry; thermal evolution; Large Igneous Province; Continental Flood Basalt; crustal flow; continental geotherm; atmospheric evolution; great oxidation event; Fortescue Group; Pilbara Craton

Auteur : Nicolas Flament
Titre : Refroidissement séculaire de la Terre solide, émergence des continents, et évolution des enveloppes externes de la Terre
Directeurs : Nicolas Coltice et Patrice Rey
Lieu et date de soutenance : 9 Décembre 2009 en l'École Normale Supérieure de Lyon

---

Résumé

Le refroidissement séculaire du manteau terrestre et de la lithosphère continentale se traduit par l'augmentation de la surface de terres émergées. L'augmentation corollaire des processus d'altération et d'érosion des silicates a des conséquences majeures pour les enveloppes externes.

Nous avons développé un modèle physique qui permet d'évaluer la surface de terres émergées en fonction de la température du manteau, de la surface totale de continents, et de la distribution des altitudes continentales. Nos résultats numériques montrent qu'à la fin de l'Archéen, moins de 15% de la surface terrestre étaient émergée, en accord avec nombre d'observations géologiques et géochimiques.

Pour estimer le refroidissement séculaire de la lithosphère continentale, nous avons combiné des modèles thermo-mécaniques avec des observations de terrain. Nos résultats, contraints par des données géologiques, suggèrent que la température au Moho a diminué de $\sim 200°C$ en 2,7 Ga dans le craton des Pilbaras.

Pour évaluer l'effet de la croissance continentale sur l'évolution de la surface de terres émergées, nous avons développé un modèle basé sur un modèle d'évolution thermique publié. Nos résultats suggèrent que la surface émergée, de moins de 5% de la surface terrestre à l'Archéen, dépend peu de la croissance continentale. Ceci permet de réconcilier l'évolution du $^{87}Sr/^{86}Sr$ océanique avec une croissance continentale précoce.

Les continents sont enrichis en phosphate, élément essentiel à la biosphère. Leur émergence aurait donc engendré une augmentation de la production d'oxygène par des micro-organismes photosynthétiques, contribuant ainsi à l'oxydation de l'atmosphère il y a 2,4 Ga.

Mots-clefs

Archéen ; émergence continentale ; freeboard ; croissance continentale ; hypsométrie ; évolution thermique ; provinces volcaniques ; basaltes continentaux ; écoulement crustal ; géotherme continental ; évolution atmosphérique ; oxydation de l'atmosphère ; Groupe Fortescue ; craton des Pilbaras

Nicolas Flament

Geophysicist

Contact details

✉ **Address**
School of Geosciences
The University of Sydney
NSW 2006 Australia

Phone
☎ (+61) 2 9351 7576
(+61) 468 686 512

Email
nicolas.flament@sydney.edu.au

Current position

Postdoctoral Fellow with Pr. Dietmar Müller, School of Geosciences, University of Sydney, Australia
Dynamic Earth Models and Surface Maps for South America, sponsored by Statoil

Higher education

2006-2009 **PhD in Earth Science, ENS Lyon and University of Sydney**
Secular cooling of the solid Earth, emergence of the continents, and evolution of Earth's external envelopes - Advisors: Dr. N. Coltice and Assoc. Pr. P. F. Rey

2003-2006 **Bachelor of Science and Master of Science (Earth Science), ENS Lyon**
Competitive entry (July 2003)
Spring semester (2005) at Uppsala Universitet, Sweden

2001-2003 ***"Classes préparatoires aux grandes écoles"*, Sainte Geneviève, Versailles**
Intensive training in mathematics, physics, chemistry, biology and earth science

Scientific interests

Key words: lithospheric processes, sea level evolution, numerical modelling, Archaean

PhD subjects

- Secular evolution of sea level
- Consequences of continental emergence on the evolution of early life and the atmosphere
- Crustal ductility and gravity-driven crustal flow
- Structural and geochemical evolution of the Fortescue Group, Pilbara Craton, WA

Methodologies

- Development of numerical codes (Fortran)
- Finite element modelling (Ellipsis3D)
- Field work - structural geology and geochemical sampling
- Trace element, strontium and neodymium isotopic geochemistry

Teaching activity

Teaching experience

- Assistant lecturer, Université Lyon 1
  192 hours from 2006 to 2009
- Casual assistant lecturer, University of Sydney (2007-2008)

Topics

- First-year geoscience tutorials, including geological time, mineralogy, planetology, seismology, plate tectonics, dynamics of the solid Earth and of its exogenic envelopes
- Cartography practicals, mapping and field geology

Publications

- **Flament, N.**, Rey, P. F., Coltice, N., Dromart, G., and Olivier, N., 2009. Lower crustal flow and subaqueous Archean Continental Flood Basalts, *in prep.*
- **Flament, N.**, Coltice, N. and Rey, P. F., 2008. A case for late-Archaean continental emergence from thermal evolution models and hypsometry, *Earth and Planetary Science Letters* 275 (3-4), 326-336, doi:10.1016/j.epsl.2008.08.029 - Object of an article in the *New Scientist* on 30/12/2008

Oral presentations

- **Flament, N.**, Coltice, N. and Rey, P. F., Consequences of the late-Archaean emergence of continents, Géosciences Rennes, 5 February 2009 and IUEM "Domaines Océaniques", Brest, 6 February 2009 - invited
- **Flament, N.**, Coltice, N. and Rey, P. F., Late-Archean continental emergence: consequences for the rise of atmospheric oxygen, **American Geophysical Union fall meeting, 2008**
  Webcast available on line (beginning at 63 min.)
- **Flament, N.**, Coltice, N. and Rey, P. F., Surface area of emerged land and depth of mid-oceanic ridges in the Archean, **Australian Earth Science Convention, 2008**
- **Flament, N.**, Coltice, N. and Rey, P. F., Secular evolution of the Earth and the rise of the continents, TGIF talk series, University of Sydney, 12 April 2007 - invited

Poster presentations

- **Flament, N.**, Rey, P. F., Coltice, N., Dromart, G., and Olivier, N., Lower crustal flow and subaqueous Archean continents, **American Geophysical Union fall meeting, 2009**
- **Flament, N.**, Rey, P. F. and Coltice, N., Modeling the thermal and mechanical response of 3.4-2.2 Ga continental crust to the emplacement of sills, **European Geosciences Union general assembly, 2008**
- **Flament, N.**, Coltice, N. and Rey, P. F., Emerged land surface in the Archean: constraints on continental growth and mantle thermal history, **European Geosciences Union general assembly, 2007**

Research experience

2006 **Six-month internship (Masters) at LST (ENS-UCBL)**
Secular evolution of sea level - Advisor: Dr. N. Coltice

2005 **Three-month internship at the Department of Earth Sciences, Uppsala Universitet**
Ice surface velocity from GPS measurements on Kibergbreen glacier, Queen Maud Land, Antarctica - Advisor: Dr. V. Pohjola

2004 **Two-month internship at LST (ENS-UCBL)**
Trace elements in gastropod shells by LA-ICPMS analysis - Advisor: Dr. B. Reynard

Miscellaneous

Full driver's licence

Language skills

- French (native)
- English (fluent, living in Sydney, Australia)
- Italian (spoken, lived two years in Rome, Italy)

Hobbies

- Sports: basketball (competition)
  , swimming, cycling
- Travelling

Computer skills

- Operating Systems: Unix/Linux, Windows
- Programming: Fortran, shell scripting
- Finite elements modelling: Ellipsis3D, Gale
- Mapping/GIS: GMT, Arcview
- Others: Word, Excel, Powerpoint, LaTeX

Professional Affiliations

- American Geophysical Union
- European Geosciences Union